SEAFLOOR HABITAT CHARACTERIZATION, CLASSIFICATION, AND MAPS FOR THE LOWER PISCATAQUA RIVER ESTUARY

BY

GEORGE RANDALL CUTTER, JR.
BA, University of Virginia, 1991
MS, College of William and Mary, 1998

DISSERTATION

Submitted to the University of New Hampshire
In Partial Fulfillment of
The Requirements for the Degree of

Doctor of Philosophy
in
Earth Sciences – Oceanography
September, 2005

This dissertation has been examined and approved.

_____

Dissertation Director, Dr. Larry A. Mayer
Professor of Earth Sciences and Ocean Engineering

_____

Dr. Kevin B. Briggs
Oceanographer, Naval Research Laboratory,
Stennis Space Center

_____

Dr. James V. Gardner
Research Professor of Earth Sciences

_____

Dr. Raymond E. Grizzle
Research Associate Professor of Zoology

_____

Dr. Lloyd C. Huff
Research Professor of Ocean Engineering

_____

Dr. Yuri Rzhanov
Research Associate Professor

_____

Dr. Larry G. Ward
Research Associate Professor of Earth Sciences

_____

Date

PREFACE

Dissertation structure

This dissertation contains eight chapters, including two chapters that were reformatted from peer-reviewed published works, and two chapters that have been submitted for publication. Each chapter stands alone as independent research; however, each presents important issues related to seafloor habitat and facies characterization and fits into the scope of the dissertation. As such, the dissertation does not read as a logical sequence, and some repetition of topics might occur between chapters. The introductory chapter attempts to provide the background and linkages that make this dissertation a coherent work. The final chapter allows for expansion of, or revision to, ideas presented in the chapters, because some conclusions were reinforced by further thought and work, and some hypotheses and conclusions were rejected with the introduction of new evidence.

Chapter 1 ("Introduction") contains an introduction intended to provide context and link the topics in the other chapters.

Chapter 2 ("Seafloor segmentation using texture") contains the text from a publication describing texture feature analysis for unsupervised classification of seafloor bathymetry (Cutter et al., 2003).

Chapter 3 ("Ground truthing using image mosaics") is based on a publication describing the use of image mosaics to ground-truth habitat delineations predicted from acoustic maps (Cutter et al., *In Press*).

Chapter 4 (“Seafloor microtopographical roughness spectra”) represents the text from a submitted manuscript describing estimation of parameters from roughness spectra of seafloor microtopographical profiles from sediment profile images (Cutter, *Submitted*). Results from spectral analysis of sediment profile imagery (SPI) images from the Piscataqua River are provided in Appendix A.

Chapter 5 (“Facies from the Lower Piscataqua River (Great Bay Estuarine System) Characterized using Physical Samples and Video Images”) contains unpublished work describing efforts to separately characterize sediment facies using physical sample data and seafloor images and methodology and results linking the two approaches. The impetus for this effort was the difficulty presented by having potentially disparate information from different data sources. The goal was to produce comparable information from different ground truthing methods and data sources. The realization of that goal is fundamentally important to the process of seafloor characterization using bathymetry and backscatter from acoustic data.

Chapter 6 (“Benthic habitat classification, characterization, and the provisional truth of ground-truth”) is based on a publication describing segmentation and classification of seafloor bathymetry and backscatter using statistical, textural, and spatial methods compared to results from ground truthing and the errors that can be involved with uncertainty associated with ground-truth data (Cutter, *2005*).

Chapter 7 (“Supervised classification of gridded multibeam bathymetry data using LFH texture features for habitat structure class prediction”) describes work done as a demonstration project for the National Oceanic and Atmospheric Administration (NOAA) Center for Coastal Monitoring and Assessment, Biogeography Program. The

effort involved prediction of reef habitat structure classes for every 1-by-1 m grid cell from a multibeam bathymetry survey area off Saint John, U.S. Virgin Islands. Habitat structure classes identified at points by divers and in video analysis data were used to develop prototype Local Fourier Histogram texture features used for supervised classification.

Chapter 8 ("Summary and Conclusions") synthesizes the topics of this dissertation. It is intended to put some of the efforts and results in perspective, and to provide guidance for researchers involved in similar activities.

References

Cutter, Jr., G. R., *Submitted*. Seafloor roughness spectra from sediment profile images. Submitted, Dec. 2004, to Journal of Marine Systems.

Cutter Jr., G. R., 2005. Benthic habitat classification and characterization using multibeam sonar data: the provisional truth of ground-truth. Proceedings of the International Conference for underwater acoustic measurements: technologies and results. F.O.R.T.H., Heraklion, Crete. 28 June – 1 July, 2005.

Cutter Jr., G. R., Rzhanov, Y., Mayer, L. A. and Grizzle, R. E., *In Press*. Ground Truthing Benthic Habitat Characteristics Using Video Mosaic Images. *In* Barnes, P. W., Thomas, J. P., (Eds.) Benthic habitats and the effects of fishing. American Fisheries Society, Symposium 41, Bethesda, Maryland.

Cutter, G. R., Rzhanov, Y., Mayer, L. A., 2003. Automated segmentation of seafloor bathymetry from multibeam echosounder data using local Fourier histogram texture features. Journal of Experimental Marine Biology and Ecology, 285/286, 355-370.

TABLE OF CONTENTS

LIST OF TABLES

LIST OF FIGURES

ABSTRACT

SEAFLOOR HABITAT CHARACTERIZATION, CLASSIFICATION, AND MAPS FOR THE LOWER PISCATAQUA RIVER ESTUARY

by

George Randall Cutter, Jr.

University of New Hampshire, September, 2005

Seafloor data from multibeam echosounders, underwater images, and physical samples were used to implement segmentations, classifications, and measurements for seafloor characterization and habitat mapping. Texture analysis, using local Fourier histogram texture features, was applied to multibeam bathymetry data in unsupervised- and supervised-classification modes. Seafloor video-image mosaics were used to characterize biogenic features and verify transitions between habitats and allowed descriptions of features that were not determinable from other imagery. Spectral-model parameters (slope and intercept) that are important to models relating acoustic backscatter to seafloor properties were calculated to describe roughness from seafloor microtopography in sediment profile images (SPI). SPI spectral-model parameters are consistent with published estimates for data from other devices such as sterophotographs, and values varied by sedimentary facies and bioturbational regime. Unsupervised classification of bathymetry using texture features produced segmentations that corresponded to known spatial distributions of seafloor sediments, but required arbitrary

choices for some parameter values and, therefore, included potential bias. Supervised classification of bathymetric texture overcame bias related to arbitrarily-chosen parameters, and produced classifications that corresponded well with identified seafloor habitats and with ground-truth data. Similar textures can exist for different seafloor attributes. In general, however, the LFH texture feature classification technique, using only gridded bathymetric data, works well to predict spatial distributions of seafloor morphologies and structure classes on a per-grid-cell basis and is robust to data noise. The results from several classification methods exposed the weakness of ground-truth data with high positioning uncertainty relative to the resolution and positioning uncertainty for shallow-water multibeam echosounder surveys. Ground-truth data with high positioning uncertainty were not reliable for assessment of delineations and classifications of seafloor bathymetry and acoustic backscatter data. With good ground-truth data, accurate habitat maps and seafloor characterizations can be produced using automated techniques.

CHAPTER 1

1. INTRODUCTION

1.1. Statement of Objectives

The overarching goal of my dissertation work was to establish means by which seafloor habitat characteristics can be imaged, detected, interpreted, and effectively mapped. I reviewed habitat concepts, marine habitat classification schemes, and habitat mapping efforts. Using multibeam echosounder (MBES) bathymetry and backscatter data and sidescan sonar (SSS) backscatter data from the Portsmouth, New Hampshire common dataset, I implemented current methodologies for habitat delineation, then described and applied new semi-automated delineation methods. I considered data from seafloor video mosaics to describe habitat characteristics at smaller spatial scales, and attempted to relate them to acoustically-sensed characteristics. I used historical sediment sample data and sediment maps to produce hypothetical habitat maps, then compared these to characterizations made using acoustic and optical data. Finally, I attempted to address the questions: Are habitat classifications made using acoustic data biologically or ecologically meaningful; do these classifications successfully delineate regions of distinct species distributions or community structure? If not, how can we modify habitat classification based on acoustic data to provide biologically meaningful classification, and what suite of tools and techniques should be applied to accomplish that?

My research focused on (1) automated and objective segmentation methods of benthic habitat mapping from multibeam sonar bathymetry and backscatter data; (2) applying quantitative analysis of imagery to derive physical and biological seafloor characteristics; (3) using techniques to provide overlapping spatial scales of optical and acoustic data; and (4) making linkages between characteristics assessed from different data sources.

1.2. Background

A common impetus for biological habitat mapping is to determine where and in what densities organisms exist in order to make stock assessments or evaluate biological resources. Classically, benthic habitat mapping and resource assessment have involved collecting point samples for benthic infauna and substrates (sediment facies) or transect tow samples for fish and epifauna. Optical imagery has often been used to describe substrates and assess occurrences of certain fauna.

In many cases, occurrence or abundances of some species might be determinable based on the substrates because associations exist between organisms and physical habitat attributes. Therefore, even if expensive biological determinations are not available, less expensive samples of physical environmental factors or organisms can be used to make inferences about the biological resources of interest and to support interpolations. Recently, habitat mapping efforts have involved the use of seafloor maps generated from multibeam echosounders (MBES) or sidescan sonars (SSS). The bathymetric and backscatter data from MBES can relate information about seafloor morphology and composition, with near complete coverage of the seafloor, and often at

high spatial resolution. Kostylev et al. (2003) have shown that scallop abundances were correlated with multibeam backscatter strengths on Browns Bank in the Gulf of Maine. They suggest that, because of strong associations between scallops and gravel-lag deposits, and because gravel lag regions had distinct backscatter intensities from contiguous sandy regions, the prediction of scallop stock can be made from multibeam backscatter data.

If strong associations exist between species and substrate and if backscatter strength indicates substrate composition, then a simple backscatter map could directly provide a basis for stock assessments. Unfortunately, strong associations are rare, and there are many complications that limit how well we can determine substrate type from multibeam backscatter and therefore the accuracy of predictions about biological resources is often hindered. What the acoustic data maps represent in terms of biological habitat depends upon what they represent in terms of physical habitat, and that in turn, depends upon many factors and complex interactions. Also, seafloor maps derived from acoustic data do not provide the complete description of the physical environment (i.e., all the important factors to biological resources). Even if the physical habitat attributes of the seafloor can be determined accurately from the acoustic data, anomalies are common. Known associations are generalizations, and there are many exceptions. Strong associations between organisms and substrates do exist, but not as commonly as weak and complex associations. However, the better the physical attributes can be described, the more likely that biological constituents might be predicted, and thus resource assessments improved.

1.2.1. Recent seafloor habitat mapping

Marine and estuarine benthic habitat mapping and classification has recently become a worldwide priority of ocean science. Maps derived from multibeam echosounders appear to provide the best basis for initial delineation of the seafloor into geological and geomorphological regions (Mayer et al., 1999; Todd et al., 1999). A physical habitat model developed from interpretation of those regions, with regards to substrate composition and water-column conditions, can be used to predict distributions of benthic species or communities using any organism–substrate interaction models, existing biological or fisheries data, or new sample data. Maps from multibeam and sidescan sonar data have been used for geological (Todd et al., 1999; Dartnell and Gardner, 2004), ecological (Kostylev et al, 2001) and fisheries (Friedlander et al., 1999; Kostylev et al., 2003) mapping, as well as habitat classification (Greene et al., 1999).

MBES bathymetry and backscatter maps have been used to delineate the seafloor into physical habitat regions and then assigned biological habitat classes based on sample imagery and biology samples (Kostylev et al., 2001). Thus, benthic habitat mapping has benefited from the areal coverage and high resolution capabilities of multibeam (Kostylev et al., 2001) and sidescan sonar systems. However, because of the complex interactions between seafloor composition, geometry, and acoustic reflection and backscatter (see Urick, 1983), multibeam and sidescan maps must be carefully ground-truthed to confirm sedimentological and biological predictions.

Seafloor habitat maps, such as those produced by Kostylev et al. (2001), rely on subjective expert interpretation of maps generated from multibeam bathymetry and backscatter data. Although manual interpretation is commonly used to delineate seafloor

habitats, the potential exists to use more objective automated or semi-automated segmentation of the seafloor using MBES or SSS data to interpret the seafloor in terms of benthic habitat. The notion that habitat can be automatically classified from acoustic data only applies to certain simple definitions of habitat given the present state of knowledge of acoustic-seafloor interactions. Even if a simple definition of habitat is used (e.g., sediment type), many assumptions are still required about how the acoustic data relate to seafloor properties. Habitat types are interpretation-based products from acoustic data. Some of the properties required to describe habitat, such as substrate type, can be inferred from the acoustic data, but with considerable potential for error. Ground-truth is still required to make the connection and essentially test the hypotheses about habitat type that we make from the automated or semi-automated classifications. Thus, what is produced from acoustic data is essentially a "hypothetical habitat map." Though, it might be argued that any map of seafloor characteristics constructed using interpolation is a hypothetical map.

Expert knowledge and interpretation are not only aspects of map interpretation in terms of habitat, but they are also components of habitat models (Brown et al., 2000; Banner and Hayes, 1996). Thus, habitat maps incorporate subjectivity and may not represent all important details. For instance, many habitat studies incorporate a restricted treatment of habitat attributes (salinity, temperature, depth, and substrate type), despite the fact that many other physical and biological interactions exist that complicate the relationships between organisms and habitat.

1.2.2. Habitat suitability indices (HSI)

Habitat suitability indices (HSI) have been created to summarize associations and affinities between habitat attributes and certain benthic megafauna and fish species (Banner and Hayes, 1996; Brown et al., 2000). If the degree of association between a species and habitat attributes can be determined, then the ability to predict biological resources and fisheries stocks from physical environmental data can be improved. HSI is a function of a few parameters that are scaled and quantized in order to quantify the strength of the affinity between a species and specific ranges of selected habitat attributes. In the scaled and quantized form, each parameter is considered a suitability index. HSI maps provide a spatial summary of a model combining all the individual suitability indices.

1.2.3. Habitat Fundamentals and Terminology

In much of the habitat-related literature, habitat usually connotes the spatial domain and physical setting providing resources and tolerable conditions supporting some aspect of an organism's life. This definition is generally consistent with Grinnell's (1917) usage of "niche" that expresses what is now generally considered physical habitat as well as environmental constraints affecting distributions of organisms. Hutchinson's (1958) sense of niche encompasses the ranges of conditions within which species survive and reproduce (Whittaker et al., 1973). A similarity exists between Hutchinson's concept and the requirements of what is deemed "essential fish habitat" (EFH) as designated by the Mangusun-Stevens Fisheries Conservation and Management Act of 1996. It can also be seen that maps of habitat suitability index (HSI) attempt to represent the fundamental niche of Hutchinson (1958) in terms of realistic, detectable, mappable environmental

parameters for which species life history attributes are known. It is also common to include biological modifiers (names of dominant species, or descriptions of biogenic features) for describing habitat types, but these can cause confusion because to some researchers habitat represents a physical entity whereas the term biotope is should be used if the description involves biological attributes.

Biotope may be distinguished from habitat in that biotope relates the presence and association of specific species or functional ecological group to a certain substrate type or condition. One of the prominent recent marine habitat classification schemes, BioMar (Picton and Costello, 1998), uses biotopes as its ultimate class unit. BioMar lists sublittoral sediments as a major habitat, and infralittoral muddy sands as a habitat complex; associated with that habitat (complex) are biotopes or biotope complexes. This terminology suggests that biotopes are refinements of habitat classes that include biological descriptors that are sometimes specific but are sometimes generalized. In the generalized case, the class unit is considered a biotope complex. For example, "shallow muddy sand faunal communities" describes a biotope complex, and "*Echinocardium cordatum* (heart urchin) and *Ensis* spp. (razor clams) in lower shore or shallow sublittoral muddy fine sand" describes a biotope (Picton and Costello, 1998). The hierarchical structure of that scheme is evident, and most recent classification schemes are similarly hierarchical (see Greene et al., 1999; Allee et al., 2000).

Whether or not the physical habitat is distinguished from biotope may not be of consequence because even biotope could be considered a generalization of biologically modified physical conditions for species that are not detected. The usage of habitat can encompass biotope (Bonsdorff et al., 1996; Kostylev et al., 2001) and may be understood

both ways. Standardization is being sought for habitat classification, so the terminology might converge. What are important are the physical and biological habitat attributes. The differences of opinion concerning relevant attributes and spatial scales are likely the source of the differences in terminology and approaches to classification.

1.2.4. Seafloor Habitat Attributes

As explained previously, habitats can be interpreted as spatial subsets of the physical environment as they pertain to an organism or group of organisms. To clarify the simplistic and overly general definitions of habitat, I reviewed published articles to see how researchers used seafloor habitat attributes in order to illustrate the concept of habitat. For example, habitat attribute descriptors in the literature include: salinity, temperature, depth, substrate, wave exposure, eelgrass, specific sediment classes (e.g., gravel, gravel over sand, muddy sand), hardbottom, sandy bottom, salt marsh, marsh edge, inner marsh, oyster reef, dissolved oxygen, cover and habitat complexity, and area. For synthesis, commonly used habitat attributes were summarized into a list of common attribute types (Table 1.1). Habitat classification schemes were not used to construct the attribute list. Note that not all of the attributes pertain to seafloor characteristics; rather some pertain to water-column conditions.

Levels of detail and generality of attributes often differ according to the focus of the habitat mapping effort and the spatial coverage. For example, compare the attributes used in some of the benthic ecological studies focused on macroinfauna (Bonsdorff et al., 1996) to those of habitat suitability index (HSI) and essential fish habitat (EFH) studies (Brown et al., 2000; Able, 1999). It is not that attribute details are not generally important, but typically that most attributes cannot be sensed in detail for the spatial

scales considered (sometimes because of the sampling devices used), or that knowledge does not exist concerning how those attribute details relate to a particular species. Detail is generally sacrificed for coverage and *vice versa*. In the case of habitat mapping, species size, motility and range determine the coverage necessary for complete mapping. For defining, modeling, or mapping habitats, expert knowledge and interpretation can be considered components of a habitat model (e.g., Brown et al., 2000).

Table 1.1. Summary list of common attributes used in published articles to describe seafloor habitat. Habitat classification schemes were not used to construct this list.

Habitat Attribute
Salinity
Temperature
Substrate (type, class, grain size)
Depth
Dissolved Oxygen
Nutrients
Hydrodynamic energy regime
Complexity
Associated fauna
Disturbance regime
Other factors to consider:
Global and regional setting (typically an unstated attribute)
Time
Sediment and particle load and transport

1.2.5. Seafloor Texture, Roughness, and Spatial Attributes

In addition to seafloor composition, the spatial distribution of seafloor features (landscape characteristics and patchiness) also influences benthic biology (Zajac et al., 2000; Guichard and Bourget, 1998) and can be considered as habitat complexity, a common habitat attribute (Table 1.1). In addition, the spatial scales of seafloor features

and environmental influences are important. Benthic species distributions, abundances and diversity are products of large and local spatial-scale processes (Menge and Olsen, 1990). Many benthic studies have detailed data concerning the local processes, but often lack detailed large spatial-scale process information, meaning that interpretations can lack regional context of the seafloor properties and processes. Zajac et al. (2000) showed that benthic community differences could be explained by regional differences in sediment grain-size class when considered at the spatial scale of Long Island Sound. When considered at sub-Sound scale, community differences could be attributed to local variations in seafloor properties. Spatial distribution and spatial scales of variability are important habitat characteristics, and both large and small spatial-scales are relevant. In addition, if differences in properties can be described, they likely correspond to variations in the benthic community. The scales of sampling and analysis are important. Hewitt et al. (1998) suggest that determining an appropriate sampling scale is not as important as sampling and modeling at multiple spatial scales. Larger spatial extent of samples allows larger spatial scale processes to be described, but only a certain amount of biological sampling is realizable because resources for sampling (funding, equipment, or time) are typically limited and, therefore , a compromise is made between sampling density and extent (Hewitt et al., 1998). The situation is analogous to the choice, mentioned previously, between detail and coverage.

Acoustic maps can help solve the sample-allocation problem. Shallow-water MBES bathymetry and backscatter data allow detection of seafloor properties at spatial scales ranging from decimeters to kilometers. MBES data can be used to describe spatial distributions and variability of apparent seafloor properties (such as facies or grain-size

class) over those scales. Maps of apparent facies distributions can facilitate sampling, analysis and interpretation of biological data at multiple spatial scales, making it possible to address some of the issues described by Menge and Olsen (1990), Zajac et al. (2000), and Hewitt et al. (1998). Detailed maps of the distribution and variation of seafloor morphology and composition, might provide the interpretive link between data collected for detailed benthic ecological work and habitat mapping efforts.

Because morphology can be used to interpret processes, morphological regions can be indicative of coherent physical environmental conditions; either consistent conditions or characteristic variation of conditions. For example, bedforms are generally indicative of steady unidirectional or oscillatory flow with velocity profiles inducing shear stresses within a certain range capable of mobilizing the sediment (by overcoming density, gravity, and friction). Bedform size and geometry for non-cohesive sediments depend primarily upon sediment grain-size distribution and flow or shear velocity. Ideally, bedforms composed of a narrow sediment grain size distribution can relate at least the relative strength of currents or size and period of waves (e.g., Allen, 1980). Even in a non-ideal case, there are two likely explanations for bedforms seen in MBES data: that the flow induced them or that they are relict features from a past process. One or the other explanation might be more reasonable based on the particular system. It may be possible to make inferences about the hydrodynamic regime given only detailed bathymetry and backscatter maps.

Even though it might not be possible to make inferences about specific conditions or hydrodynamic behavior, regions of similar seafloor morphology and composition suggest that similar processes have occurred in those regions. Therefore, if we can

identify and delineate seafloor regions with similar patterns of morphology and composition, then we have determined the spatial extents where the primary factors influencing benthic organisms are believed to be consistent or vary consistently. Seafloor morphological patterns can be identified manually by the investigator or automatically by using spectral, spatial, or textural analysis of seafloor backscatter or bathymetry.

Seafloor roughness can be quantified using spectral analyses (Fox and Hayes, 1985; Pace and Gao, 1988; Briggs, 1989; Fox, 1996). Spectral analysis has been applied to large spatial scale seafloor features (kilometer to tens of kilometers profiles from ocean ridges) (Fox and Hayes, 1985), and to microtopographic seafloor profiles representing millimeters to decimeters (Briggs, 1989; Lyons et al., 2002; Pouliquen and Lyons, 2002), and to sub-millimeter-resolution profiles from sediment profile images (Cutter, *Submitted*). Spectral analysis involves transforming data from a spatial (or temporal) to a frequency domain, and allows description of a range of spatial frequency components comprising seafloor elevation profiles. The power spectrum represents the variance contained in the frequency components comprising a function or signal. The amplitude spectrum is the square root of the power spectrum, or log of amplitude is half the log of power. Fox and Hayes (1985) and Fox (1996) used the amplitude spectrum, but the power spectrum has been applied more often. If periodic features such as bedforms exist on the seafloor, then the spectrum from a topographic profile taken perpendicular to crests will have a peak in the frequency band that represents the spatial frequency of the bedform periodicity (the wavelength). The Fox and Hayes (1985) model describes the spectral content of the seafloor elevation data in terms of a few parameters that can be used to discriminate seafloor regions based on roughness characteristics.

Two-dimensional spectra can be summarized by four parameters of the Fox (1996) model that represent 1) overall roughness, 2) strength of lineations or anisotropic roughness, 3) orientation of anisotropic components or lineation angle, and 4) amplitude variation with scale as represented by the slope of the spectrum. High values of the fourth parameter, b, suggest that roughness is dominated by large-spatial-scale roughness (low spatial-frequency) features, and low values of b suggest that roughness is dominated by small-spatial-scale roughness (high spatial-frequency) features. The parameter *b* is related to the fractal dimension in certain cases (Fox and Hayes, 1985). If the seafloor is isotropic, only two parameters are necessary to model the one or two-dimensional spectrum (Lyons et al., 2002). An alternative model for anisotropic seafloor roughness is provided by Lyons et al. (2002) where the power from periodic components is modeled using a Gaussian function centered on the wavenumber vector representing the average ripple wavelength and orientation.

Roughness is important to acoustic backscatter and spectral parameters are required to implement some of the widely used models that relate acoustic backscatter to seafloor properties (Jackson et al., 1986; APL-UW, 1994). However, it is difficult to reconcile and compare parameters from amplitude spectra as used by Fox and Hayes (1985) to parameters from studies using power spectra, such as Stanic et al. (1988), Briggs (1989), Lyons et al. (2002), Jackson et al. (1996), or Sternlicht and DeMoustier (2003).

1.2.6. Texture and Spatial-integration Scales

Typically, texture analysis has been applied to acoustic backscatter data. For instance, Huvenne et al. (2002) and Ojeda et al. (2004) used gray level correlation

matrices to segment backscatter data according to texture. High-resolution bathymetric data also have proven useful for texture analysis. Cutter et al. (2003) used a texture feature called local Fourier histogram (LFH) developed by Zhou et al. (2001) to segment bathymetry derived from shallow water MBES data.

Texture analysis generally involves texture features that describe a property, statistical distribution, or behavior occurring at a local spatial scale, but also depends upon the repetition of that property regionally. Many texture features require a certain, specified group of data points representing a spatial-integration scale. Often in the image analysis research field, block sizes (regions of pixels where the analysis is applied) are specified arbitrarily, with no real support for the choice of sizes. For example, researchers calculate their texture feature vector within N by N pixel blocks, where N can be 16, 32, 64, etc. The size of the block and N are sometimes chosen because test data (images) are composed of standard texture palettes (Brodatz textures) available as 512-by-512 pixel images and are easily divisible into squares with sides of lengths equal to powers of two.

An important issue is that the spatial-integration scale can control the form of the texture feature vector. A texture feature vector is basically a set of numerical values, each of which represents some statistical attribute or distribution of values from the texture feature analysis. If an integration scale is too small, then the texture feature might not be able to represent the texture pattern. If an integration scale is too large, then the texture feature might represent multiple textures. How to optimize spatial-integration scale, or at least how to avoid arbitrary decisions is undetermined.

1.2.7. Spatial Variation Characterization

Spatial variation of seafloor properties can be described, quantitatively modeled and perhaps classified using spatial analytical tools such as variograms (Herzfeld, 1993). The variogram is the variance of increments for a random variable

$$2\gamma(\vec{h}) = Var[Z(\vec{s}+\vec{h}) - Z(\vec{s})]$$

or

$$2\gamma(\vec{h}) = E[Z(\vec{s}+\vec{h}) - Z(\vec{s})]^2$$

(Robert and Richards, 1988). In practice, the empirical variogram is often estimated as

$$2\gamma(\vec{h}) = \frac{1}{n(h)} \sum_{all\_h} \{Z(\vec{s}+\vec{h}) - Z(\vec{s})\}^2$$

where **s** is the spatial location vector (x,y) in two dimensions, **h** is the lag distance and orientation vector, n(h) is the number of pairs of observations at lag distance h, and Z is a random variable or real-valued stochastic process (Cressie, 1989; Stein, 1999). Technically, the variogram is two times the semivariogram $\gamma(\mathbf{h})$, but the term variogram and semivariogram are commonly used interchangeably. Variograms represent spatial covariation in terms of the change of variance with the distance between samples. In the case where a process is second-order stationary such that the mean is constant and the covariance varies only with distance and not position (Cressie, 1989), then the semivariogram is related to the autocorrelation ρ(h) as

$$\gamma(\vec{h}) = C(0)[1 - \rho(h)]$$

where C(0) is the variance. The variogram describes variance according to separation distance, and at some separation distance the variogram value reaches the overall variance. That distance is considered the range or effective range of the variogram and

the value where the variogram approaches the overall variance is known as the sill. The shape of the variogram and the rate of increase describe how smoothly or abruptly and the rate that the overall variance is approached. Herzfeld (1993) used those properties to demonstrate that variogram properties could be used to distinguish and classify sediment ponds, abyssal hills, and some complex terrains. Models are often fit to empirical variograms, allowing spatial modeling and interpolation such as kriging, but model parameters can be useful for classification of MBES data as shown by Herzfeld (1993).

1.2.8. Ground truth imagery

Remotely deployed still-camera imagery can be used to ground truth MBES or SSS maps, and the area represented by the image sample generally is very small relative to the scale of features present in the acoustic data set. Acquiring video/photos at greater heights above the seafloor because greater camera-target distance produces a larger imaged area. Underwater optical imagery, however, is limited by water-column conditions, owing primarily to attenuation of light by suspended particles. Light-attenuation is most pronounced in coastal waters, but applicable throughout the oceans. Even when particle concentrations are low, light attenuation through clear seawater limits the distance, and therefore the area, that can be reliably imaged. In the deep sea where benthic boundary layer turbidity can be low, the limitation is the intensity of artificial light sources and camera receptors.

Video imagery can be used to provide continuous image data along large distances, although quantitative analysis can be difficult or tedious. Mosaics can be constructed from video image sequences to convert the many individual video frames to a

single still image representing the entire imaged tract. Mosaic images can be generated from underwater video footage of the seafloor collected by a diver or by towed camera using a featureless coregistration technique involving frequency-domain processing of images to automatically solve for affine motion parameters, translation, rotation and zoom (Rzhanov et al., 2000). Each frame gets coregistered to the previous frame and its magnification is adjusted to the previous zoom level. Using this approach the mosaic has a uniform distance scale throughout (unless errors accumulate).

Mosaics representing tens of meters or more of seafloor have been constructed and allow detection, identification, and measurement of large epifauna, large bioturbational features, substrate transitions, and seafloor attributes important to acoustics at spatial scales inherent to standard MBES and SSS deployments. Mosaic construction does not necessarily require positioning data, although positioning data are necessary for placement of the mosaics within geospatial maps and for interpretation with respect to sonar data maps.

1.2.9. Background Summary

It is clear that acoustic data from multibeam echosounders and sidescan sonars are indicative of physical habitat attributes, and only rarely will directly provide biological attributes. Some exceptions to that are when large organisms with distinctive acoustic response are present (e.g., kelp forests, dense seagrass beds, schools of fish). Generally, however, MBES and SSS are used to acquire seafloor elevation and backscatter intensity data. Acoustic backscatter intensity can be related to substrate composition, and seafloor elevation patterns relate to morphology that can indicate formation processes. However, many interactions complicate those relationships. It is my intent to explore some of those

complications and consider how we can interpret seafloor acoustic data in terms of biological habitat.

1.3. Overview of Data and Methods

The primary data set used for this research are MBES bathymetry and backscatter data from the Portsmouth Harbor Common Dataset (Mayer and Baldwin, 2001), collected in the mouth of the Piscataqua River Estuary mouth to construct seafloor maps that relate morphology to composition. Specifically, bathymetry data were collected with Reson Seabat 8125 and Reson Seabat 8101 multibeam echosounder systems. Backscatter data originated from a Kongsberg-Simrad EM3000D multibeam echosounder, and a Klein 5500 sidescan sonar.

Delineation and classification of these data sets were done separately and results were compared to an existing substrate map and data (Ward, 1995). Existing substrate data (Ward, 1995) were used to provide initial hypothetical "physical habitat models" (PHM) and "hypothetical habitat maps" (HHM). The PHMs and existing water-column data (temperature, salinity) were used to generate habitat suitability index (HSI) maps for selected species. A hypothetical biological habitat map was generated to predict how the dominant infaunal communities were distributed.

Ground-truth data include remote and diver-deployed video and still cameras and direct substrate and infaunal samples, to test the validity of the hypothetical PHM, HSI and the predicted faunal maps. Specific attention was made to regions where the seafloor morphology and backscatter maps differed because those regions might indicate transitions in composition and processes. Remote and diver-deployed imagery were used

to assess habitat-specific faunal occurrences and densities, for selected detectable species and biogenic features.

1.3.1. Data Sources

The work described in this thesis includes the following data: bathymetry, backscatter, optical imagery, and substrate and biological samples. The primary sources of data are listed below.

1.3.2. Bathymetry data

Bathymetry data consists of portions of two of the multibeam echosounder surveys from the Portsmouth Harbor Common Dataset (Mayer and Baldwin, 2001): the Reson 8101 dataset and the Reson 8125 dataset.

The Reson SeaBat 8125 multibeam echosounder data were collected by Science Applications International Corporation (SAIC) aboard the UNH vessel R/V *Coastal Surveyor*, in July, 2001. The 8125 operates at a frequency of 455 kHz, has a 120 degree swath width, and uses focused beamforming to achieve 240 beams with across-track beamwidths of 0.5 degrees and along-track beamwidth of 1 degree (Reson, unpub. 1). Depth resolution is stated to be 6 mm; swath coverage for the 8125 ranges from 3.5 to 1.7 times water depth in depths of 15 to 90 m (Reson, 2002). Position, heading, and attitude information for the 8125 survey was measured using an Applanix POS MV 320 (Positioning and Orientation System for Marine Vessels) inertial motion unit. Data were "cleaned" (selection and removal of data artifacts and false-bottom soundings) according to hydrographic processing standards and the data were gridded at various scales using CARIS HIPS (Hydrographic Information Processing System software, Universal Systems, Fredericton, New Brunswick, Canada).

The Reson 8101 data were collected by the National Oceanic and Atmospheric Administration (NOAA) from launches deployed from the NOAA ship *Whiting*, in November, 2000. The Reson 8101 operates at 240 kHz, has a 150 degree swath width and forms 101 beams with beamwidths of 1.5 degrees, and has a range resolution of 1.25 cm (Reson, unpub.2). Position, heading, and attitude for the Reson 8101 survey were measured using an Applanix POS MV 320. Data from a doppler speed log and a surface sound-velocimeter were logged to determine sound propagation speed. CTD (Seacat) casts were taken from a separate boat at four sites, with a cast at each site every two hours. Reson 8101 data were "cleaned" according to hydrographic processing standards and the data were gridded using CARIS HIPS software.

1.3.3. Acoustic backscatter data

Backscatter data from a Simrad EM3000 multibeam echosounder and a Klein 5500 sidescan sonar were also used. The Simrad EM3000 data were collected by Simrad aboard the UNH vessel R/V *Coastal Surveyor*, in June, 2000. The Simrad EM3000 operates at a frequency of 300 KHz and forms 127 beams with dimensions of 1.5 by 1.5 degrees. Spacing between beams is 0.9 degrees, generating overlapping beams.

The Klein 5500 "multibeam sidescan" sonar survey was conducted by NOAA from launches deployed from the NOAA ship *Whiting*. The Klein 5500 towfish was mounted directly to the hull of a survey launch-vessel. The Klein 5500 operates at a frequency of 455 kHz, and uses 5 steered and focused beams per side (Klein Associates, Inc., 2003).

1.3.4. Seafloor video imagery data

Underwater video cameras were deployed by divers and remotely from vessels to collect optical seafloor imagery. Two underwater video cameras were used. One video camera was a Sony TRV-310 digital handycam with an underwater housing. Illumination sources for the TRV-310 included ambient lighting, an LED array, and a 100-W halogen lamp. The TRV-310 was deployed by divers as well as attached to a frame and deployed from the vessel to act as a drift camera. The ability to determine the position of diver-deployed video was limited to time synchronization with a vessel positioning system clock and required that the diver be in a known position relative to the vessel. That method was not very reliable and resulted in high uncertainty of diver-deployed camera position. Using the video camera attached to a frame and lowered by line or cable from the vessel during slow drift provides for higher positioning accuracy. The camera in the vessel-drift mode is deployed vertically below the vessel and the offsets to the GPS antenna(s) were measured. The primary positional uncertainty relates to the scope of the line to the camera.

The second video camera was a Deep Sea Power and Light (DSPL) model 2050 video camera. This camera was used as part of a large, frame-based system (Hubbard Camera) with remote power supply and with the capability to transmit the video to the vessel. The lighting for the Hubbard Camera system consists of two video-synchronized strobe lights that are capable of reducing motion effects. The limitations of the Hubbard Camera system are the requirement of a relatively large vessel and the need for operational personnel. The benefits include better positioning than for a diver-deployed camera as well as the potential to eliminate motion artifacts from the imagery.

Positioning for the Hubbard camera has a level of uncertainty similar to the drift camera deployment, but the Hubbard camera can be deployed at higher speeds, thereby covering more seafloor.

The DSPL camera also can be deployed on a small towfish (Sea Sciences) that was modified with runners for use as a sled in case bottom-contact occurred. However, the lighting for the camera on the towfish is a limiting factor because of the height at which the towfish passed above the bottom. The DSPL video quality is mediocre and the CCD sensor tended to be oversensitive to blue wavelengths until factory adjustment. The positioning of the towfish was also problematic and generally even less reliable than diver positioning.

1.3.5. Substrate and biology sample data

Sediments were collected using either a box corer or a Shipek grab sampler. The box corer has a 25-by-25 cm (0.0625 m^2) box. The Shipek grab sampler has a scoop 10.2 cm deep, 19.8 cm wide, and 19.8 cm long, and a capacity of 3 L. Several diver cores (10 cm diameter Plexiglas tube) were collected to sample specific substrates or fauna.

Information on faunal occurrence, density, and identification were obtained using the video imagery data.

1.3.6. A note on positioning data

Uncertainty of positions for ground-truth samples or imagery affect the georeferencing of the data. Ground-truth samples or imagery collected by devices not rigidly mounted to the vessel and not fixed in relation to the position of the GPS antenna are subject to positional uncertainty. If ground-truth data cannot be properly

georeferenced, then their worth may be diminished. Georeferencing errors are particularly acute when ground truthing shallow-water multibeam data because of the high spatial resolution achievable. Shallow-water multibeam systems can resolve decimeter-scale features; features that may be relevant to individual organisms. Uncertainty in positioning of the ground-truth data can lead to inaccurate assessment of the seafloor in terms of biological habitat or geological attributes. Image mosaicing techniques may help overcome positioning errors of cameras by determining the actual motion of the camera along a track. However, unless objects with known positions are imaged, there will still be uncertainty associated with the absolute position of the track.

1.4. References for Chapter 1

Allee R. J., Dethier, M., Brown, D., Deegan, L. Ford, R. G., Hourigan, T. F., Maragos, J., Schoch, C., Sealey, K., Twilley, R., Weinstein, M. P., Yoklavich, M. 2000. U.S. Marine and estuarine ecosystem and habitat classification system. NOAA Tech. Memo. NMFS-F/SPO-43, July 2000.

Allen, J. R. L., 1980. Sand waves: a model of origin and internal structure. Sedimentary Geology, 26, 281-328.

APL-UW, 1994. APL-UW high-frequency ocean environmetal acoustic models handbook. Applied Physics Laboratory, University of Washington, Seattle, Washington. Technical Report APL-UW TR 9407, AEAS 9501, October, 1994.

Banner, A., Hayes, G., 1996. Identification of importants habitats in coastal New Hampshire. U.S. Fish and Wildlife Service, Gulf of Maine Project, Internet Report, Falmouth, Maine (http://rossby.unh.edu/edims/banner/gbay/gbay.htm#toc).

Bonsdorff, E., Diaz, R.J., Rosenberg, R. Norkko, A., and Cutter Jr., G.R., 1996. Characterization of soft-bottom benthic habitats of the Åland islands, northern Baltic Sea. Marine Ecol. Prog. Ser., 142, 235-245.

Briggs, K. B., 1989. Microtopographical roughness of shallow-water continental shelves. IEEE J. of Oceanic Engineering, 14 (4), 360-367.

Brown, S. K., Buja, K. R., Jury, S. H., Monaco, M. E., Banner, A. 2000. Habitat suitability index models for eight fish and invertebrate species in Casco and Sheepscot Bays, Maine. North American J. of Fisheries Management, 20, 408-435.

Cressie, N., 1989. Geostatistics. The American Statistician, 43 (4), 197-202.

Cutter, G. R., Rzhanov, Y., Mayer, L. A., 2003. Automated segmentation of seafloor bathymetry from multibeam echosounder data using local Fourier histogram texture features. Journal of Experimental Marine Biology and Ecology, 285/286, 355-370.

Cutter Jr., G. R., Rzhanov, Y., Mayer, L. A. and Grizzle, R. E., In Press. Ground Truthing Benthic Habitat Characteristics Using Video Mosaic Images. *In* Barnes, P. W., Thomas, J. P., (Eds.) Benthic habitats and the effects of fishing. American Fisheries Society, Symposium 41, Bethesda, Maryland.

Cutter, Jr., G. R., *Submitted*. Seafloor roughness spectra from sediment profile images. Submitted, Dec. 2004, to Journal of Marine Systems.

Dartnell, P., Gardner, J. V., 2004. Predicting seafloor facies from multibeam bathymetry and backscatter data. Photogrammetric Engineering and Remote Sensing, 70 (9), 1081-1091.

Fox, C.G., Hayes, D.E. 1985. Quantitative methods for analyzing the roughness of the seafloor, Reviews of Geophysics, 23 (1), 1-48.

Fox, C.G., 1996. Objective classification of oceanic ridge-crest terrains using two-dimensional spectral models of bathymetry: application to the Juan de Fuca Ridge. Marine Geophysical Researches, 18, 707-728.

Friedlander, A. M., Boehlert, G. W., Field, M. E., Mason, J. E., Gardner, J. V., Dartnell, P, 1999. Sidescan-sonar mapping of benthic trawl marks on the shelf and slope off Eureka, California. Fishery Bulletin, 97 (4), 786-801.

Greene, H. G., Yoklavich, M. M., Starr, R. M., O'Connell, V. M., Wakefield, W. W., Sullivan, D. E., McRea, Jr., J. E., Cailliet, G. M., 1999. A classification scheme for deep seafloor habitats. Oceanologica Acta, 22, 663-678.

Grinnell, J., 1917. The niche-relationships of the California thrasher. Auk, 34, 427-433.

Guichard, F., Bourget, E. 1998. Topographic heterogeneity, hydrodynamics, and benthic community structure: a scale-dependent cascade. Marine Ecology Progress Series, 171, 59-70.

Herzfeld, U. C. 1993. A method for seafloor classification using directional variograms, demonstrated for data from the western flank of the Mid-Atlantic Ridge. Mathematical Geology, 25 (7), 901-924.

Hewitt, J. E., Thrush, S. F., Cummings, V. J., Turner, S. J., 1998. The effect of changing sampling scales on our ability to detect effects of large-scale processes on communities. J. of Experimental Marine Biology and Ecology, 227, 251-264.

Hutchinson, G. E. 1958. Concluding remarks. Cold Spring Harbor Symposia on Quantitative Biology. 22: 415-427.

Huvenne, V. A. I., Blondel, Ph., Henriet, J.-P., 2002. Textural analyses of sidescan sonar imagery from two mound provinces in the Porcupine Seabight. Marine Geology, 189, 323-341.

Jackson, D. R., Winebrenner, D. P., Ishimaru, A., 1986. Application of the composite roughness model to high-frequency bottom backscattering. J. Acoust. Soc. Am., 79 (5), 1410-1422.

Jackson, D. R., Briggs, K. B., Williams, K. L., Richardson, M. D., 1996. Tests of models for high-frequency seafloor backscatter. IEEE Journal of Oceanic Engineering, 21 (4), 458-470.

Klein Associates, Inc., 2003. http://www.kleinsonar.com/5000series/5000series.html.

Kostylev, V. E., Todd, B. J., Fader, G. B., Courtney, R. C., Cameron, G. D., Pickrill, R. A., 2001. Benthic habitat mapping on the Scotian Shelf based on multibeam bathymetry, surficial geology and sea floor photographs. Marine Ecology Progress Series, 219, 121-137.

Kostylev, V.E., Courtney, R.C., Robert, G., and Todd, B.J. 2003. Stock evaluation of giant scallop (Placopecten magellanicus) using high-resolution acoustics. Fisheries Research, 60, 479-492.

Lyons, A. P., Fox, W. L. J., Hasiotis, T., Pouliquen, E., 2002. Characterization of the two-dimensional roughness of wave-rippled sea floors using digital photogrammetry. IEEE J. of Oceanic Engr., 27 (3), 515-524.

Mayer, L. A., Hughes-Clarke, J., Dijkstra, S., 1999. Multibeam sonar: potential applications for fisheries research. Journal of Shellfish Research, 17, 1463-1467.

Mayer, L., Baldwin, K., 2001. Shallow water survey 2001: papers based on selected presentations from the second international conference on high resolution surveys in shallow water. Marine Technology Society Journal 35, 3– 4.

Menge, B. A., Olson, A. M. 1990. Role of scale and environmental factors in regulation of community structure. TREE, 5 (2), 52-57.

Ojeda, G. Y., Gayes, P. T., Van Dolah, R. F., Schwab, W. C., 2004. Spatially quantitative seafloor habitat mapping: example from the northern South Carolina inner continental shelf. Estuarine, Coastal, and Shelf Science, 59, 399-416.

Pace, N. G., Gao, H., 1988. Swathe seabed classification. IEEE J. of Oceanic Engineering, 13 (2), 82-90.

Picton, B.E. and Costello M. J. 1998. The BioMar biotope viewer: a guide to marine habitats, fauna and flora in Britain and Ireland. http://www.itsligo.ie/biomar/BIOTOPE.HTM. Environmental Sciences Unit, Trinity College, Dublin.

Pouliquen, E., Lyons, A. P., 2002. Backscattering from bioturbated sediments at very high frequency. IEEE Journal of Oceanic Engineerring, 27 (3), 388-402.

Reson, Unpublished 1. Reson SeaBat 8125 product specification.

Reson, Unpublished 2. Reson SeaBat 8101 product specification.

Reson, 2002. Reson multibeam sonars. PAIGH Workshop. Taller de multibeam y procesamiento de alto volumen de datos. 18-22 Mar. 2002.

Robert, A., Richards, K. S., 1988. On the modelling of sand bedforms using the semivariogram. Earth Surface Processes and Landforms, 13, 459-473.

Rzhanov, Y. L. Linnett, R. Forbes, 2000. Underwater video mosaicing for seabed mapping. Proceedings of the 2000 IEEE International Conference on Image Processing, 10-13 September, 2000, Vancouver, Canada, pp. 224-227.

Stanic, S., Briggs, K. B., Fleischer, P., Ray, R. I., Sawyer, W., 1988. Shallow-water high-frequency bottom scattering off Panama City, Florida. J. Acoust. Soc. Am., 83 (6), 2134-2144.

Stein, M. L., 1999. Interpolation of spatial data: some theory for kriging. Springer-Verlag, New York, 247 pp.

Sternlicht, D. D., de Moustier, C. P., 2003. Time-dependent seafloor acoustic backscatter (10-100 kHz). J. Acoust. Soc. Am. 114 (5), 2709-2725.

Todd, Brian J; Fader, Gordon B J; Courtney, Robert C; Pickrill, Richard A., 1999. Quaternary geology and surficial sediment processes; Browns Bank, Scotian Shelf; based on multibeam bathymetry. Marine Geology, 162, no.1, 165-214.

Urick, R. J., 1983. Principles of underwater sound for engineers. McGraw-Hill, New York, 342 pp.

Ward, L. G., 1995. Sedimentology of the lower Great Bay/Piscataqua River Estuary. San Diego, CA: Department of the Navy, NCCOSC RDTE Division Report, 102 pp.

Whittaker, R. H., S. A. Levin, and R. B. Root. 1973. Niche, habitat, and ecotope. Amer. Naturalist, 107, 321-338.

Zajac, R. N., Lewis, R. S., Poppe, L. J., Twichell, D. C., Vozarik, J., DiGiacomo-Cohen, M. L., 2000. Relationships among sea-floor structure and benthic communities in Long Island Sound at regional and benthoscape scales. Journal of Coastal Research, 16 (3), 627-640.

Zhou, F., Feng, J., Shi, Q. 2001. Texture feature based on local Fourier transform. ICIP 2001 conference proceedings, pp. 610-613.

CHAPTER 2

2. SEAFLOOR SEGMENTATION USING TEXTURE

2.1. Citation

Published in Journal of Experimental Marine Biology and Ecology, volumes 285/286, pages 355-370.

Citation:

Cutter, G. R., Rzhanov, Y., Mayer, L. A., 2003. Automated segmentation of seafloor bathymetry from multibeam echosounder data using local Fourier histogram texture features. Journal of Experimental Marine Biology and Ecology, 285/286, 355-370.

2.2. Abstract

Patterns of seafloor topography represent regions of geomorphological feature types and the physiography governing the spatial distributions of benthic habitats. Topographic variability can be considered seafloor texture and can be remotely sensed by acoustic and optical devices. Benthic habitat delineations often involve distinctions based on seafloor morphology and composition derived from acoustic data maps that are ground-truthed by optical imaging tools. Habitat delineations can be done manually, although automation of the procedure could provide more objectivity and reproducible map products. Recently, a technique using Fourier transforms to produce texture features called local Fourier histograms (LFH) has been used successfully to classify standard

textures in grayscale images and automatically retrieve digital images from archives according to texture content (Zhou et al., 2001). A modified form of that approach implemented by varying the spatial scales at which local Fourier histograms were calculated. A modified LFH texture feature classification technique was applied to multibeam echosounder (MBES) data from Piscataqua River, New Hampshire, USA, for automatic delineation of a seafloor topographic map into regions of distinct geomorphology and apparent benthic habitats. Automated segmentations were done by the LFH method on one-meter gridded MBES data, applying the local Fourier transform, used to generate the LFH, at spatial scales from one to five meters. Seven seafloor texture classes were identified, corresponding to the primary substrate types and configurations in the study area as well as some previously unidentified regions and transitional zones. The texture regions serve as a physical habitat model for the seafloor, a basis for predicting benthic faunal inhabitants, their areal distributions, and serving as sampling strata for ground truthing efforts.

2.3. Introduction

Topographic variability of the seafloor influences benthic community structure and ecological processes at many spatial scales (Bourget et al., 1994; Cusson and Bourget, 1997; Guichard and Bourget, 1998; Menge and Olson, 1990; Zajac, 2001). Traditionally, topographic variability has been described based on maps constructed from acoustic (echosounder or sidescan sonar) data, whereas biogenic features have been described using optical data from still or motion imaging devices. The overriding result is a mismatch of spatial scales between data, measurements, and interpretation of seafloor

properties. Recent developments in multibeam echosounding (MBES) however, have resulted in detailed acoustic surveys that provide an unprecedented view of the seafloor at a broad range of spatial scales. Using MBES data, digital elevation models (DEM) or digital terrain maps (DTM), which are two-dimensional rasterized data representing elevation of the seafloor or depth, are produced that depict nearly continuous-coverage depth measurements of the seafloor and reveal distinguishable texture patterns that represent topographic variation patterns, or geomorphological regions. In shallow water (tens of meters deep) features with vertical dimensions of centimeters and horizontal dimensions of decimeters to meters can generally be distinguished, such that habitat and microhabitat characteristics are easily discriminated.

Benthic habitat delineation has recently become a worldwide priority for ocean science, and MBES seafloor maps appear to provide the best basis for initial delineation of the seafloor into geological and geomorphological regions (Mayer et al., 1999; Todd et al., 1999; Kostylev et al., 2001) . In turn, a physical habitat model developed by interpretation of those regions can be used to model distributions of benthic biological resources using any available biological or fisheries data, organism-substrate interaction models, or direct sampling. Recent studies have utilized MBES and acoustic backscatter data to provide geological (Todd et al., 1999) and biological habitat (Kostylev et al., 2001) maps, but their delineations were done manually. Manual segmentation (by visual appearance) and delineation are inherently subjective and therefore can be inaccurate. Simple approaches to automated segmentation based on first-order statistics of topographic data may be sufficient in some cases, but often fail to distinguish areas with different biogeological processes, morphology or composition. Thus, there exists a need

for a robust, automated delineation approach that is accurate, unbiased, and fast, especially for datasets that can contain billions of measurements.

One possible approach to automating the delineation of seafloor regions involves texture analysis of MBES-derived DTM's representing seafloor topography data. Some common texture analysis techniques include grayscale co-occurrence matrices and Gabor functions (Ware, 2000; Zhou et al., 2001). In particular, Gabor filters are based on models of human vision perception of texture; thus Gabor functions can be used to detect and segment grayscale image textures in a manner similar to that of the human visual system (Ware, 2000). However, human perception is biased, and digital terrain models of the seafloor can incorporate differences due to data projections or non-standard exaggerations incorporated for visual effect, thus reinforcing the need for a more objective methodology, less dependent on human perception.

One approach that was recently developed for texture feature construction uses local Fourier transforms (FT) to accurately describe the local spatial distribution of values (Zhou et al., 2001). It has been shown that this technique provides a reliable means of classification of grayscale texture images (Brodatz textures) as well as automatic retrieval of images from digital archives according to texture content. The texture features produced by the local FT technique, called local Fourier histograms (LFH), performed as well or better than grayscale co-occurrence matrix features for automatic classification of 13 Brodatz textures. In addition, Zhou et al. (2001) demonstrated that LFH texture features performed similarly to Gabor features for automated retrieval of Brodatz texture images, such that the average overall recognition ratio for 108 Brodatz textures was 70.56% for LFH and 69.63% for Gabor features. A technique incorporating texture

features similar to LFH, but denoted local spectral histograms (LSH), was recently developed by Liu et al. (2001) that might be more flexible, but also more subjective, in that it involves user choice of a set of filtering operations prior to generating the texture features.

We have applied the LFH texture features for automated classification and segmentation of the seafloor. A modified form of the LFH texture feature classification technique was implemented by varying the spatial scales used to calculate the local Fourier transforms. The technique was applied to multibeam echosounder data for automatic segmentation of a seafloor elevation map into regions of distinct geomorphology and apparent benthic habitats. The accuracy of segmentation results were verified using historical sediment sample data and sediment maps (Ward, 1995), as well as underwater video imagery and diver observations.

2.4. Study Area

The study area is located in the mouth of the Piscataqua River, a well-mixed estuary (Swift et al., 1996) flowing between New Hampshire and Maine, USA (Figure 2.1) and exchanging water with the Gulf of Maine. The freshwater supply to the Piscataqua River originates in a watershed in southeast New Hampshire and Maine and includes six tributaries, three of which flow first into Great Bay, although each of the tributaries are dammed at some point. The total watershed area is 2334 km^2. The channel in the river mouth is oriented north-south, then abruptly turns to near due west at Fort Point, NH. The Piscataqua is a tidally dominated system, with tidal amplitudes (half of the tidal range) of 1.3 m near the study area (Swift and Brown, 1983). Average

total discharges for all the tributaries combined is about 32 $m^3 s^{-1}$ (Short, 1992). Maximum average cross-section and time-averaged current speeds near the study area are 0.5 m s^{-1} (spring) and 0.4 m s^{-1} (neap) (Swift et al., 1996). However in narrower parts of the river upstream, current speeds can reach 2.2 m s^{-1} (Swift and Brown, 1983) to 3.1 m s^{-1} (Short, 1992).

Primary substrates in the Piscataqua River-mouth study area were previously mapped by sample data from sediment cores (Ward, 1995) and consist of intertidal and subtidal bedrock, gravelly channel sediments, and a sandy sediment region near the center of the channel. The sandy central channel region was recently determined from the MBES data and by diver and video observations to be a rippled sand wave field, consisting of 5-m to 10-m wavelength, 0.5-m to 1-m height sand waves composed of fine to medium sand and fine shell hash.

2.5. Methods

2.5.1. Dataset

The dataset used for developing an automated segmentation procedure was a one-meter gridded surface representing the bathymetry in the mouth of the Piscataqua River, New Hampshire, USA (Figure 2.2). The gridded bathymetry was constructed using data collected with a Reson 8125 multibeam echosounder aboard the R/V *Coastal Surveyor* (UNH) by Science Applications International Corporation (SAIC) as part of the Shallow Water Survey 2001 Common Dataset (see Mayer and Baldwin, 2001). Positioning was accomplished using an Applanix POS MV 320 (Positioning and Orientation System for Marine Vessels). Data were cleaned according to hydrographic standards and the grid

was constructed using HIPS (Hydrographic Information Processing System, copyright CARIS, New Brunswick, Canada); data are presented on a Universal Transverse Mercator (UTM) projection, zone 19 north. The dataset covered 839 by 2034 meters, with the center of the lower left corner grid cell originating at UTM Northing 4768915 m, Easting 360918 m (latitude 43.0602° North, longitude 70.707° West).

2.5.2. LFH texture features

I use a modified implementation of the local Fourier histogram (LFH) texture analysis and discrimination technique described by Zhou et al. (2001). The processing procedure involved calculating a local FT for every data point (grid cell, pixel or node). The Fourier coefficients characterize the spatial frequencies present in the signal, i.e. the signal's roughness. Zhou et al. (2001) describe texture features by considering only the immediate vicinity of a node in two-dimensional rasterized data. On a square grid, such as in grayscale images and DTMs, that vicinity consists of eight nearest neighbors, enumerated consecutively to form a one-dimensional signal. Fourier coefficients of this signal reflect local isotropic roughness of the area around the node.

Eight Fourier coefficients from the eight-element, one-dimensional signal may be interpreted as four magnitude and four phase values. Only magnitudes are used for the LFH texture features. The LFH texture features require spatial-integration over a group of nodes (grid cells). For all nodes in a square block 10 by 10 meters (block sizes of 5 by 5 m and 20 by 20 m were also tested), the Fourier coefficients are calculated, then accumulated into histograms. A histogram, with eight bins each, is generated for each magnitude coefficient. Thus, the block of nodes is described by a LFH texture feature vector with 32 elements formed by concatenating the individual histograms (LFH feature

vector elements 0, 1, ... 7 contain the histogram for the 0^{th}-magnitude coefficients, elements 8 through 15 contain the histogram for the 1^{st}-magnitude coefficient, etc.). In addition, the average depth value from the block was removed from coefficient 0 value (also known as the direct current or DC value, and representing the mean value of the series) prior to constructing the histograms in order to eliminate artifacts related to mean depth effects.

My implementation allows for varying radii at which the local FT was applied and the block-size used to accumulate the LFHs. The modification to Zhou et al. (2001) was to calculate the Fourier coefficients at not only the nearest neighbor data, but also data from a larger neighborhood, combined in a manner (depth averaged for eight $\pi/4$ radian angular sectors within a specified radial distance about each node) that maintained the same format input signal to the FT (eight-element, one-dimensional signal). LFH texture features from the expanded neighborhood describe texture at broader scales. An alternative method for examining multiple spatial scale texture using LFH would be to use only the eight-nearest-neighbor data, but to apply the LFH to data gridded at various scales.

2.5.3. Class grouping

Classes were constructed using fuzzy k-means cluster analysis (Minasny and McBratney, 2000). Seven cluster group classes were chosen after examination of results from 4 to 10 classes showed either lack of separation of primary sedimentary regions of Ward (1995) when too few classes were chosen, or excessive patchiness when too many classes were chosen. The number of classes chosen was meant to provide correspondence between substrate types for which prior knowledge existed (in the study

area, there were four) and additional configurations and transitional zones evident from visual inspection of the DTM. Table 2.1 summarizes the classes and areal coverages and provides general descriptions of the bottom types. In order to provide some assessment of what the texture classes represent in terms of composition, beyond the geomorphological properties apparent from visual interpretation of the acoustic data (sand waves and rock), the LFH map was compared to an existing substrate map and data from substrate point-samples (Ward, 1995).

2.5.4. Representative LFH texture features

After cluster analysis classification, representative LFH texture features were constructed using all LFHs from each class. Initial representative LFH texture features included data from all classes, even those determined to be misclassifications. Final LFH representative texture features were constructed using only data from classes determined to represent distinct regions by comparisons with Ward (1995) samples and visual interpretation of the terrain model, so that LFHs from apparent misclassifications were not used in construction of the representative LFHs. The representative LFH texture feature vector was meant to represent only the clear cases where textures clearly corresponded to particular substrate configurations.

2.6. Results

The LFH texture feature segmentations of the seafloor corresponded well with the various geomorphological and sedimentary regions mapped by Ward (1995) in the study area, allowing sedimentary classes to be assigned to the regions. LFH classification

results were robust, generating similar results across several spatial scales of application (Figure 2.3). Seven cluster classes were chosen as best representing the variety of apparent geomorphological features in the study area. Fewer classes led to clearly different morphologies being assigned membership to the same group and classified as the same, whereas more classes led to subdivisions and excessive patchiness.

Application of LFH to grid-cell nearest neighbors (radius = 1 m) corresponded directly to the procedure described by Zhou et al. (2001). The resultant map showed several regions with mixed texture classes. Because more uniform regionalization was sought, the neighborhood scales were increased. Results for radii of 1, 3, and 5-m are shown in Figure 2.3 a-c. With increasing neighborhood scale (radius), more uniform regions were produced, at the expense of potentially missing small patches of unique texture class. Using a radius of 1-m, i.e. just the eight nearest neighbors, many texture feature blocks were considered to be misclassifications because they were located in a homogeneous region of the DTM (particularly obvious in the sand wave field) (Figure 2.3a). Increase of the scale to a radius of 3 m resulted in more consistent regions. The best balance between regional consistency and oversimplification was produced using a radius of 5-m for these data at this grid size. The LFH map produced using a 5-m radius was filtered to generate more coherent regions by adopting the majority value from 30-by-30-m blocks as the new cell value (Figure 2.3). These regions also suggest sampling strata for ancillary data collection, and produced a simple map for comparison with the DTM and analysis within geographic information systems.

Relating the LFH texture feature classes to sediments by comparison to point sediment sample data and sediment maps (Ward, 1995) showed that LFH class 4

corresponded to the large sand field. LFH class 5 corresponded to subtidal and intertidal bedrock. Samples by Ward (1995) in the LFH class 5 regions revealed only sandy gravel and muddy gravelly sand; however, other samples attempted by Ward (1995) in rocky regions (including one in LFH class 5 region) listed no data because no sample was retrieved, as would result when the grab sampler landed on rock (Table 2.1). Based on the Ward (1995) map, all the other classes would be lumped into the gravel class; however, examination of the individual sediment samples in the LFH study area show that the regions delineated according to LFH class 7 were not represented by any sediment samples, only interpolation. LFH classes 1, 2, 3 and 6 were represented by eleven sediment samples that were primarily composed of sandy gravel and gravelly sand (Table 2.1).

Total areal coverages of majority-filtered (providing the class mode) LFH classes ranged from 67,438 m^2 (class 7) to 219,995 m^2 (class 4) (Table 2.1). Classes 2, 3, 4, and 6 all had coverages on the order of 200,000 m^2. Classes 1, 5, and 7 had coverages on the order of 100,000 m^2. Representative LFHs, produced using the mean of all LFHs by class, showed distinct differences among classes according to distributions of the various FT coefficients (Figure 2.4). The distributions of the four Fourier coefficients used to construct the local FT maps and the LFHs were apparent in the LFHs. The seven different LFH classes varied most by distributions of coefficients 1, 2, and 3. Variation of the distributions of coefficent 0 were not as pronounced as the other coefficients' distributions (Figure 2.4). LFH classes 5 and 7 had broad distributions of coefficient 0, the other classes all had narrow coefficient 0 distributions (Figure 2.4, LFH bins 1 through 8). LFH classes 1 and 2 had representative LFHs similar enough to suggest

consolidation of those classes, except that the distributions of coefficient 1 were slightly different (Figure 2.4, LFH bins 9 through 17). Distinctions among the other representative LFHs reinforce the concept that textural differences existed among seafloor regions segmented by LFH. None of the four individual coefficient distributions alone showed enough difference across classes to have been used for separation. Regardless, when the individual histograms were combined as the LFH feature vector, class differences were distinct. Consequently, the texture LFH features represent complex spatial variation of seafloor topography.

2.7. Discussion

Geomorphological regions were discriminated with high efficiency using LFH texture feature classification. Regions distinguished by LFH analysis were suggestive of substrate type and sediment distributions. Furthermore, LFH maps showed patterns similar to the relative backscatter intensity map (Figure 2.5) and the substrate map delineated by Ward (1995). The LFH texture feature classes from the Piscataqua River mouth were determined to represent most simply: rock outcrops, a sand wave and ripple field, and gravelly channel regions (Table 2.1). Those same regional types were delineated by Ward (1995) based on core and grab samples and some sidescan-sonar images. In addition, LFH texture classes existed for transitional regions and other bottom textures suggestive of slightly different geomorphologies that were either lumped into broad substrate classes by Ward (1995) or previously unsampled. Diver observations and underwater video showed these regions to consist of sandy sediments with large (typically > 0.5 cm) shell fragments (represented by class 1 and class 2, see Figure 2.3).

The apparent disparity between facies corresponding to LFH textures and sample data for some LFH classes was indicative of two issues: 1) grab samples in rock outcrop regions did not recover the rock itself, either recovering no sample or recovering sediment interspersed amidst the rocks, and 2) delineations and descriptions of bottom type have inherent scale-dependent biases that can affect correspondences among maps from different sources and methodologies. In addition, substrate heterogeneity is likely to accompany any particular seafloor texture; therefore, concise assignment of seafloor composition is not recommended.

Some textural differences appear to represent similar substrates with different roughness configurations that are probably related to sediment transport and spatial and temporal variations in hydrodynamic effects. Roughness and material transport are important factors to benthic organisms, affecting benthic assemblage structure and function. A reassessment of organism-sediment interaction (OSI) studies by Snelgrove and Butman (1994) emphasized the need to consider hydrodynamics and material transport in order to strengthen OSI models. If seafloor texture patterns correspond to material transport and hydrodynamic processes, then regions delineated by seafloor texture represent spatial extents of the benthic physical environment within which a process occurs at a particular frequency and with a certain intensity. Therefore, texture maps of the seafloor can provide insight about the benthic biological community by not only revealing physiographic constraints and regionalization of seafloor feature types, but also by delimiting areas within with particular hydrodynamic influences. Seafloor topographic maps analyzed for texture or roughness distributions are subtidal analogues to the synoptic maps generated by airborne spectrographic techniques for intertidal and

shallow subtidal water. Although biological attributes of the system and organism-sediment interactions may make the interpretation of spectrographic data used to construct synoptic maps more difficult, those attributes may lead to insights about how to remotely sense related processes (Paterson and Black, 1999). Similarly, physical and biological factors influencing seafloor texture at various spatial scales must be studied in order to accurately assess how and why differences in texture in acoustic maps of subtidal waters indicate differences in substrate characteristics and benthic habitats. Those efforts will likely lead to refinement of the interpretation of acoustic-derived seafloor maps and better methods for seafloor exploration.

The resolution of the Piscataqua River dataset allowed the discrimination of region types by LFH to much finer scales than previous sediment type delineations based primarily upon interpolation of sparse point data. Although apparent associations exist between LFH classes and substrate types, LFH classes are not simply representative of substrate alone; they represent bottom texture which, in a dynamic estuarine environment such as the Piscataqua River, is generated by interactions among the existing substrate composition, newly delivered sediments, fluid dynamics, and biological modifications.

Representative LFHs from correctly classified data, provide feature vectors that can then be applied to new bathymetry data. Thus, representative LFHs can serve as training features representative of particular geomorphologies, and can be used to directly determine the bottom texture and type for new data. LFH analysis can also be applied to acoustic backscatter data.

The spatial scales of feature variations were important and did cause some apparent misclassifications, the most obvious were areas with the rock outcrops that were

classified as sand wave field. The geometry of the rocks and sand waves was similar enough in those cases to inhibit discrimination by LFH analysis. The term 'apparent misclassifications' was used because there may have been a physical or biological basis for the apparent misclassifications: sediments may have accumulated in depressions between rocks or soft-bodied animals and plants may have covered the rocks, thereby affecting their morphologies.

2.8. Conclusions

I have developed an automated, objective method for delineating physical benthic habitats that can be used to model biological habitats prior to sampling the biological community, using historical biological data and assumptions about organism-substrate associations. LFH texture feature classification served as the mechanism for delineation, and was automated, except for the choices of number of classes and texture spatial-integration scale. The appropriate scales of application of LFH should be determinable by optimization procedures, allowing more automation and generalization of the procedures. In addition, despite the good initial results of LFH texture feature segmentation of seafloor topography, alternative segmentation techniques and comparisons to quantitative measures of roughness should be implemented. Areas with apparent misclassifications should be examined directly to determine their character. When applying the segmentation procedure to new data, an "unknown" or "new" class should be introduced to allow for textures that do not correspond to the existing LFH texture features. This will allow exploration and classification of new areas without restricting descriptions to only known types.

The LFH segmentations serve to regionalize seafloor geomorphological regions by textural pattern; those regions are believed to have characteristic combinations of sediments and hydrodynamic conditions. Therefore, LFH segmentations result in a predicted physical habitat model for the seafloor. That, in turn can be used to predict the initial benthic biological habitat model, particularly distributions of primary benthic community constituents or functional group types, depending on the detail of prior knowledge of the biological assemblages in the study area. One of the strengths of segmentations made using LFHs on MBES-derived bathymetry lies in their ability to provide a context for detailed *in situ* seafloor investigation data. On the other hand, interpretations about the ecosystem made using MBES should incorporate such detailed data, otherwise the descriptions are still as coarse as the data resolution. Thus, there are limits to interpretations made using only the MBES seafloor topography data that should be addressed by rigorous, accurately georeferenced, and innovative ground truthing methods. In particular, I seek methods that can provide information about types and rates of changes occuring in the transitions between regions segmented using LFH, and determine the true local variability of seafloor textures that might represent habitat patchiness. The majority-filtered map provided a simplified and easy to interpret regionalization of the seafloor in the study area, although the apparently noisy representations might be valid for certain attributes. Determination of small-spatial-scale variability could not be done using the Ward (1995) sediment map or sparse samples; therefore, I suggested a simplified depiction of seafloor region types in order to avoid speculation without supportive data. For new seafloor explorations, it is likely that even

less ground-truth data will be available; therefore, I believe that maintaining a simple initial model is a practical approach.

2.9. Acknowledgements

I thank Lt. Shep Smith, NOAA, for bathymetric grid generation; Science Applications International Corporation (SAIC) for collection of Reson 8125 multibeam echosounder data; Dr. Lloyd Huff, NOAA, for discussion and review of text; and Dr. Martin Jakobsson for GIS help. This work was supported by NOAA grant NA970G0241.

2.10. References for Chapter 2

Bourget, E., DeGuise, J., Daigle., G., 1994. Scales of substratum heterogeneity, structural complexity, and the early establishment of a marine epibenthic community. Journal of Experimental Marine Biology and Ecology, 181, 31-51.

Cusson, M., Bourget, E., 1997. Influence of topographic heterogeneity and spatial scales on the structure of the neighboring intertidal endobenthic macrofaunal community. Marine Ecology Progress Series, 150, 181-193.

Folk, R.L., 1954. The distinction between grain size and mineral composition in sedimentary-rock nomenclature. Journal of Geology, 62, 345-359.

Guichard, F., Bourget, E., 1998. Topographic heterogeneity, hydrodynamics, and benthic community structure: a scale-dependent cascade. Marine Ecology Progress Series, 171, 59-70.

Kostylev, V. E., Todd, B. J., Fader, G. B., Courtney, R. C., Cameron, G. D., Pickrill, R. A., 2001. Benthic habitat mapping on the Scotian Shelf based on multibeam bathymetry, surficial geology and sea floor photographs. Marine Ecology Progress Series, 219, 121-137.

Liu, X., Wang, D.L., Srivastava, A., 2001. Image segmentation using local spectral histograms. ICIP conference proceedings. IEEE 0-7803-6725-1/01.

Mayer, L. A., Hughes-Clarke, J., Dijkstra, S., 1999. Multibeam sonar: potential applications for fisheries research. Journal of Shellfish Research, 17, 1463-1467.

Mayer, L., and Baldwin, K., 2001. Shallow water survey 2001: Papers based on selected presentations from the second international conference on high resolution surveys in shallow water. Marine Technology Society Journal, 35, 3-4.

Menge, B.A., Olson, A.M., 1990. Role of scale and environmental factors in regulation of community structure. TREE, 5 (2), 52-57.

Minasny, B., McBratney, A.B., 2000. FuzME version 2.1,Australian Centre for Precision Agriculture,The University of Sydney, NSW 2006. (http://www.usyd.edu.au/su/agric/acpa).

Paterson, D. M., and Black, K. S., 1999. Water flow, sediment dynamics and benthic biology. Advances in Ecological Research, 29, 155-193.

Short, F. T., 1992. The estuarine hydrosystem. In: Short, F.T. (Ed.), The ecology of the Great Bay Estuary, New Hampshire and Maine: an estuarine profile and bibliography. NOAA Coastal Ocean Program/Univ. New Hampshire Sea Grant Coll. Program, Durham, NH (USA), NOAA COAST. OCEAN PROGRAM PUBL., 1992.

Snelgrove, P. V. R, and Butman, C. A., 1994. Animal-sediment relationships revisited: cause versus effect. Oceanography and Marine Biology: an Annual Review, 32, 111-177.

Swift, M. R., Brown, W. S., 1983. Distribution of bottom stress and tidal energey dissipation in a well-mixed estuary. Estuarine, Coastal and Shelf Science, 17, 297-317.

Swift, M.R., Fredriksson, D.W., Celikkol, B., 1996. Structure of an axial convergence zone from acoustic Doppler current profiler measurements. Estuarine, Coastal and Shelf Science, 43, 109-122.

Todd, Brian J; Fader, Gordon B J; Courtney, Robert C; Pickrill, Richard A., 1999. Quaternary geology and surficial sediment processes; Browns Bank, Scotian Shelf; based on multibeam bathymetry. Marine Geology, 162, no.1, 165-214.

Ward, L.G., 1995. Sedimentology of the lower Great Bay/Piscataqua River Estuary. San Diego, CA: Department of the Navy, NCCOSC RDTE Division Report.

Ware, C., 2000. Information visualization: design for perception. Morgan Kaufmann Publishers, San Francisco.

Zajac, R.N., 2001. Organism-sediment relations at multiple spatial scales: implications for community structure and successional dynamics. In: Aller, J.Y., Woodin, S.A.,

and Aller, R.C. (Eds.), Organism-sediment interactions. Belle W. Baruch Library in Marine Science, University of South Carolina Press, Columbia, SC.

Zhou, F., Feng, J., Shi, Q. 2001. Texture feature based on local Fourier transform. ICIP 2001 conference proceedings, pp. 610-613.

2.11. Tables for Chapter 2

Table 2.1. Substrate types found in each LFH class region, and total areal coverages of each LFH class. Substrate classes were based on sediment samples from Ward (1995), with type descriptions in terms of Folk's (1954) mud, sand, and gravel. Sediment classes include sandy gravel (sG), gravelly sand (gS), muddy sand (mS), sand (S), muddy gravelly sand (mgS); there was one station within class 5 (rocky) where no samples were recovered (NR); no samples were taken (NA) within LFH class 7. Areal coverage (rounded to nearest m^2) of each LFH texture feature class in the study area is reported, for raw LFH results (5-m radius, 10-by-10-m block), and majority filtered results (majority value in 30-by-30-m block around each grid cell).

LFH Class	**General Description**	**Sediment class of Ward (1995) samples located in each LFH class region**	**Raw LFH Coverage (m^2)**	**Majority LFH coverage (m^2)**
1	Smoother sedimented bottom-texture 1	sG, sG, gS, gS	111725	92960
2	Rougher sedimented bottom-texture 1	gS, sG, mS	187060	182589
3	Smoother sedimented bottom-texture 2	gS, msG, sG, sG	172785	199122
4	Sand Waves	S	221360	219995
5	Rock	NR, sG, mgS	111017	126986
6	Rougher sedimented bottom-texture 2	gS, gS, sG	185340	216774
7	Steep, smooth marginal slopes	NA	61819	67438

2.12. Figures for Chapter 2

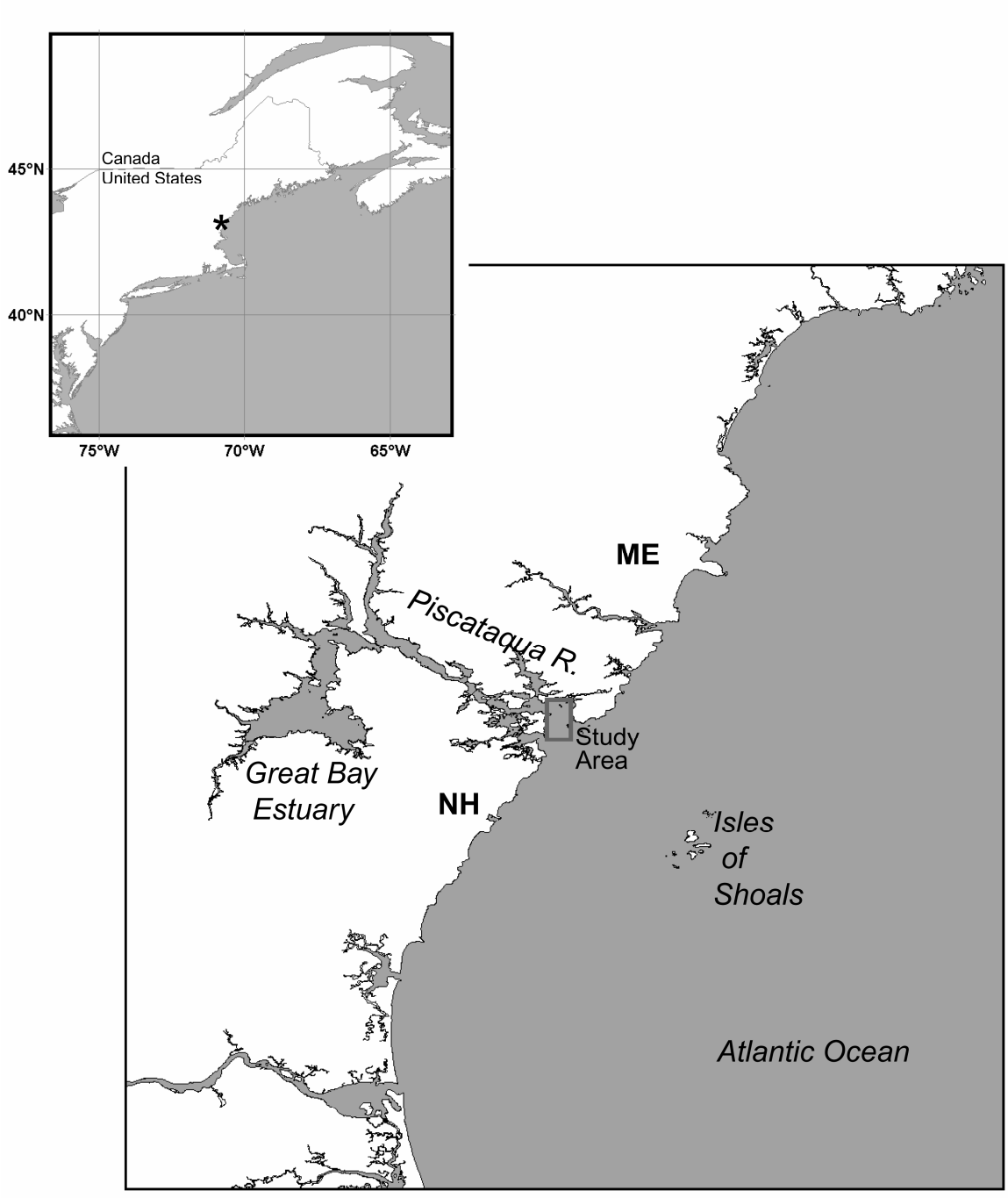

Figure 2.1. The study area consisted of a section of subtidal waters in the Piscataqua River, between New Hampshire and Maine, USA. The asterisk in the small map marks the area enlarged.

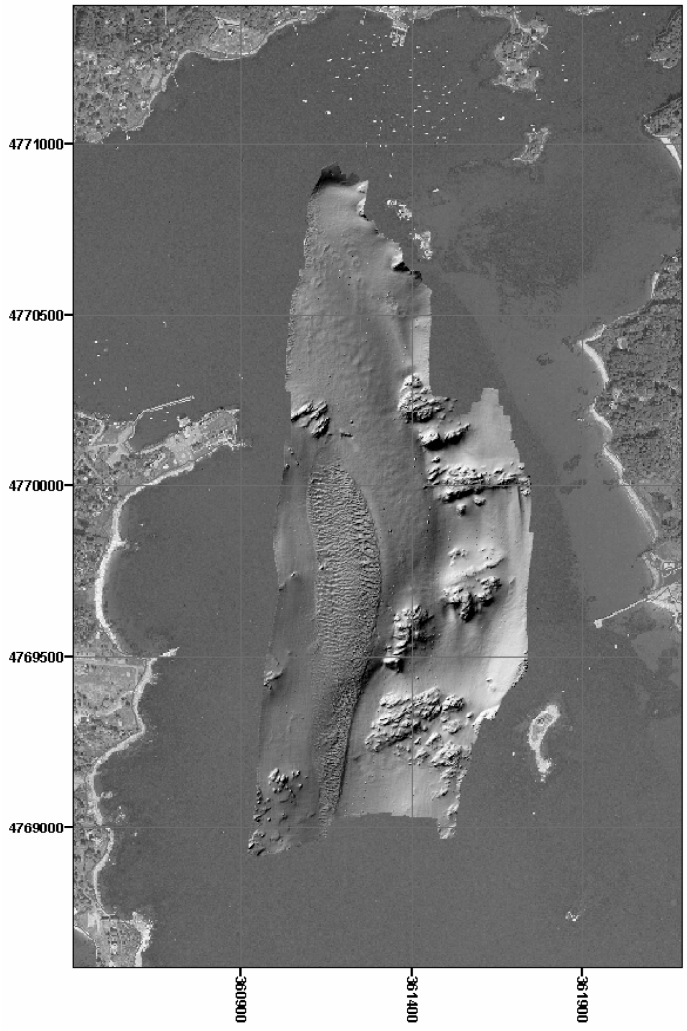

Figure 2.2. Bathymetric digital terrain model (DTM) from the mouth of the Piscataqua River, NH, gridded to 1 meter, UTM projection, zone 19N. Constructed from Reson 8125 multibeam echosounder data, collected by SAIC for NOAA & UNH JHC-CCOM, July 2000. Shading provided by artificial illumination from the north-northwest at an elevation angle of 45 degrees.

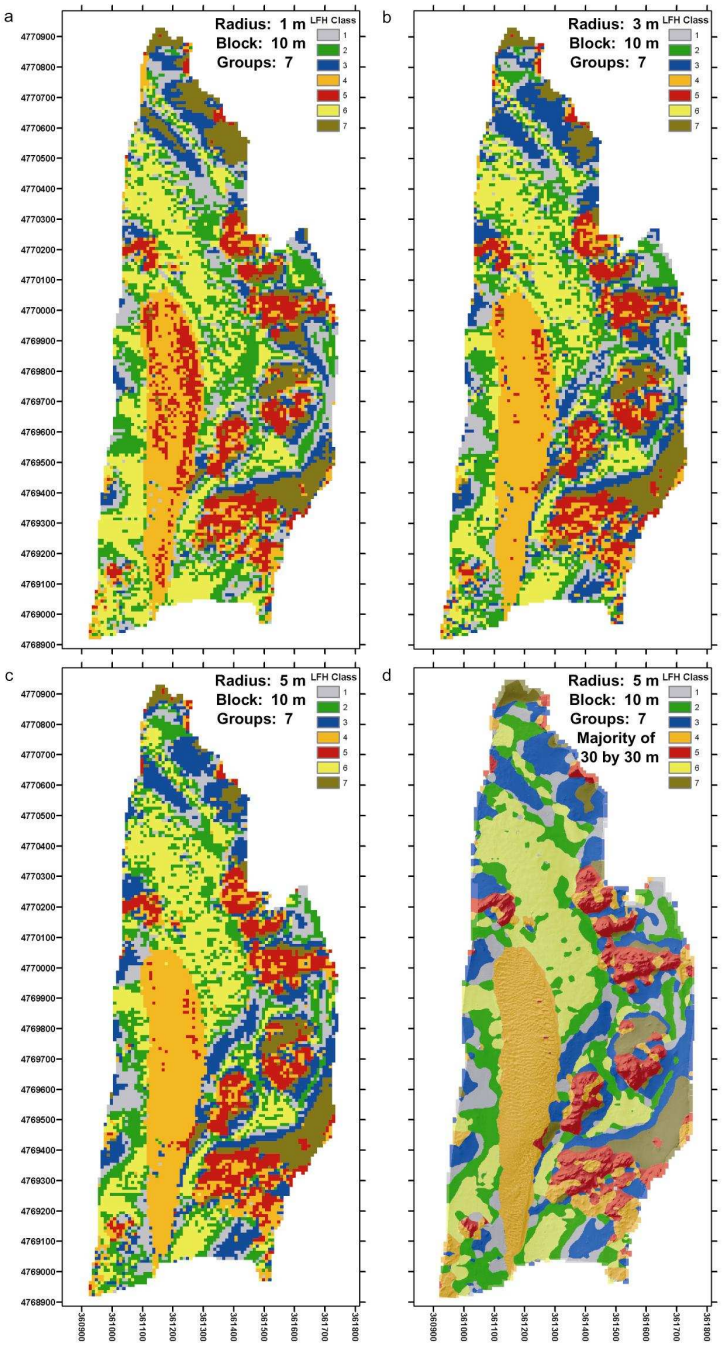

Figure 2.3. Segmentation of Piscataqua River mouth bathymetry by local Fourier Histogram (LFH) texture feature classification using coefficients 0 through 3 and varying spatial scales to generate texture features. LFH Texture feature classes from a) neighborhood radius of 1 m, b) neighborhood radius of 3 m, c) neighborhood radius of 5 m. d) neighborhood radius of 5 m where the original LFH class value for each cell was replaced by majority value (mode) from the surrounding 30-by-30-m block, and LFH map draped onto bathymetric terrain model surface. Coordinates are in UTM Eastings and Northings, zone 19 north.

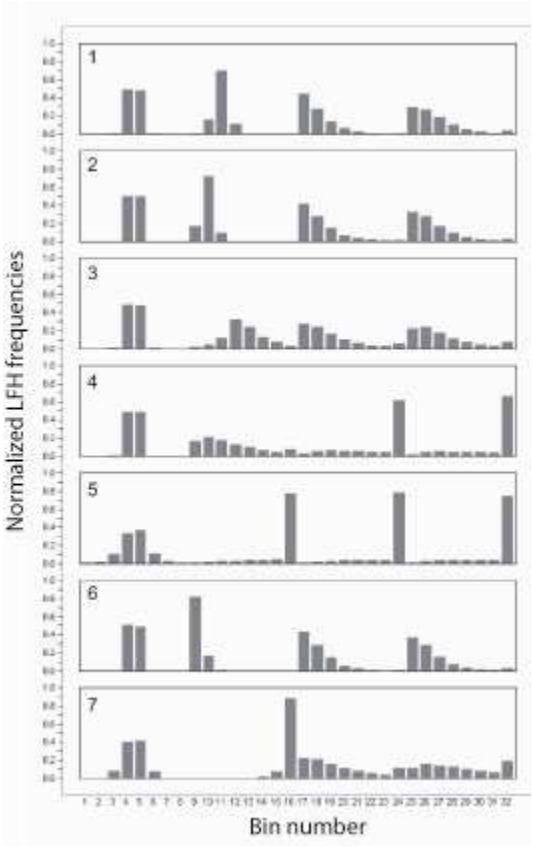

Figure 2.4. Representative histograms for seven LFH texture feature (radius=1 m, block=10 by 10 m) classes from cluster groups. Each successive eight bins represent the distribution of an individual local FT magnitude coefficient. Thus, bins 1-8 represent localFT coefficient 0 - mean, bins 9-16 represent coefficient 1 magnitude, bins 17-24 represent coefficient 2 magnitude, and bins 25-32 represent coefficient 3 magnitude. Clustering was done using fuzzy k-means method (Minasny and McBratney, 2000).

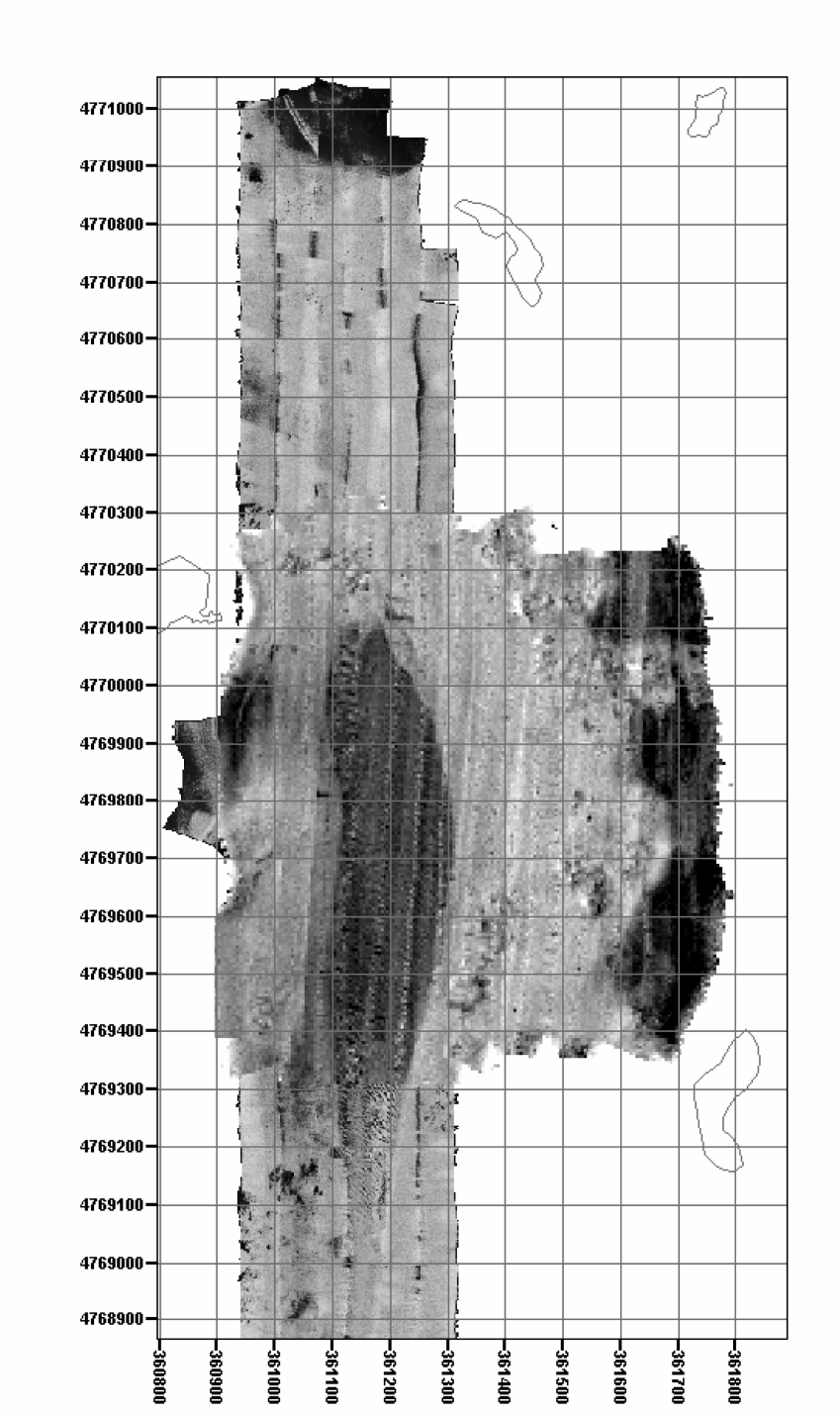

Figure 2.5. Acoustic backscatter mosaic covering part of the study area. The backscatter mosaic consists of data from a Klein 5500 sidescan-sonar and a Kongsberg-Simrad (K-S) EM3000 multibeam echosounder system, mosaiced separately, gridded to 1-m (Klein) and 5-m (K-S), then combined and gray levels adjusted so that both datasets represented the same dynamic range. The mosaic from the K-S data is shown over the mosaic of the Klein data that extended farther north and south, but less east and west.

CHAPTER 3

3. GROUND TRUTHING USING IMAGE MOSAICS

3.1. Citation

To be published in Proceedings Volume from: Symposium on the Effects of Fishing Activities on Benthic Habitats: Linking Geology, Biology, Socioeconomics, and Management. Tampa, FL, Nov. 12-14, 2002.

Citation:

Cutter Jr., G. R., Rzhanov, Y., Mayer, L. A. and Grizzle, R. E., In Press. Ground Truthing Benthic Habitat Characteristics Using Video Mosaic Images. *In* Barnes, P. W., Thomas, J. P., (Eds.) Benthic habitats and the effects of fishing. American Fisheries Society, Symposium 41, Bethesda, Maryland.

3.2. Abstract

Subtidal benthic habitats from the Piscataqua River were delineated by an automated segmentation technique using bathymetry derived from multibeam echosounder data (Cutter et al., 2003). The map produced by segmentation of seafloor textures represents a 'hypothetical benthic habitat map' that requires ground truthing. In this study, video mosaics were used to ground truth the hypothetical habitat map and to describe biological features and organism occurrences and densities. Video mosaics acquired along two transects in the Piscataqua River were used to detect substrate transitions apparent in the bathymetric map, and to quantitatively assess coverages of

distinct sediment conditions, density of megafaunal organisms (lobsters), and bioturbational features (crab feeding pits).

3.3. Introduction

Benthic habitat mapping efforts have benefited from high-resolution and total-coverage data from multibeam and sidescan-sonar systems (Kostylev et al., 2001). However, because of the complex interactions between seafloor composition, geometry and acoustic reflection and backscatter (see Urick, 1983), multibeam and sidescan maps must be ground truthed to confirm sedimentological and biological characteristics. Remotely deployed video can be used for ground truthing, but quantitative analysis can be difficult or tedious. Mosaics constructed from video-image sequences convert the many individual video frames to a single still image that represents the entire imaged tract.

To map benthic habitats of the Piscataqua River (New Hampshire and Maine) multibeam bathymetry data were analyzed by Cutter et al. (2003) using an automated segmentation and classification technique (Figure 3.1) involving classification using local Fourier histogram (LFH) texture features described by Zhou et al., (2001). Segmentations of seafloor morphologies from that analysis had good correspondence to the sediment facies in the study area (Ward, 1995) and to multibeam and sidescan-sonar acoustic-backscatter-intensity datasets. I suggest that the automatically classified texture feature map presented in Cutter et al. (2003) represents a 'hypothetical benthic habitat map' of the seafloor. The hypothetical habitat map presents the opportunity to test hypotheses about seafloor characteristics and associated benthic fauna, and, if properly

ground truthed, can be considered a true habitat map. The ability to go from a 'hypothetical habitat map' to a true map of the spatial extent and distribution of benthic habitats will be strengthened by the use of other data such as acoustic backscatter intensity, substrate composition, energy regime, and salinity. Whether or not the hypothetical habitat map accurately represents the spatial extent and distribution of benthic habitats might be strengthened by inclusion of such ancillary data The better these key environmental factors can be described, the more likely the 'hypothetical habitat map' will be an accurate representation of biological habitats. However, even if other environmental data are lacking, a 'hypothetical habitat map' can be developed to predict spatial distributions of habitat and seafloor characteristics.

A habitat map requires choice of target species or groups of species that associate and requires ground truthing data to determine how the species occur, are distributed, and utilize the seafloor. The occurrence and distribution of some species can be assessed using remote-sensing techniques. For sessile epibenthic megafauna, or those with limited-motility, video mosaics can be used to assess the presence and density of organisms as a function of seafloor region (i.e., by hypothetical benthic habitats derived from segmentation of gridded seafloor bathymetry (Cutter et al., 2003), thus providing descriptions of essential fish habitat (EFH) levels 1 and 2 (Able, 1999). EFH level 1 designates habitat-specific occurrence (presence or absence) of organisms; EFH level 2 designates distribution and abundance of organisms (Able, 1999). The purpose of this work is to demonstrate that an analysis of video mosaics can be used as a ground-truthing technique to: (1) determine where apparent transitions of substrates occur; (2) assess occurrence and density of megafauna (the northern lobster *Homarus americanus*) and; (3)

estimate coverages of substrates (bare sediments and microalgal layers) and crab feeding pits.

3.4. Data and Methods

Bathymetry data in the study area were collected aboard the R/V *Coastal Surveyor* (UNH) by Science Applications International Corporation (SAIC) using a Reson 8125 (455 kHz) dynamically focused multibeam echosounder (Mayer and Baldwin, 2001). Data were cleaned using standard hydrographic processing approaches and gridded using a weighted-mean grid with 1-m spatial resolution. Delineations of seafloor configurations representing apparent benthic habitats were produced by an automated segmentation procedure using texture feature classification applied to the gridded bathymetry data (Cutter et al., 2003).

3.5. Video Mosaic Imagery

Mosaic images were generated from underwater video footage of the seafloor collected by diver and by towed camera using a featureless coregistration technique involving frequency domain processing of images to solve automatically for affine motion parameters, translation, rotation and zoom (Rzhanov et al., 2000). Each frame was coregistered to the previous frame and its magnification was adjusted to the previous zoom level. The resulting mosaic has a uniform spatial scale throughout (unless errors accumulate). After the assembly of mosaics, colors were manually adjusted to compensate for ambient lighting effects by independently adjusting the ranges of the red, green and blue channels. Positioning data for the towed camera deployments were

provided by differential GPS, and an acoustic transponder positioning system was used for the diver deployments. Mosaic construction does not require positioning data, however positioning data are necessary for placement of the mosaics within bathymetry and backscatter maps and for the interpretation with respect to bathymetry and backscatter maps.

Video image mosaics for this study came from two locations within the study area described by Cutter et al. (2003). In the northwestern part of the study area, imagery for mosaicing was collected within an experimental enclosure for tracking lobster movements (lobster mesocosm). Across the river, to the east of the main channel, imagery for mosaicing was acquired from a rocky region.

3.6. Results

The video-image mosaic from the rocky region (Figure 3.2) reveals a transition from shelly gravel sediments to boulders and bedrock. The transition observed in the mosaic is marked in the figure with colors that correspond to the nearest texture feature class regions from the segmented bathymetry map (Figure 3.1). Several species of epifaunal sponges, bryozoans, and tunicates are evident on the rocks.

Substrate transitions are visible and are delineations easily made from a mosaic of a rocky region on the eastern side of the river mouth channel (Figure 3.2). Despite the fact that the mosaic was acquired from what appeared to be a rocky outcrop in the bathymetry image, various substrates are apparent from the mosaic. Patches of gravel, shell hash, shell valves, and boulders exist in addition to bedrock. It is evident that a variety of sediments with a wide range of grain sizes cover portions of the outcrops.

Texture feature classification determined that at least two seafloor textures exist at the scales of the analysis (1 m to 8 m). The positioning data for the video used to construct the rocky region mosaic was not precise enough to determine if the transitions delineated in the mosaic correspond to bathymetric features. The goal for future deployments is to collect positioning data that allow for accurate georeferencing of the video imagery and mosaics.

The mosaic from the lobster mesocosm (Figure 3.3) reveals a silty fine sand substrate occupied by benthic megafaunal lobsters (*Homarus americanus*) and crabs (*Cancer irroratus* and/or *C. borealis*) and large infaunal razor clams (*Ensis directus* and possibly others). The clams are evident from their siphons and empty shells and were identified by divers. Large bioturbational pits are apparent, and some are occupied by crabs and lobsters. Diver observations suggest that these pits are feeding pits excavated by crabs in pursuit of *E. directus*.

The two primary goals of the analysis of lobster mesocosm mosaic (Figure 3.3) were to detect and enumerate occurrences of the lobsters (Homarus americanus), and to delineate substrate surface conditions apparent according to three classes: (1) sediment with a micro-algal layer coverage; (2) bare sediment, although perhaps with shallow bioturbation, and; (3) deep biological-excavations. The sediment surface conditions of the lobster mesocosm are relatively easily distinguished by color. Sediment with algal cover is reddish-brown, bare sediment is olive to olive-gray, and deeply bioturbated sediment is bluish to bluish-gray due to digging and burrowing by crabs and lobsters that expose the anoxic subsurface sediments.

3.6.1. Abundance of megafauna in lobster mesocosm video mosaic

Visual analysis of the mosaic accomplishes the first goal of detecting and counting lobsters. In the mosaic, seven lobsters were present with more than 50 % of the body in the image. If only part of a lobster was seen in an image, then it was not counted.

3.6.2. Density of megafauna in lobster mesocosm video mosaic

Because all images were adjusted to the same zoom level during automated co-registration, and because the beginning of the transect contains a fence with 3.8-cm, the area coved by the mosaic could be estimated. For the portion of the mosaic analyzed, the coverage area was 5.87-m^2 and the lobster density was 1.2-m^2. This high lobster density reflected the higher frequency of occurrence of lobsters in that part of the enclosure. Other video sequences suggest a much reduced density in different parts of the mesocosm.

A density estimate from an analysis of a video sequence requires knowledge of precise distances traveled between video frames as well as the camera height from target surface. Such information could be provided by a surface positioning system but is unlikely to produce accurate estimates. Accurate estimates of imaged bottom area require either co-registration of the image series to reproduce the entire tract, or detailed instantaneous data from precise motion and position sensors incorporated with the camera. The latter option requires much more sophistication and expense than available to many studies, and was not used here.

3.6.3. Sediment surface condition in lobster mesocosm video mosaic

By eye, sediment surface condition was difficult to accurately delineate. To aid visual determination of condition, an histogram from each color (RGB) channel of the image was range-adjusted, eliminating the highest and lowest 1 % of values. Seldom was a particular area of the seafloor totally covered by one sediment condition. Coverage areas were manually-delineated and subtle differences might have been indistinguishable and small patches could have been ignored; therefore, surely some errors in the estimates exist. The coverage areas for the sediment conditions previously described were determined to be:

1. Algal or microbial covered 3.46 m^2
2. Bare or with shallow bioturbation 2.27 m^2
3. Deeply bio-excavated 0.14 m^2

3.7. Discussion

Mosaic image measurements can be made at specific intervals or for discrete areas to determine substrate conditions and estimates of organism density for any part of the seafloor imaged. The mosaic from the lobster mesocosm shows large biogenic features such as siphons of the razor clam (*E. directus*). These siphons were just large enough to resolve in the mosaic because of the height of the camera from the bottom. For the assessment of infauna or small epifauna or their features (e.g., tubes and burrows), camera-deployment requirements must be configured to maximize image resolution. Images must be collected close to the bottom, and lighting must be of sufficient intensity and uniform. One disadvantage with a deployment that maximizes resolution is reduced

coverage area. Given a fixed field-of-view of the camera, the shorter the range to the target, the smaller the imaged area. However, close-range imaging allows smaller features to be resolved and larger features to be seen with more clarity. The scale and resolution of the imagery ultimately determine the level of detail at which habitat characteristics can be quantified. In this case I was able to describe megafaunal occurrences and densities as well as megafaunal bioturbational features; those assessments relate to EFH levels 1 and 2 (Able, 1999). However, the same imagery cannot be used to assess occurrence (EFH level 1) of macrofauna or smaller organisms.

3.7.1. Issues related to optical ground truthing

A fundamental issue in habitat classification is that standard optical images, such as discrete sample seafloor photographs that typically image 1 m^2 or less, do not directly correspond to acoustically-imaged features because of resolution disparities between acoustical and optical systems. How well the photographic images represent what is sensed by the sonar cannot be accurately determined unless the optical images span the same spatial scales as the acoustic data. Videography and video mosaicing are cost-effective means (compared to other optical imaging techniques such as laser line scan) to provide optical seafloor imagery that can represent spatial scales corresponding to those of acoustic footprints (though perhaps not in all directions). It is unlikely that biological features or small bathymetric features will have acoustic responses that are clearly correlated to optical representations. Because feature-to-feature correspondence between acoustic and optical sensing is difficult, co-variability should be examined over distances or areas. Video mosaics provide optical image data that span spatial scales that can be achieved with some acoustic systems.

Why not simply acquire video or photos at greater heights above the seafloor because greater camera-target distance would produce a larger imaged area? Underwater optical imagery is limited by water-column conditions, primarily related to attenuation of light by suspended particles. This light scattering effect is most pronounced in coastal waters, but exists throughout the oceans to some degree. Even when particle concentrations are low, light attenuation through clear seawater limits the distance and therefore the area that can be imaged reliably. In the deep sea or other waters where benthic boundary layer turbidity can be minimal, the intensity of artificial light sources and camera image receptors sensitivity and resolution are limitations.

3.8. Conclusions

Video mosaics provide a cost effective way of providing large areal-coverage with high resolution and are an appropriate tool to ground truth acoustic data. It can be difficult to keep track of features or organisms seen in only part of video images; those can be identified easily in mosaiced images. To achieve accurate counts of organisms or seafloor features from analysis of video imagery, care must be taken to ensure that the data represent non-overlapping fields-of-view. Mosaics eliminate the need to repeatedly review portions of a video sequence to define sample areas that do not overlap by showing the entire coverage area. Mosaics can facilitate interpretation of processes occurring at spatial-scales not clearly evident in individual video image frames, and expand the capabilities of characterization using a common ground-truthing tool.

3.9. Acknowledgments

I thank Lt. Shep Smith, NOAA, for editing the bathymetry data and for grid generation and Science Applications International Corporation for collecting the Reson 8125 multibeam echosounder data. This work was supported by NOAA grant NA970G0241.

3.10. References for Chapter 3

Able, K. W. 1999. Measures of juvenile fish habitat quality: examples from a National Estuarine Research Reserve. Pages 134-147 in L. R. Benaka, ed. Fish habitat: essential fish habitat and rehabilitation. American Fisheries Society Symposium 22.

Cutter, G. R., Rzhanov, Y., Mayer, L. A., 2003. Automated segmentation of seafloor bathymetry from multibeam echosounder data using local Fourier histogram texture features. Journal of Experimental Marine Biology and Ecology, 285/286, 355-370.

Kostylev, V. E., Todd, B. J., Fader, G. B., Courtney, R. C., Cameron, G. D., Pickrill, R. A., 2001. Benthic habitat mapping on the Scotian Shelf based on multibeam bathymetry, surficial geology and sea floor photographs. Marine Ecology Progress Series, 219, 121-137.

Mayer, L. A., and K. Baldwin. 2001. Shallow water survey 2001: Papers based on selected presentations from the second international conference on high resolution surveys in shallow water. Marine Technology Society Journal, 35, 3-4.

Rzhanov, Y. L. Linnett, R. Forbes, 2000. Underwater video mosaicing for seabed mapping. Proceedings of the IEEE International Conference on Image Processing, 10-13 September, 2000, Vancouver, Canada, pp. 224-227.

Urick, R. J., 1983. Principles of underwater sound for engineers. McGraw-Hill, New York, 342 pp.

Ward, L. G., 1995. Sedimentology of the lower Great Bay/Piscataqua River Estuary. San Diego, CA: Department of the Navy, NCCOSC RDTE Division Report, 102 pp.

Zhou, F., Feng, J., Shi, Q. 2001. Texture feature based on local Fourier transform. Proceedings of the IEEE International conference on Image Processing (ICIP), 2001, pp. 610-613.

3.11. Figures for Chapter 3

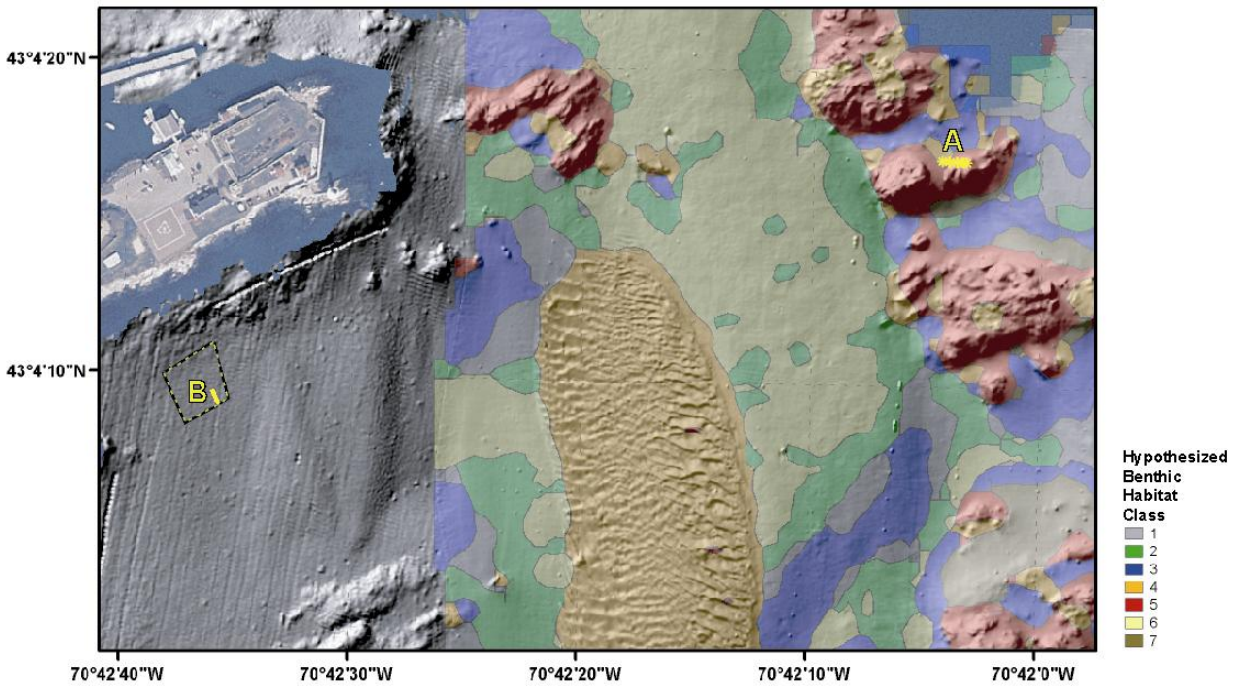

Figure 3.1. Section of the seafloor (980 by 630 m) in the mouth of the Piscataqua River, part of which was delineated using automated segmentation technique involving a modified implementation of local Fourier histogram texture feature classification applied to gridded bathymetry data from a Reson 8125 (455 kHz) multibeam echosounder (Cutter et al., in press). Seven hypothesized seafloor habitat classes resulting from the segmentation are colored in the figure. A marks the location of the transect where video for the rocky region mosaic (Figure 3.2) was acquired, and B marks the location of the lobster mesocosm experimental enclosure mosaic (Figure 3.3).

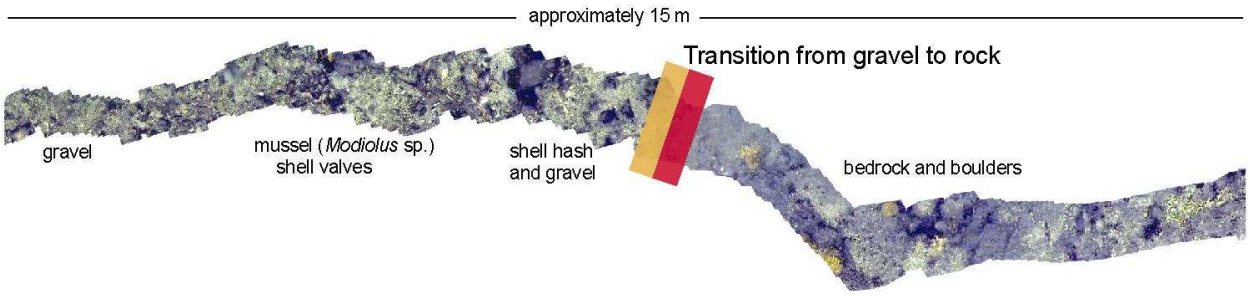

Figure 3.2. Video mosaic image showing the rocky region. The transition marked in the mosaic corresponds to the nearest boundary for texture feature class regions along the transect and represents transition from shelly gravelly sediments to bedrock with boulders. Several species of sponges, bryozoans and tunicates are evident on the rocks.

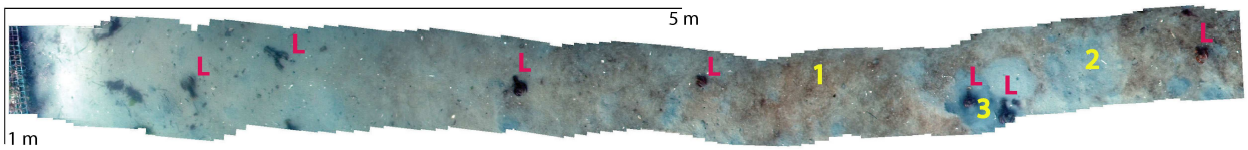

Figure 3.3. Video mosaic image from the lobster mesocosm. Lobsters (*Homarus americanus*) are labeled with L; 1 is sediment with a micro-algal layer coverage; and 2 is bare sediment, although perhaps shallow bioturbated; and 3 is deep bioturbated excavations interpreted as crab feeding pits.

CHAPTER 4

4. SEAFLOOR MICROTOPOGRAPHICAL ROUGHNESS SPECTRA

4.1. Citation

Submitted, Dec. 2004, to: The Journal of Marine Systems.

Citation:

Cutter Jr., G. R., Submitted. Seafloor roughness spectra from sediment profile images. The Journal of Marine Systems.

4.2. Abstract

Seafloor roughness spectra were calculated for 34 sediment profile images (SPI) from nine sites on the continental shelf off northern California (Eel Margin). The study area spanned nearshore sands, a transitional region, and a mid-shelf flood deposit composed of sediment that ranged from sediments from sands to clays. Sediment-water-interface (SWI) profiles were extracted by manually tracing the interface from digitized sediment profile images, then converting the trace to a one-dimensional numeric series of elevation measurements. Sample intervals were about 0.014 cm and each SWI data series spanned a distance of 14 cm. The method reported in Briggs (1989) was used to calculate spectra and spectral slope and intercept parameters. Although SPI roughness profile length scales and sampling intervals were about an order-of-magnitude smaller than those

generated from close-range stereo photogrammetry, SPI 1-dimensional spectral slopes and intercepts were similar to those derived from stereo photographs (Briggs, 1989). Mean spectral slopes (by site) ranged from -2.05 to -2.60, with an overall weighted mean slope of -2.44. Spectral intercepts were also similar to published values with an overall weighted mean of 0.0002, except in the case where the epibiota were considered to be part of the interface profile. This case produced an intercept two orders-of-magnitude larger than that from an interface profile that excluded the epibiota, as well as a lower magnitude slope. The power-law scaling of seafloor microtopographical roughness distributions appears to extend into scales of roughness represented by sediment profile images for this study area, and is similar to scaling for lower spatial-frequency roughness-element distributions. Roughness at SPI scales (mm to dm) affects the responses of acoustic wave energy used for remote sensing of the seafloor. Sediment profile images, therefore, can be useful for examining seafloor bio-geoacoustic properties.

4.3. Introduction

4.3.1. Background

A sediment profile imagery (SPI) camera system collects images of vertical cross-sections of the surficial seafloor sediments (Figure 4.1). SPI images reveal details about the sediment type, fabric, sedimentary layers, mixing depth, infauna, epifauna, biological features, microtopographical roughness and habitat quality (see, for instance: Rhoads and Cande, 1971; Rhoads and Germano, 1982 & 1986; Diaz and Schaffner, 1988; Cutter and Diaz, 2000; Diaz et al., 2003).

The sediment profile images (SPI) used for this study were previously used by Cutter and Diaz (2000) to investigate a flood deposit on the northern California continental shelf. Cutter and Diaz (2000) collected SPI from a transect of 10 stations spanning from 28-m to 83-m water depth (Figure 4.2), a transect approximately aligned with "Transect S" used during the STRATAFORM-1995 Eel Margin study (Nittrouer and Kravitz, 1996) and by Richardson et al. (2002). Cutter and Diaz (2000) described a flood deposit, a transitional region, and inshore sands in the SPI transect. The facies proposed by Cutter and Diaz (2000) were shown to be associated with distinctive acoustic-backscatter responses (Borgeld et al., 1999; Richardson et al., 2002) and with sediment geoacoustic properties including compressional and shear wave speeds and subbottom acoustic penetration depths (Richardson et al., 2002).

4.3.2. SPI and roughness measurements

Typically, the sediment-water-interface roughness from SPI has been measured only as a vertical linear extent, or maximum minus minimum height of the seafloor interface observed in the image. That measurement is desirable because it is simple and appears to provide reasonable estimates for the apparent seafloor-roughness length-scale, z_0, used to calculate seafloor shear stress for modeling sediment-transport (Wright et al., 1999). However, simple vertical difference measurements do not describe the distribution of roughness elements. For instance, a single sediment grain or a sloping interface could induce the same surface relief measurement produced by the vertical differencing method. Cutter and Diaz (2000) reported the root mean square (RMS) deviation roughness values for SPI image interfaces. RMS measurements describe the distribution of roughness in terms of deviation from a reference plane, but they do not

convey the spatial frequency distribution for roughness elements. Therefore, it is possible for an interface with many small roughness features to have the same RMS roughness as an interface with sparse, widely-spaced roughness features. The spectrum for an interface elevation series does relate the distribution of roughness in terms of spatial frequencies. A single model with two parameters can be used to describe roughness spectra for isotropic roughness. Two-parameter models have been used by Fox and Hayes (1985), Briggs (1989), Jackson and Briggs (1992), Jackson et al. (1996), and Briggs e al. (2002) for 1-D spectra and by Lyons et al. (2002) and Pouliquen et al. (2002) for 2-d spectra.

4.3.3. Eel shelf roughness

Along the SPI transect from the Eel shelf, mean RMS roughness for sediment-water-interface profiles from SPI was 0.55 cm (σ = 0.3 cm) for the inshore sands (28-m to 36-m water depth) with rippled very fine to fine sand, 0.37 cm (σ = 0.15 cm) for the transitional region (43-m to 55-m water depth), and 0.32 cm (σ = 0.06 cm) for the muddy flood deposit regions (Cutter and Diaz, 2000). Wright et al. (1999) reported roughness measurements as sediment relief determined from SPI, as simply the vertical difference between maximum and minimum elevations in the seafloor interfaces measured in SPI, and roughness lengths calculated from the measured bottom-boundary-layer flow and shear velocity relationships. Interestingly, the simple sediment relief measurements corresponded closely to apparent roughness estimates determined from inversion of boundary layer flow properties. Table 2 of Wright et al. (1999) reports z_0 for a site in 60-m water depth as 1.0 cm, and 0.8 cm for a site in 70-m water depth, and Cutter (1997) determined surface relief from SPI to be 1.3 cm for a a station in 60-m water depth

(near the instrumented Virginia Institute of Marine Science tripod measuring flow properties) and 0.9 cm for a 64.m station. However, Wright et al. (1999) had flow-based apparent roughness estimates for only two sites (60-m and 70-m water depths); therefore, the relationship might not be generally applicable.

4.3.4. Acoustic wavelength scales of SPI

Because we are trying to make spectral estimates applicable to seafloor acoustic data, we consider the acoustic wavelength scales of SPI. The seafloor profiles extracted from SPI as digitized here had a sample interval of approximately 0.014 mm and length of 150 mm, providing a resolution of about 0.028 mm and half--series length of approximately 75 mm. Scales of roughness important to acoustic wave responses are considered to be 0.1λ to 10λ (Greaves and Stephen, 2000) where λ is the wavelength of the acoustic signal. If 0.3 mm and 75 mm are used as the lower and upper bounds for the wavelength scale ranges, then the associated acoustic wavelength scales would be [0.1λ : λ : 10 λ], or [0.3 mm : 3.0 mm : 30.0 mm] and [0.75 mm : 7.5 mm : 75 mm]. Assuming transmission through seawater with sound speed (c) of 1500 m/s, the highest relevant frequencies ($f = c/\lambda$) would be 500 kHz (for λ = 3 mm) and 200 kHz (for λ = 7.5 mm). Therefore, SPI roughness profiles, capable of resolving roughness features with length scales of 0.3 to 75.0 mm, are directly relevant to the interaction of acoustic waves with the seafloor for frequencies from about 200 kHz to 500 kHz. These frequencies are typical of shallow-water multibeam echosounders and sidescan sonars. Directly resolving sand grains, pebbles, or cobbles (sediments with dimensions in the wavelength scale range) using typical multibeam echosounders or sidescan-sonars is not realistic.

Rather, sediments and features in that size range should contribute to the behavior of the scattered acoustic waves.

4.3.5. Seafloor roughness spectra

Seafloor roughness spectra have been estimated for very low spatial frequencies (and large spatial scales) using deep-sea bathymetry (*e.g*. Fox and Hayes, 1985; Fox, 1996) and acoustic backscatter data (Dziak et al., 1993; Matsumoto et al., 1993), and for high spatial frequencies using seafloor stereo photogrammetry or other methods (Stanic et al., 1988; Briggs, 1989; Stanic et al.,1989; Jackson and Briggs, 1992; Jackson et al., 1996; Briggs et al., 2002; Lyons et al., 2002; Pouliquen et al., 2002). Previous works describing seafloor roughness spectra have reported spectra for spatial frequencies as high as 5 cycles/cm (Briggs et al., 2002). This study uses data derived from SPI profiles allowing estimation of one-dimensional (1-D) roughness spectra within the range of approximately 0.07 cycles/cm (~14 cm) to more than 30 cycles/cm (~0.03 cm).

Fox (1996) used two-dimensional (2-D) spectra to describe seafloor roughness for deep-sea bathymetry based on a four-parameter model, where the two additional parameters provided estimates of anisotropy and peaks in amplitude spectra in addition to slope and amplitude. Lyons et al. (2002) used 2-D spectra from seafloor digital stereo-photos and modeled the roughness using a two-component model that incorporates statistical descriptions of the anisotropic, quasi-periodic sand ripples in addition to the 1-D power law model for isotropic components.

4.3.6. Terminology

Studies using spectral models to describe seafloor roughness have used different methodologies and terminology. Most studies of seafloor spectral roughness assume that roughness can be modeled according to a power law of the form

$$W(k)=\beta k^{-\gamma}$$

Where W(k) represents the power spectral density as a function of spatial frequency (wavenumber), k (cycles per arbitrary length unit), γ represents the spectral exponent, and spectral strength, β, represents the value of the spectrum at a specified reference wavenumber (see Fox and Hayes, 1985; Jackson et al, 1986; Lyons et al, 2002). Similar or equivalent parameters can be found with different names in different studies, for instance w_2 is used to represent spectral strength in the APL-UW (1994) model. The parameters "amplitude proportionality", "spectral strength", "spectral offset", and "spectral intercept" are related. In addition, "spectral slope", "spectral exponent", and "roll-off" are related. The "slope" and "intercept" parameters are from linear models fit by regressing spectral variance on spatial frequency.

Fox and Hayes (1985) and Fox (1996) use amplitude spectra, whereas most other studies use power spectra (amplitude is the square-root of power), and some studies report 2-D spectral parameter estimates, even though they were estimated from 1-D spectra. Therefore, parameter values from different studies cannot be directly compared unless adjusted to common form. Slope parameters are simpler to adjust than intercept or offset parameters because offsets are particular to a specified spatial frequency, usually defined as a spatial frequency of 10^0 = 1-cm. The spatial scales (spatial frequency bands) described in studies of deep-sea bathymetry do not overlap scales represented by seafloor

photographs, and therefore do not share common reference spatial frequency for the intercept or offset parameters. Extrapolation to 1-cm spatial frequency is required to make intercept or offset parameters comparable.

The terms for the spectral parameters estimated here, spectral slope and spectral intercept, were used in accordance with Stanic et al. (1988), Briggs (1989), Stanic et al. (1989), Jackson and Briggs (1992), Jackson et al. (1996), and Briggs et al. (2002). Spectral slope as calculated here is related to the spectral slope parameter of Fox and Hayes (1985), and the spectral intercept parameter reported here is analogous to the proportionality constant (â) of Fox and Hayes (1985). However, â effectively represents an intercept of the amplitude spectrum at a spatial frequency of 1 km, whereas the spectral intercept here represents the power spectrum at a spatial frequency of 1 cm.

APL-UW (1994), Jackson et al. (1986), Lyons et al. (2002), Pouliquen et al. (2002) and Sternlicht and de Moustier (2003) use two-dimensional forms of the spectral slope and intercept parameters, called spectral exponent (γ) and spectral strength (w_2 or β) in accordance with the composite roughness acoustic-backscatter model of Jackson et al. (1986). The two-dimensional spectral parameter values summarized by Sternlicht and de Moustier (2003) were derived from exponents of 1-D spectra from Jackson et al. (1986), Stanic et al. (1988), Briggs (1989), Stanic et al. (1989), Jackson and Briggs (1992), and Jackson et al. (1996). Spectral exponent can be converted from one-dimensional (γ_1) to two-dimensional (γ_2) form by

$$\gamma_2 = \gamma_1 + 1$$

(APL-UW, 1994). The "spectral exponent" in the 2-D form reported in APL-UW (1994) and Jackson et al. (1986) is the negative of the one-dimensional spectral slope value plus one:

$$\gamma_2 = -\text{Slope}_{\text{spec-1D}} + 1.$$

Two-dimensional spectral strength (β_2 or w_2) is a function of one-dimensional spectral strength (β_1) and the 2-D spectral exponent (γ_2), according to:

$$\beta_1 = \pi^{1/2}\Gamma[(\gamma_2-1)/2]\beta_2/\ \Gamma(\gamma_2/2)$$

where Γ is the gamma function (Jackson et al., 1986).

In this study, roughness spectra are estimated for seafloor profiles extracted from the SPI images based on the method described by Briggs (1989). These one-dimensional spectral parameter results could be converted to two-dimensional forms in order to provide spectral parameter estimates in accordance with those used by acoustic models such as Jackson et al. (1986) and APL-UW (1994). This study reports the values of the parameters called here spectral slope and intercept directly estimated from SPI spectra. . The spectral slope parameter effectively relates the relative contribution of low- to high-frequency roughness, such that more negative spectral slope indicates dominance of the low frequencies relative to high frequencies.

4.4. Methods

4.4.1. Study area

Images from nine of the ten SPI stations (Table 4.1) occupied by Cutter and Diaz (2000) were used for spectral roughness estimation. The stations occupied were located

approximately along the shore-normal “Transect S” used during the STRATAFORM-1995 study of the Eel Margin as shown in Figure 4.2.

4.4.2. Images and seafloor profiles

The sediment profile images were collected in December 1995 using a Benthos model 3731 sediment profiling camera and 100 ASA Fuji color slide film. The slides were digitized and seafloor profiles were extracted by manually tracing the sediment-water-interface apparent at the profile camera prism window. Small parts of the interface in the digitized SPI images were magnified in order to maximize resolution. The result of manually tracing the interface was a vector with horizontal- and vertical-dimension coordinates (x,z) that represent a data series with sampling intervals equal to pixel dimensions of 0.014 mm (Figure 4.3). The data series from SPI seafloor profiles were made piecewise continuous by eliminating elevations occurring beneath any overhangs that produced multi-valued series with multiple elevations for a single horizontal coordinate.

4.4.3. Spectral Analysis

The method of Briggs (1989) was used to estimate SPI roughness spectra. Code to process the data and estimate spectra was tested for accuracy and agreement to previous implementations by applying the code to seafloor profile data from stereo photographs used by Briggs (1989) and comparing the results. The method involves “prewhitening” the relative seafloor height data by taking the first differences of the data series (series differenced at lag of one sampling interval), applying a 20 % cosine taper window to the differenced series, calculating an uncorrected periodogram using the magnitude values from a fast Fourier transform of the data, then correcting the

periodogram for the "prewhitening" by a factor of $4\sin^2(\pi f_j \Delta)$, where f is the spatial frequency for interval j=1:N, and N is the number of samples in the series, and Δ is the digitizing interval (Briggs, 1989). The process is demonstrated graphically in Figure 4.4 where prewhitened and corrected spectra are shown. The same methodology has been used by Fox and Hayes (1985), and Jackson and Briggs (1992) to estimate seafloor spectra. Slopes and intercepts of SPI spectra were determined from ordinary-least-squares fit regressions over the entire range of spatial frequencies.

Rather than perform an ensemble average to estimate overall spectral slope of the regression, a weighted mean slope (Slope_wm) value was calculated by the following method:

$$\text{Slope\_wm} = \frac{\sum_{i=1}^{g} \sum_{j=1}^{m} w_i \cdot s_{ij}}{\sum_{i=1}^{g} \sum_{j=1}^{m} w_i}$$

where g represents the number of groups, in this case sampling sites, m represents the number of samples per site, w represents the weight, and s the sample slope. The inverse of the sample variance for each site were used for the weights.

4.5. Results and Discussion

4.5.1. SPI Spectral roughness parameters overall and by site

One image (S95_8-5) contained sea pens (Figure 4.5). The inclusion of the outline of the sea pens as part of the seafloor roughness profile was done only for comparison of such an extreme case to more typical profiles. The sea pens extended about 10 cm vertically from the sediment-water-interface, and had an ornate shape. Most

of the profile of the sea pens was overlapping along the horizontal direction; therefore, the profile data series for the sea pens used for spectral analysis resembled a large vertical spike. Such a representation and the effects upon spectral roughness parameter values was not justifiable for characterization of roughness in terms of hydraulic effects or acoustic backscatter effects. There may be cases where it would make sense to include the faunal profiles as part of the seafloor roughness profile; however, not in this case, because the effect would produce a roughness estimate that does not realistically represent physical quantities affecting acoustic scattering or hydraulic roughness. Therefore, the sea pens were excluded from the seafloor profile for calculation of statistics; however, for the profile including the sea pens the estimates of the spectral slope was -1.775 and the spectral intercept was 0.038 cm^3 (Table 4.2: S95_8-5bio).

Considering all of the individual SPI seafloor profiles, but excluding the outline with the sea pens, spectral slopes ranged from -2.06 to -2.052 (N = 34) and spectral intercepts ranged from 0.00016 to 0.0012 cm^3 (Table 4.2). The unweighted overall mean spectral slope was -2.39 (σ=0.14) and the unweighted overall mean spectral intercept was 0.00027 (σ=0.00017). The overall weighted mean spectral slope was -2.44, and overall weighted mean spectral intercept was 0.0002 cm^3.

One sample profile (S95_1-3) resulted in high values for slope and intercept, and was determined to have a disturbed interface (Figure 4.5). The source of disturbance could not be identified, but those data were excluded from the calculations of the overall statistics. For the disturbed profile from S95_1-3, the spectral slope was -2.052, and the intercept was 0.00118 cm^3 (Table 4.2).

Excluding the disturbed profile (S95_1-3) and the profile containing the sea pen (S95_8-5), the overall range of spectral slopes was -2.06 to -2.046, and the range of spectral intercepts was 0.00016 to 0.00048 cm^3. The profile with the sea pen produced an unusually low (less steep) spectral slope and a high spectral intercept compared to the rest of the observations and to other studies. The disturbed profile produced a relatively high spectral slope, and a spectral intercept that was 2.5 times higher than any of the other undisturbed profiles. Because of this effect, spectra might be a way to detect the presence of disturbance in SPI image interfaces. The unweighted overall mean spectral slope, excluding the sea pens profile and the disturbed profile from S95_1-3, was -2.40 (σ=0.13), and the unweighted overall mean spectral intercept was 0.00024 cm^3 (σ=0.000081).

Mean spectral slopes values by site (N = 9), excluding data from S95_1-3 ranged from -2.55 (σ=0.034; Site 8) to -2.22 (σ=0.23; Site 2) (Table 4.3). Mean spectral intercepts by site ranged from 0.00019 (σ=0.00003; Site 7) to 0.00035 cm^3 (σ=0.00011; Site 8) (Table 4.3).

4.5.2. Roughness parameters by depth and facies

SPI spectral slope values increased approximately linearly with increasing water depth, varying from approximately -2.55 in 30 m to -2.25 in 80 m water depth (Figure 4.6). SPI spectral intercept values decreased from approximately 0.00035 to 0.0002 cm^3 between 30 and 50 m, then increase to 0.0005 cm^3 in 80 m (Figure 4.6).

Several studies have identified distinct sediment facies in the study area, primarily nearshore sands and a mid-shelf flood deposit. Mean SPI spectral slope values became less steep going from sand to transition to flood-deposit region (Figure 4.7). Mean SPI

spectral intercept values were low in the transitional region, and were high in the sand and flood deposit facies (Figure 4.7). The higher spectral intercepts in the sand and flood-deposit regions indicated that the overall magnitude of roughness was higher in those regions compared to the transitional region.

That overall roughness magnitude was higher in the flood-deposit was expected because the deposit was known to be highly bioturbated by infauna (Cutter and Diaz, 2000). Similarly, Cutter and Diaz (2000) reported high RMS roughness for the sand and flood-deposit facies, suggesting that the high RMS in the deposit resulted from bioturbation. However, RMS alone would not distinguish the flood-deposit from the sand facies. Here, we find that although SPI spectral intercepts were not distinguishable between the sand and flood-deposit facies, the SPI spectral slopes were different (significantly at $p=0.05$, according to a Tukey-Kramer HSD test for equivalence of means). Although the sediment grain-size distributions were different between the facies, the individual grains did not comprise the roughness features. Although grains may comprise the roughness features in other geographic locations, here the bedforms and biogenic features comprise the roughness elements. Therefore, for the Eel Margin study area, the relationship between roughness and sediment grain size is not direct.

4.5.3. Possible artifacts and need for comparative studies

The sediment-profile camera is a partially destructive sampling device; it does not extract material, but it does move and compress sediment during deployment. Although the images can usually reveal whether the camera system has disturbed the seafloor, there may be some subtle, systematic, yet unidentified disturbances to the seafloor interface The SPI prism could cause unconsolidated sediment grains to shift or be suspended, and

perhaps cause sediment to bulge as the prism penetrates. To determine the extent of the potential disturbance and impacts on roughness estimates, it would be beneficial to simultaneously collect SPI and plan-view stereo images, so that the stereo images would capture the seafloor interface before and after SPI prism penetration. The SPI sediment-water-interfaces used for this study were apparently intact, and any obviously disturbed interfaces were excluded from analysis. However, it is important to establish whether the small-scale roughness feature distributions described by spectral analysis are natural, and not induced. If the SPI system does cause disturbances and alter the spectra, then accounting and correcting for the disturbances is important.

4.5.4. Anisotropy

Anisotropic roughness occurred in the sand facies in the form of sand ripples. The SPI interface profiles and spectra were not adjusted for orientation relative to the ripples. Some of the SPI profiles were aligned across ripple crests and others were aligned along the ripple-crest strike. The ripple wavelength relative to the spatial frequency band represented by the measured profile will determine how ripples influence the spectrum. In this case, the ripples observed the Eel Margin, inner shelf using SPI had wavelengths on the order of 10 to 15 cm. Those wavelengths represent about half of the lowest frequencies described by the SPI profiles and spectra. Across-strike spectra should have more negative spectral slopes representing a steeper decrease, and along-strike spectra should have less negative spectral slopes. Consequently, by ignoring orientation of SPI profiles in rippled sediments, and averaging spectral parameters over that facies, the roughness for the rippled, anisotropic regions was underestimated.

4.6. Conclusions

The combination of two spectral parameter estimates (slope and intercept) provide a better discrimination of seafloor facies and classification of seafloors than estimates of roughness from vertical elevation differences or RMS deviation. The amount of time required and level of complication involved with generating spectra from SPI profiles and estimating spectral parameters could be worth the expense. Automation of the process would make SPI valuable to more studies.

Spectral roughness estimates were made on 34 SPI images from the Eel Margin. The unweighted overall mean SPI spectral slope, excluding a profile with sea pens and a disturbed profile, was -2.40, and the unweighted overall mean spectral intercept was 0.00024 cm^3. That spectral slope value and its corresponding 2-D spectral exponent of 3.4, and the spectral intercept are within the range reported for published values. The range of SPI spectral slope values (-2.60 to -2.05) suggests that spectral slope (or spectral exponent) should not be considered a constant term for models, even for the spatial frequencies of microtopographical profiles. The relationships between spectral slope and intercept values and physical and biogenic roughness and associated seafloor facies (Figures 6 and 7) suggest that local seafloor zonation and facies distributions should be accounted for when interpreting and applying roughness spectra parameter values.

4.7. Acknowledgements

Invaluable assistance was offered by Kevin Briggs, who provided source code written by D. Percival from which the details of the methodology were determined, as well as comments and suggestions. The sediment profile images were collected for the

STRATAFORM project, December, 1995, sponsored by the Geology and Geophysics Program of the U. S. Office of Naval Research. This work was supported by NOAA grant number NA17OG2285.

4.8. References for Chapter 4

Applied Physics Laboratory, 1994. APL-UW high-frequency ocean environmental acoustic models handbook. Applied Physics Laboratory, University of Washington, Seattle, Washington. Technical Report APL-UW TR 9407, AEAS 9501, October, 1994.

Borgeld, J. C., Hughes Clark, J. E., Goff, J. A., Mayer, L. A., Curtis, J. A., 1999. Acoustic backscatter of the 1995 flood deposit on the Eel shelf. Mar. Geol. 154, 197-210.

Briggs, K. B., 1989. Microtopographical roughness of shallow-water continental shelves. IEEE Journal of Oceanic Engineering, 14 (4), 360-367.

Briggs, K. B., Tang, D., Williams, K. L., 2002. Characterization of interface roughness of rippled sand off Fort Walton Beach, Florida. IEEE J. Ocean. Engin. 27 (3), 505-514.

Cutter Jr., G. R., 1997. Spatial, geostatistical, and fractal measures of seafloor microtopography across the Eel River Shelf, off northern California. MS thesis, College of William and Mary, School of Marine Science.

Cutter Jr., G. R., Diaz R. J., 2000. Biological alteration of physically structured flood deposits on the Eel margin, northern California. Continental Shelf Research, 20, 235-253.

Diaz, R.J., Schaffner, L.C., 1988. Comparison of sediment landscapes in Chesapeake Bay as seen by surface and profile imaging. In: Lynch, M.P., Krome E.C. (Eds.), Understanding the estuary: advances in Chesapeake Bay research. Proceedings of a conference, 29-31 March, 1988, Baltimore, Maryland. Chesapeake Research Consortium publication 129. CBP/TRS 24/88.

Diaz, R.J., Cutter, G.R.,Jr., Dauer, D.M., 2003. A comparison of two methods for estimating the status of benthic habitat quality in the Virginia Chesapeake Bay. Journal of Experimental Marine Biology and Ecology. Vol. 285-286, pp. 371-381.

Dziak, R. P., Matsumoto, H, Fox, C. G. 1993. Estimation of seafloor roughness spectral parameters from multi-beam sonar acoustic backscatter data: Axial seamount, Juan de Fuca Ridge. Geophysical Research Letters, 20, (17), pp. 1863-1866, 1993.

Fox, C. G., Hayes, D. E., 1985. Quantitative methods for analyzing the roughness of the seafloor. Rev. Geophys., 23 (1), 1-48.

Fox, C.G., 1996. Objective classification of oceanic ridge-crest terrains using two-dimensional spectral models of bathymetry: Application to the Juan de Fuca Ridge**.** *Mar. Geophys. Res., 18,* 707–728.

Greaves, R.J. and Stephen, R.A., 2000. Low-grazing-angle monostatic acoustic reverberation from rough and heterogeneous seafloors. J. Acoust. Soc. Am., 108, 1013-1025.

Jackson, D. R.,Winebrenner, D. P., Ishimaru, A., 1986. Application of the composite roughness model to high-frequency bottom backscattering. J. Acoust. Soc. Am. 79 (5), 1410-1422.

Jackson, D. R., Briggs, K. B., 1992. High-frequency bottom backscattering: roughness versus sediment volume scattering. J. Acoust. Soc. Am. 92 (2), 962-977.

Jackson, D. R., Briggs, K. B., Williams, K. L., Richardson, M. D., 1996. Tests of models for high-frequency seafloor backscatter. IEEE Journal of Oceanic Engineering, 21 (4), 458-470.

Lyons, A. P., Fox, W. L. J., Hasiotis, T., Pouliquen, E., 2002. Characterization of the two-dimensional roughness of wave-rippled sea floors using digital photogrammetry. IEEE J. of Oceanic Engr., 27, 3, 515-524.

Matsumoto, H., Dziak, R. P., Fox, C. G., 1993. Estimation of seafloor microtopographic roughness through modeling of acoustic backscatter data recorded by multibeam sonar systems. J. Acoust. Soc. Am., 94 (5), 2776-2787.

Nittrouer, C. A. and Kravitz, J. H., 1996. STRATAFORM: a program to study the creation and interpretation of sedimentary strata on continental margins. Oceanography 9, 146-152.

Pouliquen, E., Lyons, A. P., 2002. Backscattering from bioturbated sediments at very high frequency. IEEE Journal of Oceanic Engineerring, 27 (3), 388-402.

Rhoads, D.C., Cande, S., 1971. Sediment profile camera for in-situ study of organism-sediment relations. Limnology and Oceanography 16, 110-114.

Rhoads, D.C., Germano, J.D., 1982. Characterization of organism-sediment relations using sediment profile imaging: an efficient method of remote ecological monitoring of the seafloor (REMOTS (Trademark) system). Marine Ecology Progress Series 8, 115-128.

Rhoads, D.C., Germano, J.D., 1986. Interpreting long-term changes in benthic community structure: a new protocol. Hydrobiologia 142, 291-308.

Richardson, M. D., Briggs, K. B., Bentley, S. J., Walter, D. J., Orsi, T. H., 2002. The effects of biological and hydrodynamic processes on physical and acoustic properties of sediments off the Eel River, California. Mar. Geol. 182, 121-139.

Stanic, S., Briggs, K. B., Fleischer, P., Ray, R. I., Sawyer, W., 1988. Shallow-water high-frequency bottom scattering off Panama City, Florida. J. Acoust. Soc. Am., 83 (6), 2134-2144.

Stanic S., Briggs K. B., Fleischer P., Sawyer W. B., Ray R. I., 1989. High-frequency acoustic backscattering from a coarse shell ocean bottom. J. Acoust. Soc. Am., 85, 125-136.

Sternlicht, D. D., de Moustier, C. P., 2003. Time-dependent seafloor acoustic backscatter (10-100 kHz). J. Acoust. Soc. Am. 114 (5), 2709-2725.

Wright, L. D., Kim, S. -C., Friedrichs, C. T., 1999. Across-shelf variations in bed roughness, bed stress and sediment suspension on the northern California shelf. Mar. Geol. 154, 99-116.

4.9. Tables for Chapter 4

Table 4.1. Position and depth data for SPI samples (from the Eel shelf) used for seafloor roughness spectral analysis. Stations are listed in order of decreasing water depth.

Station	Rep	#Prof	#Surf	Date	Time(GMT)	Lat (North)		Lon (West)	
1	1	5	6	12/6/95	222443	40	57.801	124	16.927
1	2					40	57.781	124	16.897
1	3					40	57.799	124	16.872
1	4					40	57.797	124	16.87
1	5					40	57.783	124	16.877
1	6					40	57.78	124	16.87
2	1	5	5	12/6/95	231847	40	53.62	124	15.852
2	2					40	53.624	124	15.801
2	3					40	53.619	124	15.801
2	4					40	53.611	124	15.792
2	5					40	53.616	124	15.799
3	1	5	5	12/6/95	233122	40	53.427	124	15.418
3	2					40	53.365	124	15.408
3	3					40	53.364	124	15.395
3	4					40	53.353	124	15.381
3	5					40	53.339	124	15.366
10 *	1	5	5	12/7/95	221223	40	52.977	124	14.822
10 *	2					40	52.954	124	14.825
10 *	3					40	52.951	124	14.822
10 *	4					40	52.953	124	14.827
10 *	5					40	52.947	124	14.841
4	1	5	5	12/6/95	000026	40	52.96	124	14.501
4	2					40	52.968	124	14.483
4	3					40	52.975	124	14.485
4	4					40	52.98	124	14.482
4	5					40	52.974	124	14.476
5	1	5	5	12/7/95	191453	40	53.131	124	13.875
5	2					40	53.123	124	13.894
5	3					40	53.124	124	13.895
5	4					40	53.138	124	13.887
5	5					40	53.148	124	13.867
6	1	5	5	12/7/95	193535	40	52.962	124	13.805
6	2					40	52.968	124	13.785
6	3					40	52.969	124	13.786
6	4					40	52.969	124	13.747
6	5					40	52.967	124	13.746
7	1	5	5	12/7/95	205531	40	51.988	124	13.762
7	2					40	52.001	124	13.771
7	3					40	51.998	124	13.776
7	4					40	51.994	124	13.774
7	5					40	51.995	124	13.769
9	1	1	6	12/7/95	213858	40	52.194	124	12.867
9	2					40	52.188	124	12.851
9	3					40	52.193	124	12.855
9	4					40	52.191	124	12.861
9	5					40	52.179	124	12.864
9	6					40	52.17	124	12.86
8	1	5	5	12/7/95	211642	40	51.651	124	12.723
8	2					40	51.65	124	12.736
8	3					40	51.663	124	12.744
8	4					40	51.663	124	12.746
8	5					40	51.668	124	12.727
TRIPODS									
VIMS(S-70)						40	53.648	124	16.993
VIMS(S-60)						40	53.434	124	15.158
UW(S-60)						40	53.395	124	15.333
USGS(S-50)						40	53.82	124	13.82

* Not included in spectral analysis.

Table 4.2. Roughness spectra model parameter estimates for Eel shelf SPI profiles.

Station	Slope	Intercept (cm^3)
S95_01-1	-2.380	0.00025000
S95_01-3 *	-2.052 *	0.00118000 *
S95_01-4	-2.158	0.00025421
S95_01-6	-2.439	0.00025412
S95_02-2	-2.046	0.00019575
S95_02-4	-2.133	0.00047815
S95_02-5	-2.474	0.00024183
S95_03-1	-2.419	0.00028582
S95_03-2	-2.489	0.00023817
S95_03-3a	-2.277	0.00016344
S95_03-4	-2.322	0.00021014
S95_03-5	-2.391	0.00025567
S95_04-1	-2.422	0.00024346
S95_04-2	-2.314	0.00020017
S95_04-3	-2.383	0.00015731
S95_04-4	-2.414	0.00015514
S95_04-5a	-2.387	0.00018162
S95_05-1	-2.558	0.00024006
S95_05-2	-2.507	0.00022742
S95_05-3	-2.405	0.00020862
S95_05-4	-2.316	0.00015836
S95_05-5	-2.305	0.00017596
S95_06-1	-2.596	0.00038159
S95_06-2	-2.312	0.00028182
S95_06-3	-2.400	0.00015695
S95_06-4	-2.383	0.00016272
S95_06-5	-2.571	0.00031570
S95_07-1	-2.427	0.00017832
S95_07-2	-2.337	0.00017172
S95_07-3	-2.432	0.00023701
S95_08-2	-2.513	0.00021656
S95_08-4	-2.581	0.00041174
*S95_08-5bio	-1.775 *	0.03783437 *
S95_08-5nobio	-2.552	0.00041425
S95_09-1	-2.446	0.00026566

* Excluded from analyses and summary statistic calculations.

Table 4.3. Eel shelf SPI spectral parameters, excluding 1-3 and 8-5bio: mean and standard deviation (σ) by sample site.

Site	N	Slope	σ (Slope)	Intercept (cm^3)	σ (Intercept) (cm^3)	Depth (m)
1	3	-2.326	0.148	0.000253	0.0000024	83
2	3	-2.218	0.226	0.000305	0.0001515	64
3	5	-2.380	0.083	0.000231	0.0000465	60
4	5	-2.384	0.043	0.000188	0.0000364	52
5	5	-2.418	0.113	0.000202	0.0000344	50
6	5	-2.452	0.124	0.000260	0.0000980	48
7	3	-2.399	0.053	0.000196	0.0000359	43
8	3	-2.549	0.034	0.000348	0.0001134	28
9	1	-2.446	.	0.000266	.	36
overall	33	-2.397	0.126	0.000242	0.0000808	

4.10. Figures for Chapter 4

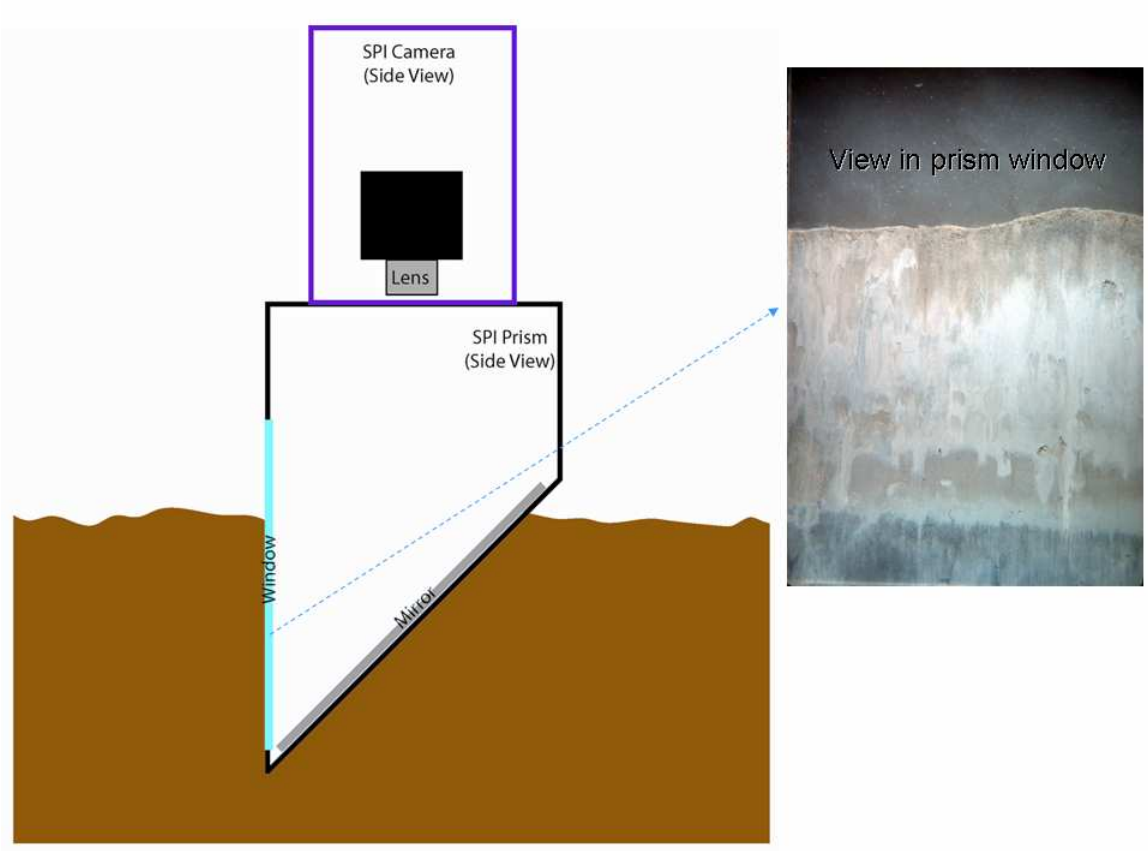

Figure 4.1. Sediment profile imagery (SPI) camera diagram and example image.

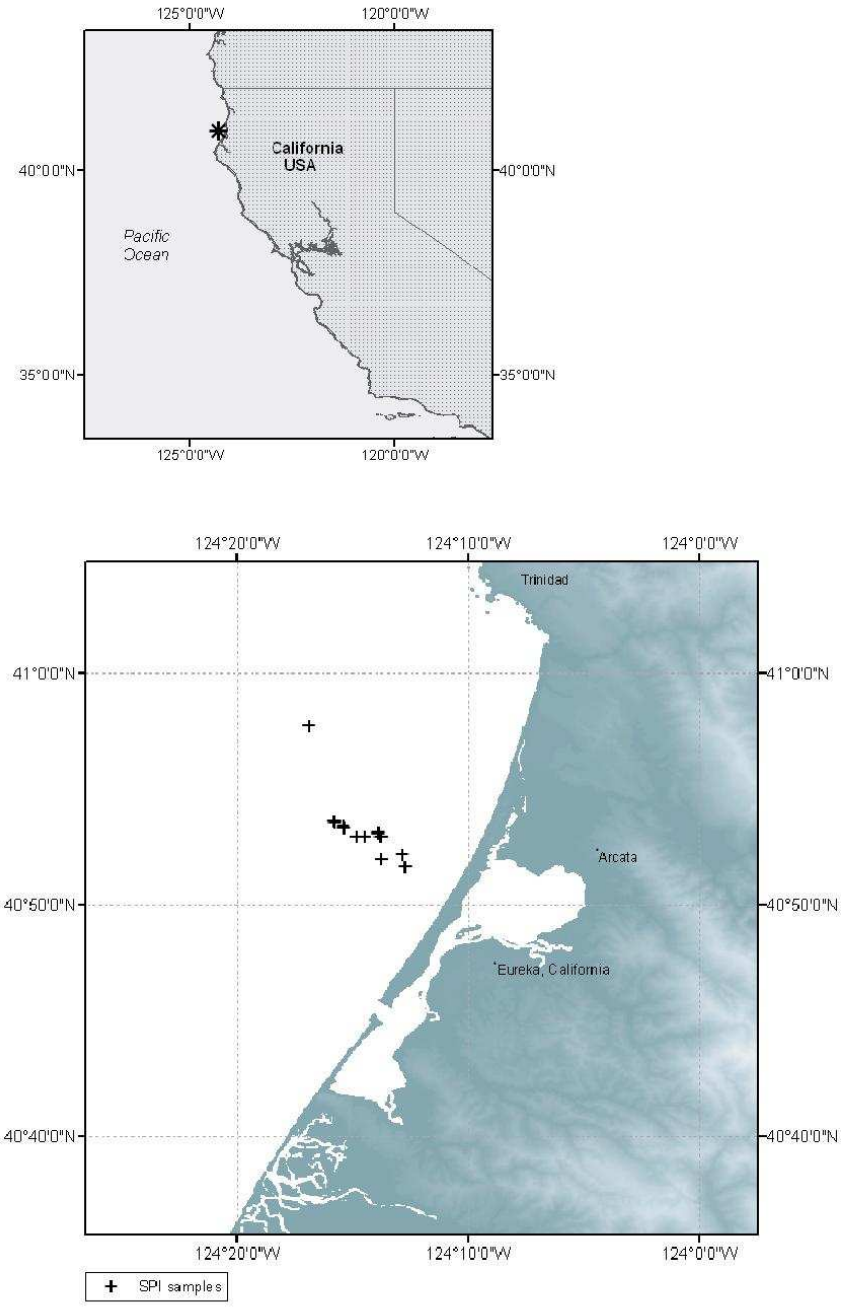

Figure 4.2. Study area off northern California, USA, near latitude , longitude 124 W. Sediment profile image (SPI) transect from the STRATAFORM-1995 study.

Figure 4.3. Example of sediment profile image, manually traced sediment-water-interface seafloor profile, and extracted profile data series obtained by manual tracing.

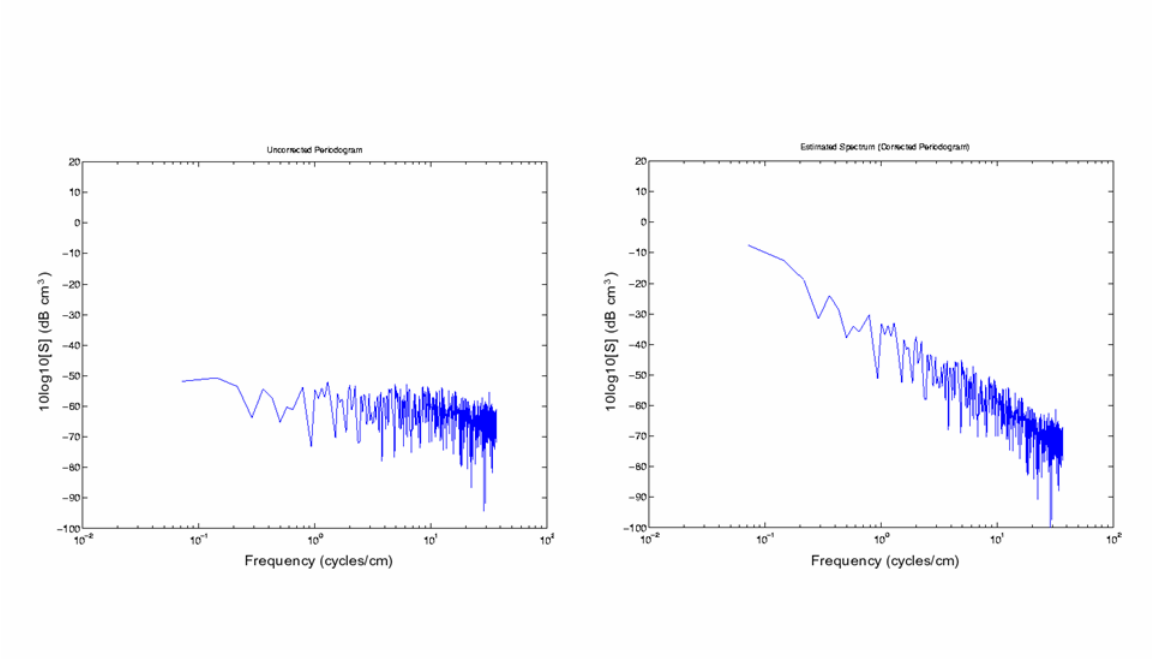

Figure 4.4. Examples of a prewhitened and estimated spectrum (corrected periodogram) from a SPI seafloor profile.

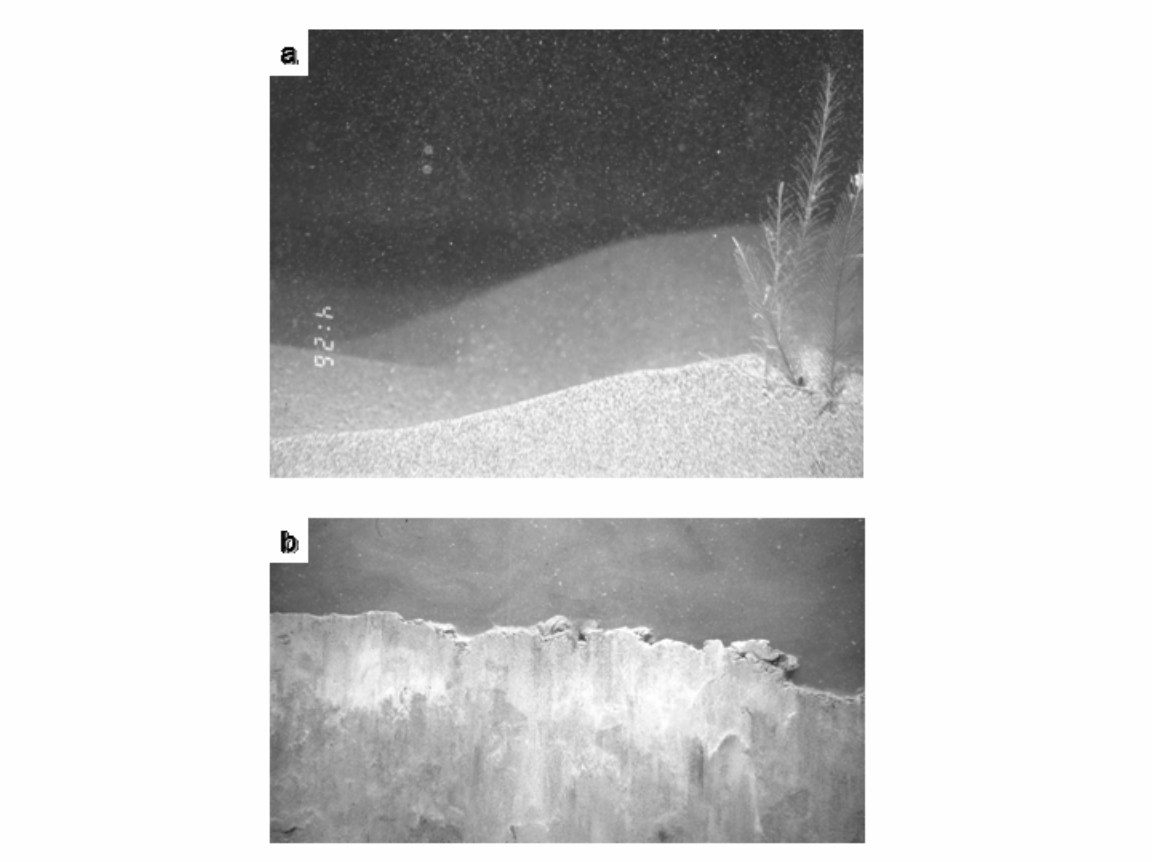

Figure 4.5. SPI images with a) sea pens, and b) disturbed interface.

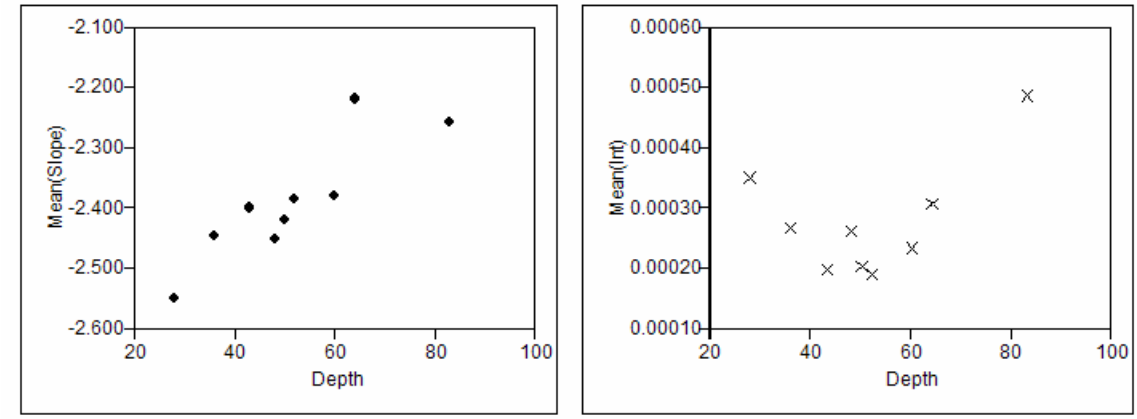

Figure 4.6. SPI spectral roughness parameters, summarized by depth. (a) Spectral slope, and (b) spectral intercept.

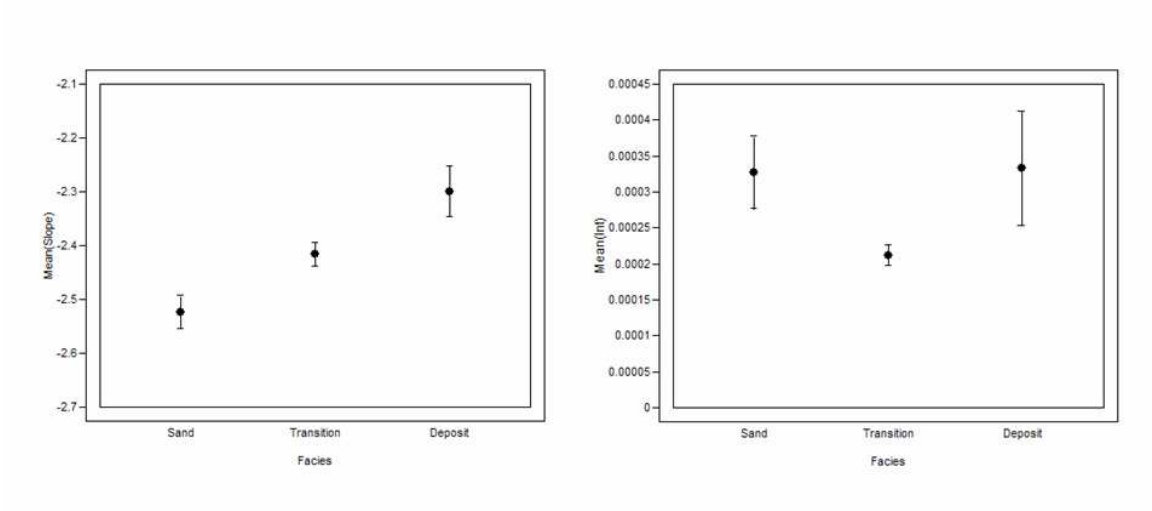

Figure 4.7. SPI spectral roughness parameters, summarized by facies. (a) Spectral slope, and (b) spectral intercept.

CHAPTER 5

5. FACIES FROM THE LOWER PISCATAQUA RIVER (GREAT BAY ESTUARINE SYSTEM) CHARACTERIZED USING PHYSICAL SAMPLES AND VIDEO IMAGES

5.1. Introduction

This chapter explores facies characteristics that may be inferred from multibeam bathymetry and acoustic backscatter data and from mosaiced seafloor video imagery, as discussed in previous chapters. Specifically, this chapter deals with characterizing seafloor facies by grain-size distributions. Sediment grain size often is important to benthic fauna and to acoustic backscatter amplitudes. Although grain size is not the only factor involved in the complex relationships among those phenomena, often it is a primary factor and sometimes grain-size can be used as a surrogate for multiple related factors. It is not specifically grain size that determines what lives in a given area or what the acoustic backscatter will be, but rather grain size or facies type often is directly related to the physical environmental conditions that have the most influence.

Sediment samples and seafloor video images were collected to provide detailed characterizations of facies for ground truthing bathymetric and backscatter data and to develop habitat maps for the lower Piscataqua River (part of the Great Bay Estuary).

Many sites in the Piscataqua River had previously been sampled and mapped by Ward (1995), however only a few samples existed within this study area. Habitat suitability index (HSI) maps had been developed previously by Banner and Hayes (1996); however, only for the upper Piscataqua River and Great Bay Estuary proper.

Fot this study, sediments were characterized using several methods, and comparisons of the results from the different methods were made and sediment grain size distributions were measured from physical samples of the seafloor. Sediment classes were also assigned based on the sample distributions. Sediment classes from video images were assigned based on visual analysis of from locations where physical samples were acquired. Sediment distributions were also estimated from analysis of video images. Comparisons were made between sediment classes determined from physical sample data and image analysis and between distributions estimated from physical sample data and image analysis.

If multibeam bathymetry and backscatter data are to be ground truthed, or empirical models relating acoustic backscatter to sediment properties are to be constructed, or habitat maps are to be developed, then data from multiple approaches to ground truthing should be compatible. It would be beneficial to be able to use the most efficient and cost-effective ground-truthing methods possible. However, if the data from different sources or methods do not agree, or the data are unable to relate the same information, then one method may not be substituted for another. This study shows that agreement between facies characterizations from physical sample and image data can be good, but it is dependent upon the level of detail.

5.2. Methods

5.2.1. Sediment sampling

Sediment samples were collected from the Piscataqua River mouth, east of Newcastle Island, New Hampshire on 04 and 05 September, 2002 from the UNH vessel R/V *Gulf Challenger*. Sample locations were chosen according to a randomized block design. Seven seafloor morphological classes derived from the texture analysis of multibeam bathymetry data within the study area (Cutter et al., 2003) were used as blocks (strata). Ten random positions were chosen within each class using the Minnesota DNR Sample Generator extension for ArcView GIS software (ESRI) (http://www.dnr.state.mn.us/mis/gis/tools/arcview/extensions/sampling/dnrsample.html). If the generated samples appeared to be too close to the edge of a defined class region or if the distribution of samples among the class regions did not appear uniformly random, then samples were regenerated. The locations of two samples within the sand wave field (SWF) were arbitrarily changed so that the SWF would be represented by two samples in the north and two in the south, and with one on the eastern and one on the western sides of the SWF. This was done because the asymmetrical shapes of the megaripple bedforms in the SWF suggested that they were formed by ebb tide currents on the east side of the SWF and flood tide currents on the west side of the SWF. Only a portion of the original study area (Cutter et al., 2003) was sampled. Most samples were allocated within an area bounded approximately with the extent of the data from the Simrad EM3000 multibeam echosounder survey. The sediment sample study area comprised a region bounded by Universal Transverse Mercator (UTM, Zone 19, WGS-1984) coordinates: E 361000, N

4769275 and E 361750, N 4770250 m. Forty sites were visited to collect sediment samples (Figure 5.1).

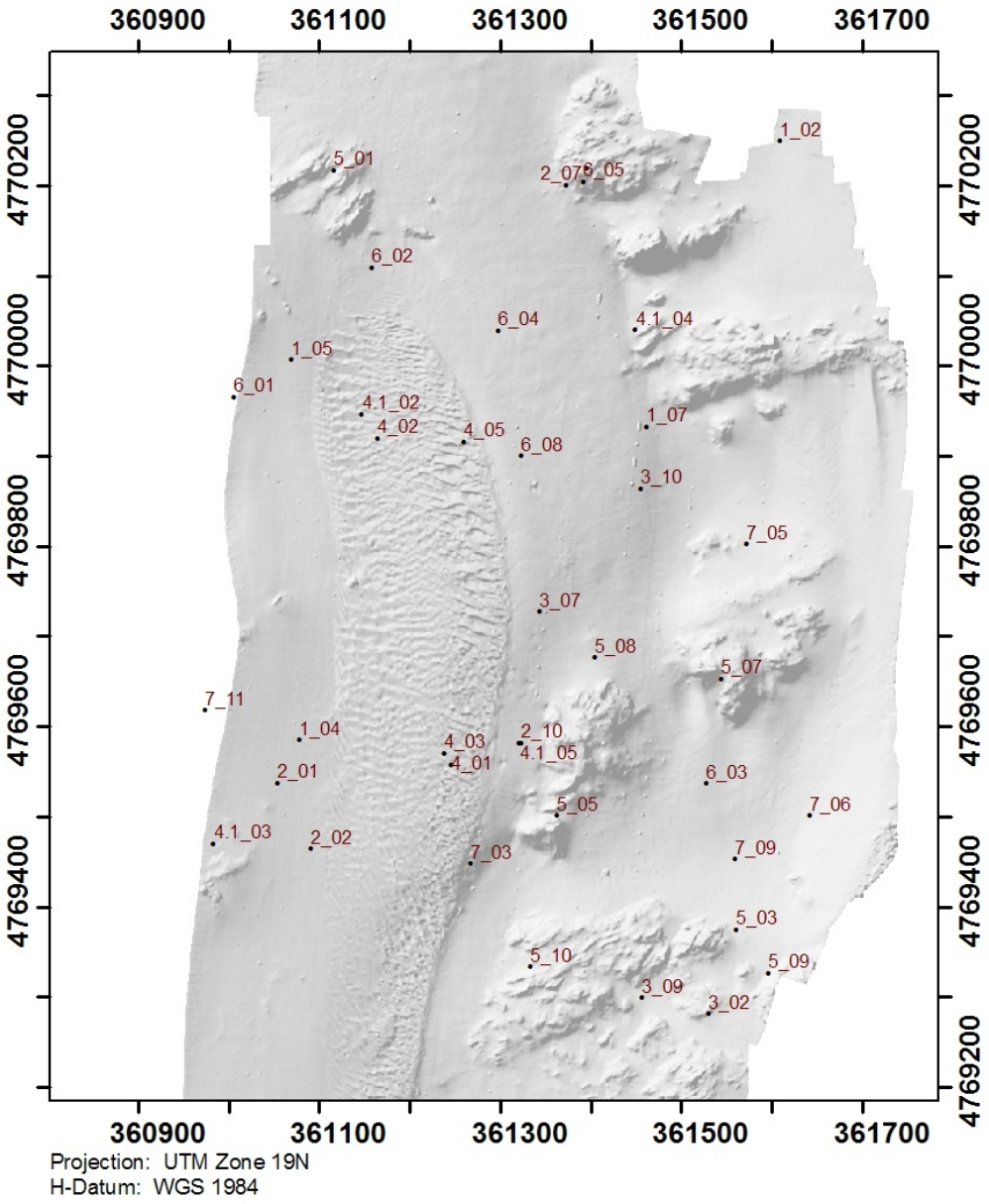

Figure 5.1. Locations of the sediment sample sites collected in 2002 (39 of the 40 sites visited are shown; 03_1 is off the map to the north). Sites are labeled with station identifier; coordinates are UTM, zone 19 north.

At each site, prior to the collection of a sediment sample, a video camera was deployed to the bottom and images were recorded while the camera frame was on bottom, with the camera looking downward. Then, the station was reoccupied by the vessel and a sediment sampler was deployed. Sample station positions from a Raytheon Raystar 398 differential Global Positioning System (DGPS) receiver system were recorded aboard the R/V *Gulf Challenger* (Table 5.1). The DGPS antenna was approximately 8 m aft of the A-frame from which the samplers were deployed.

Table 5.1. Recorded coordinates for sediment sample stations. Coordinates are longitude and latitude (decimal degrees) and UTM Easting and Northing (m).

Sample Code (Cruise-date_ID)	Longitude (degrees)	Latitude (degrees)	Easting (m)	Northing (m)
200209_01_2	-70.69985	43.07233	361609.2	4770249.5
200209_01_4	-70.70622	43.06625	361077.2	4769584.5
200209_01_5	-70.70643	43.07005	361068.1	4770006.8
200209_01_7	-70.70158	43.06945	361461.6	4769932.2
200209_02_1	-70.70650	43.06582	361053.1	4769536.8
200209_02_2	-70.70603	43.06517	361089.7	4769463.9
200209_02_7	-70.70275	43.07185	361372.1	4770200.6
200209_02_10	-70.70320	43.06627	361322.8	4769581.3
200209_03_1	-70.70425	43.07620	361259.7	4770686.2
200209_03_2	-70.70058	43.06360	361529.9	4769280.9
200209_03_7	-70.70298	43.06758	361343.5	4769727.2
200209_03_9	-70.70150	43.06375	361455.6	4769299.0
200209_03_10	-70.70165	43.06883	361454.8	4769863.8
200209_04_1	-70.70415	43.06603	361245.0	4769557.0
200209_04_2	-70.70523	43.06928	361164.1	4769919.7
200209_04_3	-70.70425	43.06615	361237.1	4769570.1
200209_04_5	-70.70407	43.06926	361259.0	4769915.9
200209_04.1_2	-70.70547	43.06951	361145.6	4769946.0
200209_04.1_3	-70.70735	43.06520	360982.5	4769469.7
200209_04.1_4	-70.70177	43.07042	361448.9	4770039.8
200209_04.1_5	-70.70323	43.06627	361320.1	4769581.4
200209_05_1	-70.70590	43.07195	361115.8	4770216.9
200209_05_2	-70.70247	43.07202	361395.5	4770218.7
200209_05_3	-70.70023	43.06445	361560.3	4769374.7
200209_05_5	-70.70270	43.06555	361361.9	4769500.9
200209_05_7	-70.70050	43.06695	361544.2	4769652.8
200209_05_8	-70.70223	43.06713	361403.5	4769676.0
200209_05_9	-70.69978	43.06402	361596.0	4769325.8
200209_05_10	-70.70302	43.06403	361332.7	4769333.0
200209_06_1	-70.70720	43.06967	361004.8	4769965.5
200209_06_2	-70.70537	43.07098	361157.1	4770108.7
200209_06_3	-70.70068	43.06590	361526.9	4769536.5
200209_06_4	-70.70363	43.07038	361296.8	4770039.2
200209_06_5	-70.70252	43.07188	361391.1	4770203.9
200209_06_8	-70.70328	43.06913	361322.5	4769899.8
200209_07_3	-70.70385	43.06505	361267.2	4769447.3
200209_07_5	-70.70020	43.06830	361571.7	4769802.2
200209_07_6	-70.69927	43.06560	361641.6	4769500.8
200209_07_9	-70.70027	43.06515	361559.2	4769452.5
200209_07_11	-70.70750	43.06653	360973.3	4769618.1

Sampling using a box corer had been planned, but because the box corer often failed to recover sediments because of large unconsolidated grains, a Shipek grab sampler was used for most samples. The Shipek grab scoop was 10.2 cm deep, the scoop top was 19.8 cm wide and 19.8 cm long, with a capacity of 3 L. Dimensions of the box corer were 25 by 25 cm (0.0625 m^2). Divers collected cores from two stations using a 10-cm diameter plastic core tube. For diver core collection, divers descended down the video camera cable deployed from the stern of the boat. Prior to the divers collecting the core, they acquired video footage of the seafloor where the core was to be acquired.

Sediment samples were recovered from 33 locations. Of the 33 samples recovered, 3 samples were successfully collected using the box corer, 28 samples were collected using the Shipek grab, and 2 samples were collected by divers (Table 5.2). In order for a sample to be accepted, the general requirement was that the depth of sediment in the device was required to be at least 5 cm, and the surface had to be intact, otherwise the sample was discarded and another acquired. One sample had less than the required depth of material, but was kept anyway because of multiple attempts with little or no recovered material.

Table 5.2. Sediment samples collected by device.

Type	**Count**
Total Sites Visited	40
No Sample	7
Samples Recovered	33
Shipek	28
Box Corer	3
Diver core	2

The identity of one sample could not be confirmed after analysis, and therefore grain size distribution data were produced for 32 of the physical samples collected (Table 5.3).

Table 5.3. List of all grab samples with USGS grain-size analysis data.

N	Cruise ID	Station ID	Sampling Device
1	200209	01_ 2	Shipek
2	200209	01_ 4	Shipek
3	200209	01_ 5	Shipek
4	200209	01_7	Shipek
5	200209	02_1	Box corer
6	200209	02_2	Box corer
7	200209	02_7	Shipek
8	200209	02_10	Shipek
9	200209	03_1	Shipek
10	200209	03_2	Shipek
11	200209	03_10	Shipek
12	200209	04_1	Box corer
13	200209	04_2	Shipek
14	200209	04_3	Shipek
15	200209	04_5	Shipek
16	200209	04.1_2	Shipek
17	200209	04.1_3	Shipek
18	200209	04.1_4	Shipek
19	200209	04.1_5	Diver core
20	200209	05_3	Shipek
21	200209	05_8	Shipek
22	200209	05_9	Shipek
23	200209	06_1	Shipek
24	200209	06_2	Shipek
25	200209	06_3	Shipek
26	200209	06_4	Shipek
27	200209	06_5	Shipek
28	200209	06_8	Shipek
29	200209	07_3	Shipek
30	200209	07_5	Shipek
31	200209	07_9	Shipek
32	200209	07_11	Diver core

Video imagery was acquired at seven additional stations where no physical samples were recovered. At these stations rocks and boulders were observed in the

video, or the sampler failed to recover material. For these seven samples, sediment grain-size distributions were estimated from video images. Table 5.4 relates which samples were subject to which analysis.

Table 5.4. Sources of sediment grain-size data are indicated for each sample station.

Phys or Image Count	USGS Count	Sample_ID	USGS grain-size analysis	Image analysis
1	1	01 2	+	+
2	2	01 4	+	+
3	3	01 5	+	+
4	4	01 7	+	+
5	5	02 1	+	+
6	6	02 2	+	+
7	7	02 7	+	+
8	8	02 10	+	+
9	9	03 1	+	+
10	10	03 2	+	+
11		03_7		+
12		03_9		+
13	11	03 10	+	+
14	12	04 1	+	+
15	13	04 2	+	+
16	14	04 3	+	+
17	15	04 5	+	+
18	16	04.1 2	+	+
19	17	04.1 3	+	+
20	18	04.1 4	+	+
21	19	04.1 5	+	+
22		05_1		+
23		05_2		+
24	20	05 3	+	+
25		05_5		+
26		05_7		+
27	21	05 8	+	+
28	22	05 9	+	+
29		05_10		+
30	23	06 1	+	+
31	24	06 2	+	+
32	25	06 3	+	+
33	26	06 4	+	+
34	27	06 5	+	+
35	28	06 8	+	+
36	29	07 3	+	+
37	30	07 5	+	+
38		07_6		+
39	31	07 9	+	+
40	32	07 11	+	+

Sediment subsamples for grain-size analysis were extracted from each grab sample using a large stainless steel spoon, then stored in plastic bags at room temperature until analysis. The remainder of the sample was prepared for macrofaunal analysis by

washing using seawater on a 500-μm sieve, and fixed with 10 % formalin solution in plastic jars. The samples were transferred from formalin to 95 % ethanol within three days to preserve them.

5.2.2. Sediment Grain Size Distributions from Physical Samples

Analysis of grain-size distribution was performed by the Laboratory of Dr. James Gardner at the USGS Western Region Coastal and Marine Geology Program, Menlo Park, California. Grain size was determined at 0.25-phi intervals. All samples were wet sieved into gravel, sand and fines (silt and clay) fractions, then analyzed as follows:

greater than -1.0 phi (2 mm) ---------- washed, dried and weighed

between 4.0 phi (63 μm) and -1.0 phi (2 mm) ---- settling tubes

less than 4.0 phi (63 μm) ---------- Beckman Coulter laser diffraction.

Menking et al. (1993) describe the USGS grain size analysis methods in some detail. The grain-size statistics for the distribution data from these methods were generated with a USGS program, SDSZ (Pers. Comm., J. Gardner, USGS, 2003). The mean and median grain size, sorting, skewness and kurtosis were calculated using three different methods, those of Folk and Ward (1957), Inman (1962) and Trask (1930). Details of the Inman and Trask statistics can be found in Menking et al. (1993). Details of the Folk and Ward (1957) statistics are provided here. The statistics were originally developed so that they could be estimated from graph analysis, therefore they use percentile values from cumulative distributions of grain-size data in phi units, where the grain size diameter (Φ) is

$$\Phi = -\log_2(D_{mm})$$

where D_{mm} is the grain-size diameter in mm, or, alternatively

$D_{mm} = 2^{-\Phi}$.

Folk and Ward (1957) (FW) grain size statistics are calculated as:

$Mean_{FW} = (\Phi_{16} + \Phi_{50} + \Phi_{84})/3$

$Median_{FW} = \Phi_{50}$

$Sorting_{FW} = (\Phi_{16} + \Phi_{84})/4 + (\Phi_{95} + \Phi_{05})/6.6$

$Skewness_{FW} = (\Phi_{16} + \Phi_{84} - 2*\Phi_{50})/2*(\Phi_{84} - \Phi_{16}) + (\Phi_{05} + \Phi_{95} + 2*\Phi_{50})/2*(\Phi_{95} - \Phi_{05})$

$Kurtosis_{FW} = (\Phi_{95} - \Phi_{05})/2.44*(\Phi_{75} - \Phi_{25})$

where $\Phi_{\#\#}$ represents the grain size in phi units at the ## percentile of the cumulative distribution (Menking et al., 1993). Results from the USGS grain-size analysis are supplied in Appendix B-1. Statistics and moments were recalculated using GRADISTAT (Blott and Pye, 2001) for quality assurance and are included in Appendix B (B-2, B-3).

5.2.3. Sediment classes from physical samples

Two approaches were used in order to have comparable data from physical samples and images. First, sediment grain size distribution data from physical samples were reduced to percentage gravel, sand, silt, clay, and then to sediment class names according to Folk (1954, 1974) and Shepard (1954), using the program SEDCLASS (Poppe et al., 2003).

5.2.4. Sediment classes from seafloor images

Initially, images were described using a sediment class name like those from the Folk's system for mud, sand, and gravel, or Shepard system for sand, silt, and clay, but modified for mud, sand, and gravel, as shown in Poppe et al. (2003). Descriptive class names produced from the images also used modifiers for shell content, so that

descriptions could accommodate all the combinations of mud, sand, and gravel plus shell. Class names were applied based on visual interpretation without specifically measuring any grains or coverage areas in the images. The class names were intended to represent the proportions of the primary component grain sizes that were visible. For instance, sediments in images were classed as sandy gravel when gravels comprised > 50 % (coverage area) and sand comprised 25 % to 49 % of the sediments. The images were analyzed in random order to prevent bias from sequential images that might be similar because of collection order.

5.2.5. Sediment grain-size distributions from images

Because the class names conveyed a relatively crude level of detail, (for instance, sandy gravel encompasses a large range of combinations of sand and gravel), another methodology was applied where percent coverage area was estimated for each visible grain-size class. During analysis of images for estimation of coverage by sediment grain size classes, lines with lengths corresponding to divisions of the Wentworth (1922) grain size scale were displayed on a reference image that was simultaneously displayed (Figure 5.2).

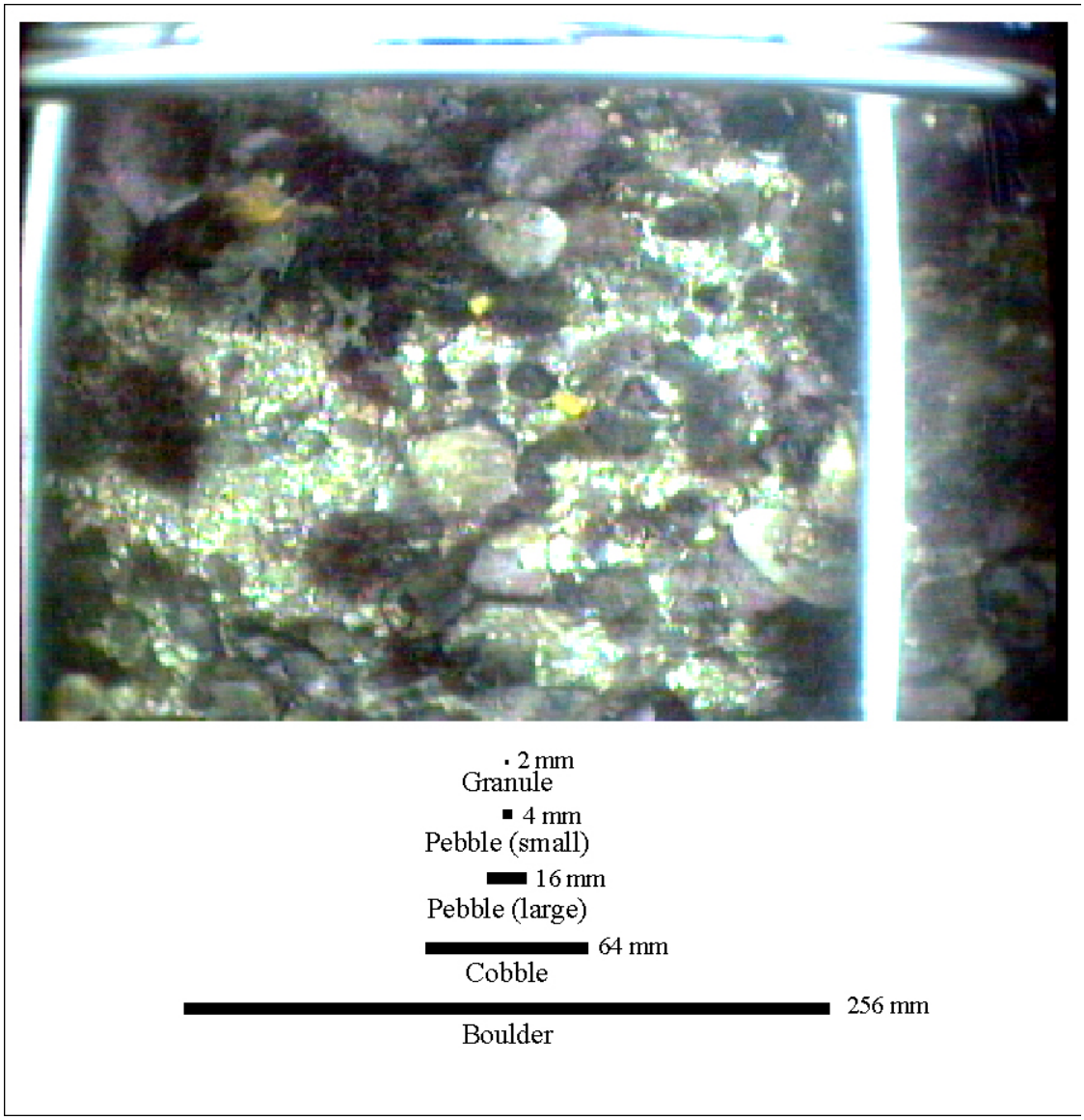

Figure 5.2. Wentworth (1922) size-class scales for grain-size class divisions visible in seafloor video images displayed during analysis for estimating grain-size distribution percent coverage area from images.

Selected grains in the image were measured using a measurement tool calibrated to a known distance, providing an object of known size to gauge others against. Having a measured object in the image facilitated estimation of coverage by size class by allowing visual discrimination of features with respect to an object known to be in a particular size

class. Scales representing bounds for the following grain-size classes were used to gauge sizes of grains and features:

BOULDER

25.6 cm = -8 Phi = Boulder size class lower bound

GRAVEL

6.40 cm = -6 Phi Cobble size class lower bound

1.60 cm = -4 Phi Large pebble size class lower bound

0.40 cm = -2 Phi = Small pebble size class lower bound

0.20 cm = -1 Phi = Granule size class lower bound.

5.2.6. Gravel fraction sediment grain size distributions from physical samples

Because grains in the gravel-fraction size-class were discernible in the images, but gravel fraction (<-1 phi, > 2 mm) had not been separated by USGS, additional processing of the sediments was required. Sediments retained on a -1 phi sieve from the USGS analysis were dried and sieved through a series of screens at 0.5-phi intervals (-1.5 phi to -6 phi). Within each size fraction, biogenic sediments (shells) were separated from lithogenic grains (rocks) and each group was weighed. Any sediments passing through the series of sieves and retained by the collection pan were also separated into shell and rock groups and weighed. The reason for separating shell from rock was that shell material could generally be clearly seen in the images. Even very small (1 mm - 2 mm) shell hash and fragments were often apparent. Shell hash (diameter of 1 mm or less) and larger shell-fragments typically were much easier to discern than lithogenic grains from the same size classes (granule or small pebble) because of their white color and contrast with background material. Shell is considered an important attribute to benthic habitat,

and a significant source of acoustic backscatter, and with potentially different acoustic scattering-effects than rock because of geometrical and mass-density differences.

Shells and rocks in this study area had quite different densities (mass per unit volume). Shells were less dense, but often had large surface areas. Therefore, percentage weight might not be equivalent to percentage coverage area when distributions from samples and images are compared, but are expected to be proportional. Use of either percent weight data or percent coverage data should enable discrimination between facies.

5.3. Results and Discussion

5.3.1. Sediment grain-size distributions from physical samples

Data tables and histograms for physical sample (grab and core) grain-size distributions for each sample are provided in Appendix B (B-4). Sampled sediment grain sizes ranged from almost 100 % sand to 100 % gravel, contained very little mud, and no sample with more than 7 % combined silt plus clay (Figure 5.3 and Table 5.5).

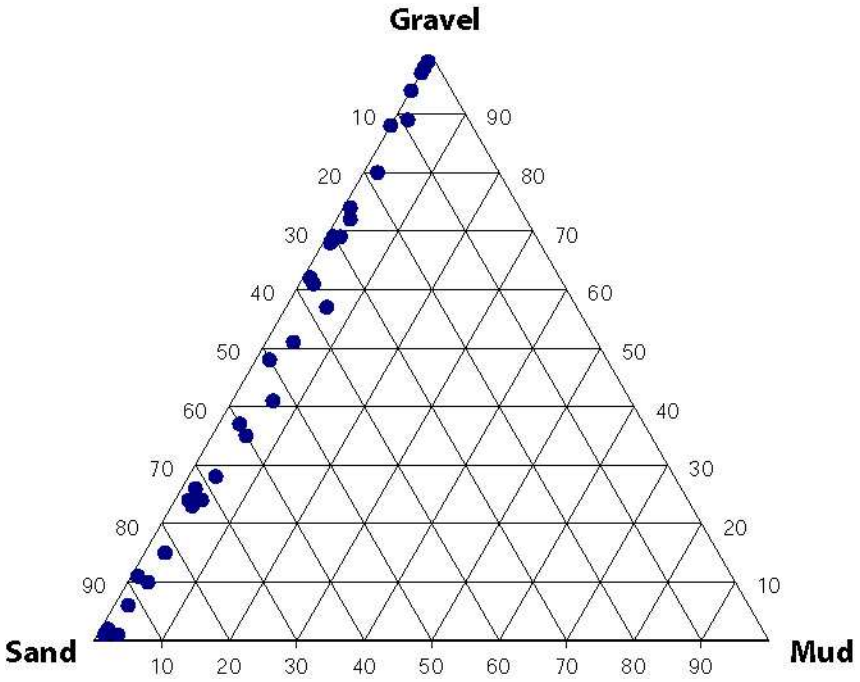

Figure 5.3. Ternary diagram showing the percentages of gravel, sand, and mud for lower Piscataqua River sediments collected 4-5 September, 2002 using a grab sampler or corer.

Median grain sizes for sediment samples based on the Folk and Ward (1957) method ranged from 2.46 phi to -1.12 phi (0.18 mm to 2.17 mm), or fine sand to granule (Table 5.5).

Table 5.5. Grain-size statistics from lower Piscataqua River sediment samples, using Folk and Ward (1957) (FW) method.

StationID	FW Mean (Φ)	FW Median (Φ)	FW Sorting (Φ)	FW Skewness (Φ)	FW Kurtosis (Φ)	FW Mean (mm)	FW Median (mm)
01_2	2.52	2.46	0.33	-0.16	0.79	*0.17*	*0.18*
01_4	1.99	1.82	0.94	-0.48	2.87	*0.25*	*0.28*
01_5	-1.04	0.01	1.43	0.96	0.50	*2.06*	*0.99*
01_7	-1.09	-0.27	1.22	0.96	9.37	*2.13*	*1.21*
02_1	1.99	1.11	1.52	-0.63	0.53	*0.25*	*0.46*
02_2	2.12	2.12	0.33	0.07	1.60	*0.23*	*0.23*
02_7	-1.12	-1.12	0.06	0.47	0.38	*2.17*	*2.17*
02_10	-1.03	-0.06	1.89	0.95	1.03	*2.04*	*1.04*
03_1	-1.01	0.07	1.52	0.95	0.55	*2.01*	*0.95*
03_2	-1.12	-1.12	0.06	0.47	0.38	*2.17*	*2.17*
03_10	-1.07	-0.09	1.32	0.96	0.52	*2.10*	*1.06*
04_1	1.16	1.11	0.78	-0.28	2.26	*0.45*	*0.46*
04_2	1.24	1.28	0.35	0.07	1.32	*0.42*	*0.41*
04_3	1.46	1.48	0.82	-0.14	2.24	*0.36*	*0.36*
04_5	1.22	1.11	0.75	-0.41	2.39	*0.43*	*0.46*
04.1_2	-1.08	-0.47	0.88	0.94	0.87	*2.11*	*1.39*
04.1_3	2.26	1.39	1.75	-0.53	0.72	*0.21*	*0.38*
04.1_4	-1.11	-1.11	0.52	0.50	9.01	*2.16*	*2.16*
04.1_5	-1.05	-0.12	1.28	0.95	0.51	*2.07*	*1.09*
05_3	-1.12	-1.12	0.06	0.47	0.38	*2.17*	*2.17*
05_8	-1.08	-0.25	1.18	0.96	0.82	*2.11*	*1.19*
05_9	-1.05	-0.14	1.36	0.95	0.79	*2.07*	*1.10*
06_1	2.26	2.19	1.03	-0.32	2.33	*0.21*	*0.22*
06_2	-1.12	-1.12	0.40	0.50	7.32	*2.17*	*2.17*
06_3	-1.12	-1.12	0.06	0.47	0.38	*2.17*	*2.17*
06_4	-1.05	-0.29	1.07	0.94	0.5	*2.07*	*1.22*
06_5	-1.07	-0.30	1.08	0.95	0.59	*2.10*	*1.23*
06_8	0.41	0.35	1.23	0.03	0.48	*0.75*	*0.78*
07_3	1.10	0.66	1.32	-0.37	0.49	*0.47*	*0.63*
07_5	-1.07	0.01	1.46	0.96	0.54	*2.10*	*0.99*
07_9	-1.11	-1.11	0.60	0.50	10.5	*2.16*	*2.16*
07_11	1.61	1.08	1.69	-0.29	0.56	*0.33*	*0.47*

Rocks and boulders existed in the study area, but were not directly sampled by the grab or corer. However, the presence of rocks and boulders were inferred if the grab sampler was repeatedly recovered with no sample, or if rocks or boulders were observed in video imagery (Table 5.6).

Table 5.6. Gravel, sand, and mud percent weight data (used for constructing ternary diagram) from analysis of sediment grab samples. A * indicates that rocks or boulders were observed in imagery.

Station_ID	Gravel	Sand	Mud	Rock/Bldr
01_2	0.45	98.12	1.43	
01_4	14.95	81.86	3.19	
01_5	60.44	37.11	2.45	
01_7	80.08	17.72	2.20	
02_1	25.36	72.39	2.25	
02_2	1.08	96.23	2.69	
02_7	98.93	0.87	0.20	
02_10	57.49	36.72	5.79	
03_1	51.70	44.69	3.61	
03_2	98.60	1.02	0.38	
03_7	.	.	.	
03_9	.	.	.	100 *
03_10	68.48	29.49	2.03	
04_1	10.70	88.30	1.00	
04_2	2.77	96.57	0.65	
04_3	6.26	91.76	1.98	
04_5	10.61	88.16	1.23	
04.1_2	72.07	25.87	2.06	
04.1_3	24.63	71.61	3.76	
04.1_4	89.07	9.33	1.60	
04.1_5	61.77	36.92	1.30	
05_1	.	.	.	100 *
05_2	.	.	.	100 *
05_3	97.05	2.78	0.17	
05_5	.	.	.	100 *
05_7	.	.	.	100 *
05_8	74.09	24.62	1.29	
05_9	61.15	37.37	1.48	
05_10	.	.	.	100 *
06_1	10.32	87.09	2.59	
06_2	94.18	5.51	0.31	
06_3	98.35	1.51	0.14	
06_4	61.55	37.49	0.96	
06_5	69.09	30.19	0.72	
06_8	47.77	50.46	1.78	
07_3	37.48	60.00	2.52	
07_5	68.05	31.01	0.94	
07_6	.	.	.	100 *
07_9	87.91	11.97	0.13	

The spatial distribution of the sediment grain-size distributions generally corresponded with expected size classes based on morphological regions evident in the multibeam bathmetry (Figure 5.4) and the sediment map of Ward (1995).

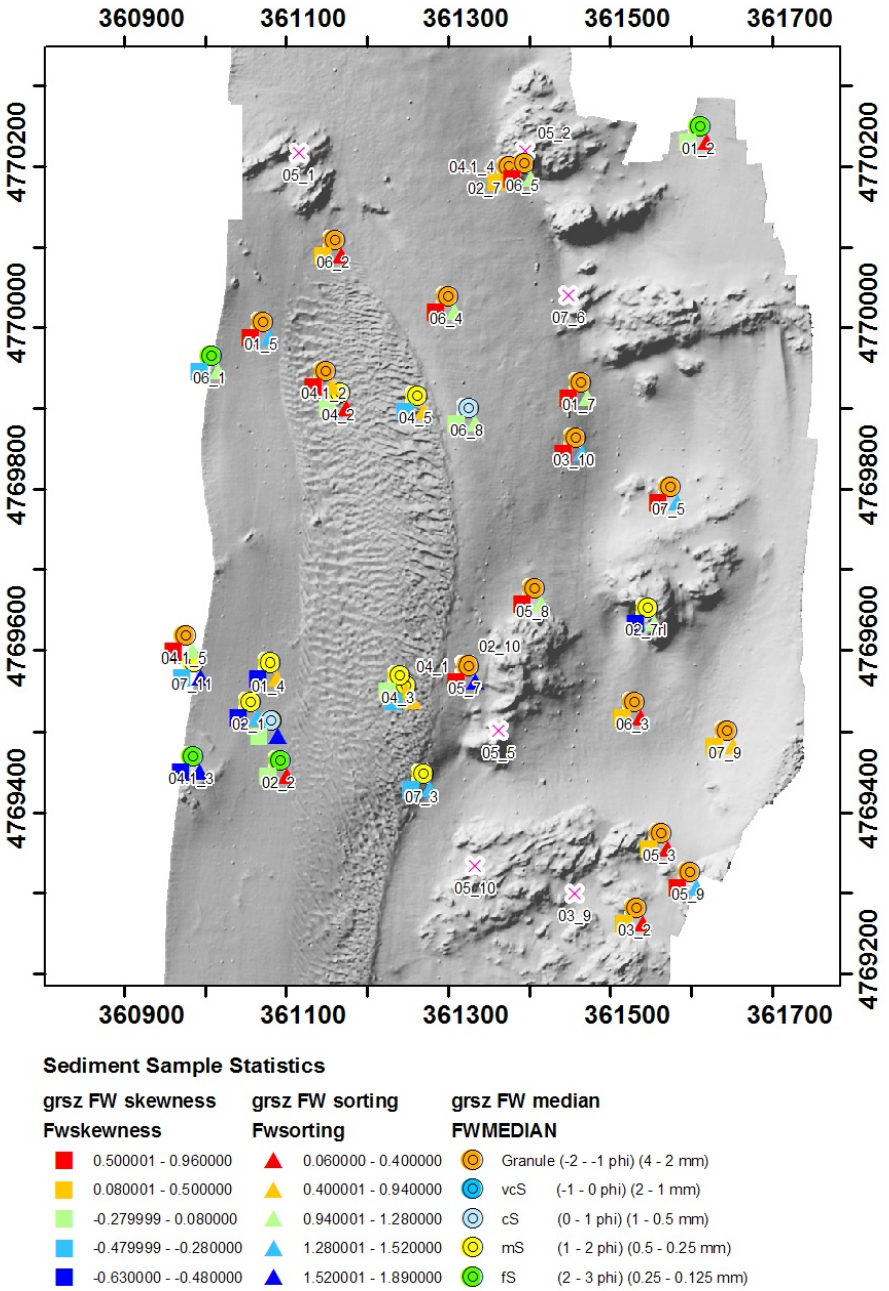

Figure 5.4. Sediment grain-size statistics from analysis of grab samples: median grain size, sorting, and skewness, according to Folk and Ward (1957) (FW) method. In the legend, grsz stands for grain size.

5.3.2. Sediment classes from physical samples

Folk (1954, 1974) and Shepard (1954) sediment class names were generated, using SEDCLASS (Blott and Pye, 2001), from sediment-sample data reduced to percentages of mass for gravel, sand, silt, and clay size fractions (Table 5.7).

Table 5.7. Folk (1954, 1974) and Shepard (1954) sediment class names from percent-mass sediment sample data.

Station_ID	Gravel %	Sand %	Silt %	Clay %	FOLK_CLASS	SHEPARD_CLASS
01_2	0.45	98.12	0.8	0.64	SLIGHTLY GRAVELLY SAND	SAND
01_4	14.95	81.86	1.93	1.26	GRAVELLY SAND	GRAVELLY
01_5	60.44	37.11	1.6	0.85	SANDY GRAVEL	GRAVEL
01_7	80.08	17.72	1.45	0.75	GRAVEL	GRAVEL
02_1	25.36	72.39	1.31	0.94	GRAVELLY SAND	GRAVELLY
02_2	1.08	96.23	1.6	1.09	SLIGHTLY GRAVELLY SAND	SAND
02_7	98.93	0.87	0.17	0.04	GRAVEL	GRAVEL
02_10	57.49	36.72	3.79	2.01	MUDDY SANDY GRAVEL	GRAVEL
03_1	51.7	44.69	2.31	1.29	SANDY GRAVEL	GRAVEL
03_2	98.6	1.02	0.33	0.04	GRAVEL	GRAVEL
03_9	.	.	.	.		
03_10	68.48	29.49	1.17	0.86	SANDY GRAVEL	GRAVEL
04.1_2	72.07	25.87	1.37	0.69	SANDY GRAVEL	GRAVEL
04.1_3	24.63	71.61	2.25	1.51	GRAVELLY SAND	GRAVELLY
04.1_4	89.07	9.33	1.32	0.28	GRAVEL	GRAVEL
04.1_5	61.77	36.92	0.83	0.47	SANDY GRAVEL	GRAVEL
04_1	10.7	88.3	0.63	0.37	GRAVELLY SAND	GRAVELLY
04_2	2.77	96.57	0.47	0.18	SLIGHTLY GRAVELLY SAND	SAND
04_3	6.26	91.76	1.16	0.82	GRAVELLY SAND	SAND
04_5	10.61	88.16	0.74	0.49	GRAVELLY SAND	GRAVELLY
05_1	.	.	.	.		
05_2	.	.	.	.		
05_3	97.05	2.78	0.14	0.03	GRAVEL	GRAVEL
05_5	.	.	.	.		
05_7	.	.	.	.		
05_8	74.09	24.62	0.84	0.45	SANDY GRAVEL	GRAVEL
05_9	61.15	37.37	1.05	0.43	SANDY GRAVEL	GRAVEL
05_10	.	.	.	.		
06_1	10.32	87.09	1.48	1.11	GRAVELLY SAND	GRAVELLY
06_2	94.18	5.51	0.23	0.08	GRAVEL	GRAVEL
06_3	98.35	1.51	0.12	0.02	GRAVEL	GRAVEL
06_4	61.55	37.49	0.69	0.27	SANDY GRAVEL	GRAVEL
06_5	69.09	30.19	0.46	0.26	SANDY GRAVEL	GRAVEL
06_8	47.77	50.46	1.08	0.7	SANDY GRAVEL	GRAVELLY
07_3	37.48	60	1.49	1.03	SANDY GRAVEL	GRAVELLY
07_5	68.05	31.01	0.59	0.4	SANDY GRAVEL	GRAVEL
07_6	.	.	.	.		
07_9	87.91	11.97	0.08	0.05	GRAVEL	GRAVEL
07_11	27.37	68.5	2.6	1.53	GRAVELLY SAND	GRAVELLY

5.3.3. Sediment classes from seafloor images

Folk (1974) grain size classes estimated from the images are reported in Table 5.8. Rock was also included as a class. Shells were only considered in terms of their size class for this dataset. Sand, sandy gravel, gravelly sand, gravel and rock were identified from the images. In addition, a simplified class name was developed by removing modifiers from Folk (1974) class names. For example, sandy gravel was simplified to gravel. Hence, three crude facies classes were applied to the image classification; sand, gravel, and rock. Images used to estimate sediment grain sizes are provided in Appendix B (B-5).

Table 5.8. Folk (1974) and simplified (sand, gravel, rock) sediment classes estimated from visual interpretation of seafloor video images from the lower Piscataqua River. S=sand, G=gravel, R=rock, GS=gravelly sand, SG= sandy gravel.

StationID	Visually-estimated Folk Class	Visually-estimated Folk Class Code	Visually-estimated Simplified (MSGR) Class Code
01_2	Sandy Gravel	SG	G
01_4	Sand	S	S
01_5	Sand	S	S
01_7	Gravel	G	G
02_1	Gravelly Sand	GS	S
02_2	Sand	S	S
02_7	Gravel	G	G
02_10	Gravel	G	G
03_1	Gravel	G	G
03_2	Sandy Gravel	SG	G
03_7	Sandy Gravel	SG	G
03_9	Rock	R	R
03_10	Gravel	G	G
04_1	Sand	S	S
04_2	Gravelly Sand	GS	S
04_3	Sand	S	S
04_5	Gravelly Sand	GS	S
04.1_2	Gravel	G	G
04.1_3	Sand	S	S
04.1_4	Gravel	G	G
04.1_5	Sandy Gravel	SG	G
05_1	Rock	R	R
05_2	Rock	R	R
05_3	Sandy Gravel	SG	G
05_5	Rock	R	R
05_7	*Gravel*	*G*	*G*
05_7	*Rock*	*R*	*R*
05_7	*Gravel*	*G*	*G*
05_7	*Rock*	*R*	*R*
05_8	Gravel	G	G
05_9	Gravel	G	G
05_10	Gravel	G	G
06_1	Gravelly Sand	GS	S
06_2	Gravel	G	G
06_3	Sandy Gravel	SG	G
06_4	Sandy Gravel	SG	G
06_5	Gravel	G	G
06_8	Sandy Gravel	SG	G
07_3	Gravel	G	G
07_5	Sandy Gravel	SG	G
07_6	Gravelly Sand	GS	S
07_9	Gravelly Sand	GS	S
07_11	Gravelly Sand	GS	S

5.3.4. Comparison of sediment classes from physical samples and images

Comparisons of sediment classes estimated from visual analysis and sample data are shown in Table 5.9.

Table 5.9. Comparison of sediment classes estimated from images and physical-samples (+ indicates that the classes were identified as the same; - indicates that classes were identified as different; "." indicates that no comparison was made).

N	StationID	Image	Image Folk Class	Sample Folk Class	Image:Sample Folk Class Comparison	Image Simplified Class	Sample Simplified Class	Image:Sample Simplified Class Comparison
1	01_2	00_1-2	SG	GS	0	G	S	0
2	01_4	01_1-4	S	GS	0	S	S	1
3	01_5	02_1-5	S	SG	0	S	G	0
4	01_7	42_1-7	G	G	1	G	G	1
5	02_1	03_2-1	GS	GS	1	S	S	1
6	02_2	14_2-2	S	GS	0	S	S	1
7	02_7	50_2-7	G	G	1	G	G	1
8	02_10	37_2-10	G	MSG	0	G	G	1
9	03_1	04_3-1	G	SG	0	G	G	1
10	03_2	17_3-2	SG	G	0	G	G	1
11	03_7	36_3-7	SG		.	G		.
12	03_9	45_3-9	R		.	R		.
13	03_10	40_3-10	G	SG	0	G	G	1
14	04_1	06_4-1b	S	GS	0	S	S	1
15	04_2	24_4-2	GS	GS	1	S	S	1
16	04_3	44_4-3	S	GS	0	S	S	1
17	04_5	35_4-5	GS	GS	1	S	S	1
18	04.1_2	23_4.1-2	G	SG	0	G	G	1
19	04.1_3	26_4.1-3	S	GS	0	S	S	1
20	04.1_4	49_4.1-4	G	G	1	G	G	1
21	04.1_5	53_4.1-5	SG	SG	1	G	G	1
22	05_1	27_5-1	R		.	R		.
23	05_2	32_5-2	R		.	R		.
24	05_3	43_5-3	SG	G	0	G	G	1
25	05_5	38_5-5	R		.	R		.
26	*05_7*	*19_5-7*	*G*		.	*G*		.
	05_7	*20_5-7b*	*R*		.	*R*		.
	05_7	*51_5-7c*	*G*		.	*G*		.
27	05_8	39_5-8	G	SG	0	G	G	1
28	05_9	46_5-9	G	SG	0	G	G	1
29	05_10	41_5-10	G		.	G		.
30	06_1	21_6-1	GS	GS	1	S	S	1
31	06_2	28_6-2	G	G	1	G	G	1
32	06_3	29_6-3	SG	G	0	G	G	1
33	06_4	30_6-4	SG	SG	1	G	G	1
34	06_5	31_6-5	G	SG	0	G	G	1
35	06_8	34_6-8	SG	SG	1	G	G	1
36	07_3	18_7-3	G	SG	0	G	G	1
37	07_5	33_7-5	SG	SG	1	G	G	1
38	07_6	48_7-6	GS		.	S		.
39	07_9	47_7-9	GS	G	0	S	G	0
40	07_11	54_7-11	GS	GS	1	S	S	1

Summaries of comparison results for each classification scheme are shown in Tables 5.8, 5.9, and 5.10. Poor agreement existed between Folk (1974) classes estimated from images and samples when modifiers for secondary components were used (e.g. sandy gravel), with 59 % disagreement (Table 5.10).

Table 5.10. Folk (1974) class determined from visual analysis of video compared to Folk class from sediment samples. Listed is the frequency of samples for which classes agreed or disagreed, and percentage (dis)agreement is given in parentheses.

Image:Sample Comparison	Frequency
No Data	11
0 (Different)	19 (59 %)
1 (Same)	13 (41 %)

When shell fragments identified in images were grouped in the gravel size-class, agreement improved only slightly; half of the Folk classes from images and samples agreed (Table 5.11).

Table 5.11. Folk (1974) class, including modifiers, determined from visual analysis of video, accounting for shell fragments in the gravel class, compared to simplified sediment class from sediment samples. Listed is the frequency of samples for which classes agreed or disagreed, and percentage (dis)agreement is given in parentheses.

Image:Sample Comparison	Frequency
No Data	11
0 (Different)	16 (50 %)
1 (Same)	16 (50 %)

Simplifying sediment classes by removing modifiers for secondary components resulted in 91 % agreement between classifications from images and samples (Table 5.12). Hence, when only crude facies classes (such as mud, sand, gravel, and rock) were used, visual interpretation matched results of sediment sample analysis in nearly all cases.

Table 5.12. Simplified-class determined from visual analysis of video compared to simplified sediment class from sediment samples. Listed is the frequency of samples for which classes agreed or disagreed, and percentage (dis)agreement is given in parentheses.

Image:Sample Simplified-Class Comparison	Frequency
No Data	11
0 (Different)	3 (9 %)
1 (Same)	29 (91 %)

A graphical summary of comparisons between sediment classes made from physical sample data and images is shown in Figure 5.5.

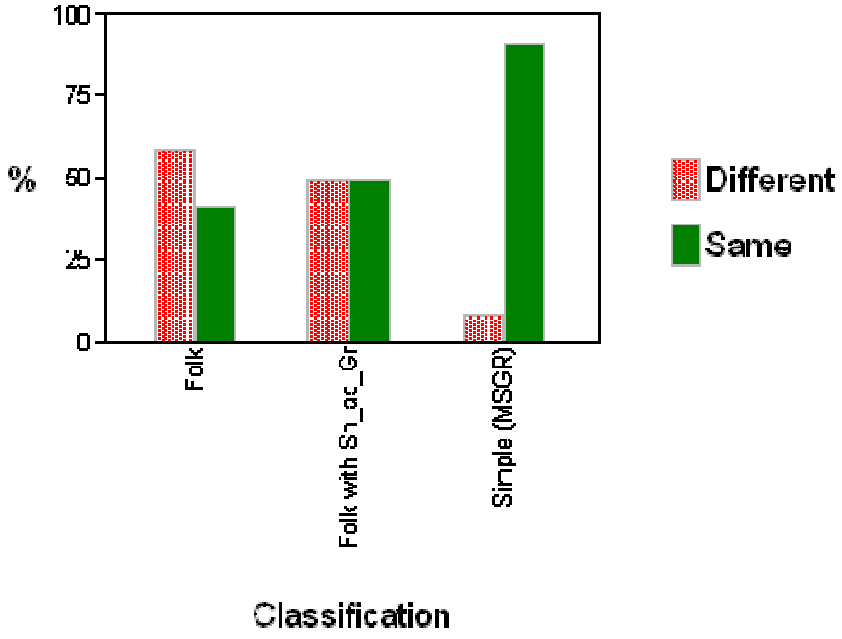

Figure 5.5. Summary of comparisons of sediment classifications made using physical sample data and images. "Folk" is from the classification to Folk class with modifiers, "Folk with Sh_as_Gr" is the classification made where shell hash was considered to be gravel-size, and Simple (MSGR) is the classification to only primary components (mud, sand, gravel, rock).

Better agreement was expected between the classification results from images and samples. It was expected that sandy gravels and gravelly sands would be identified in images with higher rates of accuracy. The low rate of agreement (50 %) could be explained by several possibilities, including actual differences because of local spatial variability (images and samples were not necessarily from the exact same location), poor visual judgment or visual bias, or sediments with close to 50 % sand and 50 % gravel would appear as either sandy gravel or gravelly sand, depending on what was exposed at the interface. Sediments were visually identified in several cases as gravel when analyses

determined that they were sandy gravel, and sand was not evident in the image either because of sparse or low areal-coverage or because of poor image resolution.

5.3.5. Sediment grain-size distributions from images

Sediment grain-size classes with ranges that spanned one to two phi units were used to estimate sediment grain-size coverages from images (Table 5.13). Lithogenic (rock) and biogenic (shell) components were separated for gravel size classes. It was determined that the recombined size classes were visually distinguishable in seafloor video images, either by measuring features in images or visually estimating sizes of grains, or by color and texture.

Table 5.13. Sediment grain-size classes used for analysis of seafloor video images and for comparison with recombined sediment grain size distribution data. For the sediment class name codes, Rk = rock, Bldr = boulder, G = gravel, S = sand, Lith = lithogenic, Sh = shell (biogenic), cobb = cobble, peb = pebble, lg = large, sm = small, grain = granule.

Recombined Size Classes	Recombined Sediment Class Name Codes	Min. Size (Phi)	Max. Size (Phi)	Min. Size (mm)	Max. Size (mm)
Rk.Bldr	Rk.Bldr	NA	-8.0	256	NA
-8.0 to -6.0 Φ (lith)	G_Lith_cobb	-8.0	-6.0	64	256
-5.5 to -4.0 Φ (lith)	G_Lith_peb_lg	-6.0	-4.0	16	64
-3.5 to -2.0 Φ (lith)	G_Lith_peb_sm	-4.0	-2.0	4	16
-2.0 to -1.0 Φ (lith)	G_Lith_grain	-2.0	-1.0	2	4
-8.0 to -6.0 Φ (shell)	G_Sh_cobb	-8.0	-6.0	64	256
-5.5 to -4.0 Φ (shell)	G_Sh_peb_lg	-6.0	-4.0	16	64
-3.5 to -2.0 Φ (shell)	G_Sh_peb_sm	-4.0	-2.0	4	16
-2.0 to -1.0 Φ (shell)	G_Sh_grain	-2.0	-1.0	2	4
-0.75 to 1.0 Φ	S_coarse	-1.0	1.0	0.5	2
1.25 to 4.0 Φ	S_fine	1.0	4.0	0.0625	0.5
> 4.25 Φ	Mud	4.0	14.0	0.00006	0.0625

Coverage areas estimated from video images for each sediment grain size class are shown in Table 5.14. Coverages of lithogenic ("lith") and biogenic ("sh" for shell) materials in the gravel size classes were separately estimated. Rocks or boulders were present in 6 of the 40 images. Mud could not be identified in any images. Previously, analysis of sediment samples did not separate the gravel fractions, but it is clear from the data in Table 5.14 that substantial amounts of gravel in different gravel size classes (cobble, pebble, and granule) existed in the study area.

Lithogenic cobbles were rare, but when present they occupied from 1 % to 31 % of the coverage area (Table 5.14). Large and small lithogenic pebbles were common and occupied substantial coverage areas. Lithogenic granules were sometimes found to cover 1 % to 50 % of the area, but often could not be distinguished. Gravel-sized shell material was commonly present, and was found in all but one image. Cobble-sized shell valves were occasionally present, and covered from 1 % to 5 % of the area. Small and large pebbles and granule-size shell material was common and covered from less than 1 % to 50 % of the coverage area when present (Table 5.14).

Sand was sometimes distinguishable by color or texture patterns, but not necessarily as grains. Mud was not identified in any images. In seafloor video from other study areas mud has been identifiable (by color and texture). At the sites sampled within this study area, grab sample data showed that mud was rare and present in small quantities.

Table 5.14. Percentage of coverage area for each sediment size class estimated from seafloor video images acquired at sediment sample sites. The coverage area percentages sum to 100 % except in cases where the lithology was not determinable in part of the image. (“.” = indeterminate). G = gravel, lith = lithogenic, sh = shell, Rk = rock, Bldr = boulder, cobb = cobble, peb_lg = large pebble, peb_sm = small pebble, grain = granule.

Label	Rk/ Bldr	G_Lith_ cobb	G_lith_ peb_lg	G_lith_ peb_sm	G_lith_ grain	G_sh_ cobb	G_sh_ peb_lg	G_sh_ peb_sm	G_sh_ grain	Sand	Mud
01_02	0	0	10	10	.	0	1	1	1	77	.
01_04	0	0	0	0.1	.	0	1	0.1	0.1	98.7	.
01_05	0	0	5	1	.	0	0	5	5	84	.
01_07	0	0	80	10	.	5	1	1	0.1	0	.
02_01	0	0	0	5	.	0	0	5	1	89	.
02_02	0	0	0	1	50	0	1	1	10	37	.
02_07	0	0	75	9	.	0	5	10	1	.	.
02_10	0	0	10	75	.	0	1	10	3	1	.
03_01	0	0	10	80	.	0	0	1	9	0	.
03_02	0	0	31	31	.	0	2	5	31	.	.
03_07	0	1	1	60	.	0	1	1	1	35	.
03_09	80	0	5	0	.	0	10	0.1	0.1	.	.
03_10	0	0	75	20	.	0	0	1	1	3	.
04_01	0	0	0	0.1	.	0	0	0.1	40	59.8	.
04_02	0	0	0	1	10	2	0	10	25	52	.
04_03	0	0	0	0	1	0	0	1	10	88	.
04_05	0	0	0	0	40	0	0	1	10	49	.
04.1_02	0	0	72	25	.	0	1	1	1	.	.
04.1_03	0	0	0	0.1	.	0	1	1	1	96.9	.
04.1_04	0	0	88	10	.	0	1	1	.	.	.
04.1_05	0	0	25	25	10	0	2	10	10	20	.
05_01	75	.	.	.	.	.	.	.	.	.	.
05_02	85	5	0	0	.	0	0	1	9	0	.
05_03	0	0	50	1	.	0	20	1	1	25	.
05_05	99	0	0	0	.	0	0	0	1	0	.
05_07	100	0	0	0	.	0	0	0	0	0	.
05_08	0	0	90	1	.	0	1	2	3	3	.
05_09	.	0	30	30	.	0	1	30	.	.	.
05_10	50	10	10	10	1	0	5	3	3	0	.
06_01	0	0	0	1	.	1	25	10	10	53	.
06_02	0	31	33	33	.	0	0	1	1	1	.
06_03	0	0	50	38.9	.	0	0	1	0.1	10	.
06_04	0	.	50	25	.	0	0	1	1	10	.
06_05	0	0	49.5	49.5	.	0	0	0	1	0	.
06_08	0	0	60	20	.	0	10	1	1	5	.
07_03	0	0	10	25	.	0	1	10	50	4	.
07_05	0	0	1	48.9	.	0	1	0.1	0.1	48.9	.
07_06	0	0	5	10	.	0	5	1	1	88	.
07_09	0	0	10	10	.	0	0	1	0	79	.
07_11	0	0	1	30	1	0	1	1	1	65	.

Figures of the grain size coverage data shown in Table 5.14 are provided in Appendix B (B-6).

5.3.6. Gravel-fraction sediment grain-size distributions from physical samples

The initial grain size analysis of sediment samples did not separate the gravel size class fraction (grains with diameters > 2mm, or < -1 Φ). Because many of the samples from this study area contained substantial proportions of gravel-sized sediment, the grain-size distributions often contained a well-separated sand fraction and a large single value representing the gravel fraction, such as in the example from sample 200209_02_10 (Figure 5.6).

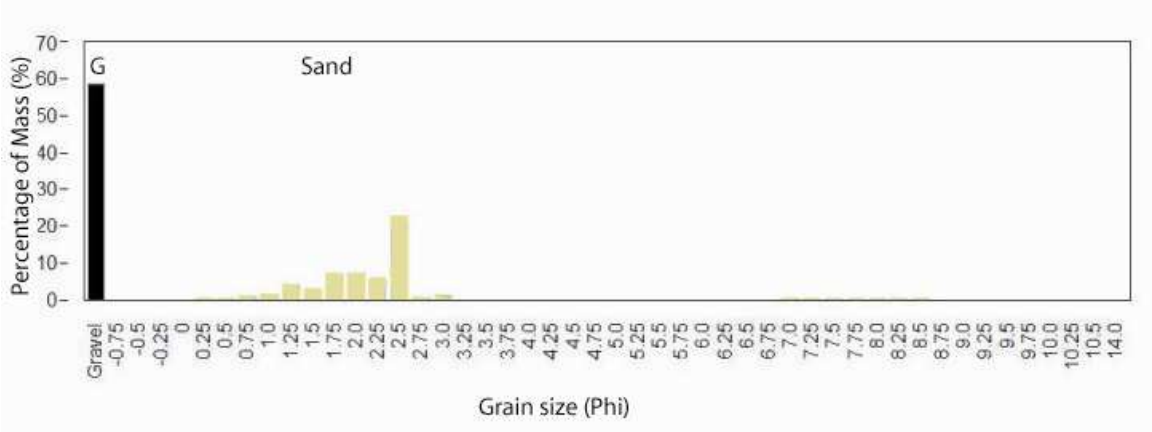

Figure 5.6. Example of grain-size distribution from original analysis of sediment samples. Percentage of mass is plotted. Sand is shown as gold, gravel (retained on a -1 phi sieve), labeled as G, is shown as black.

Most of what could be visually identified from seafloor video images was gravel-sized sediment. Therefore, the gravel fractions from the samples were separated by dry sieving. An example of the result (for the same sample as in Figure 5.6) is shown in Figure 5.7.

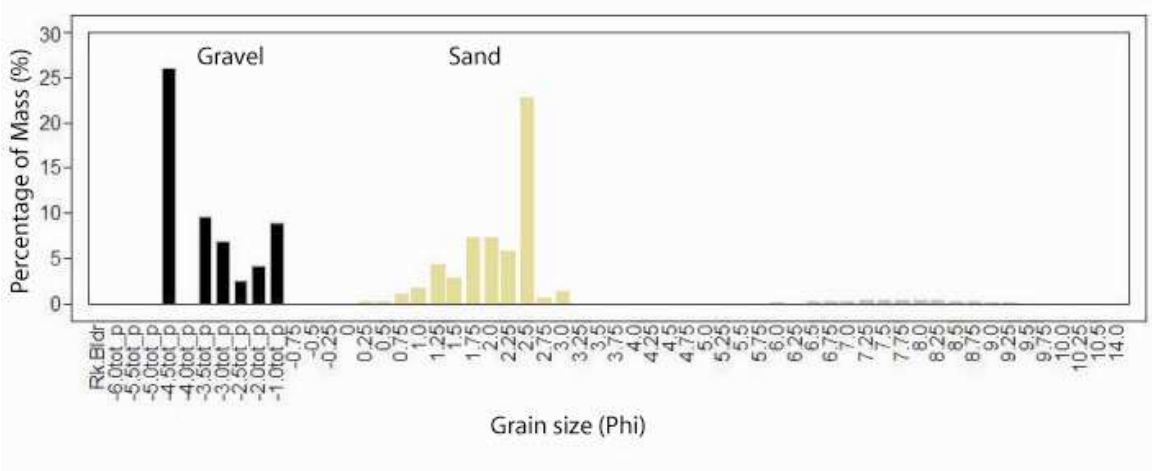

Figure 5.7. Sediment distribution plot after including the separated gravel fraction. Sand is shown as gold, gravel is shown as black.

In addition to separating the gravel fraction, the lithogenic and shell materials were separated for each of the gravel size class intervals (-1 to – 6 Φ), producing a distribution such as that shown in Figure 5.8.

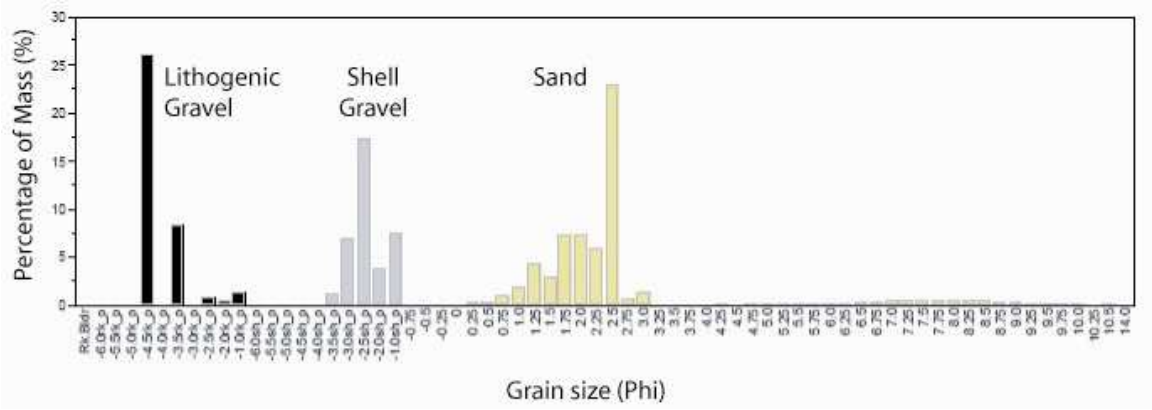

Figure 5.8. Histogram of sediment grain-size data showing percent weight data for separated gravel size classes for lithogenic (black) and shell (gray) materials. Sand and mud size-class data are also shown (gold).

Because most of those size class intervals could not be distinguished visually, the size classes were recombined into classes with the 1 to 2 phi intervals shown in Table 5.13. That resulted in size class distributions like the one shown in Figure 5.9.

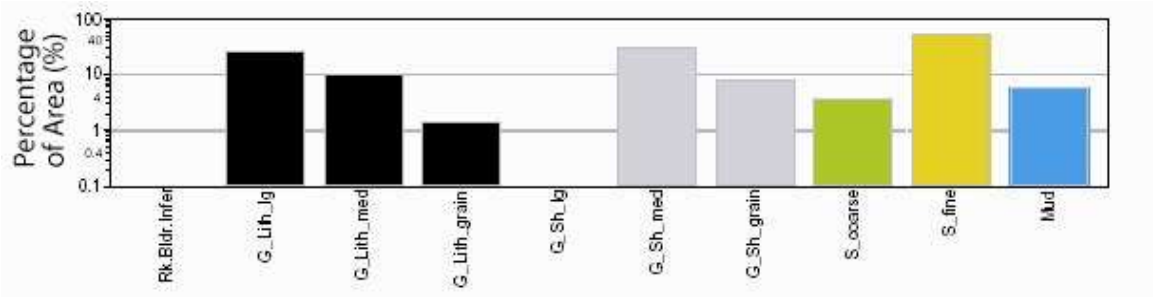

Figure 5.9. Sediment grain size grab sample data histogram using the recombined size classes that could be distinguished visually and were also used for grain-size distribution data from images.

The sediment grab-sample grain-size data resulting from the recombined scheme are summarized in Table 5.15.

Table 5.15. Percentage of weight (mass) for each recombined sediment size class estimated from grab, corer, or diver core sample data. "." = no data, G = gravel, lith = lithogenic, sh = shell, Rk = rock, Bldr = boulder, cobb = cobble, peb_lg = large pebble, peb_sm = small pebble, grain = granule.

Station	Rock Bldr Inferred	-8.0 to -6.0 Φ G lith Cobb	-5.5 to -4.0 Φ G lith Peb_lg	-3.5 to -2.0 Φ G lith Peb_sm	-2 to -1.0 Φ G lith Grain	-8.0 to -6.0 Φ G sh Cobb	-5.5 to -4.0 Φ G sh Peb_lg	-3.5 to -2.0 Φ G sh Peb_sm	-2 to -1.0 Φ G sh Grain	-.75 to 4.0 Φ Sand	> 4 Φ Mud
01_2	0	0	0	0	0	0	0	0.23	0.23	98.12	1.42
01_4	0	0	0	5.44	0.50	0	0	6.23	2.77	81.85	3.22
01_5	0	0	57.76	0	0.13	0	0	1.36	1.29	37.09	2.44
01_7	0	0	59.57	14.19	1.11	0	0	2.50	2.70	17.71	2.21
02_1	0	0	0	19.57	2.86	0	0	1.08	1.82	72.37	2.25
02_2	0	0	0	0.16	0.27	0	0	1.45	1.12	96.22	2.75
02_7	0	0	96.67	0.91	0.07	0	0	0.73	0.60	1.75	0.43
02_10	0	0	26.09	9.85	1.41	0	0	29.40	7.61	56.73	5.79
03_1	0	0	13.26	23.71	2.50	0	0	6.54	5.59	44.70	3.62
03_2	0	0	95.99	0	0	0	0	1.57	1.02	1.00	0.36
03_7	.	.	.	.	.	.	.	.	.	.	.
03_9	100	.	.	.	.	.	.	.	.	.	.
03_10	0	0	39.18	22.71	1.61	0	0	2.07	3.27	28.73	2.00
04_1	0	0	0	0	1.29	0	0	2.51	6.89	88.31	1.01
04_2	0	0	0	0.12	0.13	0	0	0.30	2.15	96.58	0.82
04_3	0	0	0	0.19	0.19	0	0	0.87	4.87	91.78	1.98
04_5	0	0	0	0.21	0.42	0	0	1.98	7.98	88.16	1.24
04.1_2	0	0	0	56.23	11.24	0	0	1.44	3.26	25.87	2.06
04.1_3	0	0	7.11	9.58	2.81	0	0	0	0.52	71.62	3.70
04.1_4	0	0	48.14	35.60	1.29	0	0	1.22	2.66	9.36	1.60
04.1_5	0	0	32.07	24.43	1.22	0	0	2.13	1.97	36.93	2.00
05_1	100	.	.	.	.	.	.	.	.	.	.
05_2	100	.	.	.	.	.	.	.	.	.	.
05_3	0	0	93.82	2.79	0.10	0	0	0.11	0.20	2.66	0.25
05_5	100	.	.	.	.	.	.	.	.	.	.
05_7	100	.	.	.	.	.	.	.	.	.	.
05_8	0	0	43.58	25.24	2.48	0	0	1.53	1.63	24.63	1.27
05_9	0	0	18.93	25.83	11.25	0	0	2.42	2.40	37.35	1.47
05_10	100	.	.	.	.	.	.	.	.	.	.
06_1	0	0	0	4.03	0.24	0	0	3.33	2.68	81.86	2.58
06_2	0	0	95.68	0	0.14	0	0	0.21	0.52	5.53	0.32
06_3	0	0	83.03	14.04	1.32	0	0	0.19	0.14	1.53	0.14
06_4	0	0	49.30	7.58	1.92	0	0	0.15	0.27	37.48	0.95
06_5	0	0	52.43	12.02	3.11	0	0	0.39	1.30	30.21	0.89
06_8	0	0	22.86	18.06	4.54	0	0	0.49	1.92	50.44	2.40
07_3	0	0	13.64	8.36	4.64	0	2.75	2.66	5.39	60	2.53
07_5	0	0	49.04	17.61	0.75	0	0	0.28	0.47	31.00	1.20
07_6	100	.	.	.	.	.	.	.	.	.	.
07_9	0	0	78.57	9.41	0	0	0	0	0	11.96	0.08
07_11	0	0	0	15.79	10.13	0	0	0.89	0.61	68.49	4.13

Using the recombined size class scheme, results from analysis of sediment samples could be compared to results from analysis of images. Side-by-side plots comparing the

sediment data from samples to images in Table 5.14 and Table 5.15 are provided for all samples in Appendix B (B-6).

5.3.7. Comparison of sediment grain size distributions from physical samples and images

Sediment size-class distributions estimated from analysis of seafloor imagery resembled recombined distributions measured from the gravel-separated grab samples. It is clear from the graphs that agreement between sediment size class distributions determined from both methods is good, although not for all samples. Note that grab sample data represent percent mass and image data represent percent coverage area and, therefore, identical numbers should not be expected. Also note that analysis of video images for sediment distribution was done independent of, and without reliance on, sediment grab sample results. Figure 5.10 shows examples for one sample site.

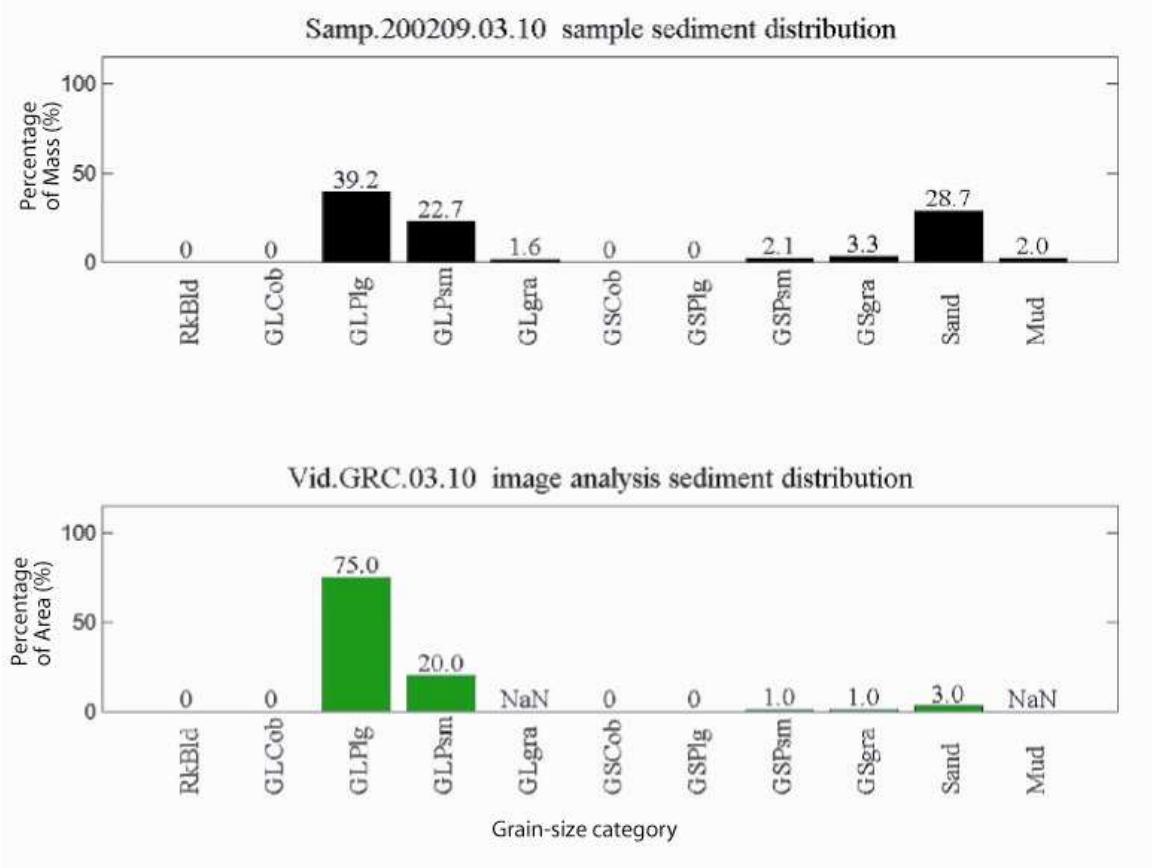

Figure 5.10. Example of comparison between sediment grain size distribution from grab sample to sediment distribution estimated using a video image from station 3-10. Numeric labels represent percentages: percentage of mass for sample, and percent cover for image. NaN represents no data. The categories represent: (RkBld) Rock or Boulder, (GLCob) lithogenic gravel in cobble range, (GLPlg) lithogenic gravel in large pebble range, (GLPsm) lithogenic gravel in small pebble range, (GLgra) lithogenic gravel in granule range, (GSCob) gravel-sized biogenic shell cobble range, (GLPlg) gravel-sized biogenic shell in large pebble range, (GLPsm) gravel-sized biogenic shell in small pebble range, (GLgra) gravel-sized biogenic shell in granule range, (Sand) all sediments in the sand size classes, (Mud) all sediments in the silt and clay size classes.

Despite that apparent good agreement existed between data from physical samples and images based on visual inspection of the graphs, it is desirable to place a quantitative descriptor on how well sediment size class distributions estimated from analysis of seafloor imagery resemble distributions measured from grab samples. Use of such a

statistic was not intended to determine whether the estimates represented the same seafloor data, but rather to provide some quantitative assessment of how well the data from different sources agreed and how well one type of data might be expected to predict the other. An insignificant value for a chi-square statistic might simply mean that the test did not apply. Because the grab sample and image sample were not simultaneously acquired, some differences could be explained by spatial variability of properties due to positional differences during reoccupation of the station. Alternatively, visual bias could have been the cause.

5.3.8. Goodness of fit, distance, similarity

Chi-square and Kolmogorov-Smirnov (KS) goodness-of-fit tests were reviewed for applicability to the task. The KS test and the chi-square test are non-parametric (Zar, 1984). Although it was calculated for these comparisons, the chi-square test is probably not appropriate for comparing these data for several reasons. The data represent percentages (percent weight and percent cover). Zar (1984) warns that chi-square statistic calculated from converting frequency data to percentages is not valid; however, it is unclear whether this applies to data that begin as percentages. There are many categories with missing data or low percentages (<5 %) and, therefore, the chi-square statistic would be suspect in these cases. The KS test is probably more appropriate for the data and also is calculated for assessing agreement.

5.3.9. Distances, Similarity, and Dissimilarity measures

5.9.1.3. Bray-Curtis similarity and dissimilarity

Bray-Curtis similarity is often employed by ecologists, usually for grouping or ordination of biological community data. Bray-Curtis similarity is generally considered equivalent to Sorensen's index (Gallagher, 1998). The original formulation of Bray-Curtis similarity (BCs) (Bray and Curtis, 1957) is the form used by COMPAH96 (Gallagher, 1998), a popular clustering package.

$$BCs = 2*SUM(\min(x_j,x_k)) / SUM (x_j+x_k)$$

where x_j is the physical-sample data-array, x_k is the image data-array, i and j range from 1:n, SUM represents summation over the length (n) of the array, and min stands for minimum.

Here, the Bray-Curtis dissimilarity (BCd) is used, where

$$BCd = 1 – BCs.$$

Alternatively, the Bray-Curtis dissimilarity index (BCd) can be found in the form:

$$BCd = SUM(abs(x_j-x_k) / SUM (x_j+x_k)$$

where abs stands for the absolute value, and multiplication by 2 is not included.

5.9.2.3. Euclidean distance

The Euclidean distance (D_Eucl) between two vectors, x and y, is

$$D\_Eucl = [SUM(x_i-y_i)^2]^0.5$$

where i is number of dimensions, or variables, contained by each vector.

In matrix form, Euclidean distance between vectors X and Y is the norm of X-Y

$$D\_Eucl = || X-Y ||$$

which is equivalent to

$$D\_Eucl = [(X-Y)^2]^{0.5}$$

The squared Euclidean distance is

$$D\_Eucl2 = [X-Y]^T[X-Y]$$

where T indicates the transpose. Euclidean distances are not standardized and, therefore, may be uninterpretable if the variables are measured in different units. In such a case, it is desirable to adjust for the effects of different scales or units by standardization.

5.9.3.3. Mahalanobis Distance

A related distance, the Mahalanobis Distance (D_Mahal), compensates for unequal variances (that can be introduced by different units) between variables, and uses the covariance matrix for standardization:

$$D\_Mahal = [X-Y]^T[C]^{-1}[X-Y]$$

(modified from Davis, 1986) and C is the covariance matrix for X and Y.

There are not straightforward ways to assign probability of occurrence to distances or dissimilarities (such as the Euclidean, Bray-Curtis, and Mahalanobis) in order to assess whether the observed value exceeds some threshold for acceptance. The analyst must judge how to categorize the values if a decision is to be made about whether the data agree or not. Often, minimum distance criteria are applied to determine group membership based on a distance/dissimilarity value. However, in this case, I am trying to assess agreement between data from samples and images. It is preferred to judge against some standard, rather than arbitrarily deciding on a threshold value. Therefore, two statistical tests are applied: the chi-square and Kolmogorov-Smirnov goodness of fit tests.

5.9.4.3. Chi-square statistic

The Chi-square test statistic is calculated as:

$$X^2 = \sum_{j=1}^{k} \frac{\left(O_j - E_j\right)^2}{E_j}$$

for the jth class of k classes, using image data as O (observed), sample data as E (expected). If the value of E was equal to zero, then 0.5 was added. A chi-square test was performed, comparing the calculated X^2 to X^2 critical for 10 degrees of freedom at a probability level of 0.05 (X^2crit_a:0.05,df:10 = 18.307). A chi-square statistic value that exceeds critical value is considered significant at that probability level. The probability level of 0.05 suggests that 1 in 20 times (5 %), a larger than the critical value could occur by chance. Significance of the chi-square statistic generally suggests that the null hypothesis, that the two distributions are the same, can be rejected. However, caution should be used in the interpretation of significance in this case because of the differences between the data and the questionable validity of chi-square test for these data.

5.9.5.3. Kolmogorov-Smirnov test

A Kolmogorov-Smirnov (KS) test for continuous data was performed as another way to assess agreement between the sediment distributions from the samples and the images. The KS test is a non-parametric goodness-of-fit test designed specifically for ordered categories (Zar, 1984). The sediment size class data are organized in ordered categories; therefore, the KS test seems appropriate. The KS test statistic represents the maximum value of the deviation (difference) between the observed cumulative

distributions and the theoretical (or specified) cumulative frequency distribution (cfd) (Zar, 1984). Often, the KS test is used to determine whether data are normally distributed (or Poisson, or logistic, etc.). In these comparisons between image and physical sample data, the image data represent the observed and the sample data are used as the specified distribution.

5.3.10. Summary of Agreement Assessment

Euclidean distance and Bray-Curtis dissimilarity between sediment sample distribution and image distribution vectors relate how well the data from two different analyses agree. Table 5.16 contains values of Euclidean distance and Bray-Curtis dissimilarity for all samples with good paired data, i.e., where both grab samples and video image samples existed and both represented trusted data.

Table 5.16. Euclidean distance (D_Eucl), Bray-Curtis dissimilarity (BCd), Chi-square statistic value (ChiSq) and significance for sediment distribution data vectors from separate analysis of grab sample and images.

Sample_ID	BC_Dissim	Euclid_D	ChiSq	ChiSqSig	KS_D	KS_p	KS_sig
1_02	0.23	25.5	456.7	Sig	0.364	0.461	NS
1_04	0.18	19.2	22.2	Sig	0.364	0.461	NS
1_05	0.55	70.8	133.7	Sig	0.182	0.993	NS
1_07	0.28	28.1	93.5	Sig	0.364	0.461	NS
2_01	0.21	22.8	31.6	Sig	0.273	0.808	NS
2_02	0.61	77.9	3356.7	Sig	0.182	0.993	NS
2_07	.	.	.	.	.	.	
2_10	0.71	89.7	503.9	Sig	0.273	0.808	NS
3_01	0.60	72.4	188.8	Sig	0.364	0.461	NS
3_02	0.66	78.1	2659.7	Sig	0.364	0.461	NS
3_07	.	.	.	.	.	.	
3_09	.	.	.	.	.	.	
3_10	0.36	44.3	59.7	Sig	0.364	0.461	NS
4_01	0.33	43.8	166.7	Sig	0.273	0.808	NS
4_02	0.45	52.0	543.3	Sig	0.364	0.461	NS
4_03	.	.	.	.	.	.	
4_05	0.42	55.7	1764.9	Sig	0.182	0.993	NS
4.1_02	0.73	83.5	10571.2	Sig	0.364	0.461	NS
4.1_03	0.26	28.3	38.5	Sig	0.364	0.461	NS
4.1_04	.	.	.	.	.	.	
4.1_05	.	.	.	.	.	.	
5_01	0.14	25.0	11.0	NS	0.091	1.000	NS
5_02	0.15	18.2	251.1	Sig	0.273	0.808	NS
5_03	.	.	.	.	.	.	
5_05	0.01	1.4	9.0	NS	0.091	1.000	NS
5_07	0.00	0.1	5.2	NS	0.091	1.000	NS
5_08	0.49	56.8	99.3	Sig	0.273	0.808	NS
5_09	.	.	.	.	.	.	
5_10	0.48	53.3	801.4	Sig	0.636	0.023	Sig
6_01	0.38	39.7	1351.8	Sig	0.273	0.808	NS
6_02	0.66	77.5	4276.9	Sig	0.364	0.461	NS
6_03	0.34	42.2	102.0	Sig	0.182	0.993	NS
6_04	0.27	32.6	66.8	Sig	0.182	0.993	NS
6_05	0.38	48.3	148.1	Sig	0.364	0.461	NS
6_08	0.52	59.8	328.2	Sig	0.182	0.993	NS
7_03	0.69	74.2	456.5	Sig	0.273	0.808	NS
7_05	0.50	60.1	118.7	Sig	0.273	0.808	NS
7_06	.	.	.	.	.	.	
7_09	.	.	.	.	.	.	
7_11	.	.	.	.	.	.	

The values of D_Eucl and BC suggest moderate agreement overall between sample and image estimates for percent weight and percent cover of sediment grain size classes, with a large range of distances and dissimilarities, and apparently several pairs with large disagreement (Figure 5.11).

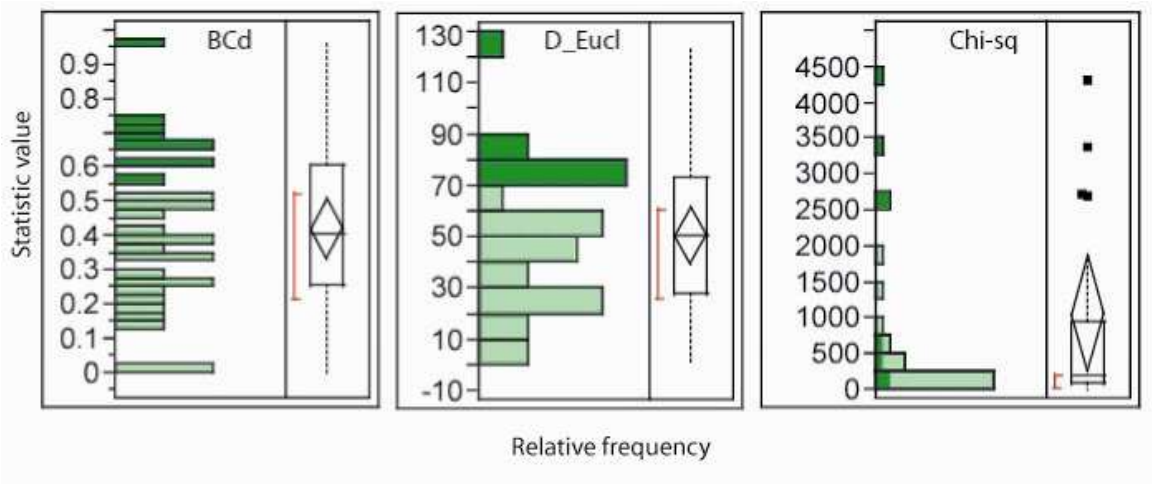

Figure 5.11. Distributions of Euclidean distance (D_Eucl), Bray-Curtis dissimilarity (BCd), and Chi-square statistic.

D_Eucl and BCd generally related the same relative information about agreement between samples. Dark bars in Figure 5.10 represent where D_Eucl > 70 %. In most of these cases, there is also high BCd (> 0.55).

Chi-square statistic values for all samples (except 3 from rock/boulder facies) exceeded chi-square critical value for 10 degrees of freedom (df). Those results should be considered cautiously. First, it is not clear that the chi-square test is valid for these data. Second, the data represent different attributes: percent mass, and percent coverage area. Standardization might be required; for example, for samples such as 05_02 that was inferred to have 100% rock or boulder by weight, because a sample was not recovered,

and 85% coverage of rock/boulder was observed in the image, the resultant chi-square statistic value exceeded the critical chi-square value.

According to the KS test done using the CRAN-R statistical analysis software (Ihaka and Gentleman, 1996), only one station had different distributions: Station 5_10 (where no sample was recovered and, therefore, 100% rock/boulder inferred, but the image revealed rock, cobble, and large pebbles). Thus, the chi-square test suggested that nearly all distributions disagreed, but the Kolmogorov-Smirnov test suggested that nearly all of them agreed.

The distance/dissimilarity statistics should probably only be used to judge relative agreement between sample and image sediment distribution data. What becomes very clear is that the chi-square statistic should not be calculated for data with cells containing zeros or when many cells contain low values. For frequency data, usually a warning that chi-square test is suspect is issued if >20 % of the cells contain counts < 5; that occurred frequently with these samples. For these data, we hope that we have Type 1 statistical errors (erroneously rejecting the null hypothesis).

5.3.11. Geographic explanation?

Recall that the samples and images were not simultaneously acquired and not necessarily at exactly the same locations. Therefore, the above results suggest a hypothesis that where the largest differences occurred (large D, BC, or X^2) we might expect to find more heterogeneous, variable spatial distributions. Examination of the bathymetry or backscatter data might be able to support the expectation based on evident morphology and backscatter variation. We can also test the hypothesis by examining video transect data. If actual spatial heterogeneity is not the cause, then what is the

cause? Perhaps there is something about the sediment sample that does not get discriminated by visual interpretation or perhaps the visual classification was erroneous because the grains were incorrectly identified by visual examination. There were eight samples where D > 70 % (Table 5.17).

Table 5.17. List of sampled stations where sediment distributions from grab sample and image analysis had large differences (Euclidean distance > 70 %).

Sample_ID	Euclid_D
01_5	70.84
02_10	89.69
02_2	77.90
03_1	72.38
03_2	78.11
04.1_2	83.46
06_2	77.46
07_3	74.17

Highlighting the samples where D > 70 % on the bathymetry data provides only some support for explaining the differences based on spatial location or proximity to transitions (Figure 5.12). Approximately half of these samples were located near a strong morphological transition, or within a morphological region characterized by large roughness features. The green circles are where better agreement existed, and red asterisks are where agreement was relatively poor.

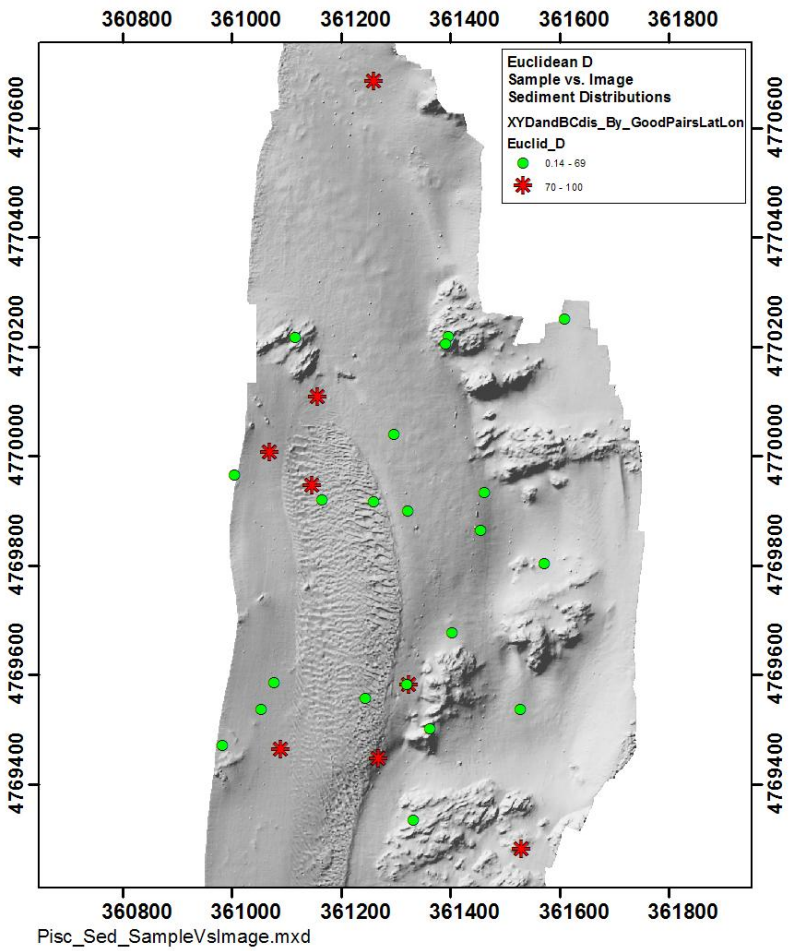

Figure 5.12. Locations where large Euclidean distances resulted between sediment distributions estimated from grab samples and images.

Placing some of the paired sediment distributions on the map for selected samples labeled with relative level of agreement can help determine whether differences were related to geographic distributions of attributes (Figure 5.13). Categories levels describing level of agreement were: best ($D<25$; $0.3 < BCdis < 0.5$), good ($25 < D < 42$; $0.51 < BCdis < 0.55$), moderate ($42 < D < 55$; $0.56 < BCdis < 0.66$), low ($56 < D < 70$; $0.67 < BCdis < 0.74$), and poor agreement ($D > 70$; $0.75 < BCdis < 0.82$)

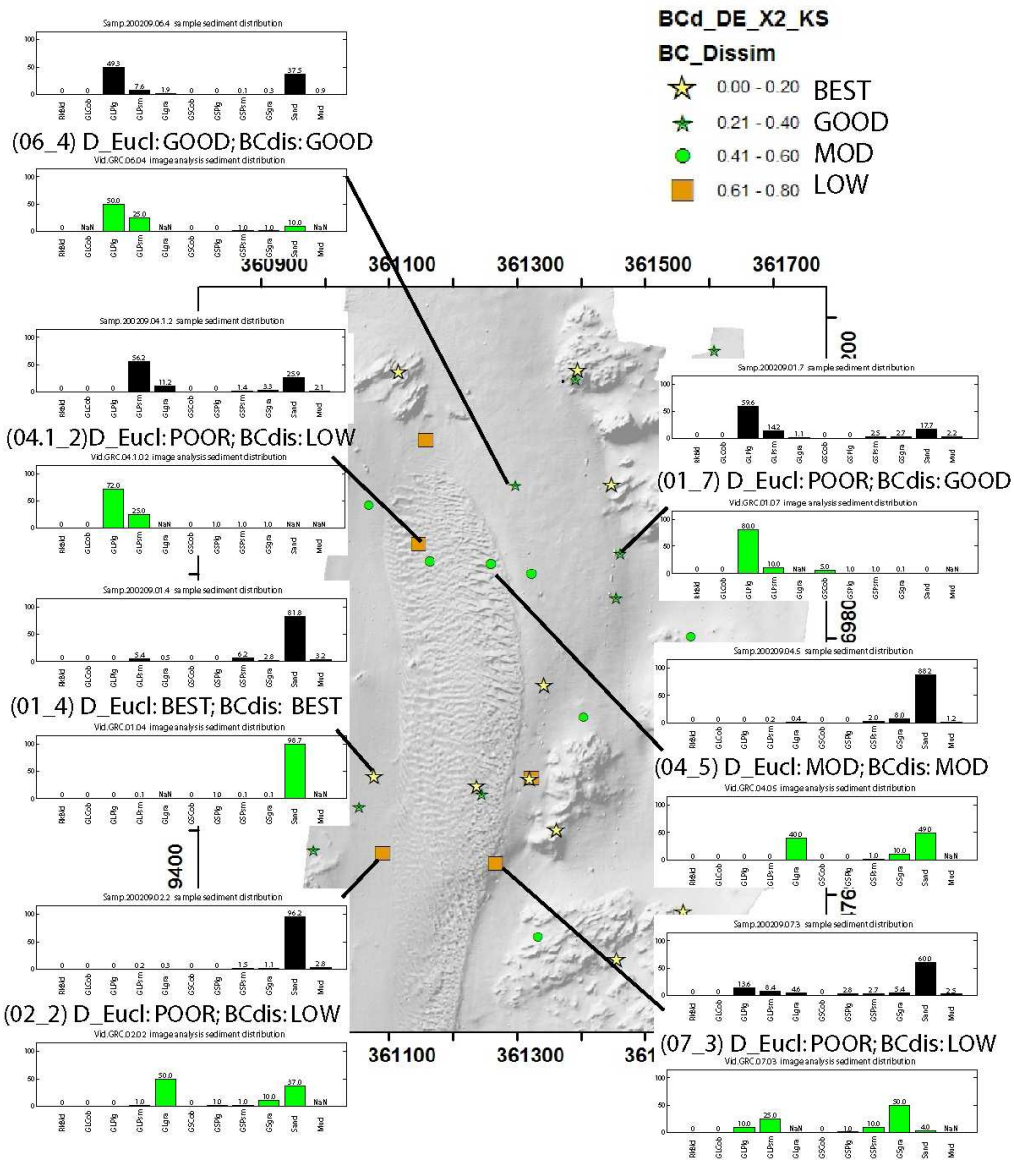

Figure 5.13. Sample stations colored by Euclidean distance between sediment distributions estimated from grab samples and from images. Examples of the distributions estimated and the relative quality of their agreement are shown for selected stations. Sample data are in the upper plots (black) and image analysis data are in the lower plots (green).

Categorizing relative agreement according to the ranges observed for the dissimilarity and distance measures seems overly strict. If the grain-size distributions from images and physical samples were offset by a value in only one size-class, then the agreement could

be categorized as poor based on relative dissimilarity. This categorization allows no flexibility in the interpretation of sediment grain size from images. For instance, if the grains were judged as being large pebbles rather than small, and coarse sand was deemed to be granule, then agreement might be "low" or "poor" according to distance or dissimilarity measures. However, most of the cases with "low" or "poor" agreement were considered to be reasonably good. It can be seen in Figure 5.13 that "low" or "poor" agreement sometimes resulted from differences in adjacent size-class categories (where grain size had been estimated visually to be one class smaller or larger than what the sample contained). For instance, consider distributions from 07_3: the grab sample analysis distribution determined 60 % sand (by mass), and the image analysis distribution was 50 % in the class representing shell in the granule size class (G_Sh_grain: 2 – 4 mm). Perhaps what appeared to be granule-sized shell hash in the image was actually sand-sized material. Perhaps sand was misidentified as shell hash in the image. Perhaps local spatial variation existed and both distributions were accurate.

All of the sample-*versus*-image sediment grain size histogram plots are provided in Appendix B.

5.4. Conclusions

Estimating percent coverage area for each grain size class from seafloor video imagery requires much more time and effort than assigning a class name by estimating an overall modal grain size from an image. In addition, there is considerable uncertainty about whether particular patterns or colors in images represent grains of a particular size. Grains often cannot be easily distinguished, if at all, except for occasional large grains.

In most cases, grains are overlapping, therefore, even pebbles and cobbles can be difficult to accurately assess.

If a crude classification is all that is required for ground truthing acoustic data, for verifying extrapolations of sample data, or for physical habitat characterization, then rapid and relatively accurate determinations of primary sediment facies can be resolved from moderate to good quality seafloor video images. If more detailed grain size distribution data are required, it is possible to use images from underwater cameras to estimate grain size distributions (or facies characteristics) that have good agreement with sample data, as has been demonstrated by this study. These results are beneficial because acquiring and processing images from shallow water is less time consuming and less expensive than complete grain-size analyses of sediments. Many more images can be acquired and analyzed, thus increasing spatial coverage. Also, images can reveal information about some facies that cannot be recovered easily or at all by many sampling devices.

5.5. References for Chapter 5

Banner, A., Hayes, G., 1996. Identification of importants habitats in coastal New Hampshire. U.S. Fish and Wildlife Service, Gulf of Maine Project, Internet Report, Falmouth, Maine (http://rossby.unh.edu/edims/banner/gbay/gbay.htm#toc).

Blott, S. J., Pye, K. 2001. Gradistat: a grain size distribution and statistics package for the analysis of unconsolidated sediments. Earth Surface Processes and Landforms, 26, 1237-1248.

Cutter, G. R., Rzhanov, Y., Mayer, L. A., 2003. Automated segmentation of seafloor bathymetry from multibeam echosounder data using local Fourier histogram texture features. Journal of Experimental Marine Biology and Ecology, 285/286, 355-370.

Folk, R.L., 1954. The distinction between grain size and mineral composition in sedimentary-rock nomenclature. Journal of Geology, 62, 345-359.

Folk, R.L., 1974. Petrology of Sedimentary Rocks. Hemphill Publishing Co., Austin, TX, 182 pp.

Folk, R.L., and Ward, W.C., 1957. Brazos River bar, a study in the significance of grain-size parameters. Journal of Sedimentary Petrology, 27, 3-27.

Ihaka, R., Gentleman, R., 1996. R: A language for data analysis and graphics. Journal of Computational and Graphical Statistics, 5, 299-314.

Inman, D.L., 1962. Measures for describing the size distribution of sediments. Journal of Sedimentary Petrology, 22, 125-145.

Menking, K. M., Hannah, M. M. , Fitts,J. P., Bischoff, J. L., and Anderson, R.S., 1993. Sedimentary and mineralogical analyses of Core OL-92: Sediment Size Analyses of the Owens Lake Core. In George I. Smith and James L. Bischoff (Eds), U.S. Geological Survey Open-File Report 93-683. (http://pubs.usgs.gov/of/of93-683/report.html).

Shepard, F.P., 1954. Nomenclature based on sand–silt–clay ratios. Journal of Sedimentary Petrology 24 (3), 151–158.

Trask, P.D., 1930. Mechanical analysis of sediments by centrifuge. Economic Geology 25 581-599.

Ward, L. G., 1995. Sedimentology of the lower Great Bay/Piscataqua River Estuary. San Diego, CA: Department of the Navy, NCCOSC RDTE Division Report, 102 pp.

Wentworth CK. 1922. A scale of grade and class terms for clastic sediments. Journal of Geology 30: 377–392.

Zar, J. H., 1984. Biostatistical analysis. 2nd edition. Prentice-Hall, Inc., Englewood Cliffs, New Jersey, 718 pp.

CHAPTER 6

6. BENTHIC HABITAT CLASSIFICATION, CHARACTERIZATION, AND THE PROVISIONAL TRUTH OF GROUND-TRUTH

6.1. Citation

Published in: Proceedings of the International Conference on Underwater Acoustic Measurements: Technologies and Results. Heraklion, Crete, Greece, 28 June – 1 July, 2005.

Citation:

Cutter Jr., G. R., 2005. Benthic habitat classification, characterization, and the provisional truth of ground-truth. Proceedings of the International Conference on Underwater Acoustic Measurements: Technologies and Results. Heraklion, Crete, Greece, 28 June – 1 July, 2005.

6.2. Introduction

Acoustic remote sensing of the seafloor often involves multibeam echosounders that provide very high resolution bathymetric and backscatter data from acoustic ranging and signal strengths. Increasingly, multibeam bathymetry and backscatter maps are being used as a basis for seafloor habitat maps, such as in Kostylev et al. (2001). Sedimentary

facies maps have been generated from expert interpretation (Todd et al., 1999) and hierarchical decision tree analysis of backscatter and bathymetry data (Dartnell and Gardner, 2004). Key to inferring seafloor facies and habitat characteristics from bathymetry and acoustic backscatter data are ground-truth sample data.

Ground-truth data are critical to interpreting, classifying, and characterizing remotely sensed seafloor data. Sample data are used to (1) validate physics-based model predictions, (2) build empirical models, (3) assign class names and perhaps associated characteristics to results of unsupervised classification, and (4) develop prototype feature vectors for supervised classification of remotely sensed seafloor data. Regardless of the approach, similar problems will likely be encountered, and similar decisions will be required that are related to the so-called "ground-truth" sample data.

This work relates a combination of methods used to segment and classify multibeam bathymetry and backscatter maps into apparent, "hypothetical" seafloor habitat types. Derivative products of bathymetry and backscatter were used in combination with ground-truth data. Physical samples and seafloor video images constitute the ground-truth data. Segmentation and classification of bathymetry and backscatter was carried out by manual delineation, value ranges, local variance, texture feature analysis, and spatial covariance model parameter values. This study demonstrates how classifications and predicted characteristics are dependent on the interpretation and spatial aspects of the ground-truth data.

6.3. Data and analysis

The study area for this work was a portion of the subtidal lower Piscataqua River Estuary that flows between New Hampshire and Maine, USA. The study area represented a small part of the area surveyed for the Portsmouth Common Dataset 2001 (Mayer and Baldwin, 2001). Data used for this work were from surveys collected in support of the Second International Conference on High-Resolution Surveys in Shallow Water by Science Applications International Corporation (SAIC) in July, 2001, and by Simrad in June, 2001, in conjunction with University of New Hampshire Joint Hydrographic Center and Center for Coastal and Ocean Mapping. The bathymetry dataset was from the SAIC survey that used a dual-head Reson 8125 multibeam echosounder (Byrne et al., 2001). Backscatter data were from the survey by Simrad and UNH that used a Simrad EM3000-D multibeam echosounder. Positioning and orientation for both surveys were recorded using an Applanix/TSS POS/MV 320 inertial motion unit. Data were cleaned and processed according to hydrographic standards, then gridded with 1 m grid cell sizes (Figure 6.1).

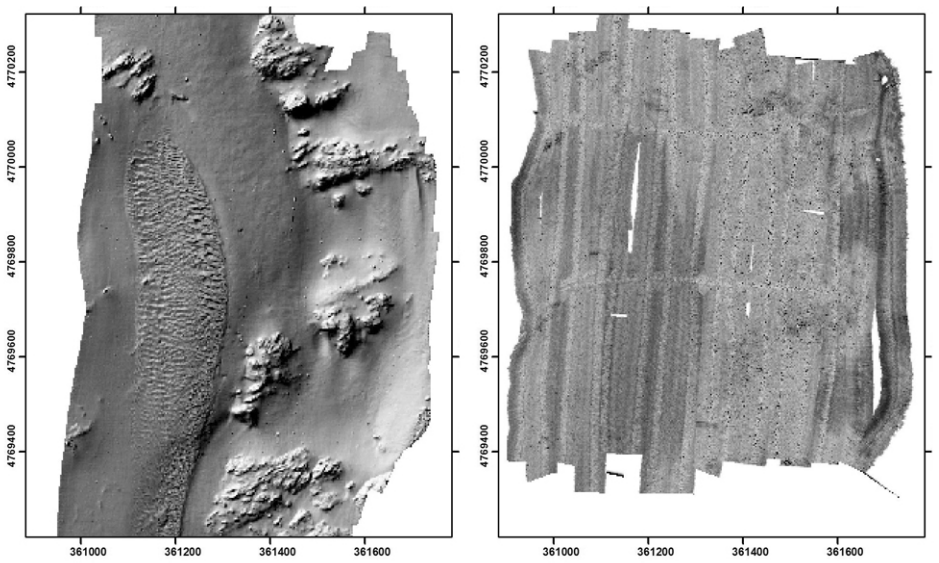

Figure 6.1. Bathymetry gridded from Reson 8125 data and acoustic backscatter mosaic grid from Simrad EM3000D data for part of the Piscataqua River Estuary. In the backscatter mosaic (on the right), dark represents low backscatter strength, light represents high backscatter strength. Coordinates are Eastings and Northings (m) from UTM zone 19 north.

An existing sediment distribution map (Ward, 1995) for the study area served as a standard for assessing the segmentation results. Segmentation of bathymetry and backscatter data grids was done initially by manually delineating the maps into regions that appeared to be distinctive visually. Manual delineation of seafloor morphology or backscatter is a simple, reliable way to impose spatial extent and coverage of distinct facies and habitats. Human perception makes manual delineation quite effective in the case of excessively noisy data. However, manual delineation requires much subjectivity, and boundaries are not often clear. Analyst bias is a concern with manual delineation, as is reproducibility. To avoid potential analyst bias, other segmentations were applied using techniques based on backscatter median value: classification of local Fourier histogram (LFH) texture features using unsupervised (Cutter et al., 2003), and supervised schemes; and spatial covariance model parameters fit to variograms from bathymetry.

6.4. Results and discussion

Regions identified by manually delineating bathymetry and backscatter maps based on distinctive morphologies and/or backscatter values tended to match the spatial delineations for primary lithologies reported by Ward (1995). Those were: rock, gravel, and sand. The rocky regions and sandy region characterized by megaripples were easily identified visually in the bathymetry. The remaining area corresponded to regions identified by Ward (1995) to be primarily composed of gravel.

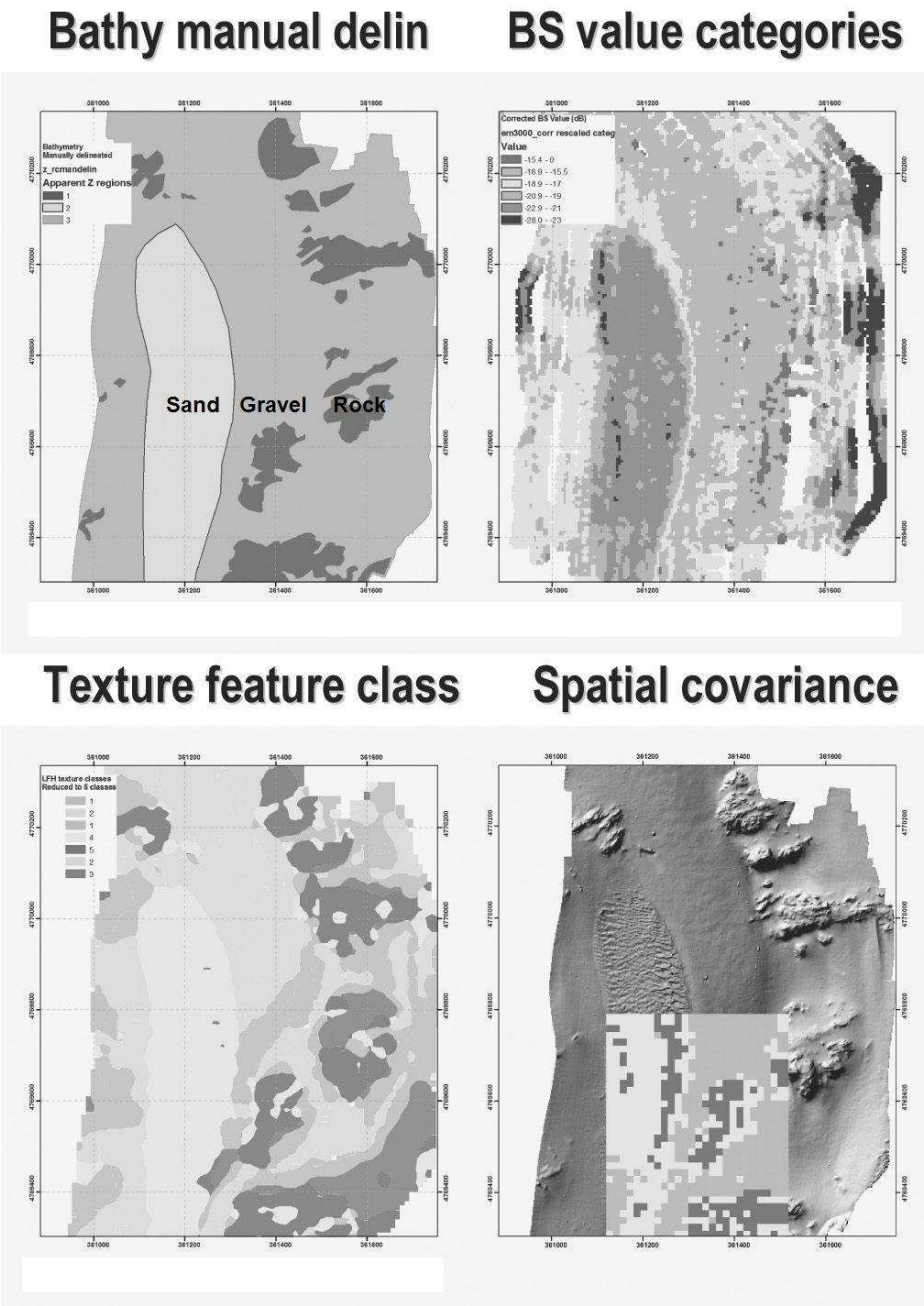

Figure 6.2. Results from segmentation of bathymetry data from manual delineation, classification of backscatter value statistics, LFH texture feature classification, and spatial covariance model parameter classification.

Segmentation results from all the techniques resulted in regional groupings of similar morphologies or backscatter values, and all correspond to the primary facies of Ward (1995) to a reasonable degree based on visual comparison. What we sought,

however, was a more detailed characterization, for sediment class, at least. Although it is tempting to predict sediment class from a physics-based model such as Jackson et al. (1986), there were several reasons for avoiding that. These include: the operational frequency of the EM3000 sonar (300 kHz) that is higher than the range considered to be valid for the Jackson et al. (1986) model; an offset that existed between levels from each of the dual heads; the backscatter data were gridded and not corrected for seafloor geometry; and because modelled sediment properties are ideal and this study area contained many coarse sediment mixtures.

A variogram from part of the backscatter dataset shows that the data were noisy, or highly variable, over the smallest sample interval distances (Figure 6.3). The variogram

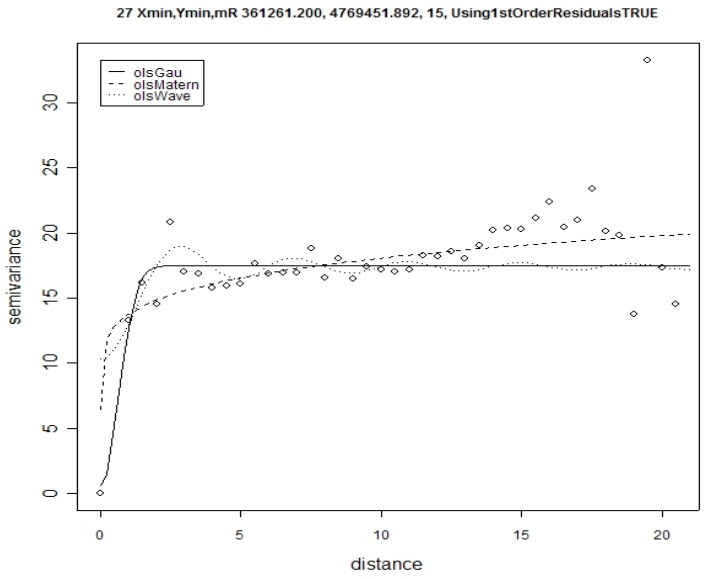

Figure 6.3. Data noise or high variability is suggested by this variogram for a subset of the backscatter data.

from the backscatter data also suggests that the backscatter data are not generally useful for segmentation and classification techniques that rely upon quantitative descriptions of local spatial or statistical properties. Also, the variogram supports the use of low-pass

filtered backscatter data. Because the backscatter data were noisy and were not corrected for seafloor geometry, characterizations of seafloor attributes from these backscatter data should be limited to homogenous regions with uncomplicated geometries.

With good quality, low noise data such as the multibeam bathymetry from this shallow water study area, spatial variation can be used to discriminate between some morphologies. Similar to the approach described by Herzfeld (1993), variograms were used here to segment and classify bathymetric data into the three primary facies based on differences in spatial covariance properties of bathymetry by facies (Figure 6.4). Specifically, parameters from spatial covariance models fit to empirical variogram data by ordinary least squares were used for segmentation of bathymetry for a portion of the study area. Results of the segmentation of bathymetry using an index constructed from covariance model parameters are shown in Figure 6.2.

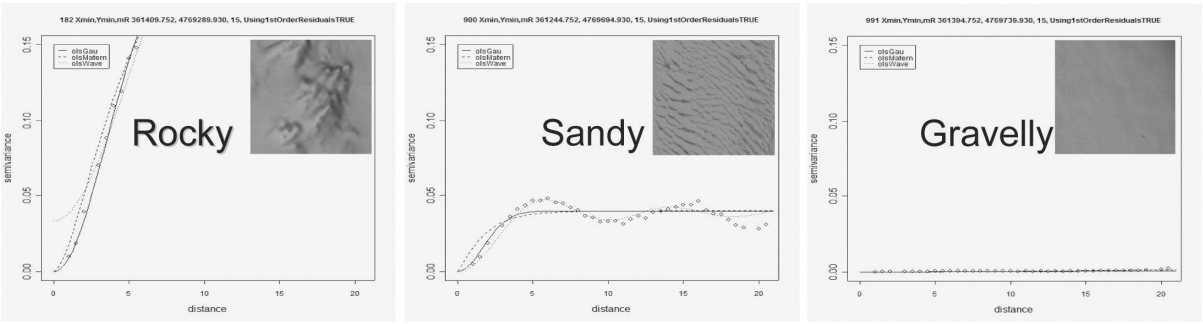

Figure 6.4. Representative variograms for bathymetry by facies, suggesting that facies had characteristic morphologies distinguishable by spatial properties.

Samples used to construct the existing sediment map (Ward, 1995) suggested that within the gravelly facies, sediment grain size distributions could range from gravelly-sand to sandy-gravel. Manual delineations of bathymetry resulted in differences from the existing sediment map of Ward (1995). These differences were due to the multibeam data resolution and coverage compared to the data used to construct the Ward (1995)

sediment map. The new delineations were generally refinements of the Ward (1995) sediment map that was based on sparse samples and interpretation of limited-coverage sidescan sonar data. Ground-truth data were needed to assess the accuracy of delineations, and seafloor video images were used for the ground truthing (Figure 6.5).

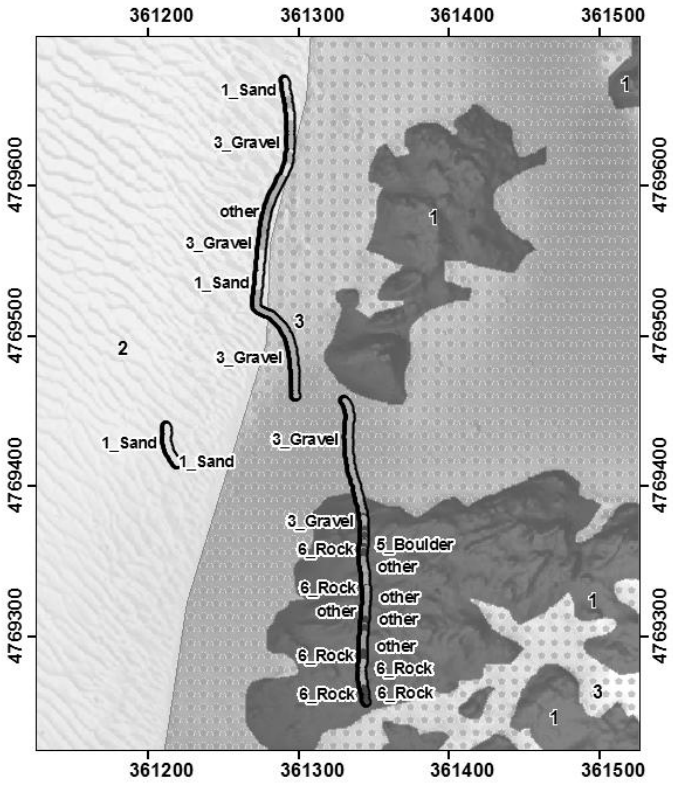

Figure 6.5. Regions from manual delineation of bathymetry relating to the three primary facies; rocky facies is dark, gravelly is stippled, and sandy is rippled. Video transect data are coded and labelled by facies interpreted from video images.

Away from boundaries between facies, video data corroborated predicted facies. Ground-truth video data from the delineation corresponding to sand facies sometimes revealed gravel facies and, hence, misclassification (Table 6.1). Most cases where video indicated misclassification were from samples collected along a transitional zone or at the boundary (Figure 6.5).

Table 6.1. Contingency table for counts of facies interpreted from video imagery (V) by manually delineated bathymetric regions (Z).

Count	**Sand(V)**	**Gravel(V)**	**Boulder(V)**	**Rock(V)**	**Other(V)**
Sandy(Z)	98	89	0	0	14
Gravelly(Z)	0	131	0	0	0
Rocky(Z)	1	61	21	42	75
	99	281	21	42	89

The unsupervised LFH texture feature classification technique (Cutter et al., 2003) results at the per-grid-cell level without spatial filtering resulted in several regional groupings that corresponded to subtle morphologies that were evident in the bathymetric data upon close reinspection. Thus, the following questions arose: what might the texture classes represent, and were they associated with real features, with data artifacts, or with processing artifacts? If real features were represented, then were the differences in texture and morphology associated with differences among sediment classes or with differences of morphology for a single sediment class organized by different flow characteristics. To determine whether these texture feature classes and subtle morphological differences were associated with previously unidentified sedimentary attributes, seafloor video imagery data were examined (Figure 6.6).

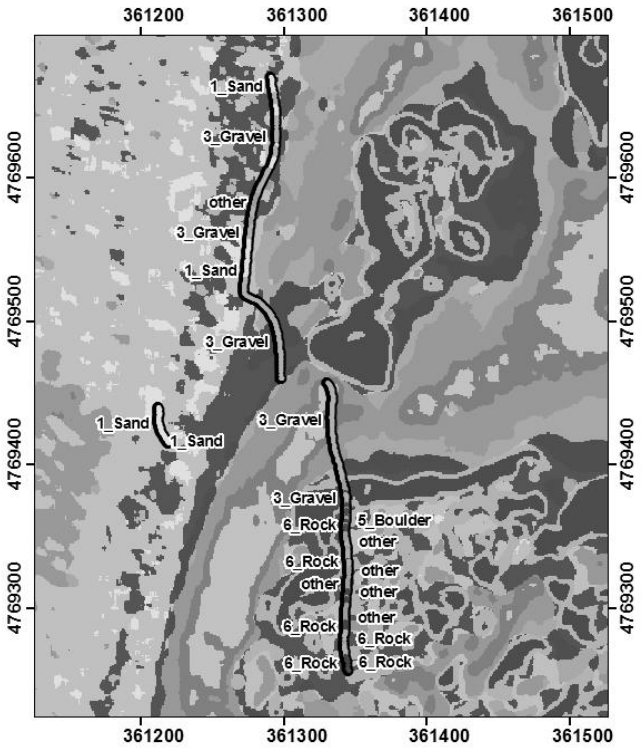

Figure 6.6. Supervised classification results LFH texture features from bathymetry. Video transect labelled with facies identified from video images.

Supervised classification uses prior information about characteristics known to exist. Techniques involving spatial or textural attributes help eliminate most user bias and avoid introduction of artificial strict boundaries. Supervised classification of bathymetry was performed using LFH texture feature prototypes developed at training locations where characteristics had been identified in video data. Results clearly indicated that if training sample locations where prototypes were developed were not accurately located, then segmentations did not agree with known sediment distributions. Also, the rocky region contained several patches of shelly-, sandy-, and gravelly-sediments. Within the region manually delineated as rocky according to large roughness features, only 21% of the non-overlapping imaged fields directly revealed rock (Table

6.1). Most of the image samples from the apparently rocky region revealed other sediments, predominantly biogenic shell.

Without careful attention to both the location and characterization related by the training sample image data, the results of the supervised LFH classifications done using training samples from the rocky region shown in Figure 6.5 could predict sand, gravel, boulder, or other facies. Like many other texture features, the LFH is constructed using an arbitrary spatial-integration scale. If that spatial-integration scale covered more than one sediment class zone, then the texture feature and resultant classification could represent a combination class. If the training sample came from a small patch surrounded by another facies with a characteristic morphology, then the texture feature actually would represent a morphology (and associated facies) different from that identified. Several resultant segmentations from supervised texture feature classification misrepresented spatial distributions of the classes used for training. These results did not necessarily represent failures of the texture feature as a classification tool, but rather that in some cases the morphology did not represent the facies identified in the ground-truth imagery. Additionally, some facies identified from the imagery did not have clear or consistent bathymetric expression at the spatial scales involved with the texture feature analysis.

6.5. Conclusions

Zonation is not always accurate because sometimes “regional-level” variation occurs locally. Ground-truth samples are not always able to provide verification for the interpretation of a bathymetry or backscatter map. Sampling methodology and

experimental design can lead to inaccurate assessments. Positioning uncertainty and habitat transitions can confound efforts to characterize the seafloor. If positioning cannot be constrained, characterization and classification detail level will be limited. Some questions can be addressed even if ground-truth position uncertainty is high, however compromise could required for the precision of characterization. Ground truthing high-frequency MBES data from shallow water requires accurate positioning, and perhaps requires non-traditional methods. There can be cases where ground-truth data and properties inferred from bathymetry or backscatter data do not agree, yet both have validity. Interpretation of habitat characteristics and classifications must account for the possibility that different data sources and spatial-scale mismatches might not lead to different and apparently incompatible classifications.

6.6. Acknowledgements

This work was supported by NOAA grant number NA17OG2285, and the NOAA Joint Hydrographic Center Fellowship for Ocean Mapping, 2004.

6.7. References for Chapter 6

Byrne, S., Clifford, B., Simmons, W., Depner, J., Reed, B., Moestikiwati, J., Smith, G., Processing Data for Seafloor Mapping: Integration and Metrics. Marine Technology Society Journal, 35, 4, 2001.

Cutter, G. R., Rzhanov, Y., Mayer, L. A., Automated segmentation of seafloor bathymetry from multibeam echosounder data using local Fourier histogram texture features. Journal of Experimental Marine Biology and Ecology, 285/286, 355-370, 2003.

Dartnell, P., Gardner, J. V., Predicting seafloor facies from multibeam bathymetry and backscatter data. Photogrammetric Engineering and Remote Sensing, 70 (9), 1081-1091, 2004.

Herzfeld, U. C., A method for seafloor classification using directional variograms, demonstrated for data from the western flank of the Mid-Atlantic Ridge. Mathematical Geology, 1993.

Jackson, D. R., Winebrenner, D. P., Ishimaru, A., Application of the composite roughness model to high-frequency bottom backscattering. J. Acoust. Soc. Am., 79, 1410-1422, 1986.

Kostylev, V. E., Todd, B. J., Fader, G. B., Courtney, R. C., Cameron, G. D., Pickrill, R. A., Benthic habitat mapping on the Scotian Shelf based on multibeam bathymetry, surficial geology and sea floor photographs. Marine Ecology Progress Series, 219, 121-137, 2001.

Mayer, L., Baldwin, K., Shallow water survey 2001: papers based on selected presentations from the second international conference on high resolution surveys in shallow water. Marine Technology Society Journal 35 (4), 3-4, 2001.

Todd, Brian J; Fader, Gordon B J; Courtney, Robert C; Pickrill, Richard A., Quaternary geology and surficial sediment processes; Browns Bank, Scotian Shelf; based on multibeam bathymetry. Marine Geology, 162, no.1, 165-214, 1999.

Ward, L. G., Sedimentology of the lower Great Bay/Piscataqua River Estuary. San Diego, CA: Department of the Navy, NCCOSC RDTE Division Report, 1995, 102 pp.

CHAPTER 7

7. SUPERVISED CLASSIFICATION OF GRIDDED MULTIBEAM BATHYMETRY DATA USING LFH TEXTURE FEATURES FOR HABITAT STRUCTURE CLASS PREDICTION

7.1. Introduction

Bathymetric surveys were conducted in 2004 off Saint John, USVI by the Center for Coastal Monitoring and Assessment, Biogeography Program of NOAA. Cruise Number NF-04-06-VI, aboard NOAA Ship Nancy Foster, was conducted in support of near shore and deepwater habitat characterization research (NOAA, 2004). The extent of the Saint John survey is shown in Figure 7.1; coordinates (in meters) are from Universal Transverse Mercator (UTM) projection, zone 20 north. Bathymetric data were acquired using a pole-mounted Reson SeaBat 8101-ER multibeam echosounder. Details about data collection equipment, procedures, and processing can be found in the Data Acquisition and Certification Report (NOAA, 2004).

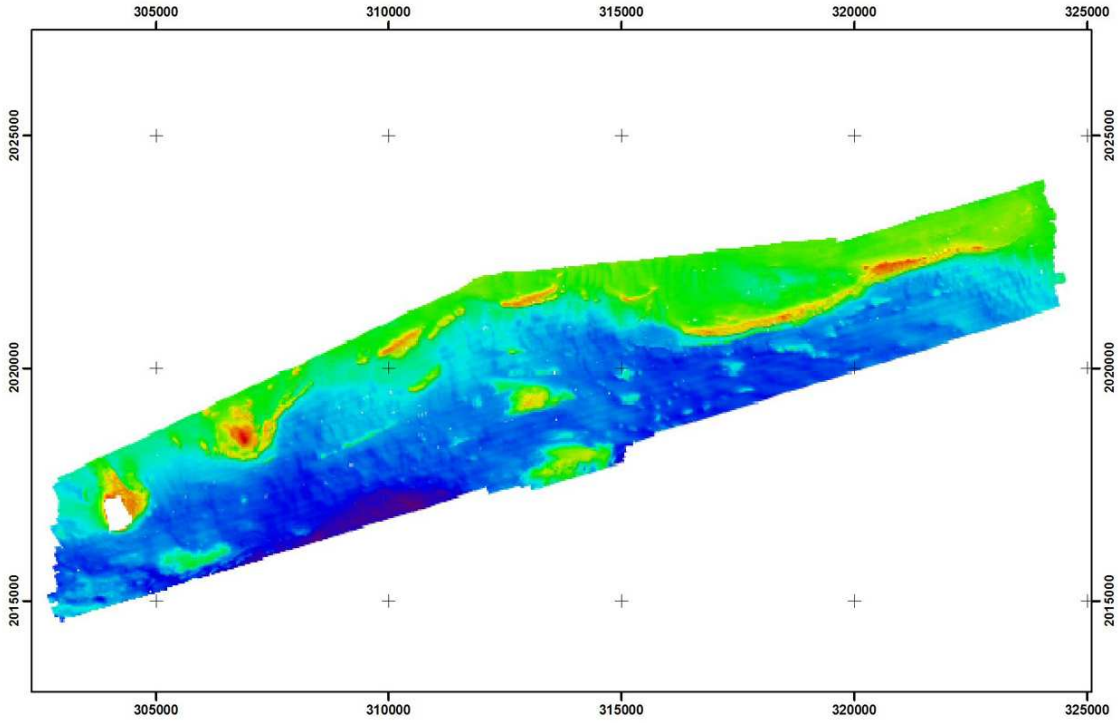

Figure 7.1. DTM from main bathymetric survey area from 2004 Nancy Foster mission off Saint John, U.S. Virgin Islands.

Habitat classification and characterization within the Saint John survey area was a primary interest to NOAA. Cutter et al. (2003) and Cutter (2005) have demonstrated the applicability of LFH texture feature classification for segmentation of bathymetric data and generation of hypothetical habitat maps. Based on those initial studies, NOAA requested that Local Fourier Histogram (LFH) texture feature classification be applied to the USVI bathymetry data.

Local Fourier Histogram texture features were developed for identification and retrieval of images from large databases based on image content. Technical details concerning the LFH texture feature can be found in Zhou et al. (2001). LFH

classification has been applied to gridded bathymetric data in unsupervised (Cutter et al., 2003), and supervised schemes (Cutter, 2005).

7.2. Data

Within the Saint John survey area, two subareas were chosen for gridding at high resolution (1 m by 1 m) and use for demonstration of LFH classification: West, and Central subareas (Figure 7.2).

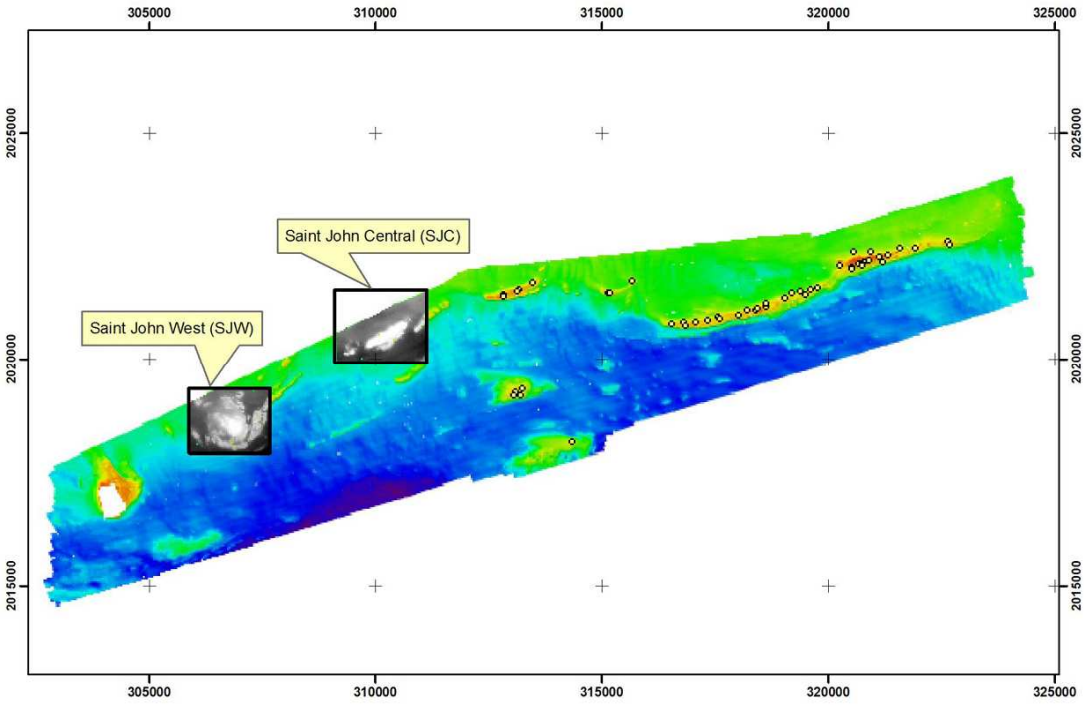

Figure 7.2. Saint John West (SJW) and Saint John Central (SJC) subareas considered for higher resolution gridding and classification.

Gridded bathymetric data from the two subareas were provided by NOAA for use in LFH texture feature classification. The data represented edited (hydrographically-cleaned) CARIS HIPS MBES soundings, binned to 1 m with shoal-biased selection, exported to

comma-separated ASCII-text files. Data were projected using UTM projection, from UTM zone 20 north, based on datum NAD83, with depths in meters (Pers. Comm., A. Otter, NOAA, 2005).

The Saint John West (SJW) subarea data were chosen for LFH analysis because ground-truth data from diver observations and video image analysis existed there (Figure 7.3).

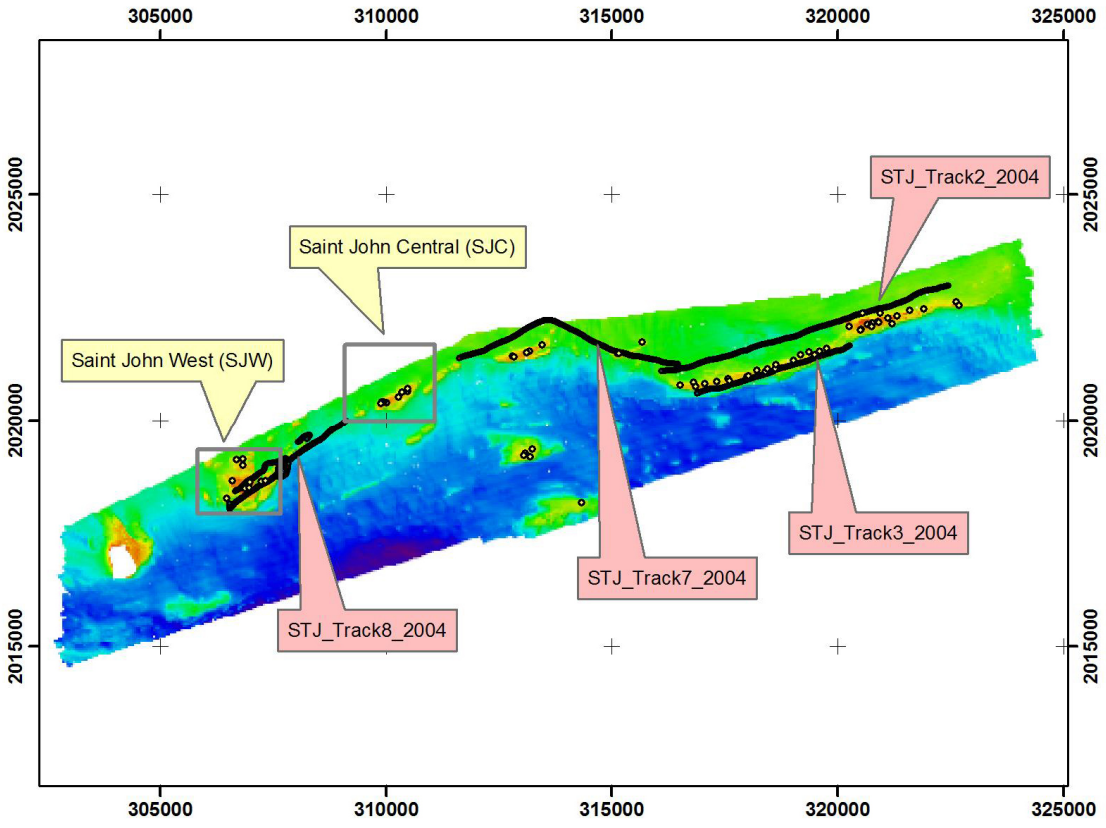

Figure 7.3. Video transects (black lines) and dive sites (points) from which ground-truth data for habitat characteristics were available.

This work represents a demonstration of supervised classification of gridded bathymetric data using LFH texture features. The gridded bathymetry dataset used was

the Saint John West (SJW) 2004 survey subarea, with 1 m by 1 m grid cell size (Figure 7.4).

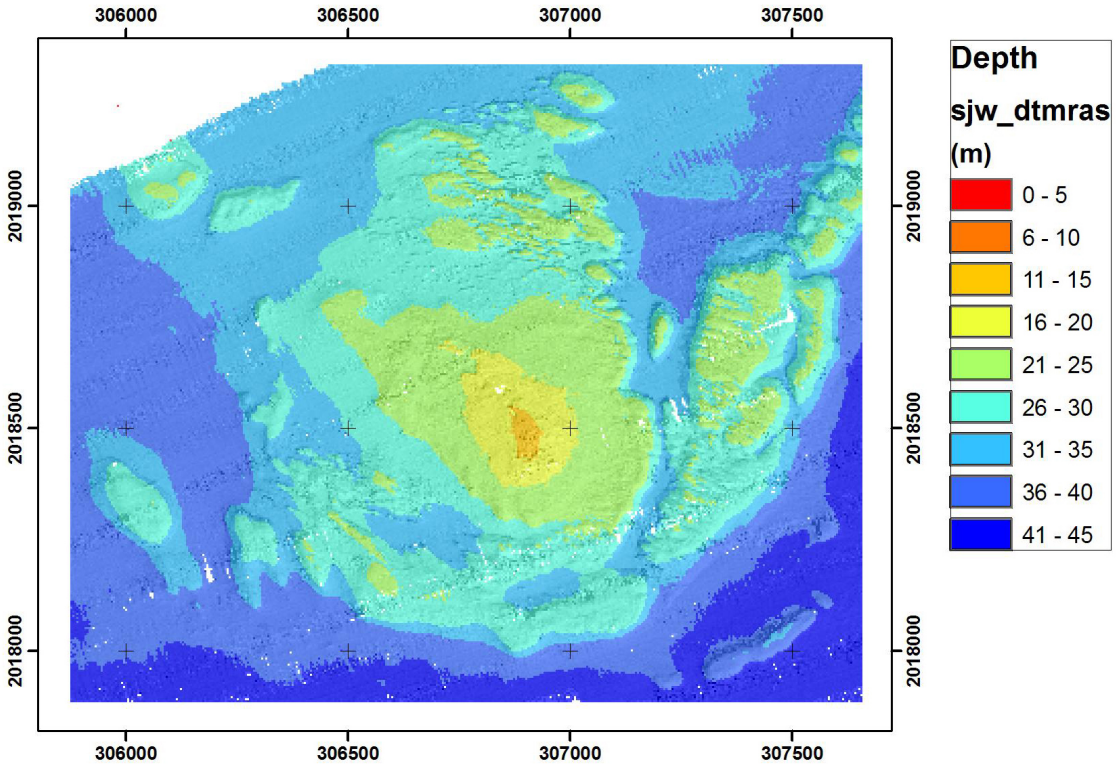

Figure 7.4. High-resolution grid (1-m grid-cell size) of the Saint John West (SJW) subarea, used for texture feature analysis.

7.3. Analysis

7.3.1. Habitat Structure Class Training Data

Data from diver observations and video image analysis were provided by NOAA for the SJW area. Observations from these data describing seafloor structure were used for supervised LFH classification. Dive data contained a variable called "HABITAT_STRUCTURE" and video data contained a variable called "STRUCTURE" that appeared to sufficiently describe features with bathymetric expression that would

have characteristic LFH texture feature vectors and therefore be useful as LFH class names. Within SJW, data from11 dive sites were available with diver identified habitat structure class (Figure 7.5).

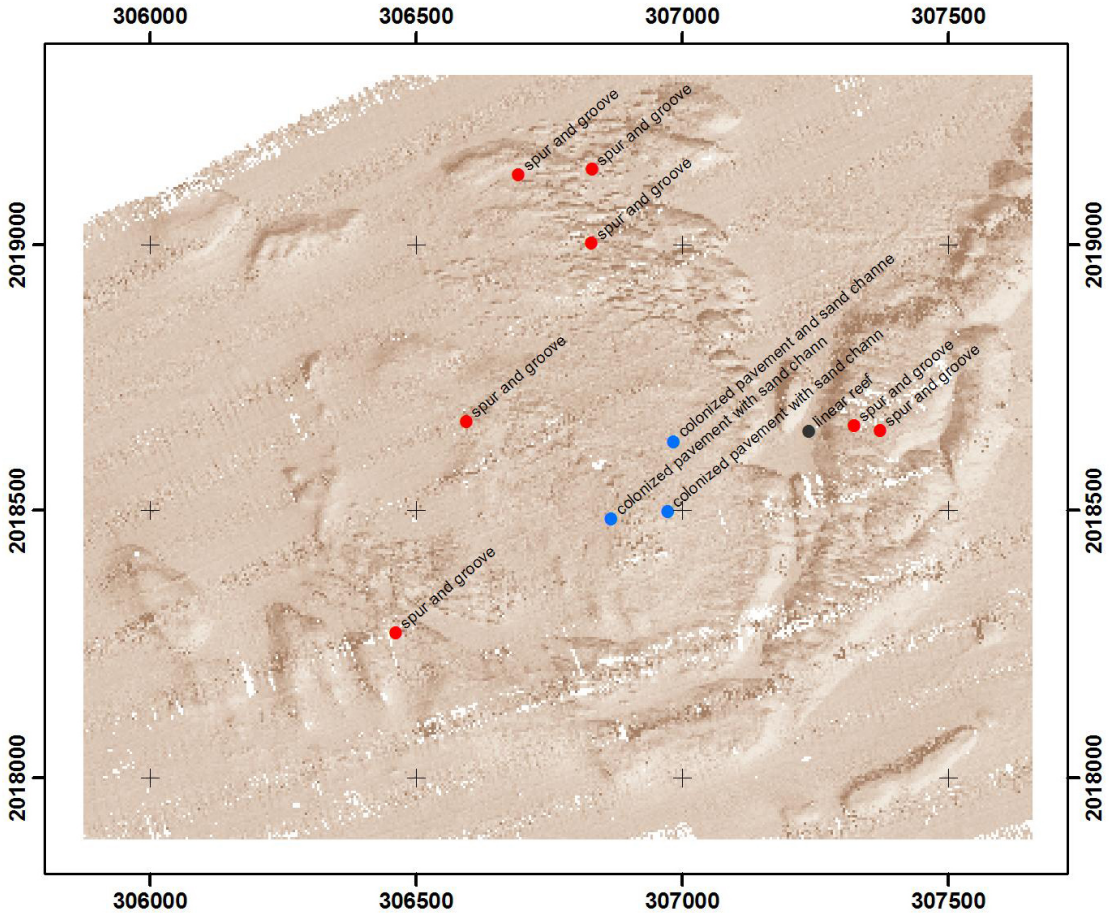

Figure 7.5. Saint John West (SJW) area bathymetry and dive sites labeled with diver identified habitat structure class.

Also, data from a video camera deployment (STJ_Track8_2004) occurred within SJW (Figure 7.6). Video images were visually interpreted as described by Battista and Kendall (Unpublished), included here as Appendix C. These ground-truth data were used

for determining training data classes and locations for developing prototypes for supervised LFH classification.

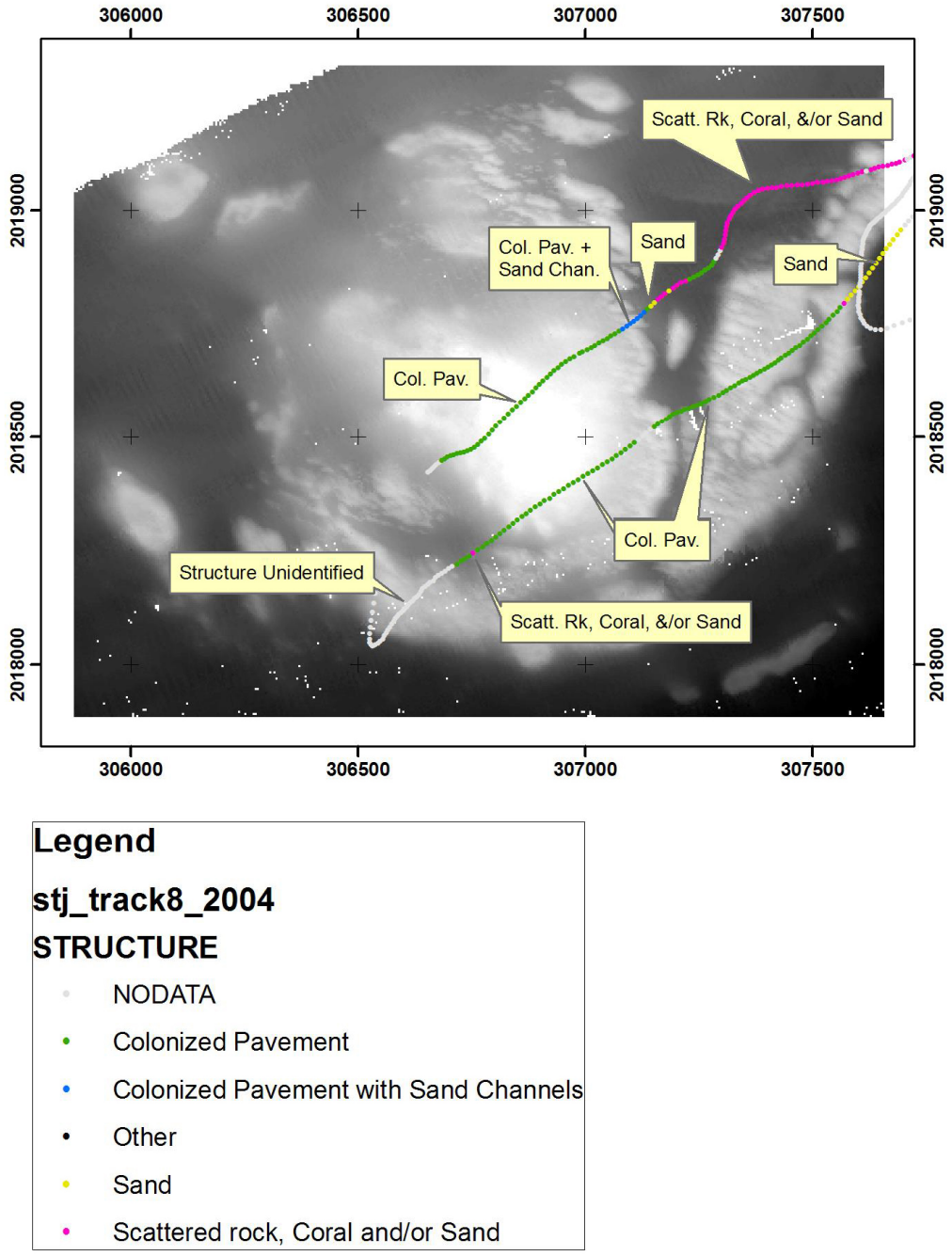

Figure 7.6. Saint John West (SJW) area bathymetry and video transects encoded and labeled by video analysis results for habitat structure class.

Dive data from sites within SJW identified three types of habitat structure: Spur and Groove ; Colonized Pavement and Sand Channels; and Linear Reef (Figure 7.7, labeled SG, CP+SC, and LR). Video data identified four types of structure within SJW: Colonized Pavement; Colonized Pavement and Sand Channel; and Scattered Rock, Coral, and/or Sand; and Sand (Figure 7.7).

Within the SJW area, six habitat structure classes, listed in Table 7.1, were identified by divers and video.

Table 7.1. Habitat structure classes identified by divers or video analysis, and abbreviated codes used during classification.

Code	**Structure Class Name**	**Identified By**
SG	Spur and Groove	Divers
CP+SC	Colonized Pavement and Sand Channels	Divers and Video Analysis
LR	Linear Ridge	Divers
CP	Colonized Pavement	Video Analysis
sRCS	Scattered Rock, Coral, and/or Sand	Video Analysis
S	Sand (unconsolidated sediments)	Video Analysis

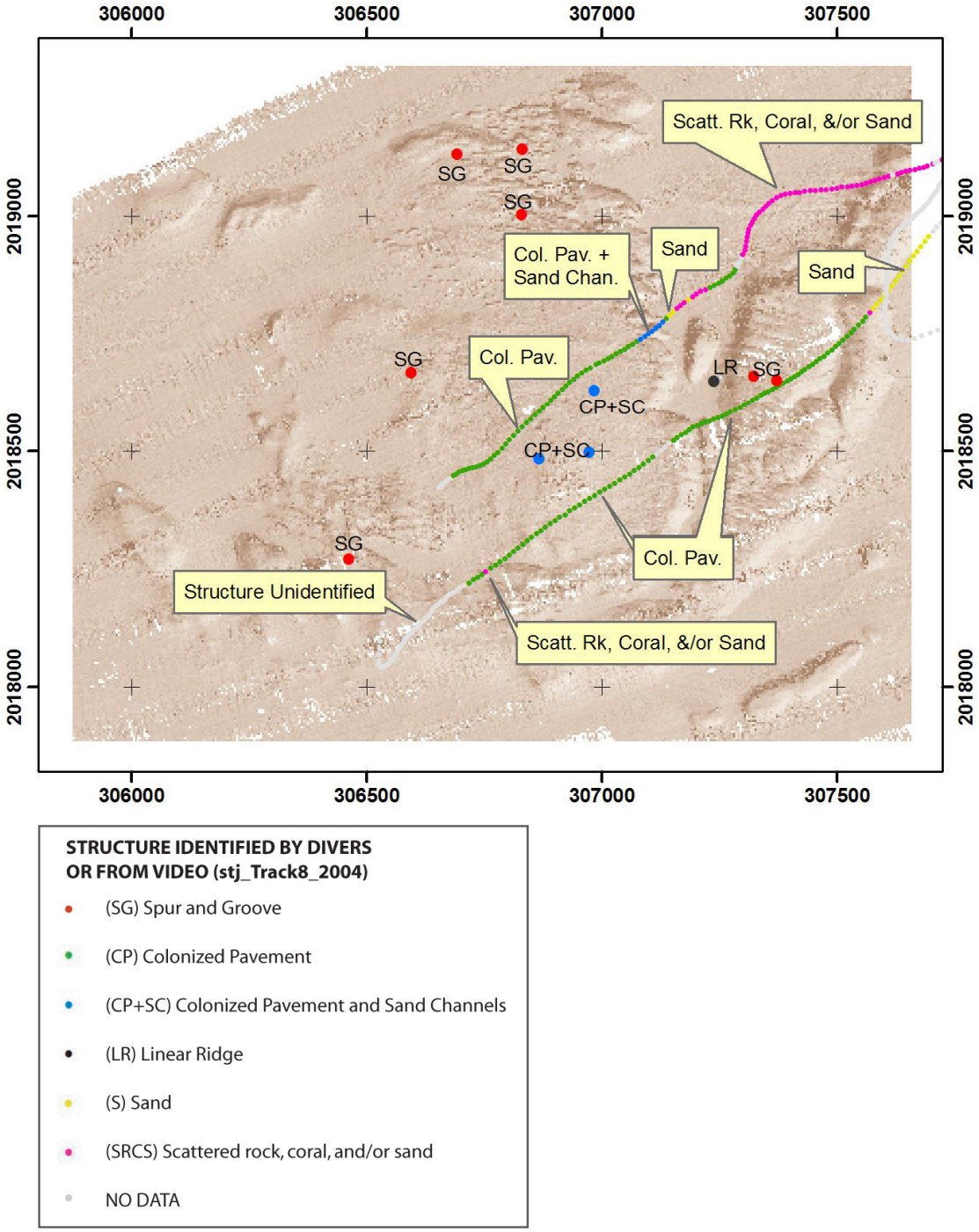

Figure 7.7. Saint John West (SJW) area bathymetry and video transects and dive sites encoded by habitat structure type class.

Examination of the ground-truth dive and video data in conjunction with the bathymetric data led to choices of locations where LFH texture feature vector prototypes would be generated. It appeared that some of the ground-truthed interpretations fit certain morphological patterns evident in the bathymetric data, however some interpretations seemed to occur across several morphologies. For instance, the video-derived structure type "Scattered rock, coral and or sand" extended across what appeared to be distinct bathymetric feature types in the DTM (Figure 7.7). Similarly, the dive data habitat structure type "Spur and groove" occurred in some places where the DTM did not appear to have a noticeable spur and groove pattern. This is not a criticism of the ground-truth data, but rather an explanatory basis for the choice in training point locations for the LFH analysis.

7.3.2. Training samples location coordinates

Figure 7.8 shows the ground-truth data subsets initially selected as potential training sample locations. Six classes representing types of diver-identified habitat structure or video analyst-identified structure were considered. It was determined that training samples would be developed for locations from which two types of structure were identified by divers (Spur and Groove, and Colonized Pavement and Sand Channels), three types of structure identified from video (Sand; Colonized Pavement; and Scattered Rock, Coral, and/or Sand), and one location where video identified Colonized Pavement, but nearby dive data identified Spur and Groove (Figure 7.7 and Figure 7.8; Table 7.2).

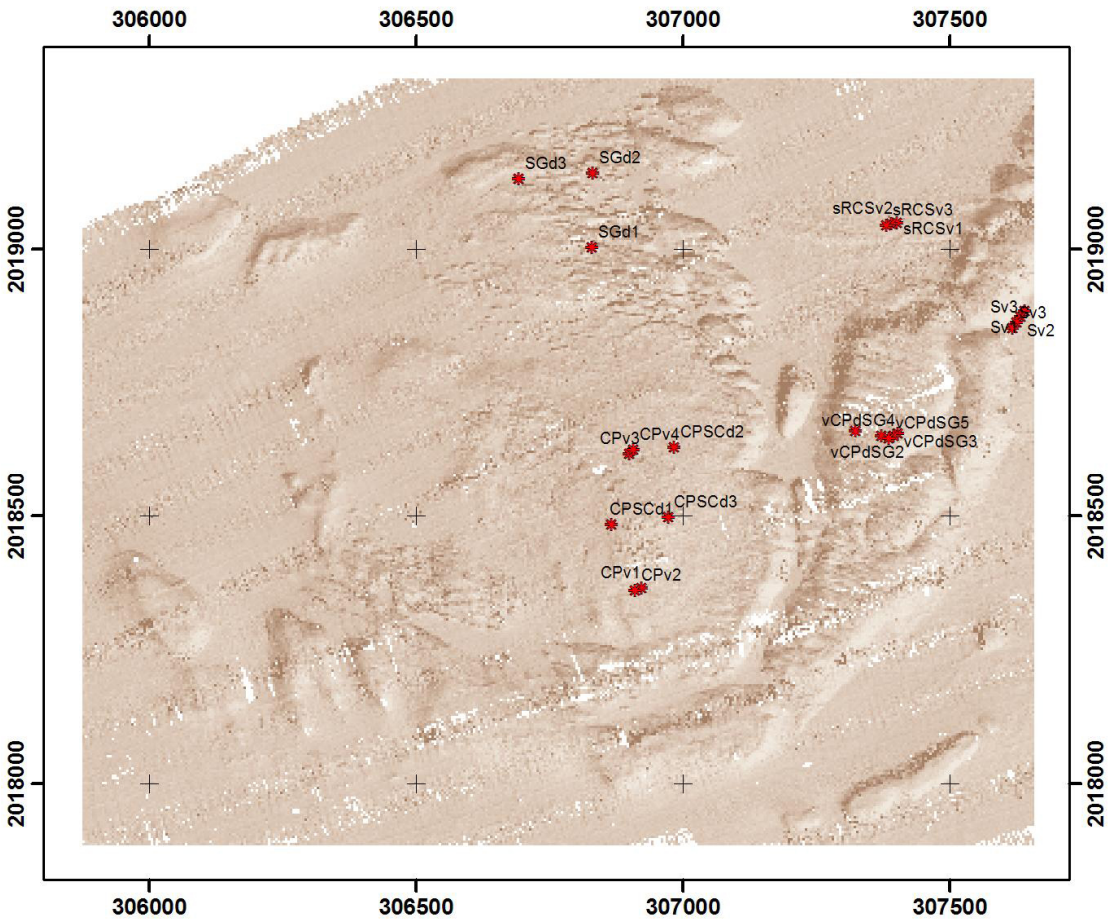

Figure 7.8. Locations of potential training samples for supervised classificaton.

Table 7.2. Coordinates of potential training samples for LFH classification of Saint John, western subregion ("SJW") representing selected dive and video data. Coordinates from UTM zone 20 north, WGS-1984. Preclass_ID codes key: Sv = Sand from video; CPSCd = Colonized Pavement and Sand Channel from divers; CPv = Colonized Pavement from video; sRCSv = scattered Rock, Coral, or Sand from video; vCPdSG = Colonized Pavement from video and Spur and Groove from divers; SGd = Spur and Groove from divers.

StationID	Easting (m)	Northing (m)	Preclass_ID
vS1	307639.70	2018884.25	Sv1
vS2	307632.27	2018873.65	Sv2
vS3	307624.20	2018863.56	Sv3
vS4	307616.70	2018853.20	Sv3
MSRO128	306865.35	2018483.89	CPSCd1
MSRO189	306983.16	2018631.04	CPSCd2
MSRO199	306971.26	2018498.33	CPSCd3
vCP1	306920.86	2018365.39	CPv1
vCP2	306909.66	2018360.24	CPv2
vCP3	306899.11	2018617.91	CPv3
vCP4	306907.00	2018625.71	CPv4
v_sRCS1	307399.69	2019049.79	sRCSv1
v_sRCS2	307389.42	2019048.28	sRCSv2
v_sRCS3	307379.95	2019044.13	sRCSv3
MSRO201	307321.91	2018660.87	vCPdSG1
MSRO150	307371.53	2018651.52	vCPdSG2
v192	307401.31	2018656.01	vCPdSG3
v193	307393.42	2018651.32	vCPdSG4
v194	307385.57	2018646.84	vCPdSG5
MSRO160	306829.29	2019003.41	SGd1
MSRO192	306829.61	2019141.78	SGd2
MSRO193	306692.02	2019132.08	SGd3

One location representing each of those structure types (or combinations of types) was used to develop initial training sample LFH prototypes (Figure 7.9; Table 7.3).

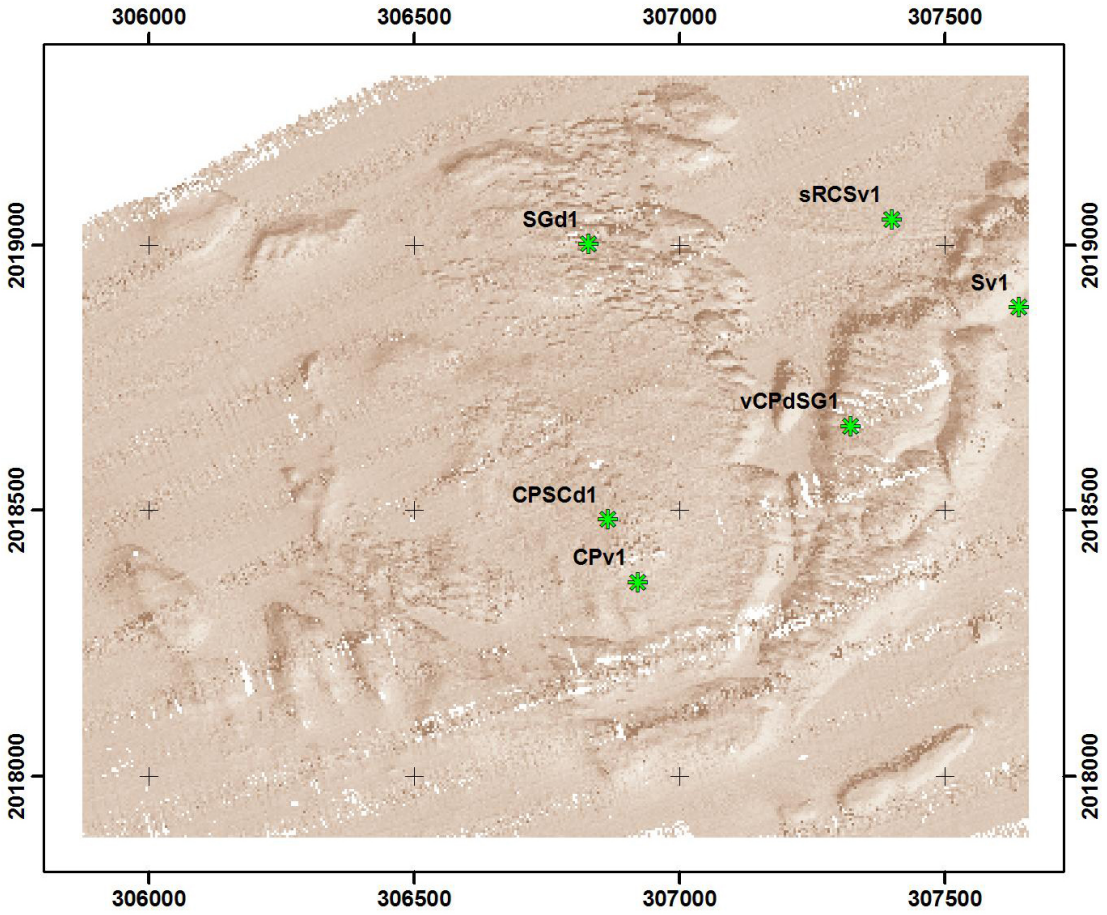

Figure 7.9. Locations of training samples labeled with habitat classifications from divers or video analysis.

Table 7.3. Coordinates of training samples for LFH classification of Saint John, western subregion ("SJW") representing selected dive and video data. Only one point from each interpreted class used for this classification. Coordinates from UTM zone 20 north, WGS-1984. Preclass_ID key: same as in Table 7.2.

StationID	Easting (m)	Northing (m)	Preclass_ID
1-vS1	307639.709	2018884.252	Sv1
2-MSRO128	306865.351	2018483.89	CPSCd1
3-vCP1	306920.863	2018365.392	CPv1
4-v_sRCS1	307399.696	2019049.799	sRCSv1
5-MSRO201	307321.917	2018660.87	vCPdSG1
6-MSRO160	306829.291	2019003.41	SGd1

Preliminary analysis suggested that there were several artifacts in the bathymetric grid apparently related to the survey operation, processing, and/or gridding. The artifacts were most pronounced in the outer beam regions of the multibeam swath (Figure 7.10).

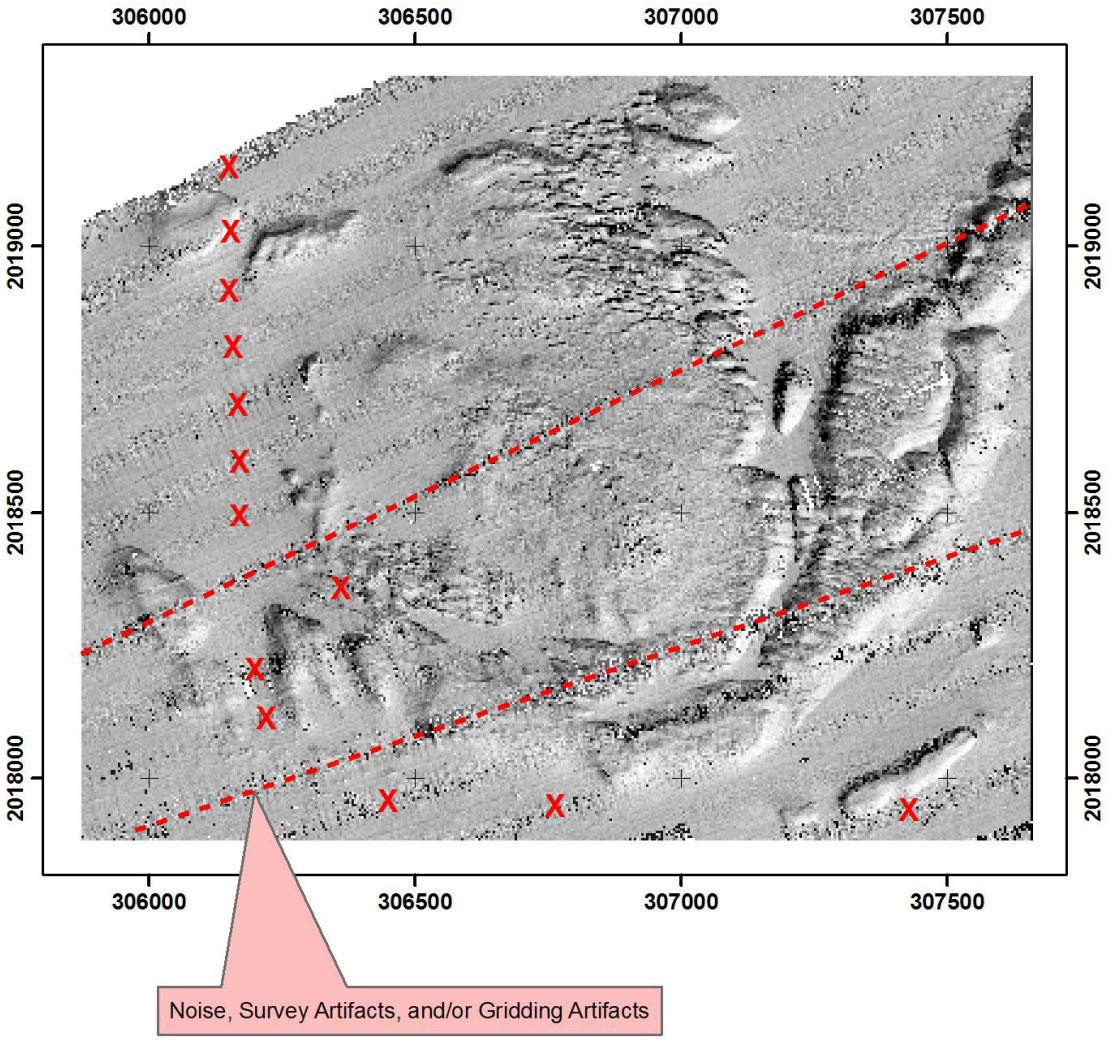

Figure 7.10. Noise, survey- or gridding-aritifacts in the gridded multibeam bathymetry.

An additional training sample location was included in attempt to represent the artifacts as a class, generally referred to as “Noise” hereafter. The six structure type training sample locations along with the noise class location (in the western part of SJW) used for initial LFH classification are shown in Figure 7.11 and listed in Table 7.4.

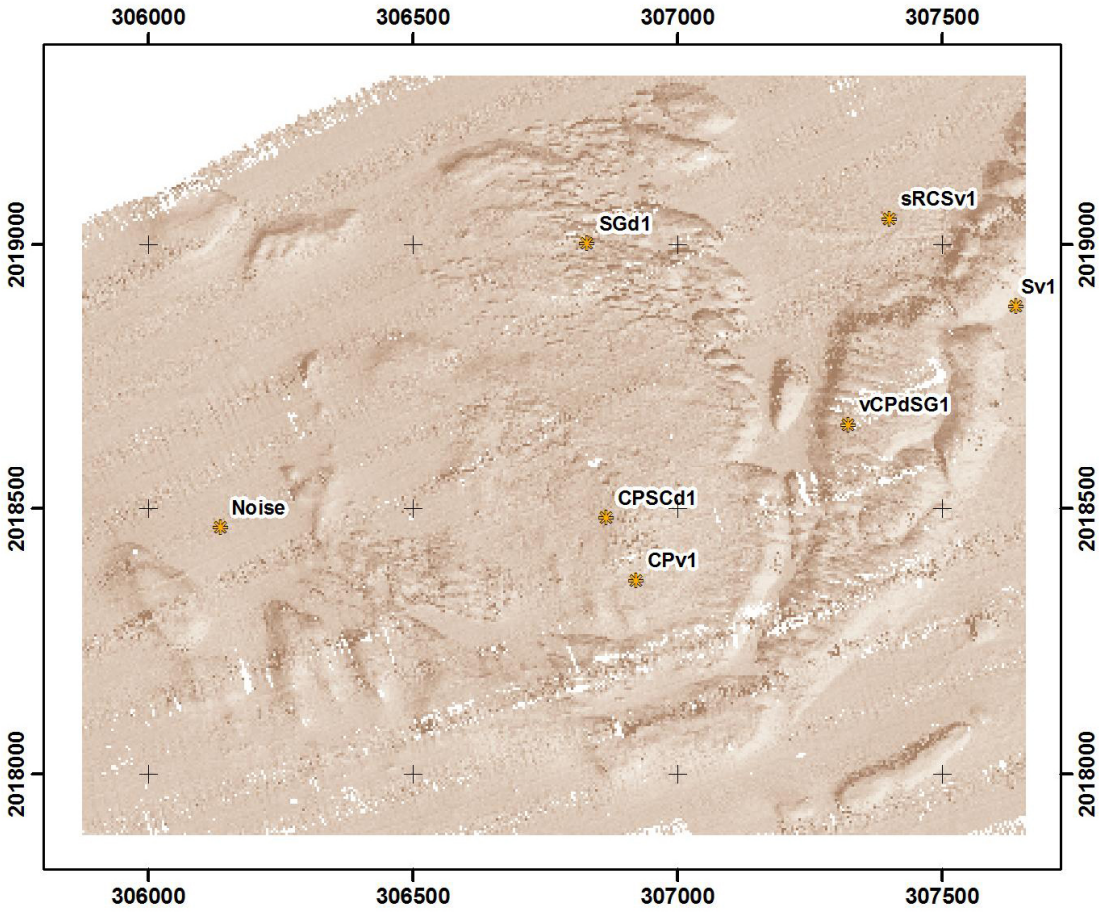

Figure 7.11. The seven locations with training data used for LFH texture feature classification.

Table 7.4. Coordinates of training samples for LFH classification of Saint John, western subregion ("SJW") representing selected dive and video data and a noise class sample. Only one point from each interpreted class used for this classification. Coordinates from UTM zone 20 north, WGS-1984. Preclass_ID key: same as in Table 7.2, except for N = noise.

StationID	Easting (m)	Northing (m)	Preclass_ID
1-vS1	307639.709	2018884.252	Sv1
2-MSRO128	306865.351	2018483.890	CPSCd1
3-vCP1	306920.863	2018365.392	CPv1
4-v_sRCS1	307399.696	2019049.799	sRCSv1
5-MSRO201	307321.917	2018660.870	vCPdSG1
6-MSRO160	306829.291	2019003.410	SGd1
7-Noise	306136.000	2018465.500	N1

7.3.3. Local Fourier Histograms (LFH)

Local Fourier Histogram (LFH) texture features were calculated using the procedure described in Cutter et al., (2003) and Cutter (2005). LFH feature vectors were accumulated within 15 by 15 m blocks around each grid cell. Supervised classification of LFH feature vector data was implemented using a minimum distance classifier method described in Cutter (2005).

7.4. Results and Discussion

7.4.1. Local Fourier Maps (LFMs)

The LFH texture features represent distributions of three (or optionally, four) component values. Development of the LFH texture features involves a preliminary step during which products called Local Fourier Maps (LFM) by Zhou et al. (2001) are generated. Each cell of the LFM represents the value of a Fourier transform coefficient for the series

of data in the neighborhood immediately surrounding each grid cell. The three LFM's generally relate to the behavior or variance of the data at relatively low, medium, and high spatial frequencies, with the particular spatial frequencies determined by the data grid cell size and also how distances are measured with respect to nearest neighbor cell groups.

LFM1 represents coefficient 1 that can be considered to represent the variance or magnitude of a spatial frequency (f) occurring at 1 cycle per period (the period being 8 grid cells and thus 8*1 = 8 m). Similarly, LFM2 represents 2 cycles per period, and LFM3 represents 3 cycles per period. Therefore, in a non-strict but intuitive sense (see Cutter 2005), LFM1, 2, and 3 can be considered to represent feature length scales of 8, 4, and 2.7 meters for this 1-m cell-size data grid. Components 1, 2 and 3 from the Fourier transform are used here for the LFH classification, as implemented by Cutter (2005). LFM's are developed from the bathymetric data alone without consideration of training samples or spatial-integration scales.

LFM1, 2, and 3 are shown in Figure 7.12, 7-13, and 7-14.

LFM1 (Figure 7.12) is color coded using the red band of an RGB colorspace, with intensity representing weighted value (1000x).

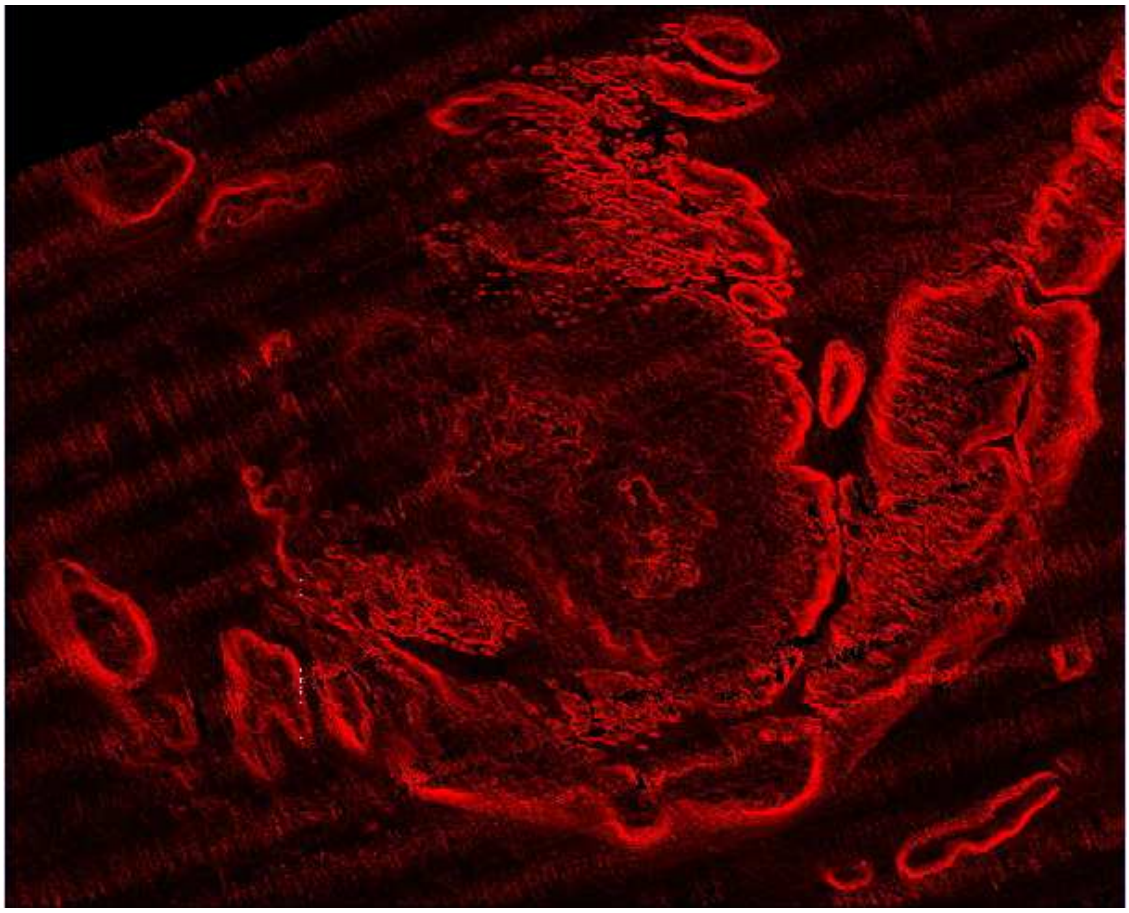

Figure 7.12. Color-coded values for local Fourier transform component 1 (LFM1), representing low spatial-frequency variation; higher intensities represent larger values.

LFM2 (Figure 7.13) is color coded using the green band of an RGB colorspace, with intensity representing weighted value (2000x).

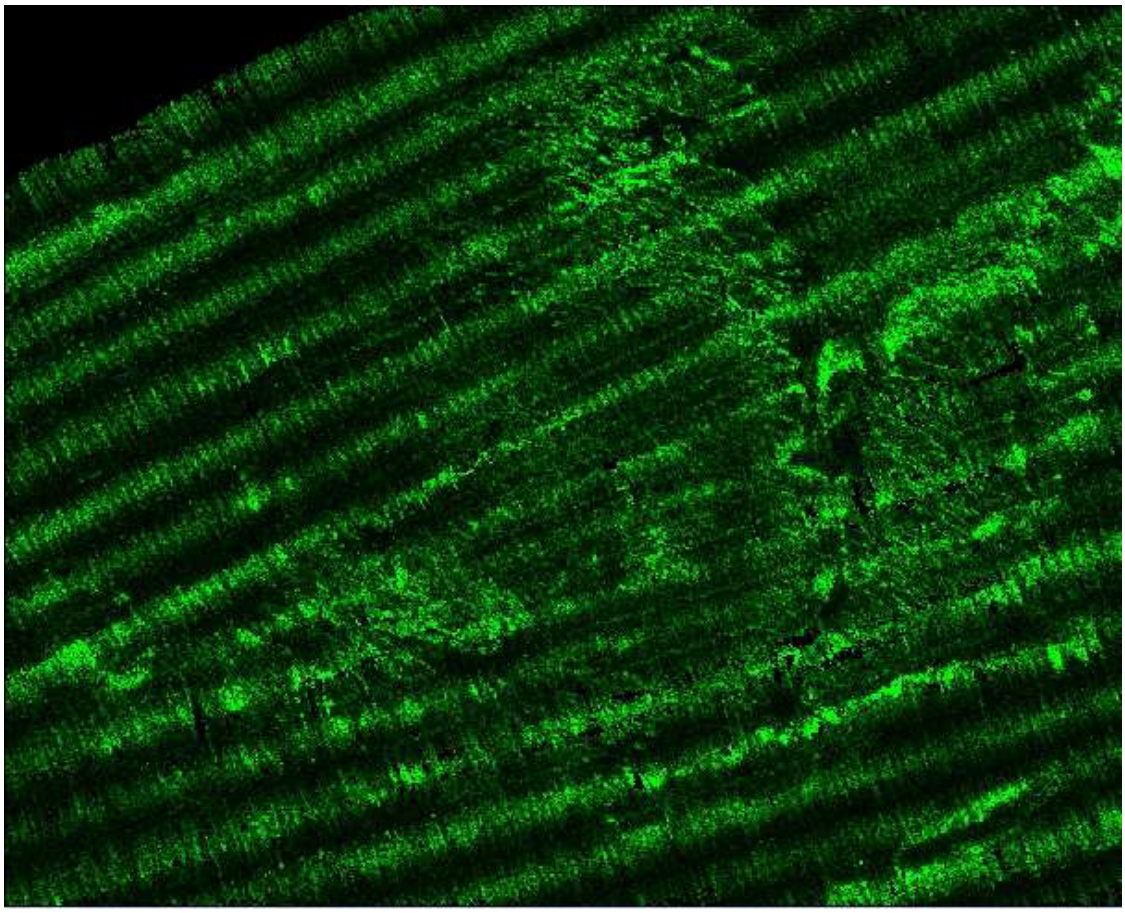

Figure 7.13. Color-coded values for local Fourier transform component 2 (LFM2), representing intermediate spatial-frequency variation; higher intensities represent larger values.

LFM3 (Figure 7.14) is color coded using the blue band of an RGB colorspace, with intensity representing weighted value (2000x).

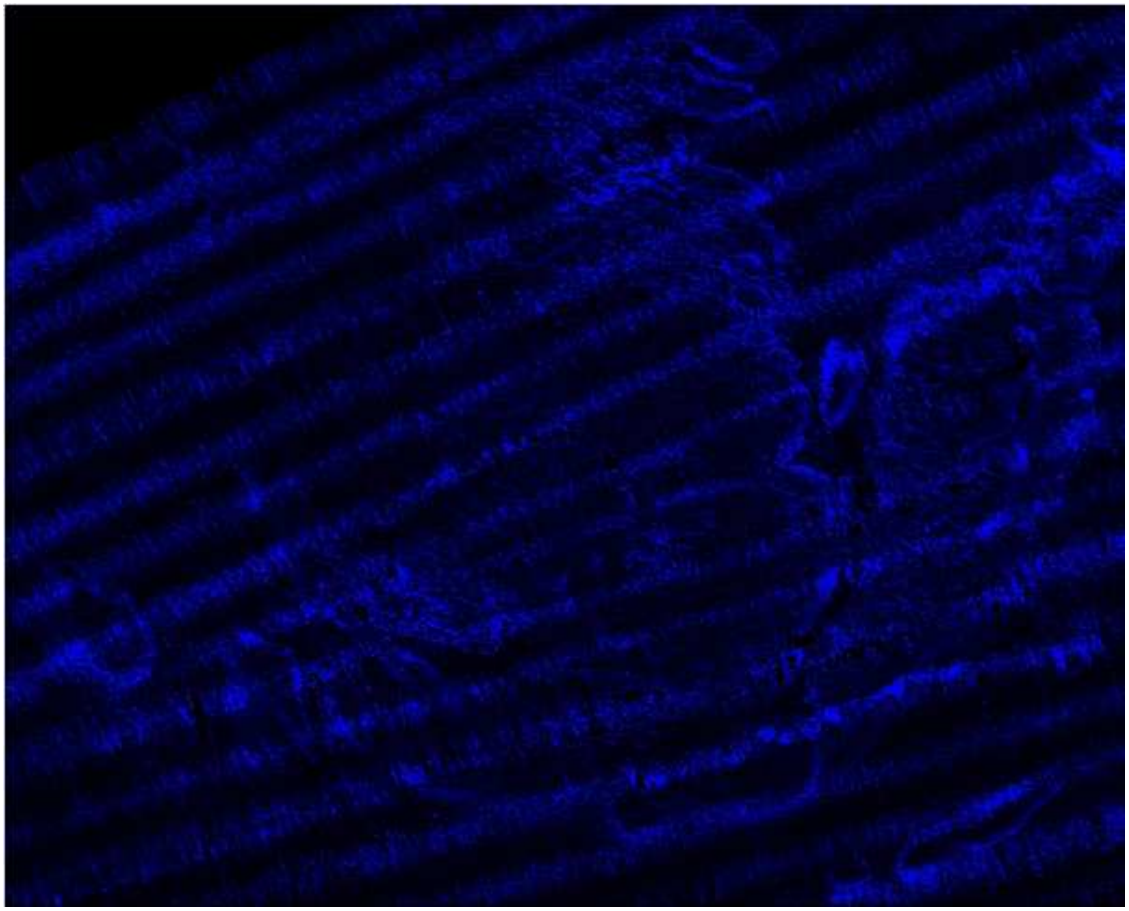

Figure 7.14. Color-coded values for local Fourier transform component 3 (LFM3), representing high spatial-frequency variation; higher intensities represent larger values.

7.4.2. LFMRGB psuedospectral

It has proven useful to combine these color coded LFM's into a pseudospectral-like image referred to as LFMRGB by Cutter (2005). The LFMRGB image represents color combinations and intensities that visually relate the component spatial frequencies and their relative magnitudes, from all three spatial frequencies at once. Hence, the LFMRGB visually depicts what the LFH basically signifies: a texture feature vector simultaneously representing multiple roughness scales (Figure 15).

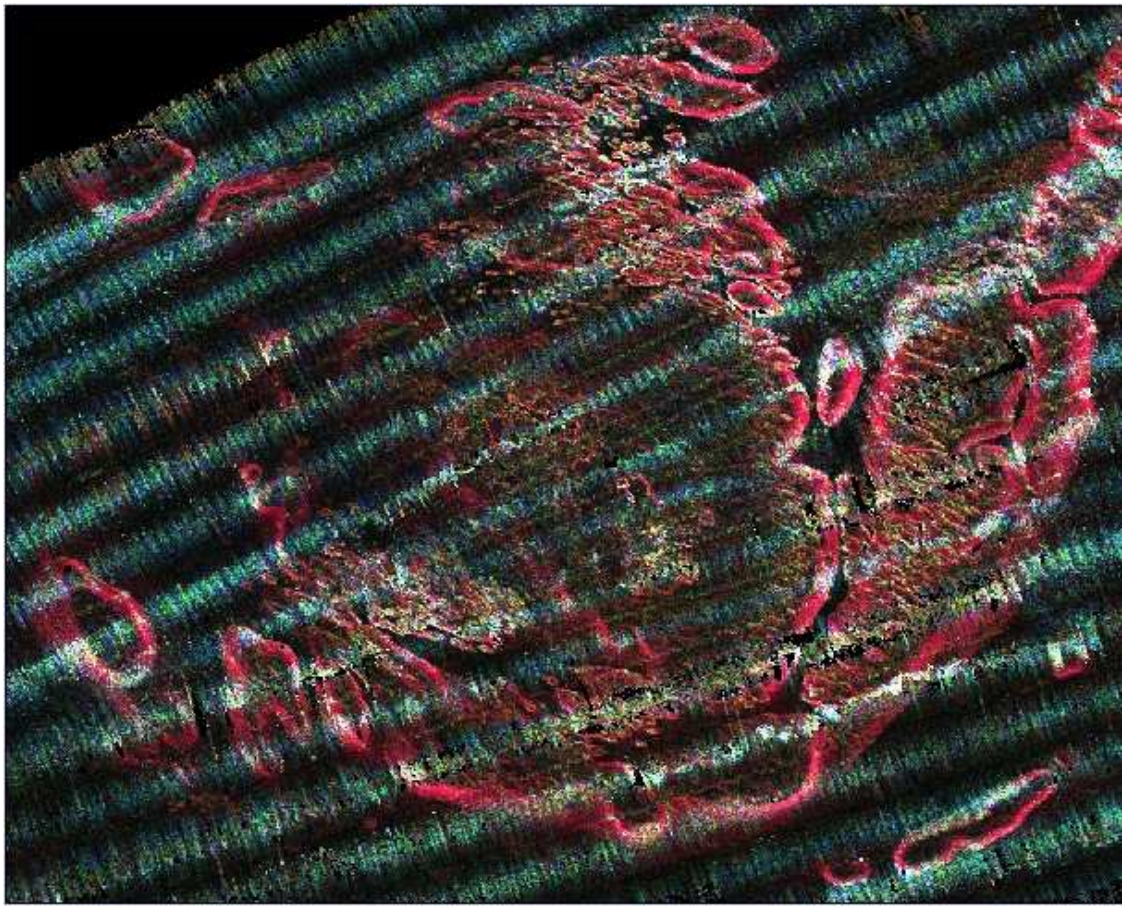

Figure 7.15. The pseudospectral LFMRGB map, an additive combined product of the color encoded products from low, intermediate and high spatial-frequency variation (Red: LFM1, Green: LFM2, Blue: LFM3). See text for detailed explanation.

In the LFMRGB image, bright red occurs where low spatial frequency roughness dominates; where green is bright, middle spatial frequency roughness dominates; and bright blue represents dominance by high spatial frequency elements. Combinations of colors occur that represent combination of roughness element frequency bands. For example red and green combined in equal proportions to produce yellow, therefore yellow would be indicative of an equal combination of low and medium frequency elements. In this case, components representing spatial frequencies are weighted to accommodate value ranges of 8-bit color bands, therefore yellow represents equal combinations of weighted low and medium spatial frequency component values.

The LFMRGB map (Figure 7.15) reveals the strong presence of noise or data artifacts occurring at the medium and high spatial frequencies (approximately > 2 m to 4 m feature lengths), seen as blue-green linear bands along-survey-tracks. The low spatial frequency (red in Figure 7.15) is dominated by signal from the seafloor morphological features, and some combination of low and medium morphological feature combinations are evident (as yellow in Figure 7.15) between the noise bands.

Texture feature vectors are constructed using the data from LFM1, LFM2, and LFM3. At any grid cell, an LFH texture feature represents the distribution of the values of LFM1, 2, and 3 within a specified block size, or spatial-integration scale. For additional technical and mathematical details, see Zhou et al. (2001), Cutter et al. (2003), and Cutter (2005).

7.4.3. LFH Classification of Habitat Structure

Supervised LFH Texture feature classification, using prototypes developed at training sample locations for the 6 habitat structure classes and the 1 noise class (Table 7.4) resulted in the hypothetical habitat map shown in Figure 7.16.

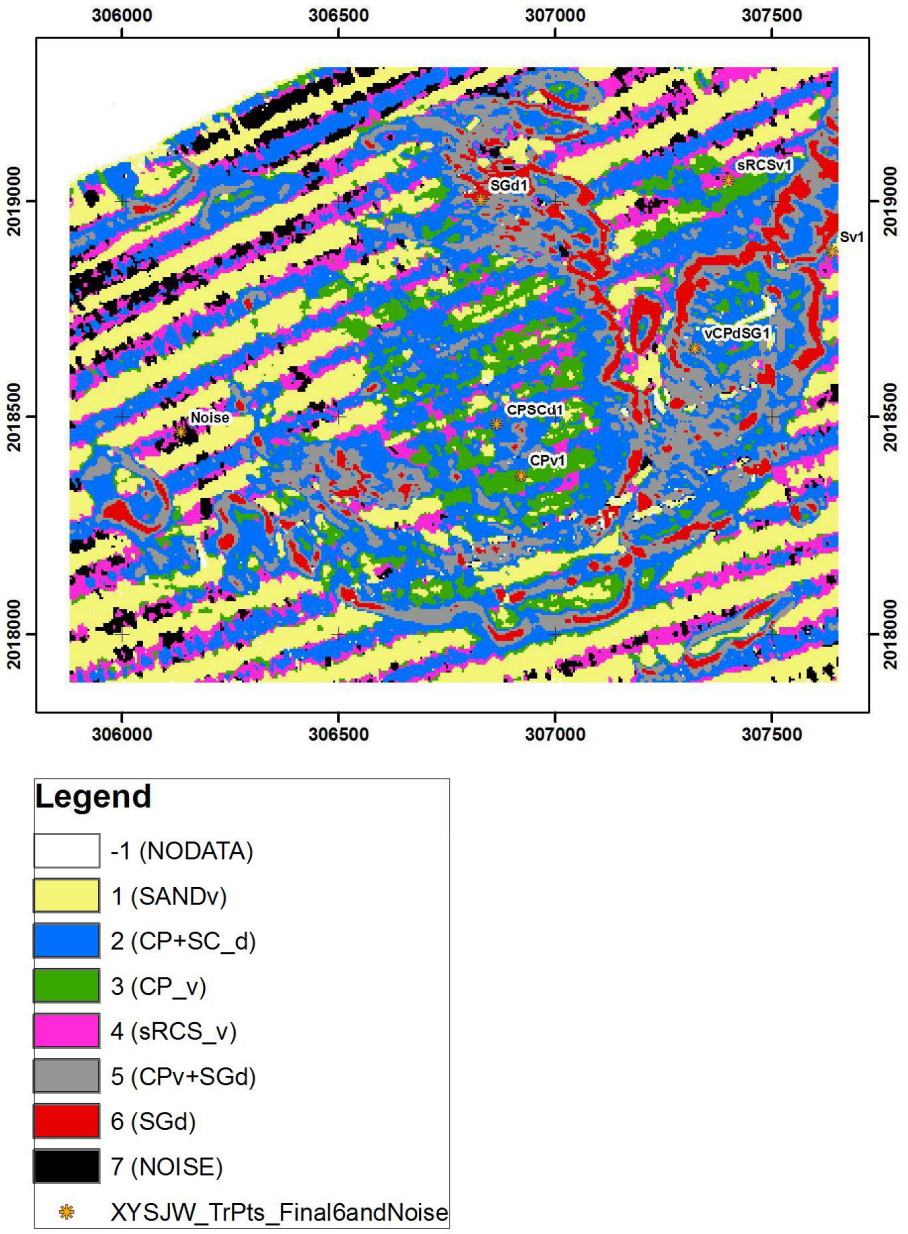

Figure 7.16. Map segmentation produced using supervised LFH classification with all training data classes.

The LFH class “Noise” (colored black in Figure 7.16) accounted for some of the data artifacts. However, some of the other LFH texture feature classes still were influenced by noise, as the survey lines are evident and composed of two classes meant to represent levels of habitat structure. Specifically, the Colonized Pavement and Sand Channel class from dive data (CP+SC_d), shown in blue, was attributed to much of the noisy data (Figure 7.16). The Scattered Rock, Coral, and/or Sand class from video data (sRCS_v), shown as magenta in Figure 7.16, was also attributed mostly to noise. The reason for this result could be that training samples were located in noise, or that the LFH feature vectors for the actual noise and the classes CP+SC_d and sRCS_v were similar. Eliminating the CP+SC_d and sRCS_v classes from consideration results in the map shown in Figure 7.17 that represents four habitat structure classes.

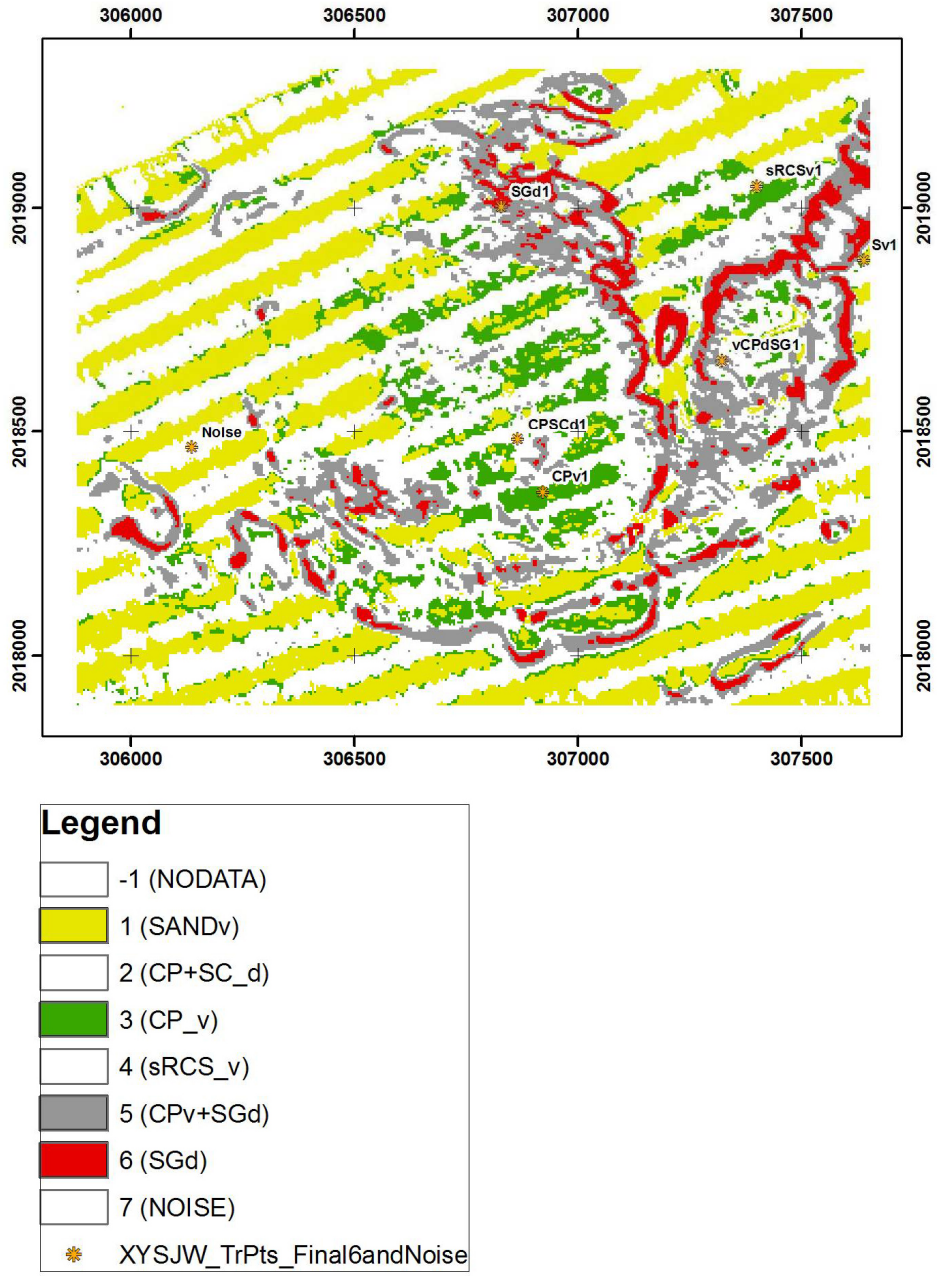

Figure 7.17. Map segmentation produced using supervised classification. Classes that were influenced by noise or artifacts are shown as white. The segmentation from the remaining classes corresponds to morphological regions evident in the bathymetry.

The noise-eliminated LFH hypothetical habitat class map (Figure 7.17) represents the structure levels of: Sand (SANDv); Colonized Pavement (CPv); Spur and Groove

(SGd); and either Colonized Pavement and/or Spur and Groove (CPv+SGd, previously also called “vCPdSG”). Recall the CPv+SGd class was developed for a location where the dive and video data differed within a small distance.

7.4.4. Evaluation and Preliminary Validation

If we examine the ground-truth data and the LFH class map simultaneously (Figure 7.18), we see that there appears to be good agreement between the classifications made by video analyst and spatial distributions depicted by the LFH map.

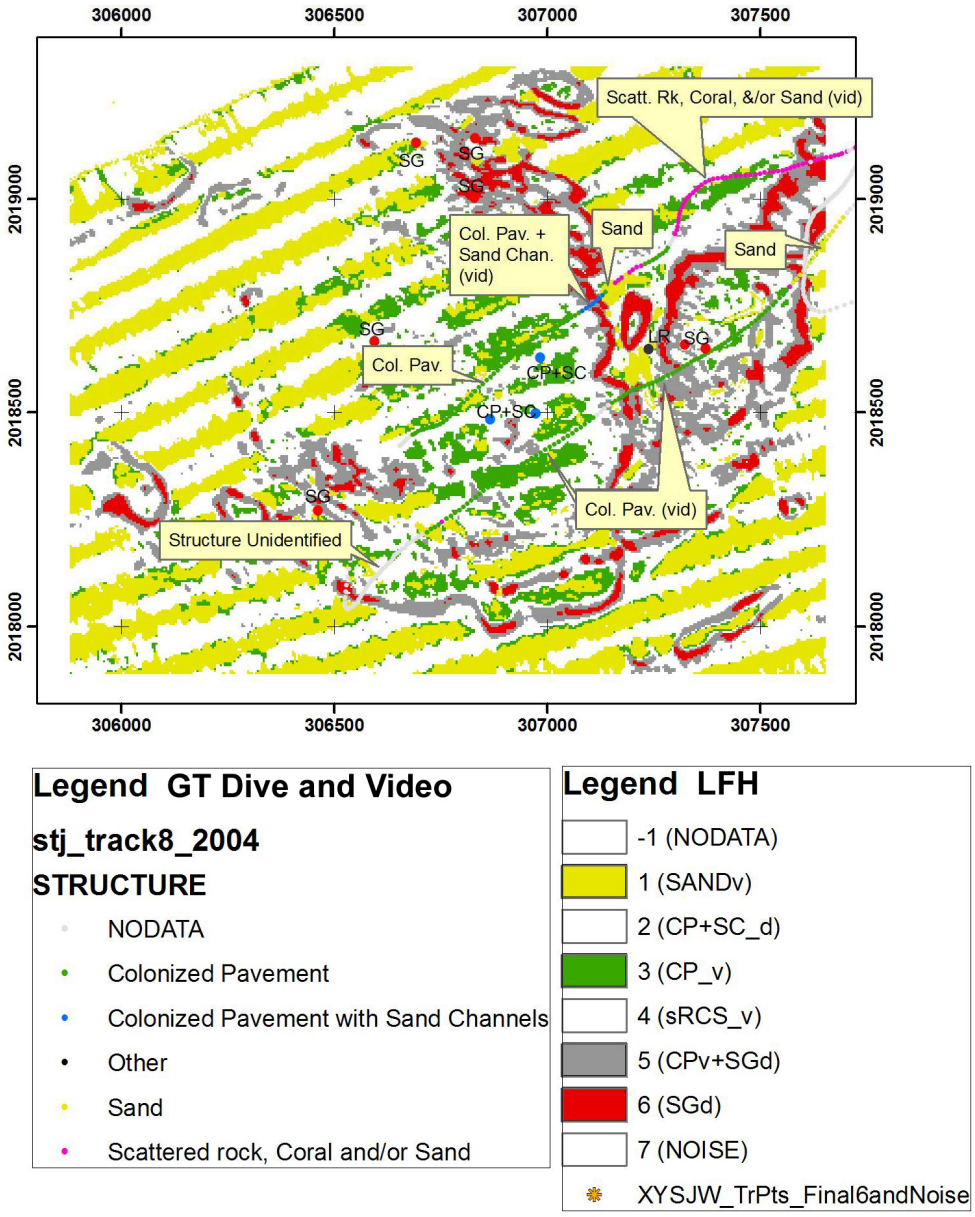

Figure 7.18. Supervised classification results and video and diver classifications. The same colors were used to represent class levels for the texture feature classes and diver/video data classes. Class labels are included on the map.

Since the LFH classes mixed with noise are removed, we see that the CP+SC_d class described by divers occurred in three locations within the data noise regions. The only class that is clearly inconsistently described by the ground-truth data and the LFH class map is the "Scattered Rock, Coral, and/or Sand" class from the video interpretation data. The LFH classification did not discriminate that class from noise, and predicted other classes occurring where video sRCS_v occurred. Otherwise, the "Sand" class distribution predicted by LFH appears consistent with the ground-truth data, as does the "Spur and Groove" LFH class.

The LFH class CPv+SGd is difficult to assess because dive data appear to be somewhat inconsistent with video data. If we believe the video data, then the CPv+SGd LFH class, shown as gray, would be the same as the CP_v class, shown as green (Figure 7.18). In that case, the match between the LFH class map and the video data would be better in the eastern part of SJW (near 307400, 2018700). Figure 7.19 reproduces Figure 7.18, without intrusive labeling, representing a noise-eliminated LFH hypothetical habitat

class map with ground-truth data.

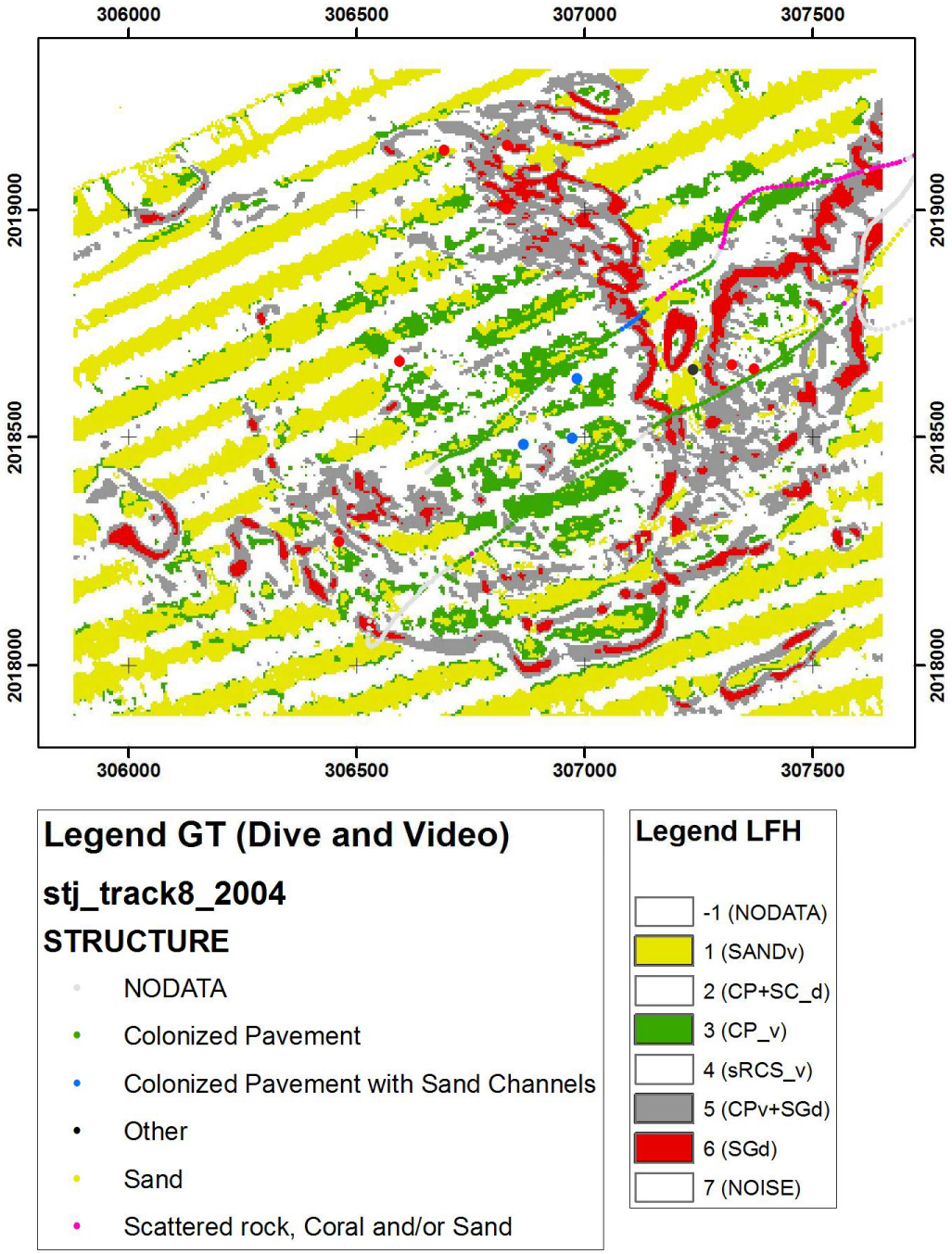

Figure 7.19. Supervised classification results and video and diver classifications. The same colors were used to represent class levels for the texture feature classes and diver/video data classes. The video-transect ground-truth data generally verify LFH texture feature classification.

7.5. Accuracy Assessment

7.5.1. Initial overall assessment

Video data from STJ_Track8_2004 will be used for initial validation and accuracy assessments of characterizations predicted from LFH classes. Except for colonized pavement, the prediction accuracy of several of the LFH classes appeared low, particularly for the CP+SCd (colonized pavement and sand channels according to divers) and sRCSv (scattered rock, coral, and/or sand according to video) classes (Table 7.5), if no consideration is given to complicating factors.

Table 7.5. Contingency table for habitat structure LFH class (LFH-OrigClass) by habitat structure indicated by video (VidStruct).

Count Row %	CP+SCv	CPv	SANDv	sRCSv	
CP+SCd	3 3.85	60 76.92	0 0.00	15 19.23	78
CPv	0 0.00	40 75.47	1 1.89	12 22.64	53
CPv+SGd	1 3.23	18 58.06	3 9.68	9 29.03	31
NODATA	0 0.00	1 33.33	1 33.33	1 33.33	3
NOISE	0 .	0 .	0 .	0 .	0
SANDv	1 5.26	8 42.11	4 21.05	6 31.58	19
SGd	2 20.00	5 50.00	1 10.00	2 20.00	10
sRCSv	0 0.00	14 53.85	4 15.38	8 30.77	26
	7	146	14	53	220

Recall that CP+SCd and sRCSv LFH classes were considered to be confounded by artifacts in the bathymetric grid. Therefore, they were ultimately combined into the

"NOISE" class. The "NOISE" LFH class represented bathymetry grid data dominated by artifacts, and contained 104 of the 220 video observations that were coincident with LFH prediction locations (Table 7.6).

Table 7.6. Contingency table for VidStruct By LFH-NewClass2 LFH classes with NOISE LFH class containing Noise, CP+SCd and sRCSv.

Count Row %	CP+SCv	CPv	SANDv	sRCSv	
CPv or CPv+SGd	1 1.19	58 69.05	4 4.76	21 25.00	84
NODATA	0 0.00	1 33.33	1 33.33	1 33.33	3
NOISE (and CP+SCd or sRCSv)	3 2.88	74 71.15	4 3.85	23 22.12	104
SANDv	1 5.26	8 42.11	4 21.05	6 31.58	19
SGd	2 20.00	5 50.00	1 10.00	2 20.00	10
	7	146	14	53	220

7.5.2. Colonized pavement

When the LFH classes “CPv” (colonized pavement according to video data) and “CPv+SGd” (colonized pavement according to video data, but spur and groove according to divers) were combined, the result was that 58 of the 84 cases where CPv or CPv+SGd was predicted by LFH, ground-truth video confirmed to be CPv by video. Hence, in this case we are ignoring diver data that suggested that spur and groove existed near where video indicated colonized pavement. The prediction of CPv by LFH was (58/84) 69 % accurate when allowed to also contain the CPv+SGd class.

For the case where we did not combine CPv and CPv+SGd classes, LFH predicted CPv, 40 of 53 cases where CPv was predicted by LFH, ground-truth video confirmed to be CPv by video. Under these circumstances, the prediction of CPv by LFH was (40/53) 75 % accurate (Table 7.7).

Table 7.7. Contingency table for VidStruct by LFH classes with CPv and CPv+SGd classes considered separately.

Count Row %	CP+SCv	CPv	SANDv	sRCSv	
CPv	0 0.00	40 75.47	1 1.89	12 22.64	53
CPv+SGd	1 3.23	18 58.06	3 9.68	9 29.03	31
NODATA	0 0.00	1 33.33	1 33.33	1 33.33	3
NOISE	3 2.88	74 71.15	4 3.85	23 22.12	104
SANDv	1 5.26	8 42.11	4 21.05	6 31.58	19
SGd	2 20.00	5 50.00	1 10.00	2 20.00	10
	7	146	14	53	220

7.5.3. Sand

The prediction of “SANDv” (sand according to video data) by LFH was (4/19) 21 % accurate according to ground-truth video. LFH predicted “SANDv” in 15 cases where either sRCSv (scattered rock, coral, and/or sand), CPv (colonized pavement), or CP+SCd (colonized pavement with sand channels) existed according to video data. However, there are additional factors to consider: similar classes and sampling coverage.

7.5.4. Similar classes

If the video classification “sRCSv” (scattered rock, coral, and/or sand) is considered to represent mostly unconsolidated material, and to be indistinguishable in the bathymetry from unconsolidated sand (“SANDv”), then SANDv and sRCSv can be combined into a single class called unconsolidated. The LFH results suggest that those two classes were not really distinguishable by texture.

When SAND and sRCSv classes were combined into a single class (UNCONS), the accuracy of LFH classification improved. Under the circumstance where LFH classes SANDv and sRCSv were combined into a class called UNCONS (unconsolidated), the prediction of UNCONS by LFH was (10/19) 53 % accurate (Table 7.8).

Table 7.8. Contingency table for VidStruct by LFH class, where structure classes “SANDv” and “sCRSv” were combined into a single class representing unconsolidated material (“UNCONS”).

Count Row %	CP+SCv	CPv	UNCONS	
CPv	0 0.00	40 75.47	13 24.53	53
CPv+SGd	1 3.23	18 58.06	12 38.71	31
NODATA	0 0.00	1 33.33	2 66.67	3
NOISE	3 2.88	74 71.15	27 25.96	104
SGd	2 20.00	5 50.00	3 30.00	10
UNCONS	1 5.26	8 42.11	**10** 52.63	19
	7	146	67	220

7.5.5. Sampling coverage

The relatively low accuracy for LFH prediction of sandy or unconsolidated structure habitats was also a function of the video sampling. Very little video coverage existed in the regions where “SAND” was predicted by LFH (Figure 7.20). The majority of the area predicted to be “SAND” by LFH was considered to be valid and more accurate than indicated by video data according to inspection of the bathymetry.

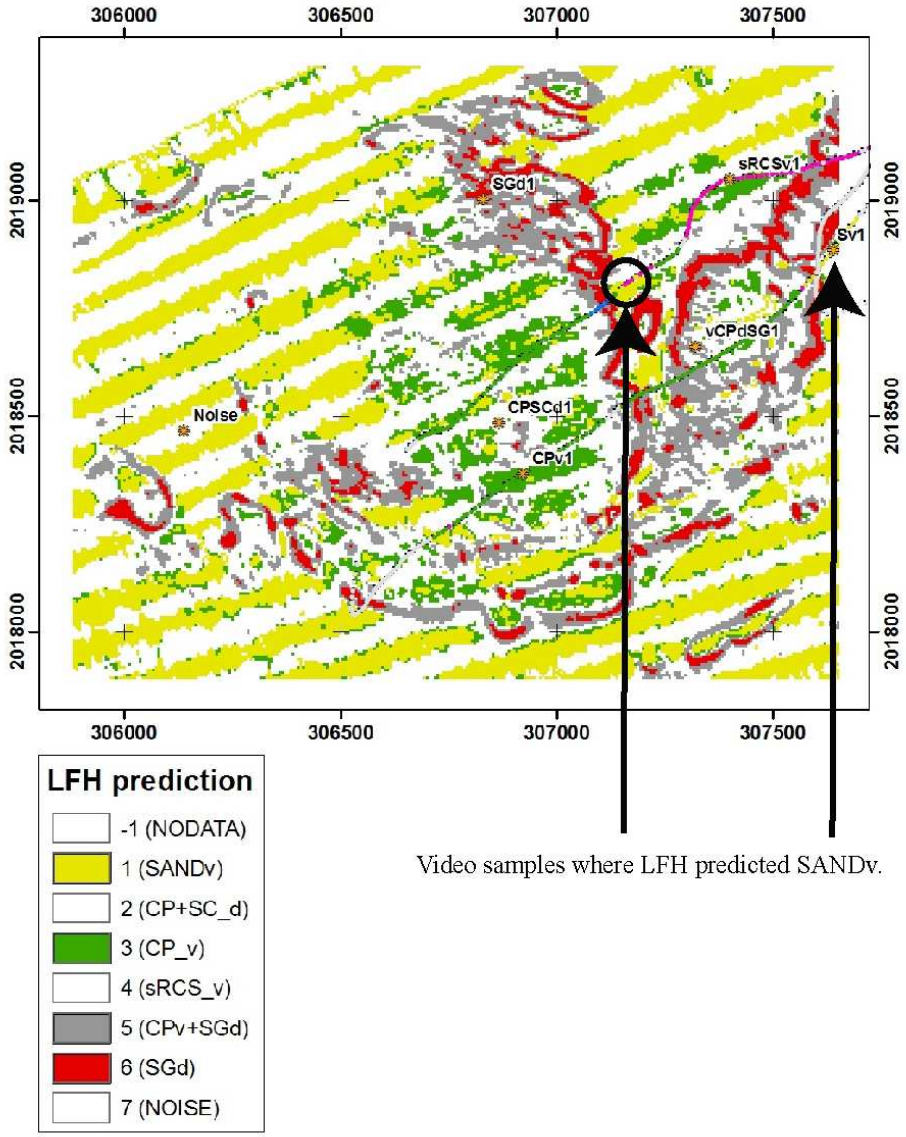

Figure 7.20. Map segmentation produced by supervised classification of LFH texture features. Arrows indicate the locations of the few locations where sand was identified from video imagery.

7.5.6. Spur and Groove

Spur and groove habitat structure was identified only by divers. Formal assessment of LFH class prediction for spur and groove (SGd) was not done because nearly all dive locations were in bathymetric noise.

7.6. Conclusions

Noise and data artifacts were revealed by LFMRGB, allowing development of a specific texture class for representing noise. In addition, the LFM's might provide a means for filtering the data noise, prior to analysis and classification.

The texture feature analysis of the bathymetry predicts that the sand class exists on the tops of some of the reef plateaus (Figure 7.18). Whether that is true or not is not determinable from the texture feature analysis. Additional constraints can be placed upon the classification of the LFH texture features by either considering additional data or incorporating other attributes (suggested by backscatter value, for instance). If that is not done, then similar morphologies will produce similar textures, and not be separated, even if the substrates or structures differ.

Distinct types of seafloor materials can be organized to generate similar morphologies that texture alone will not discriminate. In general, however, the LFH texture feature classification technique, using only gridded bathymetric data, works quite well to predict spatial distributions of seafloor morphologies and structure classes, on a cell-wise basis.

7.7. Acknowledgments

This work was supported by NOAA grant number NA17OG2285. Invaluable assistance and data were provided by T. Battista, A. Otter, M. Monaco, and others from the Biogeography Program of NOAA (NOS, NCCOS, CCMA).

7.8. References for Chapter 7

Cutter, G. R., Rzhanov, Y., Mayer, L. A., 2003. Automated segmentation of seafloor bathymetry from multibeam echosounder data using local Fourier histogram texture features. Journal of Experimental Marine Biology and Ecology, 285/286, 355-370.

Cutter Jr., G. R., 2005. Seafloor Texture Analysis of Saipan Anchorage Bathymetry using Local Fourier Histogram (LFH) Texture Features: LFH class maps from Saipan bathymetry using unsupervised classification and supervised classification based upon seafloor video image data. Final Report to the NMFS Pacific Islands Fisheries Center, F/PIC Natl. Marine Fisheries Service, Order number JJ133F04SE0124, Requisition/Ref. No. NFFR7400-4-00124, January 2005.

NOAA, 2004. Data Acquisition and Certification Report. Cruise Number NF-04-06-VI, W00123, W00124, and W00125, NOAA Ship Nancy Foster. St. Croix, St. John, and St. Thomas, U.S. Virgin Islands. Cruise Instructions dated January 2004. Chief Scientist: Mark E. Monaco, Lead Hydrographer: Sean C. Rooney.

Zhou, F., Feng, J., Shi, Q., 2001. Texture feature based on local Fourier transform. ICIP 2001 conference proceedings, pp. 610-613.

CHAPTER 8

8. SUMMARY AND CONCLUSIONS

Mapping seafloor habitats was a primary goal of this dissertation work and was accomplished using bathymetry and acoustic backscatter data from multibeam echosounders (MBES). This dissertation also reviews habitat concepts, marine habitat classification schemes, and habitat mapping efforts. MBES bathymetry data and acoustic backscatter data provided means of distinguishing habitats and facies. Habitats and facies could often be distinguished from high-resolution MB bathymetry grids, alone. When the seafloor contained even subtle, but consistent, morphological patterns, habitats could be delineated by eye from MB bathymetry. Apparent habitats were delineated using analyst interpretation (manual delineation), and using texture analysis and spatial covariance properties. Manual delineation was suitable for producing crude delineations of primary facies and habitats that corresponded to regions composed of prominent morphological features or patterns. When bathymetry or backscatter data were at higher resolutions, it was more difficult to determine where to define boundaries because so many feature details could be distinguished. Individual features such as rock outcrops or boulders, and subtle morphological differences that were not visible in lower-resolution maps could be seen in higher-resolution maps. Delineation then became a problem of

feature-identification rather than zonation. Hence, the efficacy of manual delineation methods can be reduced when data are high resolution.

Texture analysis and spatial covariance properties provided the basis for quantitative methods used to infer spatial distributions and zonations of seafloor characteristics. Texture feature analysis and spatial covariance classification served to overcome some of the bias of manual delineation methods for bathymetry and backscatter maps. Texture feature analysis could distinguish many different morphologies and identify them on a per-grid-cell basis. Per-grid-cell texture-feature classification is an improvement over manual delineation because it is often unclear where boundaries should be drawn or if boundaries should be drawn at all during manual delineation. Boundaries are not always apparent in seafloor bathymetry or backscatter data. Divisions between facies, habitats, or morphological regions sometimes exist, but are not often very distinct. Transitions between facies and habitats can be subtle or undetectable. Habitat patches can be small. In these cases, the automated methods that are based on statistical distributions of attributes measurable from bathymetry or backscatter maps can produce better delineations.

The results of texture feature classification was a segmentation; that is essentially a delineation of every map grid cell. Often, segmentation results resemble results of manual delineation because of feature zonations. However, segmentation methods are able to distinguish and classify much smaller map units than manual delineation methods. Segmentation by texture can produce products that appear noisy or overly heterogeneous, with many small units, and hence difficult to interpret and verify. Ground-truthing data representing similar spatial scales to the smallest variations in the segmentation products

are required to validate that different textures, for instance, correspond to differences in seafloor attributes. Backscatter data might be able to suggest that differences appear to exist for seafloor characteristics, but backscatter data must also be ground truthed.

Linkages were established between characteristics assessed using physical grab samples and seafloor video imagery. By regrouping and reanalyzing data from these different sources, inferences could be made using either source. Collecting and interpreting imagery is generally less expensive in terms of time and funds. Data from both are required from some locations in order to establish correspondence, but then data from imagery could be used alone for characterizations. Efforts that make ground-truth data from different sources compatible enhance the ability to make accurate characterization of seafloor attributes.

Imagery allows non-invasive inspection and larger coverage area than physical samples, but image detail can be limited. Also, assessing video image sequences for seafloor characteristics or biological resource assessments can be difficult and tedious. A mosaiced image produced from a sequence of images using co-registration techniques can overcome some of the difficulty involved with analyzing video sequences. However, producing mosaics can be time-consuming and mosaics can incorporate errors and can obscure features.

Results suggest that to achieve accurate counts of organisms or seafloor features from analysis of video imagery, care must be taken to ensure that the data samples represent non-overlapping fields-of-view. Mosaics eliminate the need to repeatedly review portions of a video-image sequence to determine the bounds of non-overlapping sampled fields-of-view by showing the entire coverage area. Image mosaics can

facilitate interpretation of processes occurring at spatial-scales not clearly evident in individual video image frames, and expand the capabilities of characterization. The mosaicing (image co-registration) process can be time-consuming, and accurate co-registration is not possible for all imagery. Video-image sequences or individual images from discrete locations can be as, or more, effective for determining seafloor characteristics or assessing biological resources. It is important to control how characteristics are measured or counted in video image sequences to avoid bias and have consistent, reproducible results.

Spectral model parameters that describe seafloor roughness that are important to empirical and theoretical models relating acoustic backscatter to seafloor properties can be estimated from sediment profile images. The combination of two spectral parameter estimates (slope and intercept) provide a better discrimination of seafloor facies and classification of seafloors than estimates of roughness from vertical elevation differences or RMS deviation. Spectral slope value and intercepts estimated from SPI are within the range reported for published values. The range of SPI spectral slope values (-2.60 to -2.05) suggests that spectral slope (or spectral exponent) should not be considered a constant term for models, even for the spatial frequencies of microtopographical profiles. The relationships between spectral slope and intercept values and physical and biogenic roughness and associated seafloor facies suggest that local seafloor zonation and facies distributions should be accounted for when interpreting and applying roughness spectra parameter values.

The number of classes and spatial-integration scale had to be specified arbitrarily for unsupervised classification of seafloor bathymetry. A single spatial-integration scale

was generally not sufficient for a study area; each morphological region tended to have a distinct spatial covariance properties. Hence, spatial covariance of bathymetry or backscatter could be used for classification and segmentation of habitats. Also, it was apparent that spatial covariance properties might provide a way to optimize defining spatial-integration scales used for unsupervised classification. However, the choice of number of classes for unsupervised classification would remain arbitrary.

Supervised classification provided a way to infer seafloor characteristics for entire bathymetric survey maps based on only sparse ground-truth data, and the number of classes were predetermined from ground-truth data. Results reported in this dissertation from supervised classification of MBES bathymetry using texture features had good correspondence with hold-out ground-truth data and spatial distributions of morphologies visible in the map. It was found that the verity of accuracy assessments from ground-truth data were provisional upon the circumstances of data collection, including positioning error. Positioning error also allowed inaccurate classification. If the positions of ground-truth data used for developing classification prototypes were inaccurate, then classes assigned to morphological textures at the reported locations could have been intended for nearby, but different morphologies. It is critical to account for heterogeneity if ground-truth positioning data have high uncertainty relative to the detail of the bathymetry or backscatter data used for classification.

It is important to allow for unknown, unidentified classes when implementing supervised classification to prevent data from being forced to fit into classification scheme developed from observations for only part of the area studied. Good, robust

classification results can be produced using supervised classification based on bathymetric texture and sparse ground-truth data

Supervised classification of bathymetric texture was implemented to account for data artifacts and prevent artifacts from affecting classifications. Distinct types of seafloor materials can be organized to generate similar morphologies that texture alone will not discriminate. In general, however, the LFH texture feature classification technique, using only gridded bathymetric data, works well to predict spatial distributions of seafloor morphologies and structure classes on a per-grid-cell basis and is robust to data artifacts. If systematic methods are included to account for conditions that do not fit a classification scheme, it is possible to produce consistent, accurate, and low-bias habitat maps and seafloor characterizations using semi-automated methods including classification using LFH texture features, spatial- and roughness-model parameters, or acoustic backscatter data.

APPENDICES

APPENDIX A

ROUGHNESS SPECTRA PARAMETERS FROM SEDIMENT PROFILE IMAGES FROM THE LOWER PISCATAQUA RIVER

A.1. Introduction

It has been shown that seafloor roughness spectra can be described using a power-law model, for spatial scales from centimeters to many kilometers (Fox and Hayes, 1985). Parameters describing the relationship between spectral power (or amplitude) and spatial frequency have been used for modeling acoustic backscatter from the seafloor (Jackson et al., 1986; APL-UW, 1994; Sternlicht and de Moustier, 2003). Although the backscatter models use two-dimensional forms of the parameters, typically the parameters are estimated from one-dimensional profiles that are extracted from seafloor elevation data from singlebeam and multibeam echosounders, stereophotographs, diver traces (Fox and Hayes, 1985; Stanic et al., 1988, 1989; Briggs, 1989; Jackson and Briggs, 1992) or laser lines.

This study uses sediment profile images to provide the seafloor elevation profile data. Profiles from digitized sediment profile imagery (SPI) images provide data series with a sub-millimeter resolution and 10 to 15 cm length. Thus, these images extend into a new spatial frequency band for seafloor spectral roughness measurement. The spatial frequency band represented by SPI images is important because it encompasses the

acoustic wavelength scales for many of the high-resolution multibeam echosounders, sidescan sonars, and interferometric sonars now in use.

A.2. Methods

Sediment profile images were acquired using a Diaz digital model SPI that incorporated a Minolta Dimage-8 digital camera. Images were collected on 19 May, 2003 from eight sites in the lower Piscataqua River, east of Newcastle Island, New Hampshire (Table A.1). The UNH research vessel R/V *Gulf Challenger* was used for the deployments.

A camera deployment involved lowering the system by winch wire to the seafloor, whereupon slack is provided for 20 to 30 s. During that time, the camera prism penetrates into the seafloor. In automatic operation mode, the camera descent begins a 5-s time delay sequence after which two images are captured with a 5-s delay between them. The camera was used in remote-controlled mode for this deployment. Remote control was accomplished using a cable from the camera to the surface vessel that terminated in a manual triggering device and carried a live video signal from the camera for remote monitoring of the operation. The time delay between touchdown and image capture allows the prism time to penetrate into the seafloor at a rate controlled by a water-filled piston that acts to dampen the penetration rate. During each deployment, two to four pseudoreplicate images were captured.

Analyses

Roughness spectra were calculated using the method of Briggs (1989). Images from sites 1, 5, 6, 7, and 8 (Figure A.1) were used to estimate spectra. First, the seafloor

interface was traced manually from the digital image, scaled according to known spatial scales so that data were generated in cm size-units rather than pixels. The seafloor profile data were a set of elevations and distances, (x,z). These data were submitted to the processing steps described by Briggs (1989) and implemented in D. Percival's FORTRAN code (unpublished). The first step was a pre-whitening operation (see Fox and Hayes, 1985) accomplished by taking the first differences of the elevation series then removing the mean. A 20% cosine taper was applied to the differenced, detrended series. A fast Fourier transform (FFT) was applied, producing coefficient values whose squared magnitudes were used as the uncorrected periodogram. The periodogram was corrected for the prewhitening operation and represents the estimated power spectrum.

The estimated power (S) and frequency (f) were log-transformed and a linear model fit to the log-log data. If the power approached white noise (flat spectrum) at the higher frequencies, then those frequencies were excluded from the fit and the linear model was recalculated to the restricted range. Noise rejection was necessary in all cases for the six images analyzed. The slope of the linear model and the intercept at a spatial frequency of 1 cycle/cm were recorded as the spectral parameters.

A.3. Results and Discussion

The SPI images analyzed came from two distinct facies within the lower Piscataqua River. Images 1 – 4 came from a gravel deposit and 5 – 8 were from a rippled sand dune (or sand wave) field that was easily distinguishable in bathymetric grids from multibeam echosounder data. Spectral slopes and intercepts were distinct for the two facies.

The spectral slope for the SPI image profile from the gravel deposit was -3.40 (Figure A.2), much larger than published values for gravel and larger in magnitude than the maximum value suggested by the APL-UW (1994) model. The spectral slope, as estimated here, is the negative of the one-dimensional (1-D) form of the spectral exponent (γ), as it is denoted by the acoustic modelers. The 2-D form of the exponent, γ_2, is $\gamma_2 = \gamma_1 + 1$ (Jackson et al., 1986). Therefore, in this case, the value of γ_2 from the gravel deposit of the lower Piscataqua River, was 4.40. The APL-UW (1994) model suggests an upper limit of 3.99 for the two-dimensional (2-D) form of the spectral exponent parameter. The spectral intercept for the gravel deposit SPI image, 0.00071, was also high relative to published values.

The absolute values of the spectral parameters for the the rippled sand dunes were not unusual with respect to published values. Spectral slopes for SPI image profiles from the rippled sand dunes ranged from -2.16 to -2.57, and intercepts ranged from 0.00015 to 0.00030 (Table A.2, Figure A.3, Figure A.4).

A.4. Conclusions

The sediment profile camera does not penetrate well, or at all sometimes, into sediments of pebble to cobble size. Therefore, the SPI camera is not a robust tool for examining in further detail the apparently unusual results obtained for the spectral parameters from the gravel deposit. For such sediments, a stereo photography system would produce better results, although perhaps at slightly lower resolution and spatial frequency scales. Other alternatives such as laser profilimetry are worth considering as options for collecting seafloor profile data.

A.5. Acknowledgments

I thank R. J. Diaz for the use of his sediment profile camera system for this survey. Also, I thank Kevin Briggs for invaluable discussion and for providing FORTRAN code and executable program from D. Percival that provided the basis for my coding efforts and establishing that results from these analyses were compatible with previous studies. This work was supported by NOAA grant number NA17OG2285.

A.6. References for Appendix A

APL-UW (Applied Physics Laboratory-University of Washington), 1994. APL-UW high-frequency ocean environmental acoustic models handbook. Applied Physics Laboratory, University of Washington, Seattle, Washington. Technical Report APL-UW TR 9407, AEAS 9501, October, 1994.

Briggs, K. B., 1989. Microtopographical roughness of shallow-water continental shelves. IEEE Journal of Oceanic Engineering, 14 (4), 360-367.

Fox, C. G., Hayes, D. E., 1985. Quantitative methods for analyzing the roughness of the seafloor. Rev. Geophys., 23 (1), 1-48.

Jackson, D. R.,Winebrenner, D. P., Ishimaru, A., 1986. Application of the composite roughness model to high-frequency bottom backscattering. J. Acoust. Soc. Am. 79 (5), 1410-1422.

Jackson, D. R., Briggs, K. B., 1992. High-frequency bottom backscattering: roughness versus sediment volume scattering. J. Acoust. Soc. Am. 92 (2), 962-977.

Sternlicht, D. D., de Moustier, C. P., 2003. Time-dependent seafloor acoustic backscatter (10-100 kHz). J. Acoust. Soc. Am. 114 (5), 2709-2725.

A.7. Tables for Appendix A

Table A.1. Sediment profile image (SPI) sample site locations for the Piscataqua River study area.

Sample code	Time (UTC)	Latitude (degrees decimal minutes)	Longitude (degrees decimal minutes)
PSPI1	16:08:17	43 03.484 N	070 42.156 W
PSPI2	16:11:55	43 03.587 N	070 42.207 W
PSPI3	16:14:55	43 03.706 N	070 42.237 W
PSPI4	16:25:40	43 03.814 N	070 42.267 W
PSPI5	16:29:00	43 03.919 N	070 42.270 W
PSPI6	16:31:30	43 03.994 N	070 42.297 W
PSPI7	16:34:00	43 04.086 N	070 42.319 W
PSPI8	16:36:10	43 04.181 N	070 42.322 W

Table A.2. Values of slope and intercept describing one-dimensional spectra from sediment profile images collected in the lower Piscataqua River, 2003.

Pspi	Slope	Int	SedClass	Note	Facies
1	-3.4003	0.0007068	Pebble,Cobble	-	Pebble-cobble gravel deposit
5	-2.1622	0.0002331	gravelly-Sand	gravel-size shell fragments	Rippled sand dunes
6	-2.1747	0.0001502	gravelly-Sand	gravel-size shell fragments	Rippled sand dunes
7	-2.5739	0.0002969	gravelly-Sand	gravel-size shell fragments	Rippled sand dunes
8	-2.4186	0.0002060	gravelly-Sand	gravel-size shell fragments	Rippled sand dunes

A.8. Figures for Appendix A

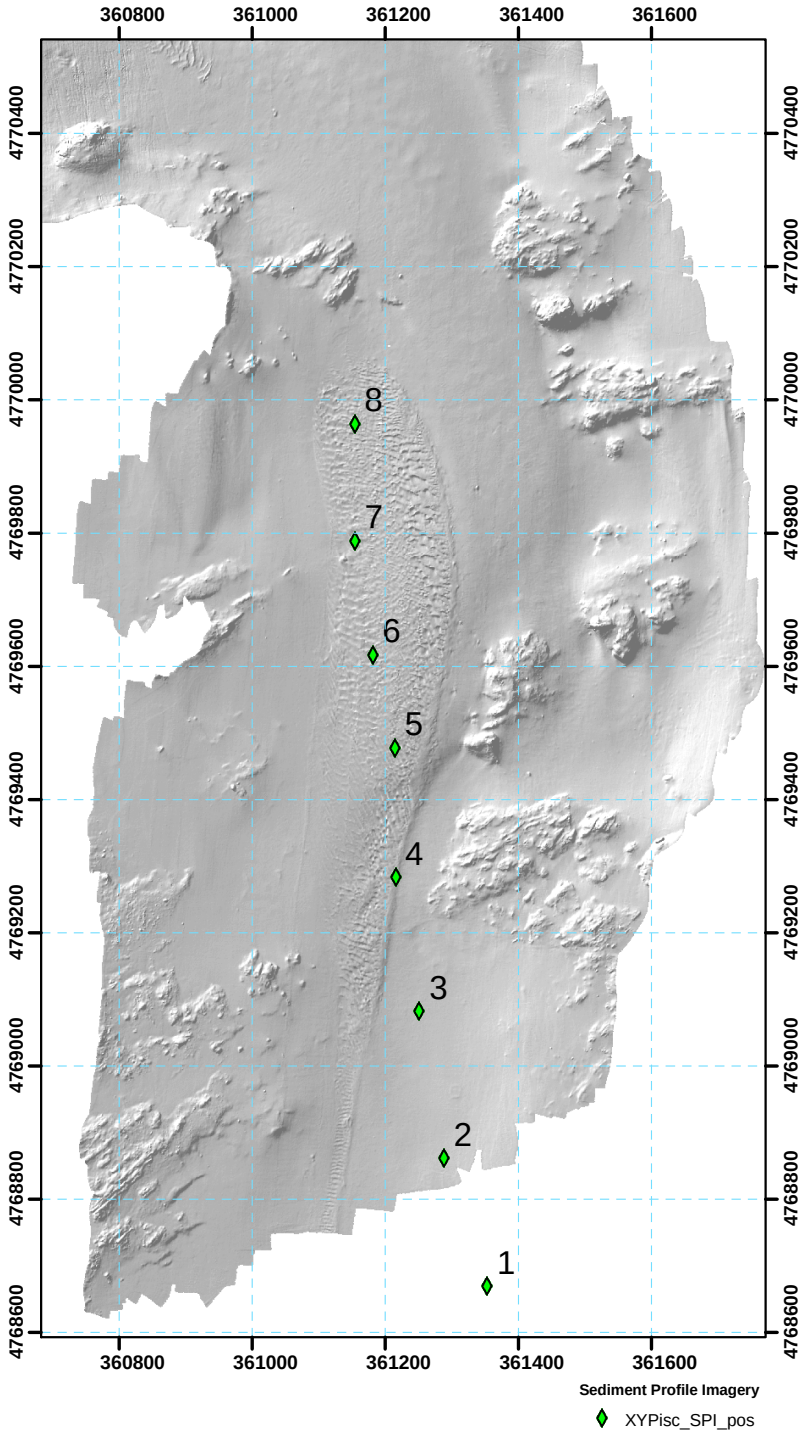

Figure A.1. Sediment profile image (SPI) sample site locations in the lower Piscataqua River.

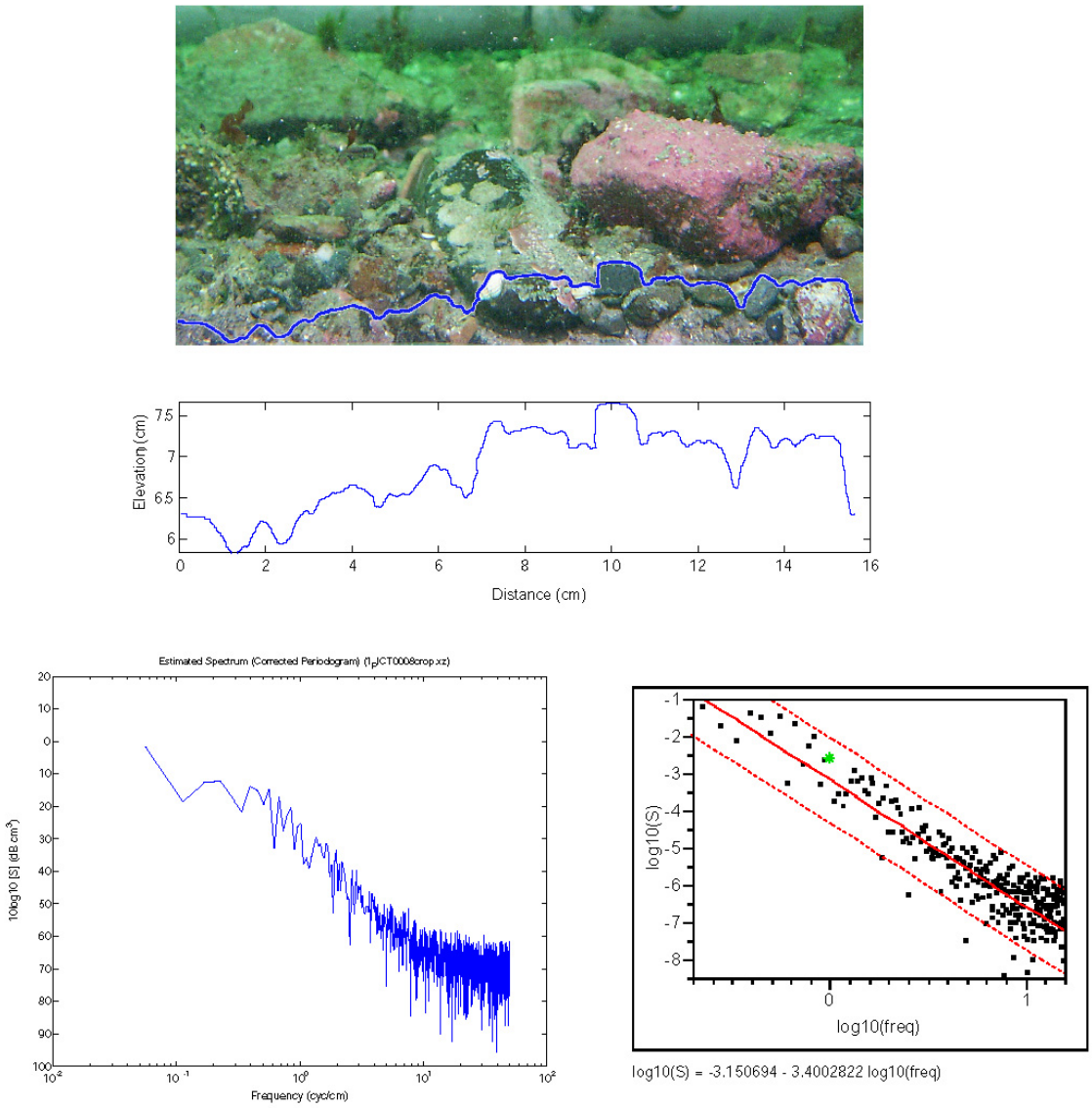

Figure A.2. Sediment profile image, seafloor profile and spectrum from Piscataqua River SPI sample site 1 (slope = -3.4003, intercept = 0.0007068).

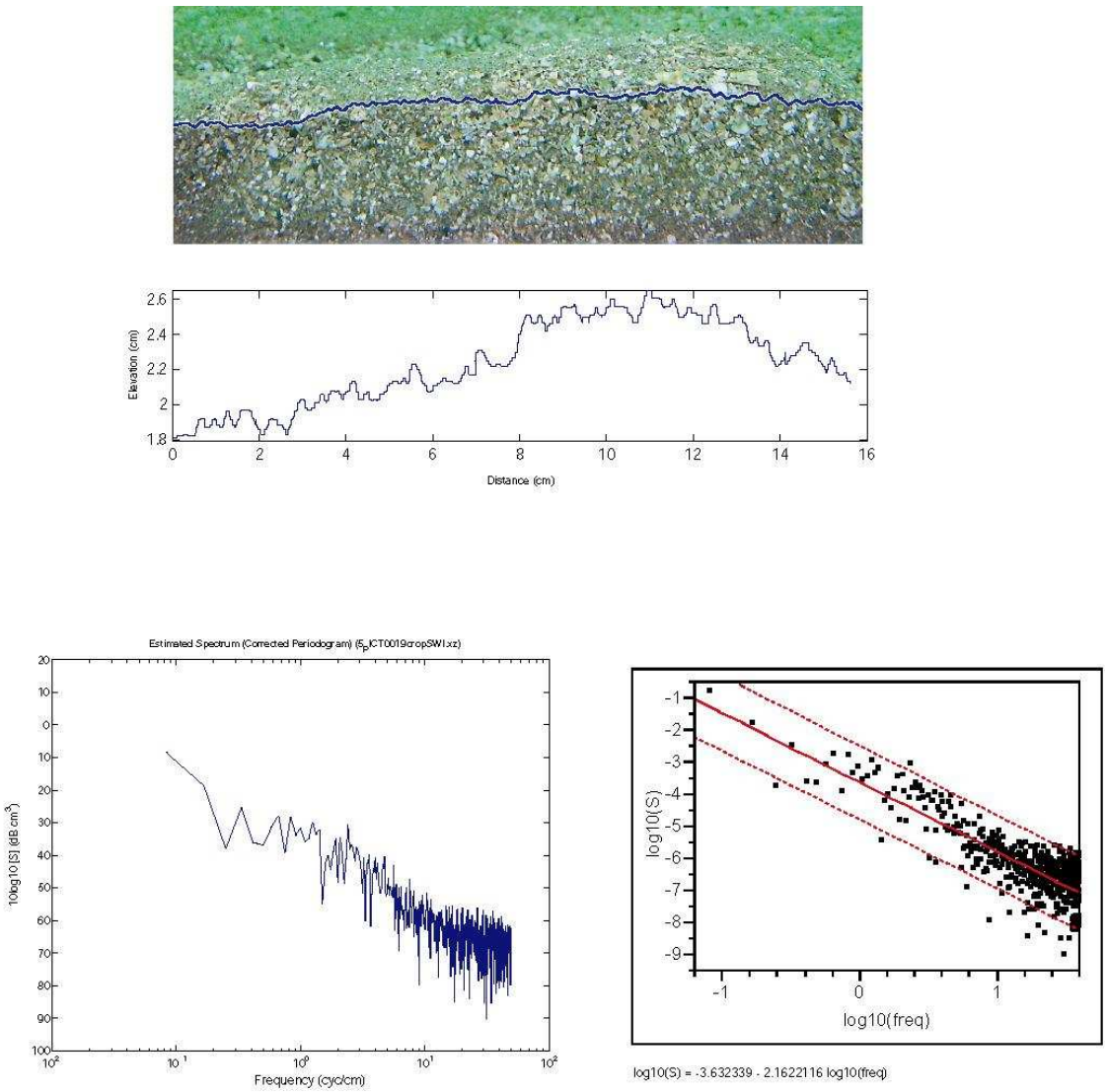

Figure A.3. Sediment profile image, seafloor profile and spectrum from Piscataqua River SPI sample site 5 (slope = -2.1622 , intercept = 0.0002331).

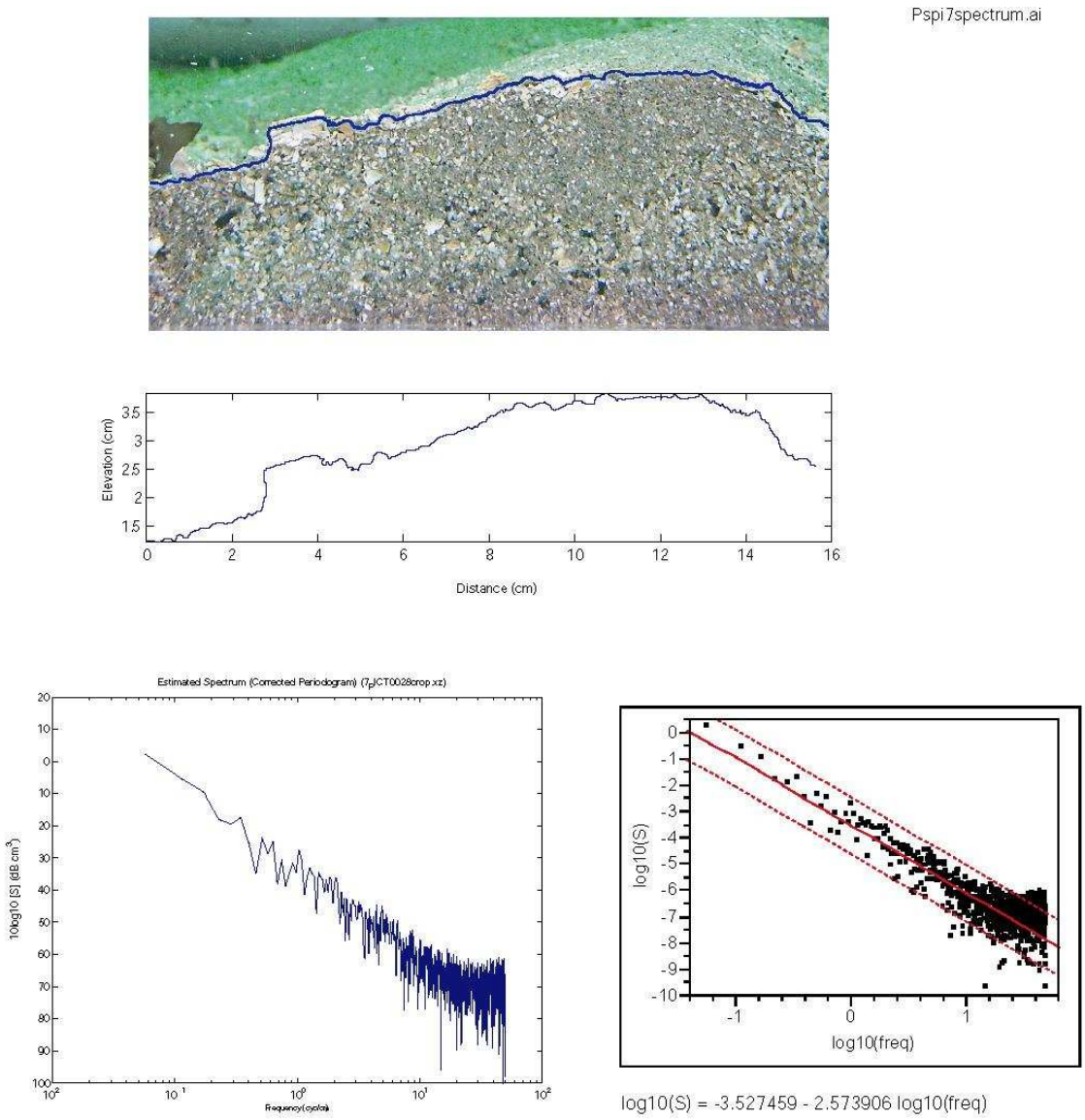

Figure A.4. Sediment profile image, seafloor profile and spectrum from Piscataqua River SPI sample site 7 (slope = -2.5739, intercept = 0.0002969).

APPENDIX B

DATA AND IMAGES USED FOR SEDIMENT GRAIN-SIZE CHARACTERIZATION

B-1. SEDIMENT GRAIN-SIZE DISTRIBUTION DATA FROM SAMPLES, GRAVEL NOT SEPARATED; USGS ANALYSIS

Table B.1. Sediment grain-size analysis data for the lower Piscataqua River; USGS method.

Station ID	N	Exclude	Cruise ID	Batch #	Analytical Method	# of classes	Coarse size limit	Intermediat fract bound	Total wt of subsamp	-1 phi	-0.75 phi
01_2	1		200209	Jgardner	124	48	-1.25	3.75	39.735	0.45	0
01_4	2		200209	Jgardner	124	48	-1.25	3.75	48.316	14.95	0
01_5	3		200209	Jgardner	124	48	-1.25	3.75	87.276	60.44	0
01_7	4		200209	Jgardner	124	48	-1.25	3.75	117.987	80.08	0
02_1	5		200209	Jgardner	124	48	-1.25	3.75	51.104	25.36	0
02_2	6		200209	Jgardner	124	48	-1.25	3.75	50.95	1.08	0
02_7	7		200209	Jgardner	124	48	-1.25	3.75	271.443	98.93	0
02_7rl		No record, maybe 3_7	200209	Jgardner	124	48	-1.25	3.75	41.721	23.83	0
02_10	8		200209	Jgardner	124	48	-1.25	3.75	67.527	57.49	0
03_1	9		200209	Jgardner	124	48	-1.25	3.75	52.415	51.7	0
03_2	10		200209	Jgardner	124	48	-1.25	3.75	222.934	98.6	0
03_7		Lost - No Data	200209	Jgardner							
03_10	11		200209	Jgardner	124	48	-1.25	3.75	132.654	68.48	0
04_1	12		200209	Jgardner	124	48	-1.25	3.75	58.076	10.7	0
04_2	13		200209	Jgardner	124	48	-1.25	3.75	67.024	2.77	0
04_3	14		200209	Jgardner	124	48	-1.25	3.75	51.517	6.26	0
04_5	15		200209	Jgardner	124	48	-1.25	3.75	66.52	10.61	0
04.1_2	16		200209	Jgardner	124	48	-1.25	3.75	59.794	72.07	0
04.1_3	17		200209	Jgardner	124	48	-1.25	3.75	79.463	24.63	0
04.1_4	18		200209	Jgardner	124	48	-1.25	3.75	97.829	89.07	0
04.1_5	19		200209	Jgardner	124	48	-1.25	3.75	143.474	61.77	0
05_3	20		200209	Jgardner	124	48	-1.25	3.75	154.575	97.05	0
05_8	21		200209	Jgardner	124	48	-1.25	3.75	96.045	74.09	0
05_9	22		200209	Jgardner	124	48	-1.25	3.75	42.587	61.15	0
06_1	23		200209	Jgardner	124	48	-1.25	3.75	67.801	10.32	0
06_2	24		200209	Jgardner	124	48	-1.25	3.75	91.536	94.18	0
06_3	25		200209	Jgardner	124	48	-1.25	3.75	128.638	98.35	0
06_4	26		200209	Jgardner	124	48	-1.25	3.75	115.632	61.55	0
06_5	27		200209	Jgardner	124	48	-1.25	3.75	216.691	69.09	0
06_8	28		200209	Jgardner	124	48	-1.25	3.75	119.482	47.77	0
07_3	29		200209	Jgardner	124	48	-1.25	3.75	98.73	37.48	0
07_5	30		200209	Jgardner	124	48	-1.25	3.75	201.185	68.05	0
07_9	31		200209	Jgardner	124	48	-1.25	3.75	70.589	87.91	0
07_11	32		200209	Jgardner	124	48	-1.25	3.75	80.472	27.37	0

Table B.1 (Continued). Sediment grain-size analysis data for the lower Piscataqua River; USGS method.

Station ID	-0.5 phi	-0.25 phi	0 phi	0.25 phi	0.5 phi	0.75 phi	1 phi	1.25 phi	1.5 phi	1.75 phi	2 phi	2.25 phi
01 2	0	0	0	0	0	0	0	0	1.96	0.98	7.85	15.7
01 4	0	0	0	0	0	0	0	3.27	2.46	10.64	19.65	21.28
01 5	0	0	0	0	0	0	0	1.11	1.48	4.08	7.79	9.28
01 7	0	0	0	0	0.18	0.35	0.53	0.71	2.3	3.01	3.37	3.19
02 1	0	0	0	0	0	0	0.72	0.72	2.17	7.96	13.75	19.54
02 2	0	0	0	0	0	0	0	0	0.96	8.66	24.06	30.79
02 7	0	0	0.04	0	0.11	0	0.07	0.16	0.09	0.9	0.09	0.08
02 7rl	0	0	0	0	1.49	2.98	3.73	16.38	11.17	15.63	13.4	6.7
02 10	0	0	0	0.37	0.37	1.1	1.83	4.4	2.94	7.34	7.34	5.87
03 1	0	0	0	0	0.89	1.34	1.79	3.57	4.47	6.7	5.8	5.36
03 2	0	0	0	0	0.08	0.09	0.06	0.15	0.07	0.1	0.06	0.06
03 7												
03 10	0	0	0	0	0	0	0	1	2.95	4.13	7.37	6.49
04 1	0	0	0	2.65	2.65	3.53	13.25	28.26	14.13	11.48	7.95	3.53
04 2	0	0	0	0	1.93	0.97	10.62	36.7	22.21	16.42	6.76	0.97
04 3	0	0	0	0	0.92	3.67	5.51	22.02	13.76	15.6	16.52	8.26
04 5	0	0	0.88	0.88	3.53	3.53	7.93	31.74	16.75	14.11	5.29	2.64
04.1 2	0	1.29	1.81	2.58	1.55	3.1	3.88	7.75	2.07	1.03	0.26	0.26
04.1 3	0	0	0.72	0.72	0.72	0	0.72	0	0.72	1.43	5.73	14.32
04.1 4	0	0	0.19	0.56	0.28	0.47	0.75	1.03	0.47	1.12	1.21	1.12
04.1 5	0	0	0	0.74	0	0.74	1.48	4.43	3.69	7.38	7.38	5.91
05 3	0	0	0	0	0	0	0	0.06	0.11	0.11	0.14	0.04
05 8	0	0	0	0.25	0.98	1.23	1.48	3.2	2.46	3.94	4.67	3.2
05 9	0.75	0.75	2.24	1.49	2.24	0.37	7.84	2.61	1.49	2.61	1.87	1.87
06 1	0	0	0	0	0	0	0.87	2.61	2.61	6.1	10.45	16.55
06 2	0	0	0	0	0	0.06	0.22	0.55	0.72	1.21	1.16	0.77
06 3	0	0	0	0.05	0.09	0.09	0.06	0.12	0.12	0.12	0.18	0.17
06 4	0	0	0	0.37	0.75	2.62	3	11.99	7.12	6.75	3	1.5
06 5	0	0.91	0	0.6	0.91	2.72	1.81	6.04	4.23	6.34	4.23	1.51
06 8	0	0	1.01	0.5	2.02	2.52	1.51	6.56	7.06	11.6	10.09	4.54
07 3	0	0	0	1.2	1.2	6	2.4	7.2	9	7.2	10.8	9.6
07 5	0	0	0	0	0	0	0.31	1.55	1.55	2.79	4.34	4.65
07 9	0	0	0	0	0.24	0	0.12	0.24	0.24	0.48	0.96	1.91
07 11	0	1.37	1.37	0.68	2.05	1.37	3.42	4.79	5.48	4.79	6.16	7.53

Table B.1 (Continued). Sediment grain-size analysis data for the lower Piscataqua River; USGS method.

Station ID	2.5 phi	2.75 phi	3 phi	3.25 phi	3.5 phi	3.75 phi	4 phi	4.25 phi	4.5 phi	4.75 phi	5 phi	5.25 phi
01 2	21.59	22.57	22.57	3.92	0.98	0	0	0.02	0.02	0.03	0.03	0.04
01 4	15.55	4.91	3.27	0.82	0	0	0	0.03	0.03	0.05	0.06	0.08
01 5	7.05	3.71	1.11	1.11	0.37	0	0	0.05	0.03	0.06	0.06	0.06
01 7	1.42	1.06	0.71	0.53	0.35	0	0	0.03	0.02	0.04	0.05	0.05
02 1	16.65	5.79	2.17	2.17	0	0.72	0.01	0.05	0.04	0.04	0.05	0.06
02 2	22.13	4.81	3.85	0.96	0	0	0	0.2	0.04	0.06	0.07	0.08
02 7	0.03	0.06	0.03	0.02	0	0.01	0.06	0.03	0.02	0	0.01	0
02 7rl	1.49	1.49	0	0	0	0	0.02	0.04	0.03	0.04	0.05	0.05
02 10	22.94	0.73	1.47	0	0	0	0.03	0.07	0.04	0.05	0.07	0.1
03 1	4.47	3.57	3.57	2.23	0.45	0.45	0.04	0.13	0.09	0.1	0.11	0.11
03 2	0.05	0.06	0.07	0.06	0.04	0.05	0	0.01	0.01	0.01	0.02	0.02
03 7												
03 10	4.42	1.18	0.59	0.59	0	0	0.01	0.03	0.02	0.03	0.04	0.05
04 1	0.88	0	0	0	0	0	0	0.01	0.01	0.02	0.03	0.03
04 2	0	0	0	0	0	0	0	0.01	0.01	0.01	0.02	0.02
04 3	1.84	0.92	0.92	1.84	0	0	0	0.02	0.03	0.04	0.06	0.06
04 5	0.88	0	0	0	0	0	0	0.02	0.02	0.02	0.03	0.04
04.1 2	0.26	0	0	0	0	0	0.03	0.05	0.04	0.05	0.06	0.07
04.1 3	15.03	12.89	6.44	5.01	5.01	1.43	0.73	0.14	0.11	0.11	0.12	0.12
04.1 4	0.75	0.47	0.37	0.19	0.19	0.19	0	0.03	0.04	0.05	0.07	0.08
04.1 5	2.22	0.74	0.37	0.37	0.37	0.37	0.74	0.01	0.02	0.03	0.03	0.03
05 3	0.28	0.33	0.39	0.67	0.36	0.14	0.03	0.01	0	0.01	0.01	0.01
05 8	1.72	0.49	0.25	0.49	0.25	0	0.02	0.04	0.02	0.03	0.03	0.04
05 9	1.12	2.24	4.48	3.36	0	0	0.02	0.05	0.03	0.04	0.05	0.05
06 1	18.29	13.06	7.84	1.74	1.74	0	0	0.05	0.05	0.06	0.07	0.08
06 2	0.33	0.11	0.06	0.11	0.11	0.11	0.01	0.01	0.01	0.02	0.01	0.01
06 3	0.15	0.12	0.14	0.06	0.02	0.02	0.02	0.01	0.01	0.01	0.01	0.01
06 4	0.37	0	0	0	0	0	0.01	0.02	0.01	0.02	0.02	0.03
06 5	0.6	0	0.3	0	0	0	0.01	0.02	0.01	0.02	0.02	0.02
06 8	2.02	0.5	0.5	0	0	0	0.01	0.03	0.02	0.03	0.04	0.05
07 3	4.2	0.6	0.6	0	0	0	0	0.01	0.02	0.03	0.03	0.04
07 5	5.27	4.65	4.03	1.24	0.31	0.31	0	0.02	0.02	0.02	0.03	0.03
07 9	2.51	2.87	1.79	0.36	0.24	0	0	0	0	0	0	0
07 11	9.59	8.22	5.48	3.42	1.37	1.37	0.03	0.2	0.14	0.15	0.15	0.15

Table B.1 (Continued). Sediment grain-size analysis data for the lower Piscataqua River; USGS method.

Station ID	5.5 phi	5.75 phi	6 phi	6.25 phi	6.5 phi	6.75 phi	7 phi	7.25 phi	7.5 phi	7.75 phi	8 phi	8.25 phi
01 2	0.05	0.05	0.05	0.03	0.07	0.06	0.06	0.07	0.07	0.07	0.07	0.07
01 4	0.09	0.1	0.1	0.07	0.16	0.14	0.18	0.2	0.22	0.23	0.22	0.21
01 5	0.07	0.08	0.08	0.06	0.13	0.12	0.13	0.15	0.17	0.18	0.17	0.15
01 7	0.06	0.07	0.07	0.05	0.13	0.11	0.13	0.15	0.16	0.17	0.16	0.14
02 1	0.06	0.07	0.07	0.05	0.1	0.09	0.11	0.12	0.13	0.14	0.14	0.14
02 2	0.09	0.1	0.1	0.06	0.14	0.01	0.12	0.14	0.15	0.16	0.15	0.16
02 7	0.01	0.01	0.01	0.01	0.01	0.01	0.01	0.01	0.01	0.02	0.01	0.01
02 7rl	0.06	0.06	0.07	0.05	0.12	0.1	0.1	0.1	0.1	0.09	0.09	0.08
02 10	0.12	0.13	0.14	0.1	0.29	0.3	0.4	0.47	0.5	0.52	0.49	0.45
03 1	0.12	0.12	0.13	0.09	0.2	0.16	0.18	0.19	0.2	0.2	0.2	0.19
03 2	0.03	0.03	0.03	0.02	0.04	0.03	0.02	0.02	0.02	0.01	0.01	0.01
03 7												
03 10	0.05	0.06	0.06	0.04	0.09	0.08	0.1	0.11	0.12	0.13	0.13	0.13
04 1	0.04	0.04	0.04	0.03	0.06	0.05	0.05	0.05	0.06	0.06	0.06	0.05
04 2	0.02	0.03	0.03	0.02	0.05	0.04	0.04	0.04	0.04	0.04	0.03	0.03
04 3	0.07	0.07	0.07	0.05	0.1	0.08	0.09	0.1	0.1	0.11	0.11	0.11
04 5	0.04	0.04	0.05	0.03	0.07	0.06	0.06	0.07	0.07	0.07	0.07	0.07
04.1 2	0.08	0.08	0.08	0.06	0.13	0.1	0.11	0.11	0.11	0.12	0.11	0.11
04.1 3	0.13	0.13	0.14	0.09	0.19	0.1	0.15	0.16	0.17	0.18	0.18	0.18
04.1 4	0.09	0.09	0.09	0.06	0.14	0.11	0.11	0.1	0.1	0.09	0.08	0.06
04.1 5	0.04	0.04	0.04	0.03	0.07	0.06	0.8	0.08	0.09	0.09	0.09	0.08
05 3	0.01	0.01	0.01	0.1	0.02	0.01	0.01	0.01	0.01	0.01	0.01	0
05 8	0.04	0.04	0.04	0.03	0.07	0.06	0.07	0.08	0.08	0.08	0.08	0.07
05 9	0.05	0.06	0.06	0.04	0.09	0.08	0.09	0.09	0.09	0.09	0.08	0.08
06 1	0.08	0.09	0.09	0.06	0.13	0.1	0.11	0.12	0.13	0.13	0.13	0.13
06 2	0.01	0.01	0.02	0.01	0.02	0.02	0.02	0.02	0.02	0.02	0.01	0.01
06 3	0.01	0.01	0.01	0.01	0.01	0.01	0.01	0.01	0.01	0	0	0
06 4	0.03	0.03	0.04	0.03	0.07	0.06	0.07	0.07	0.07	0.07	0.06	0.05
06 5	0.02	0.03	0.03	0.2	0.04	0.03	0.04	0.04	0.04	0.04	0.04	0.04
06 8	0.05	0.06	0.06	0.04	0.09	0.07	0.09	0.1	0.11	0.12	0.12	0.12
07 3	0.05	0.06	0.07	0.05	0.11	0.11	0.14	0.17	0.19	0.2	0.2	0.19
07 5	0.3	0.03	0.03	0.02	0.05	0.04	0.05	0.05	0.05	0.05	0.05	0.05
07 9	0	0	0	0	0.01	0	0	0	0.01	0.01	0.01	0.01
07 11	0.16	0.16	0.16	0.1	0.21	0.16	0.16	0.17	0.17	0.18	0.18	0.18

Table B.1 (Continued). Sediment grain-size analysis data for the lower Piscataqua River; USGS method.

Station ID	8.5 phi	8.75 phi	9 phi	9.25 phi	9.5 phi	9.75 phi	10 phi	10.25 phi	10.5 phi	14 phi	% Gravel	% Sand
01 2	0.07	0.07	0.06	0.06	0.05	0.05	0.04	0.04	0.12	0	0.45	98.12
01 4	0.19	0.16	0.14	0.11	0.09	0.08	0.07	0.05	0.16	0	14.95	81.86
01 5	0.13	0.11	0.09	0.07	0.05	0.04	0.03	0.03	0.14	0	60.44	37.11
01 7	0.12	0.1	0.08	0.06	0.05	0.04	0.03	0.03	0.11	0	80.08	17.72
02 1	0.13	0.11	0.1	0.09	0.07	0.06	0.05	0.05	0.13	0	25.36	72.39
02 2	0.15	0.13	0.12	0.1	0.09	0.08	0.06	0.05	0.14	0	1.08	96.23
02 7	0.01	0.01	0.01	0.01	0.1	0.1	0	0	0	0	98.93	0.87
02 7rl	0.08	0.01	0.06	0.05	0.04	0.04	0.03	0.02	0.06	0	23.83	74.47
02 10	0.39	0.31	0.24	0.17	0.12	0.09	0.06	0.04	0.13	0	57.49	36.72
03 1	0.18	0.15	0.13	0.11	0.1	0.08	0.08	0.07	0.2	0	51.7	44.69
03 2	0.01	0	0	0	0	0	0	0	0.01	0	98.6	1.02
03 7												
03 10	0.12	0.11	0.1	0.08	0.07	0.05	0.05	0.04	0.11	0	68.48	29.49
04 1	0.05	0.05	0.04	0.03	0.03	0.03	0.02	0.02	0.05	0	10.7	88.3
04 2	0.03	0.2	0.02	0.02	0.01	0.01	0.01	0.01	0.03	0	2.77	96.57
04 3	0.11	0.1	0.1	0.09	0.07	0.05	0.04	0.03	0.12	0	6.26	91.76
04 5	0.07	0.06	0.05	0.05	0.04	0.03	0.03	0.02	0.06	0	10.61	88.16
04.1 2	0.1	0.09	0.08	0.07	0.06	0.05	0.04	0.03	0.07	0	72.07	25.87
04.1 3	0.18	0.17	0.16	0.14	0.13	0.11	0.1	0.08	0.23	0	24.63	71.61
04.1 4	0.05	0.04	0.03	0.02	0.02	0.01	0.01	0.01	0.02	0	89.07	9.33
04.1 5	0.07	0.06	0.05	0.04	0.03	0.03	0.02	0.02	0.05	0	61.77	36.92
05 3	0	0	0	0	0	0	0	0	0	0	97.05	2.78
05 8	0.07	0.06	0.05	0.04	0.03	0.03	0.02	0.02	0.05	0	74.09	24.62
05 9	0.07	0.05	0.05	0.03	0.03	0.02	0.02	0.02	0.06	0	61.15	37.37
06 1	0.13	0.12	0.11	0.1	0.09	0.08	0.08	0.06	0.2	0	10.32	87.09
06 2	0.01	0.01	0.01	0.01	0.01	0.01	0	0	0.01	0	94.18	5.51
06 3	0	0	0	0	0	0	0	0	0	0	98.35	1.51
06 4	0.04	0.03	0.03	0.02	0.02	0.01	0.01	0.01	0.03	0	61.55	37.49
06 5	0.04	0.03	0.03	0.02	0.02	0.02	0.01	0.01	0.03	0	69.09	30.19
06 8	0.11	0.09	0.08	0.07	0.05	0.04	0.03	0.03	0.7	0	47.77	50.46
07 3	0.17	0.15	0.12	0.1	0.07	0.06	0.05	0.04	0.1	0	37.48	60
07 5	0.05	0.04	0.04	0.03	0.03	0.02	0.02	0.02	0.06	0	68.05	31.01
07 9	0.01	0.01	0	0	0	0	0	0	0.01	0	87.91	11.97
07 11	0.18	0.17	0.16	0.15	0.13	0.12	0.1	0.09	0.25	0	27.37	68.5

Table B.1 (Continued). Sediment grain-size analysis data for the lower Piscataqua River; USGS method.

Station ID	% Silt	% Clay	% Mud	Gravel/San	Sand/Silt	Silt/Clay	Sand/Clay	Sand/Mud	Gravel/Mud	1st momen	Variance	Std. deviati
01 2	0.8	0.64	1.43	0	123.27	1.25	153.71	68.41	0.31	2.54	0.63	0.79
01 4	1.93	1.26	3.19	0.18	42.4	1.54	65.18	25.69	4.69	1.76	2.6	1.61
01 5	1.6	0.85	2.45	1.63	23.23	1.88	43.61	15.16	24.69	0.29	3.82	1.96
01 7	1.45	0.75	2.2	4.52	12.23	1.94	23.75	8.07	36.48	-0.4	2.82	1.68
02 1	1.31	0.94	2.25	0.35	55.14	1.39	76.84	32.1	11.25	1.44	3.07	1.75
02 2	1.6	1.09	2.69	0.01	60.16	1.47	88..36	35.79	0.4	2.24	1.05	1.03
02 7	0.17	0.04	0.2	113.79	5.17	4.73	50	4.27	486.17	-1.09	0.19	0.44
02 7rl	1.17	0.53	1.7	0.32	63.82	2.18	139.19	43.76	14	0.97	2.12	1.46
02 10	3.79	2.01	5.79	1.57	9.7	1.89	18.29	6.34	9.92	0.42	5.1	2.23
03 1	2.31	1.29	3.61	1.16	19.33	1.79	34.55	12.4	14.34	0.55	4.29	2.07
03 2	0.33	0.04	0.38	96.8	3.05	7.75	23.63	2.7	261.38	-1.07	0.31	0.56
03 7												
03 10	1.17	0.86	2.03	2.32	25.22	1.36	34.42	14.55	33.79	-0.04	3.26	1.81
04 1	0.63	0.37	1	0.12	140.13	1.71	239.6	88.42	10.71	1.05	1.15	1.07
04 2	0.47	0.18	0.65	0.03	204.71	2.58	527.34	147.46	4.23	1.25	0.5	0.71
04 3	1.16	0.82	1.98	0.07	79.36	1.4	111.41	46.35	3.16	1.48	1.45	1.2
04 5	0.74	0.49	1.23	0.12	118.43	1.53	181.05	71.6	8.62	1.07	1.24	1.11
04.1 2	1.37	0.69	2.06	2.79	18.87	1.99	37.5	12.55	34.97	-0.46	2.09	1.45
04.1 3	2.25	1.51	3.76	0.34	31.84	1.49	47.42	19.05	6.55	1.74	3.98	2
04.1 4	1.32	0.28	1.6	9.55	7.08	4.63	32.83	5.83	55.65	-0.74	1.65	1.29
04.1 5	0.83	0.47	1.3	1.67	44.27	1.78	78.69	28.33	47.4	0.05	2.83	1.68
05 3	0.14	0.03	0.17	34.85	20.07	5.06	101.55	16.76	584.02	-1.01	0.47	0.68
05 8	0.84	0.45	1.29	3.01	29.17	1.88	54.87	19.04	57.32	-0.34	2.3	1.52
05 9	1.05	0.43	1.48	1.64	35.56	2.44	86.64	25.21	41.26	-0.02	2.83	1.68
06 1	1.48	1.11	2.59	0.12	58.78	1.33	78.39	33.59	3.98	2.09	2.22	1.49
06 2	0.23	0.08	0.31	17.08	24.14	2.83	68.22	17.83	304.56	-0.94	0.67	0.82
06 3	0.12	0.02	0.14	65.16	12.33	7.3	89.96	10.84	706.63	-1.07	0.22	0.47
06 4	0.69	0.27	0.96	1.64	54.18	2.56	138.73	38.96	63.97	-0.14	1.97	1.41
06 5	0.46	0.26	0.72	2.29	64.93	1.8	116.94	41.75	95.56	-0.33	1.8	1.34
06 8	1.08	0.7	1.78	0.95	46.84	1.54	72.21	28.41	26.89	0.35	2.82	1.68
07 3	1.49	1.03	2.52	0.62	40.32	1.44	58.02	23.79	14.86	0.7	3.16	1.78
07 5	0.59	0.4	0.94	2.19	52.71	1.66	87.32	32.87	72.14	-0.01	3.04	1.74
07 9	0.08	0.05	0.13	7.34	157.99	1.52	240.67	95.38	700.56	-0.7	1.39	1.18
07 11	2.6	1.53	4.12	0.4	26.38	1.7	44.85	16.61	6.64	1.32	4.02	2

Table B.1 (Continued). Sediment grain-size analysis data for the lower Piscataqua River; USGS method.

Station ID	3rd momen	4th momen	F&W media	F&W mean	F&W sortin	F&W skew	F&W kurtos	I. median	I. mean	I. sorting	I. skewness	I. skewness
01 2	4.62	44.31	2.52	2.46	0.33	-0.16	0.79	2.52	2.43	0.34	-0.25	-0.13
01 4	0.98	9.18	1.99	1.82	0.94	-0.48	2.87	1.99	1.74	0.66	-0.38	-1.74
01 5	1.48	6.12	-1.04	0.01	1.43	0.96	0.5	-1.04	0.53	1.71	0.92	1.11
01 7	2.95	13.59	-1.09	-0.27	1.22	0.96	9.37	-1.09	0.15	1.35	0.92	1.32
02 1	0.48	6.08	1.99	1.11	1.52	-0.63	0.53	1.99	0.67	1.76	-0.75	-0.61
02 2	4.28	30.93	2.12	2.12	0.33	0.07	1.6	2.12	2.12	0.28	-0.01	0.32
02 7	14.95	265.67	-1.12	-1.12	0.06	0.47	0.38	-1.12	-1.12	0.09	0	0.64
02 7rl	1	9.14	1.29	0.7	1.26	-0.52	1.03	1.29	0.41	1.49	-0.59	-0.52
02 10	1.89	6.91	-1.03	-0.06	1.89	0.95	1.03	-1.03	0.42	1.6	0.91	2.24
03 1	1.47	6.19	-1.01	0.07	1.52	0.95	0.55	-1.01	0.6	1.77	0.91	1.16
03 2	11.69	157.02	-1.12	-1.12	0.06	0.47	0.38	-1.12	-1.12	0.09	0	0.64
03 7												
03 10	2.04	8.82	-1.07	-0.09	1.32	0.96	0.52	-1.07	0.39	1.59	0.92	1.1
04 1	1.68	19.21	1.16	1.11	0.78	-0.28	2.26	1.16	1.09	0.59	-0.11	-1.19
04 2	3.56	49.33	1.24	1.28	0.35	0.07	1.32	1.24	1.3	0.3	0.17	-0.06
04 3	2.5	19.83	1.46	1.48	0.82	-0.14	2.24	1.46	1.49	0.5	0.06	-1.29
04 5	2.05	20.65	1.22	1.11	0.75	-0.41	2.39	1.22	1.06	0.55	-0.31	-1.46
04.1 2	3.73	21.41	-1.08	-0.47	0.88	0.94	0.87	-1.08	-0.17	1.03	0.89	1.17
04.1 3	0.46	5.02	2.26	1.39	1.75	-0.53	0.72	2.26	0.95	2.04	-0.64	-0.51
04.1 4	4.27	24.19	-1.11	-1.11	0.52	0.5	9.01	-1.11	-1.11	0.1	0	16.13
04.1 5	1.59	7.01	-1.05	-0.12	1.28	0.95	0.51	-1.05	0.34	1.53	0.91	1.11
05 3	6.68	54.69	-1.12	-1.12	0.06	0.47	0.38	-1.12	-1.12	0.09	0	0.64
05 8	2.49	11.9	-1.08	-0.25	1.18	0.96	0.82	-1.08	0.16	1.36	0.92	1.2
05 9	1.83	7.58	-1.05	-0.14	1.36	0.95	0.79	-1.05	0.31	1.5	0.91	1.35
06 1	0.7	9.98	2.26	2.19	1.03	-0.32	2.33	2.26	2.15	0.69	-0.15	-1.63
06 2	5.52	43.29	-1.12	-1.12	0.4	0.5	7.32	-1.12	-1.12	0.09	0	13.09
06 3	10.56	140.46	-1.12	-1.12	0.06	0.47	0.38	-1.12	-1.12	0.09	0	0.64
06 4	1.82	9.71	-1.05	-0.29	1.07	0.94	0.5	-1.05	0.09	1.28	0.89	1.11
06 5	2.13	11.01	-1.07	-0.3	1.08	0.95	0.59	-1.07	0.09	1.28	0.9	1.14
06 8	1.5	8	0.41	0.35	1.23	0.03	0.48	0.41	0.32	1.49	-0.06	0.14
07 3	1.45	7.92	1.1	0.66	1.32	-0.37	0.49	1.1	0.44	1.58	-0.41	-0.36
07 5	1.43	5.31	-1.07	0.01	1.46	0.96	0.54	-1.07	0.55	1.74	0.93	1.11
07 9	2.67	9.87	-1.11	-1.11	0.6	0.5	10.5	-1.11	-1.11	0.1	0	18.79
07 11	0.98	5.73	1.61	1.08	1.69	-0.29	0.56	1.61	0.82	1.92	-0.41	-0.22

Table B.1 (Continued). Sediment grain-size analysis data for the lower Piscataqua River; USGS method.

Station ID	I. kurtosis	T. median	T. mean	T. sorting	T. skewnes	T. kurtosis
01 2	0.61	0.17	0.18	1.22	1.01	0.28
01 4	2.05	0.25	0.26	1.22	1.02	0.03
01 5	0.11	2.06	1.23	2.98	0.13	0.46
01 7	0.32	2.13	2.14	1.06	1	0.06
02 1	0.2	0.25	1.11	3.13	6.5	0.44
02 2	1.2	0.23	0.23	1.12	1.03	0.19
02 7	-0.32	2.18	2.18	1.04	1	-5.45
02 7rl	0.15	0.41	0.53	1.61	1.37	0.12
02 10	1.5	2.05	1.25	2.71	0.16	0.45
03 1	0.17	2.01	1.22	2.9	0.14	0.45
03 2	-0.32	2.18	2.18	1.04	1	-5.47
03 7						
03 10	0.11	2.1	1.28	2.62	0.17	0.45
04 1	1.67	0.45	0.44	1.22	0.93	0.05
04 2	1.15	0.42	0.41	1.15	0.93	0.23
04 3	2.7	0.36	0.36	1.27	0.95	0.23
04 5	1.84	0.43	0.44	1.2	1.01	0.05
04.1 2	0.18	2.11	1.63	1.49	0.51	0.33
04.1 3	0.18	0.21	0.6	2.59	3.7	0.21
04.1 4	15.17	2.16	2.16	1.05	1	0.07
04.1 5	0.12	2.07	1.27	2.58	0.17	0.45
05 3	-0.32	2.18	2.18	1.05	1	-5.56
05 8	0.21	2.12	1.48	1.77	0.36	0.37
05 9	0.35	2.06	1.37	2.06	0.27	0.39
06 1	2.3	0.21	0.22	1.32	1.05	0.03
06 2	12.13	2.17	2.17	1.05	1	0.31
06 3	-0.32	2.18	2.18	1.05	1	-5.48
06 4	0.12	2.07	1.33	2.26	0.23	0.45
06 5	0.14	2.1	1.39	2.01	0.28	0.42
06 8	0.09	0.75	1.25	2.6	1.23	0.45
07 3	0.1	0.47	1.2	2.75	2.72	0.45
07 5	0.12	2.09	1.26	2.79	0.15	0.45
07 9	17.83	2.16	2.16	1.05	1	0.05
07 11	0.25	0.33	1.11	3.36	3.4	0.44

B-2. GRAIN-SIZE STATISTICS FROM GRADISTAT, SAMPLE DATA WITH GRAVEL NOT SEPARATED

Table B.2. Sediment grain-size analysis data for the lower Piscataqua River; GRADISTAT results, gravel not-separated.

SAMPLE STATISTICS

		200209_01_2	200209_01_4	200209_01_5	200209_01_7
	ANALYST AND DATE:	,	,	,	,
	SIEVING ERROR:				
	SAMPLE TYPE:	Unimodal, Well Sorted	Trimodal, Moderately Sorted	Bimodal, Poorly Sorted	Unimodal, Poorly Sorted
	TEXTURAL GROUP:	Slightly Gravelly Sand	Gravelly Sand	Sandy Gravel	Gravel
	SEDIMENT NAME:	Slightly Very Fine Gravelly Fine Sand	Very Fine Gravelly Fine Sand	Sandy Very Fine Gravel	Very Fine Gravel
METHOD OF MOMENTS Arithmetic (μm)	MEAN($\overline{x}_a$):	195.6	534.8	1409.9	1799.1
	SORTING(σ_a):	144.5	693.4	953.6	766.1
	SKEWNESS(Sk_a):	11.70	1.921	-0.437	-1.528
	KURTOSIS(K_a):	160.3	4.772	1.203	3.369
METHOD OF MOMENTS Geometric (μm)	MEAN($\overline{x}_g$):	180.3	323.0	870.5	1390.3
	SORTING(σ_g):	1.396	2.377	3.191	2.537
	SKEWNESS(Sk_g):	1.752	1.300	-0.597	-1.811
	KURTOSIS(K_g):	16.20	3.932	1.628	4.833
METHOD OF MOMENTS Logarithmic (ϕ)	MEAN($\overline{x}_\phi$):	2.471	1.630	0.200	-0.475
	SORTING(σ_ϕ):	0.481	1.249	1.674	1.343
	SKEWNESS(Sk_ϕ):	-1.752	-1.300	0.597	1.811
	KURTOSIS(K_ϕ):	16.20	3.932	1.628	4.833
FOLK AND WARD METHOD (μm)	MEAN(M_G):	178.8	282.0	996.4	1204.0
	SORTING(σ_G):	1.319	1.937	2.737	2.336
	SKEWNESS(Sk_G):	0.057	0.451	-0.916	-0.925
	KURTOSIS(K_G):	0.921	2.435	0.517	10.10
FOLK AND WARD METHOD (ϕ)	MEAN(M_Z):	2.483	1.826	0.005	-0.268
	SORTING(σ_I):	0.399	0.954	1.453	1.224
	SKEWNESS(Sk_I):	-0.057	-0.451	0.916	0.925
	KURTOSIS(K_G):	0.921	2.435	0.517	10.10
FOLK AND WARD METHOD (Description)	MEAN:	Fine Sand	Medium Sand	Coarse Sand	Very Coarse Sand
	SORTING:	Well Sorted	Moderately Sorted	Poorly Sorted	Poorly Sorted
	SKEWNESS:	Symmetrical	Very Coarse Skewed	Very Fine Skewed	Very Fine Skewed
	KURTOSIS:	Mesokurtic	Very Leptokurtic	Very Platykurtic	Extremely Leptokurtic
	MODE 1 (μm):	196.0	231.0	2180.0	2180.0
	MODE 2 (μm):		2180.0	231.0	
	MODE 3 (μm):		462.5		
	MODE 1 (ϕ):	2.356	2.119	-1.119	-1.119
	MODE 2 (ϕ):		-1.119	2.119	
	MODE 3 (ϕ):		1.117		
	D_{10} (μm):	128.8	165.8	185.3	257.3
	D_{50} (μm):	177.9	252.2	2058.1	2128.3
	D_{90} (μm):	257.3	2112.6	2296.3	2311.7
	(D_{90} / D_{10}) (μm):	1.998	12.74	12.39	8.986
	(D_{90} - D_{10}) (μm):	128.5	1946.8	2110.9	2054.5
	(D_{75} / D_{25}) (μm):	1.489	1.610	8.828	1.109
	(D_{75} - D_{25}) (μm):	71.01	125.6	1954.2	220.0
	D_{10} (ϕ):	1.958	-1.079	-1.199	-1.209
	D_{50} (ϕ):	2.491	1.987	-1.041	-1.090
	D_{90} (ϕ):	2.957	2.593	2.432	1.959
	(D_{90} / D_{10}) (ϕ):	1.510	-2.403	-2.028	-1.620
	(D_{90} - D_{10}) (ϕ):	0.999	3.672	3.631	3.168
	(D_{75} / D_{25}) (ϕ):	1.260	1.431	-1.756	0.872
	(D_{75} - D_{25}) (ϕ):	0.574	0.687	3.142	0.149
	% GRAVEL:	0.5%	14.9%	60.5%	80.1%
	% SAND:	99.5%	85.1%	39.5%	19.9%
	% MUD:	0.0%	0.0%	0.0%	0.0%
	% V COARSE GRAVEL:	0.0%	0.0%	0.0%	0.0%
	% COARSE GRAVEL:	0.0%	0.0%	0.0%	0.0%
	% MEDIUM GRAVEL:	0.0%	0.0%	0.0%	0.0%
	% FINE GRAVEL:	0.0%	0.0%	0.0%	0.0%
	% V FINE GRAVEL:	0.5%	14.9%	60.5%	80.1%
	% V COARSE SAND:	0.0%	0.0%	0.0%	0.0%
	% COARSE SAND:	0.0%	0.0%	0.0%	1.1%
	% MEDIUM SAND:	10.8%	36.0%	14.5%	9.4%
	% FINE SAND:	82.4%	45.0%	21.2%	6.4%
	% V FINE SAND:	6.3%	4.0%	3.9%	3.1%
	% V COARSE SILT:	0.0%	0.0%	0.0%	0.0%
	% COARSE SILT:	0.0%	0.0%	0.0%	0.0%
	% MEDIUM SILT:	0.0%	0.0%	0.0%	0.0%
	% FINE SILT:	0.0%	0.0%	0.0%	0.0%
	% V FINE SILT:	0.0%	0.0%	0.0%	0.0%
	% CLAY:	0.0%	0.0%	0.0%	0.0%

Table B.2 (Continued). Sediment grain-size analysis data for the lower Piscataqua River; GRADISTAT results, gravel not-separated.

	SAMPLE	200209_02_1	200209_02_10	200209_02_2	200209_02_7
	ANALYST				
	SIEVING				
	SAMPLE	Bimodal, Poorly Sorted	Bimodal, Poorly Sorted	Unimodal, Well Sorted	Unimodal, Very Well Sorted
	TEXTURA	Gravelly Sand	Sandy Gravel	Slightly Gravelly Sand	Gravel
	SEDIMENT	Very Fine Gravelly Fine Sand	Sandy Very Fine Gravel	Slightly Very Fine Gravelly Fine Sand	Very Fine Gravel
METHOD OF MOMENTS Arithmetic (μm)	MEAN ($\bar{x}_a$	727.6	1182.1	252.4	2139.6
	SORTING	849.3	962.1	209.1	273.5
	SKEWNE	1.112	0.054	8.427	-6.698
	KURTOS	2.266	1.037	77.97	46.27
METHOD OF MOMENTS Geometric (μm)	MEAN ($\bar{x}_g$	393.3	676.5	227.7	2071.7
	SORTING	2.838	3.261	1.456	1.404
	SKEWNE	0.811	-0.235	1.378	-7.762
	KURTOS	2.185	1.485	17.23	66.53
METHOD OF MOMENTS Logarithmic (ϕ)	MEAN ($\bar{x}_\phi$	1.346	0.564	2.135	-1.051
	SORTING	1.505	1.705	0.542	0.490
	SKEWNE	-0.811	0.235	-1.378	7.762
	KURTOS	2.185	1.485	17.23	66.53
FOLK AND WARD METHOD (μm)	MEAN (M	463.1	625.1	230.7	2168.6
	SORTING	2.864	2.854	1.285	1.053
	SKEWNE	0.629	0.056	-0.090	0.000
	KURTOS	0.521	0.510	1.227	0.738
FOLK AND WARD METHOD (ϕ)	MEAN (M	1.111	0.678	2.116	-1.117
	SORTING	1.518	1.513	0.362	0.075
	SKEWNE	-0.629	-0.056	0.090	0.000
	KURTOS	0.521	0.510	1.227	0.738
FOLK AND WARD METHOD (Description)	MEAN:	Medium Sand	Coarse Sand	Fine Sand	Very Fine Gravel
	SORTING	Poorly Sorted	Poorly Sorted	Well Sorted	Very Well Sorted
	SKEWNE	Very Coarse Skewed	Symmetrical	Symmetrical	Symmetrical
	KURTOS	Very Platykurtic	Very Platykurtic	Leptokurtic	Platykurtic
	MODE 1	2180.0	2180.0	231.0	2180.0
	MODE 2	231.0	196.0		
	MODE 3				
	MODE 1	-1.119	-1.119	2.119	-1.119
	MODE 2	2.119	2.356		
	MODE 3				
	D_{10} (μm):	163.2	185.2	164.6	2026.7
	D_{50} (μm):	252.3	561.0	230.4	2168.6
	D_{90} (μm):	2210.9	2279.9	304.1	2320.4
	(D_{90} / D_{10}	13.55	12.31	1.848	1.145
	(D_{90} - D_{10}	2047.7	2094.7	139.5	293.7
	(D_{75} / D_{25}	9.910	10.28	1.362	1.088
	(D_{75} - D_{25}	1802.5	1954.1	71.53	183.5
	D_{10} (ϕ):	-1.145	-1.189	1.717	-1.214
	D_{50} (ϕ):	1.987	0.834	2.118	-1.117
	D_{90} (ϕ):	2.615	2.433	2.603	-1.019
	(D_{90} / D_{10}	-2.285	-2.046	1.516	0.839
	(D_{90} - D_{10}	3.760	3.622	0.886	0.195
	(D_{75} / D_{25}	-2.298	-2.017	1.235	0.896
	(D_{75} - D_{25}	3.309	3.362	0.446	0.122
	% GRAVE	25.4%	47.9%	1.1%	97.8%
	% SAND:	74.6%	52.1%	98.9%	2.2%
	% MUD:	0.0%	0.0%	0.0%	0.0%
	% V COA	0.0%	0.0%	0.0%	0.0%
	% COARS	0.0%	0.0%	0.0%	0.0%
	% MEDIU	0.0%	0.0%	0.0%	0.0%
	% FINE G	0.0%	0.0%	0.0%	0.0%
	% V FINE	25.4%	47.9%	1.1%	97.8%
	% V COA	0.0%	0.0%	0.0%	0.0%
	% COARS	0.7%	3.1%	0.0%	0.2%
	% MEDIU	24.6%	18.3%	33.7%	1.2%
	% FINE S	44.2%	25.8%	61.5%	0.2%
	% V FINE	5.2%	4.8%	3.7%	0.5%
	% V COA	0.0%	0.0%	0.0%	0.0%
	% COARS	0.0%	0.0%	0.0%	0.0%
	% MEDIU	0.0%	0.0%	0.0%	0.0%
	% FINE S	0.0%	0.0%	0.0%	0.0%
	% V FINE	0.0%	0.0%	0.0%	0.0%
	% CLAY:	0.0%	0.0%	0.0%	0.0%

Table B.2 (Continued). Sediment grain-size analysis data for the lower Piscataqua River; GRADISTAT results, gravel not-separated.

	SAMPLE	200209_02_7rl	200209_03_1	200209_03_10	200209_03_2
	ANALYST				
	SIEVING				
	SAMPLE	Trimodal, Poorly Sorted	Unimodal, Poorly Sorted	Unimodal, Poorly Sorted	Unimodal, Very Well Sorted
	TEXTURA	Gravelly Sand	Sandy Gravel	Sandy Gravel	Gravel
	SEDIMENT	Very Fine Gravelly Medium Sand	Sandy Very Fine Gravel	Sandy Very Fine Gravel	Very Fine Gravel
METHOD OF MOMENTS Arithmetic (μm)	MEAN($\bar{x}_a$)	801.1	1262.1	1583.8	2154.2
	SORTING	780.0	955.5	891.4	221.4
	SKEWNE	1.155	-0.103	-0.833	-8.561
	KURTOSI	2.437	1.052	1.708	75.08
METHOD OF MOMENTS Geometric (μm)	MEAN($\bar{x}_g$)	533.1	746.3	1091.5	2103.0
	SORTING	2.360	3.250	2.871	1.342
	SKEWNE	0.600	-0.430	-1.012	-9.744
	KURTOSI	2.447	1.629	2.366	101.4
METHOD OF MOMENTS Logarithmic (ϕ)	MEAN($\bar{x}_\phi$)	0.907	0.422	-0.126	-1.072
	SORTING	1.239	1.700	1.522	0.425
	SKEWNE	-0.600	0.430	1.012	9.744
	KURTOSI	2.447	1.629	2.366	101.4
FOLK AND WARD METHOD (μm)	MEAN(M_z)	615.5	956.7	1064.5	2170.1
	SORTING	2.401	2.928	2.542	1.053
	SKEWNE	0.507	-0.908	-0.920	0.000
	KURTOSI	1.078	0.589	0.544	0.738
FOLK AND WARD METHOD (ϕ)	MEAN(M_z)	0.700	0.064	-0.090	-1.118
	SORTING	1.264	1.550	1.346	0.074
	SKEWNE	-0.507	0.908	0.920	0.000
	KURTOSI	1.078	0.589	0.544	0.738
FOLK AND WARD METHOD (Description)	MEAN:	Coarse Sand	Coarse Sand	Very Coarse Sand	Very Fine Gravel
	SORTING	Poorly Sorted	Poorly Sorted	Poorly Sorted	Very Well Sorted
	SKEWNE	Very Coarse Skewed	Very Fine Skewed	Very Fine Skewed	Symmetrical
	KURTOSI	Mesokurtic	Very Platykurtic	Very Platykurtic	Platykurtic
	MODE 1	2180.0	2180.0	2180.0	2180.0
	MODE 2	462.5			
	MODE 3	327.5			
	MODE 1	-1.119	-1.119	-1.119	-1.119
	MODE 2	1.117			
	MODE 3	1.616			
	D_{10} (μm):	242.0	147.3	218.2	2029.2
	D_{50} (μm):	414.5	2010.9	2093.4	2170.1
	D_{90} (μm):	2201.8	2285.6	2304.1	2320.7
	(D_{50} / D_{10})	9.099	15.52	10.56	1.144
	(D_{50} - D_{10})	1959.8	2138.3	2085.9	291.5
	(D_{75} / D_{25})	2.459	8.379	6.787	1.088
	(D_{75} - D_{25})	438.9	1918.5	1895.2	182.1
	D_{10} (ϕ):	-1.139	-1.193	-1.204	-1.215
	D_{50} (ϕ):	1.271	-1.008	-1.066	-1.118
	D_{90} (ϕ):	2.047	2.763	2.196	-1.021
	(D_{90} / D_{10})	-1.798	-2.317	-1.824	0.841
	(D_{90} - D_{10})	3.186	3.956	3.401	0.194
	(D_{75} / D_{25})	3.984	-1.730	-1.398	0.897
	(D_{75} - D_{25})	1.298	3.067	2.763	0.121
	% GRAVE	23.8%	51.7%	69.0%	98.6%
	% SAND:	76.2%	48.3%	31.0%	1.4%
	% MUD:	0.0%	0.0%	0.0%	0.0%
	% V COA	0.0%	0.0%	0.0%	0.0%
	% COARS	0.0%	0.0%	0.0%	0.0%
	% MEDIU	0.0%	0.0%	0.0%	0.0%
	% FINE G	0.0%	0.0%	0.0%	0.0%
	% V FINE	23.8%	51.7%	69.0%	98.6%
	% V COA	0.0%	0.0%	0.0%	0.0%
	% COARS	8.2%	4.0%	0.0%	0.2%
	% MEDIU	56.6%	20.5%	15.6%	0.4%
	% FINE S	9.7%	17.0%	12.8%	0.2%
	% V FINE	1.6%	6.8%	2.6%	0.5%
	% V COA	0.0%	0.0%	0.0%	0.0%
	% COARS	0.0%	0.0%	0.0%	0.0%
	% MEDIU	0.0%	0.0%	0.0%	0.0%
	% FINE S	0.0%	0.0%	0.0%	0.0%
	% V FINE	0.0%	0.0%	0.0%	0.0%
	% CLAY:	0.0%	0.0%	0.0%	0.0%

Table B.2 (Continued). Sediment grain-size analysis data for the lower Piscataqua River; GRADISTAT results, gravel not-separated.

	SAMPLE	200209_04.1_2	200209_04.1_3	200209_04.1_4	200209_04.1_5
	ANALYST		,	,	,
	SIEVING				
	SAMPLE	Unimodal, Moderately Sorted	Polymodal, Poorly Sorted	Unimodal, Moderately Well Sorte	Unimodal, Poorly Sorted
	TEXTURA	Sandy Gravel	Gravelly Sand	Gravel	Sandy Gravel
	SEDIMENT	Sandy Very Fine Gravel	Very Fine Gravelly Fine Sand	Very Fine Gravel	Sandy Very Fine Gravel
METHOD OF MOMENTS Arithmetic (μm)	MEAN($\overline{x}_a$	1735.7	692.2	1978.4	1458.3
	SORTING	730.4	860.1	580.5	914.0
	SKEWNE	-1.120	1.117	-2.583	-0.496
	KURTOSI	2.417	2.306	7.812	1.282
METHOD OF MOMENTS Geometric (μm)	MEAN($\overline{x}_g$	1437.4	330.1	1719.6	976.6
	SORTING	2.126	3.184	2.043	2.893
	SKEWNE	-1.948	0.772	-3.101	-0.807
	KURTOSI	6.759	2.062	11.73	2.192
METHOD OF MOMENTS Logarithmic (ϕ)	MEAN($\overline{x}_\phi$	-0.523	1.599	-0.782	0.034
	SORTING	1.088	1.671	1.031	1.532
	SKEWNE	1.948	-0.772	3.101	0.807
	KURTOSI	6.759	2.062	11.73	2.192
FOLK AND WARD METHOD (μm)	MEAN(M	1386.2	383.0	2150.5	1078.8
	SORTING	1.864	3.365	1.444	2.506
	SKEWNE	-0.887	0.527	-0.462	-0.909
	KURTOSI	0.932	0.705	9.778	0.555
FOLK AND WARD METHOD (ϕ)	MEAN(M	-0.471	1.385	-1.105	-0.109
	SORTING	0.898	1.751	0.530	1.326
	SKEWNE	0.887	-0.527	0.462	0.909
	KURTOSI	0.932	0.705	9.778	0.555
FOLK AND WARD METHOD (Description)	MEAN:	Very Coarse Sand	Medium Sand	Very Fine Gravel	Very Coarse Sand
	SORTING	Moderately Sorted	Poorly Sorted	Moderately Well Sorted	Poorly Sorted
	SKEWNE	Very Fine Skewed	Very Coarse Skewed	Very Fine Skewed	Very Fine Skewed
	KURTOSI	Mesokurtic	Platykurtic	Extremely Leptokurtic	Very Platykurtic
	MODE 1	2180.0	2180.0	2180.0	2180.0
	MODE 2		196.0		
	MODE 3		98.00		
	MODE 1	-1.119	-1.119	-1.119	-1.119
	MODE 2		2.356		
	MODE 3		3.356		
	D_{10} (μm):	462.5	103.0	744.1	229.8
	D_{50} (μm):	2104.0	211.4	2150.5	2062.1
	D_{90} (μm):	2306.4	2206.7	2316.5	2297.2
	(D_{50} / D_{10}	4.987	21.42	3.113	9.996
	(D_{50} - D_{10}	1843.9	2103.7	1572.4	2067.4
	(D_{75} / D_{25}	2.194	6.976	1.097	6.605
	(D_{75} - D_{25}	1212.7	930.9	199.9	1872.1
	D_{10} (ϕ):	-1.206	-1.142	-1.212	-1.200
	D_{50} (ϕ):	-1.073	2.242	-1.105	-1.044
	D_{90} (ϕ):	1.113	3.279	0.426	2.122
	(D_{50} / D_{10}	-0.923	-2.872	-0.352	-1.768
	(D_{50} - D_{10}	2.318	4.421	1.638	3.321
	(D_{75} / D_{25}	0.019	-22.375	0.886	-1.386
	(D_{75} - D_{25}	1.134	2.802	0.134	2.724
	% GRAVE	72.1%	24.6%	89.0%	61.3%
	% SAND:	27.9%	75.4%	11.0%	38.7%
	% MUD:	0.0%	0.0%	0.0%	0.0%
	% V COA	0.0%	0.0%	0.0%	0.0%
	% COARS	0.0%	0.0%	0.0%	0.0%
	% MEDIU	0.0%	0.0%	0.0%	0.0%
	% FINE G	0.0%	0.0%	0.0%	0.0%
	% V FINE	72.1%	24.6%	89.0%	61.3%
	% V COA	3.1%	0.7%	0.2%	0.0%
	% COARS	11.1%	2.2%	2.1%	2.9%
	% MEDIU	11.1%	7.9%	3.8%	22.7%
	% FINE S	0.5%	48.7%	2.7%	9.2%
	% V FINE	2.1%	15.9%	2.2%	3.8%
	% V COA	0.0%	0.0%	0.0%	0.0%
	% COARS	0.0%	0.0%	0.0%	0.0%
	% MEDIU	0.0%	0.0%	0.0%	0.0%
	% FINE S	0.0%	0.0%	0.0%	0.0%
	% V FINE	0.0%	0.0%	0.0%	0.0%
	% CLAY:	0.0%	0.0%	0.0%	0.0%

Table B.2 (Continued). Sediment grain-size analysis data for the lower Piscataqua River; GRADISTAT results, gravel not-separated.

	SAMPLE	200209_04_1	200209_04_2	200209_04_3	200209_04_5
	ANALYST				
	SIEVING				
	SAMPLE	Bimodal, Moderately Sorted	Unimodal, Well Sorted	Trimodal, Moderately Sorted	Bimodal, Moderately Sorted
	TEXTURA	Gravelly Sand	Slightly Gravelly Sand	Gravelly Sand	Gravelly Sand
	SEDIMENT	Very Fine Gravelly Medium Sand	Slightly Very Fine Gravelly Medium Sand	Very Fine Gravelly Medium Sand	Very Fine Gravelly Medium Sand
METHOD OF MOMENTS Arithmetic (μm)	MEAN($\bar{x}_a$	630.2	470.9	478.9	624.8
	SORTING	554.8	304.8	457.4	553.8
	SKEWNE	2.249	4.835	3.155	2.275
	KURTOS	6.570	27.39	12.02	6.654
METHOD OF MOMENTS Geometric (μm)	MEAN($\bar{x}_g$	497.7	426.6	378.8	493.4
	SORTING	1.851	1.471	1.840	1.849
	SKEWNE	0.953	1.128	0.799	0.946
	KURTOS	4.865	13.26	5.930	5.138
METHOD OF MOMENTS Logarithmic (ϕ)	MEAN($\bar{x}_\phi$	1.007	1.229	1.400	1.019
	SORTING	0.888	0.556	0.860	0.886
	SKEWNE	-0.953	-1.128	-0.799	-0.946
	KURTOS	4.865	13.26	5.930	5.138
FOLK AND WARD METHOD (μm)	MEAN(M_z	464.5	412.2	359.1	466.2
	SORTING	1.711	1.280	1.760	1.688
	SKEWNE	0.266	-0.154	0.139	0.324
	KURTOS	2.003	1.221	1.999	2.282
FOLK AND WARD METHOD (ϕ)	MEAN(M_z	1.106	1.279	1.478	1.101
	SORTING	0.775	0.356	0.815	0.755
	SKEWNE	-0.266	0.154	-0.139	-0.324
	KURTOS	2.003	1.221	1.999	2.282
FOLK AND WARD METHOD (Description)	MEAN:	Medium Sand	Medium Sand	Medium Sand	Medium Sand
	SORTING	Moderately Sorted	Well Sorted	Moderately Sorted	Moderately Sorted
	SKEWNE	Coarse Skewed	Fine Skewed	Coarse Skewed	Very Coarse Skewed
	KURTOS	Very Leptokurtic	Leptokurtic	Very Leptokurtic	Very Leptokurtic
	MODE 1 (	462.5	462.5	462.5	462.5
	MODE 2 (	2180.0		327.5	2180.0
	MODE 3 (			2180.0	
	MODE 1 (	1.117	1.117	1.117	1.117
	MODE 2 (	-1.119		1.616	-1.119
	MODE 3 (			-1.119	
	D_{10} (μm):	277.7	304.5	222.9	299.5
	D_{50} (μm):	452.8	430.5	365.0	445.3
	D_{90} (μm):	2021.7	556.9	623.8	2019.1
	(D_{90} / D_{10}	7.280	1.828	2.799	6.742
	(D_{90} - D_{10}	1744.0	252.3	400.9	1719.6
	(D_{75} / D_{25}	1.564	1.354	1.694	1.473
	(D_{75} - D_{25}	200.8	125.8	192.2	169.6
	D_{10} (ϕ):	-1.016	0.845	0.681	-1.014
	D_{50} (ϕ):	1.143	1.216	1.454	1.167
	D_{90} (ϕ):	1.848	1.715	2.166	1.739
	(D_{90} / D_{10}	-1.820	2.031	3.181	-1.716
	(D_{90} - D_{10}	2.864	0.871	1.485	2.753
	(D_{75} / D_{25}	1.763	1.414	1.697	1.607
	(D_{75} - D_{25}	0.646	0.437	0.761	0.559
	% GRAVE	10.7%	2.8%	6.3%	10.6%
	% SAND:	89.3%	97.2%	93.7%	89.4%
	% MUD:	0.0%	0.0%	0.0%	0.0%
	% V COA	0.0%	0.0%	0.0%	0.0%
	% COARS	0.0%	0.0%	0.0%	0.0%
	% MEDIU	0.0%	0.0%	0.0%	0.0%
	% FINE G	0.0%	0.0%	0.0%	0.0%
	% V FINE	10.7%	2.8%	6.3%	10.6%
	% V COA	0.0%	0.0%	0.0%	0.9%
	% COARS	22.1%	13.5%	10.1%	15.9%
	% MEDIU	61.8%	82.0%	67.9%	67.9%
	% FINE S	4.4%	1.0%	11.9%	3.5%
	% V FINE	1.0%	0.8%	3.8%	1.2%
	% V COA	0.0%	0.0%	0.0%	0.0%
	% COARS	0.0%	0.0%	0.0%	0.0%
	% MEDIU	0.0%	0.0%	0.0%	0.0%
	% FINE S	0.0%	0.0%	0.0%	0.0%
	% V FINE	0.0%	0.0%	0.0%	0.0%
	% CLAY:	0.0%	0.0%	0.0%	0.0%

Table B.2 (Continued). Sediment grain-size analysis data for the lower Piscataqua River; GRADISTAT results, gravel not-separated.

	SAMPLE	200209_05_3	200209_05_8	200209_05_9	200209_06_1
	ANALYST				
	SIEVING				
	SAMPLE	Unimodal, Very Well Sorted	Unimodal, Poorly Sorted	Unimodal, Poorly Sorted	Bimodal, Moderately Sorted
	TEXTURA	Gravel	Sandy Gravel	Sandy Gravel	Gravelly Sand
	SEDIMENT	Very Fine Gravel	Sandy Very Fine Gravel	Sandy Very Fine Gravel	Very Fine Gravelly Fine Sand
METHOD OF MOMENTS Arithmetic (μm)	MEAN ($\overline{x}_a$	2121.1	1705.2	1508.9	435.4
	SORTING	340.2	807.7	868.6	615.4
	SKEWNE	-5.619	-1.138	-0.608	2.429
	KURTOS	32.63	2.344	1.503	7.059
METHOD OF MOMENTS Geometric (μm)	MEAN ($\overline{x}_g$	2005.7	1304.2	1051.5	266.1
	SORTING	1.597	2.477	2.821	2.270
	SKEWNE	-5.839	-1.445	-1.088	1.589
	KURTOS	35.85	3.686	2.748	5.021
METHOD OF MOMENTS Logarithmic (ϕ)	MEAN ($\overline{x}_g$	-1.004	-0.383	-0.073	1.910
	SORTING	0.676	1.308	1.496	1.183
	SKEWNE	5.839	1.445	1.088	-1.589
	KURTOS	35.85	3.686	2.748	5.021
FOLK AND WARD METHOD (μm)	MEAN (M	2167.2	1189.8	1102.4	233.9
	SORTING	1.054	2.287	2.606	1.984
	SKEWNE	0.000	-0.917	-0.914	0.398
	KURTOS	0.738	0.896	0.830	2.285
FOLK AND WARD METHOD (ϕ)	MEAN (M	-1.116	-0.251	-0.141	2.096
	SORTING	0.075	1.194	1.382	0.988
	SKEWNE	0.000	0.917	0.914	-0.398
	KURTOS	0.738	0.896	0.830	2.285
FOLK AND WARD METHOD (Description)	MEAN:	Very Fine Gravel	Very Coarse Sand	Very Coarse Sand	Fine Sand
	SORTING	Very Well Sorted	Poorly Sorted	Poorly Sorted	Moderately Sorted
	SKEWNE	Symmetrical	Very Fine Skewed	Very Fine Skewed	Very Coarse Skewed
	KURTOS	Platykurtic	Platykurtic	Platykurtic	Very Leptokurtic
	MODE 1 (	2180.0	2180.0	2180.0	196.0
	MODE 2 (				2180.0
	MODE 3 (				
	MODE 1 (	-1.119	-1.119	-1.119	2.356
	MODE 2 (				-1.119
	MODE 3 (				
	D_{10} (μm):	2024.3	273.6	158.4	135.3
	D_{50} (μm):	2167.2	2110.6	2061.4	216.5
	D_{90} (μm):	2320.1	2307.9	2297.0	2027.3
	(D_{90} / D_{10}	1.146	8.436	14.50	14.98
	(D_{90} - D_{10}	295.8	2034.3	2138.6	1891.9
	(D_{75} / D_{25}	1.089	2.960	4.225	1.709
	(D_{75} - D_{25}	184.8	1477.8	1683.6	121.9
	D_{10} (ϕ):	-1.214	-1.207	-1.200	-1.020
	D_{50} (ϕ):	-1.116	-1.078	-1.044	2.207
	D_{90} (ϕ):	-1.017	1.870	2.659	2.885
	(D_{90} / D_{10}	0.838	-1.550	-2.216	-2.830
	(D_{90} - D_{10}	0.197	3.077	3.858	3.905
	(D_{75} / D_{25}	0.896	-0.352	-0.822	1.438
	(D_{75} - D_{25}	0.123	1.566	2.079	0.773
	% GRAVE	97.1%	74.1%	61.2%	10.9%
	% SAND:	2.9%	25.9%	38.8%	89.1%
	% MUD:	0.0%	0.0%	0.0%	0.0%
	% V COA	0.0%	0.0%	0.0%	0.0%
	% COARS	0.0%	0.0%	0.0%	0.0%
	% MEDIU	0.0%	0.0%	0.0%	0.0%
	% FINE G	0.0%	0.0%	0.0%	0.0%
	% V FINE	97.1%	74.1%	61.2%	10.9%
	% V COA	0.0%	0.0%	3.7%	0.0%
	% COARS	0.0%	3.9%	11.9%	0.9%
	% MEDIU	0.4%	14.3%	8.6%	23.0%
	% FINE S	1.0%	5.7%	9.7%	58.8%
	% V FINE	1.5%	2.0%	4.9%	6.4%
	% V COA	0.0%	0.0%	0.0%	0.0%
	% COARS	0.0%	0.0%	0.0%	0.0%
	% MEDIU	0.0%	0.0%	0.0%	0.0%
	% FINE S	0.0%	0.0%	0.0%	0.0%
	% V FINE	0.0%	0.0%	0.0%	0.0%
	% CLAY:	0.0%	0.0%	0.0%	0.0%

Table B.2 (Continued). Sediment grain-size analysis data for the lower Piscataqua River; GRADISTAT results, gravel not-separated.

	SAMPLE	200209_06_2	200209_06_3	200209_06_4	200209_06_5
	ANALYST				
	SIEVING				
	SAMPLE	Unimodal, Well Sorted	Unimodal, Very Well Sorted	Bimodal, Poorly Sorted	Unimodal, Poorly Sorted
	TEXTURA	Gravel	Gravel	Sandy Gravel	Sandy Gravel
	SEDIMENT	Very Fine Gravel	Very Fine Gravel	Sandy Very Fine Gravel	Sandy Very Fine Gravel
METHOD OF MOMENTS Arithmetic (μm)	MEAN($\bar{x}_a$)	2069.9	2148.9	1503.5	1637.7
	SORTING	442.9	240.4	860.4	817.5
	SKEWNE	-3.791	-7.690	-0.505	-0.880
	KURTOS	15.44	60.74	1.292	1.837
METHOD OF MOMENTS Geometric (μm)	MEAN($\bar{x}_g$)	1921.2	2095.4	1125.0	1268.7
	SORTING	1.663	1.339	2.384	2.336
	SKEWNE	-4.195	-8.619	-0.783	-1.188
	KURTOS	20.14	80.18	2.260	3.069
METHOD OF MOMENTS Logarithmic (ϕ)	MEAN($\bar{x}_\phi$)	-0.942	-1.067	-0.170	-0.343
	SORTING	0.734	0.421	1.253	1.224
	SKEWNE	4.195	8.619	0.783	1.188
	KURTOS	20.14	80.18	2.260	3.069
FOLK AND WARD METHOD (μm)	MEAN(M_z)	2161.4	2169.5	1217.6	1227.4
	SORTING	1.335	1.053	2.137	2.156
	SKEWNE	-0.454	0.000	-0.891	-0.904
	KURTOS	7.974	0.738	0.546	0.632
FOLK AND WARD METHOD (ϕ)	MEAN(M_z)	-1.112	-1.117	-0.284	-0.296
	SORTING	0.417	0.074	1.096	1.108
	SKEWNE	0.454	0.000	0.891	0.904
	KURTOS	7.974	0.738	0.546	0.632
FOLK AND WARD METHOD (Description)	MEAN:	Very Fine Gravel	Very Fine Gravel	Very Coarse Sand	Very Coarse Sand
	SORTING	Well Sorted	Very Well Sorted	Poorly Sorted	Poorly Sorted
	SKEWNE	Very Fine Skewed	Symmetrical	Very Fine Skewed	Very Fine Skewed
	KURTOS	Extremely Leptokurtic	Platykurtic	Very Platykurtic	Very Platykurtic
	MODE 1	2180.0	2180.0	2180.0	2180.0
	MODE 2			462.5	
	MODE 3				
	MODE 1	-1.119	-1.119	-1.119	-1.119
	MODE 2			1.117	
	MODE 3				
	D_{10} (μm):	2014.7	2028.2	332.9	320.4
	D_{50} (μm):	2161.4	2169.5	2063.1	2093.1
	D_{90} (μm):	2318.9	2320.6	2297.4	2304.0
	(D_{90} / D_{10})	1.151	1.144	6.902	7.191
	(D_{90} - D_{10})	304.2	292.4	1964.5	1983.6
	(D_{75} / D_{25})	1.092	1.088	4.832	4.061
	(D_{75} - D_{25})	190.0	182.6	1750.0	1675.2
	D_{10} (ϕ):	-1.213	-1.215	-1.200	-1.204
	D_{50} (ϕ):	-1.112	-1.117	-1.045	-1.066
	D_{90} (ϕ):	-1.011	-1.020	1.587	1.642
	(D_{90} / D_{10})	0.833	0.840	-1.323	-1.364
	(D_{90} - D_{10})	0.203	0.194	2.787	2.846
	(D_{75} / D_{25})	0.892	0.897	-0.990	-0.755
	(D_{75} - D_{25})	0.127	0.121	2.273	2.022
	% GRAVE	94.2%	98.3%	61.6%	69.0%
	% SAND:	5.8%	1.7%	38.4%	31.0%
	% MUD:	0.0%	0.0%	0.0%	0.0%
	% V COA	0.0%	0.0%	0.0%	0.0%
	% COARS	0.0%	0.0%	0.0%	0.0%
	% MEDIU	0.0%	0.0%	0.0%	0.0%
	% FINE G	0.0%	0.0%	0.0%	0.0%
	% V FINE	94.2%	98.3%	61.6%	69.0%
	% V COA	0.0%	0.0%	0.0%	0.9%
	% COARS	0.3%	0.3%	6.7%	6.0%
	% MEDIU	3.6%	0.5%	28.9%	20.8%
	% FINE S	1.8%	0.6%	1.9%	2.4%
	% V FINE	0.7%	0.3%	1.0%	0.9%
	% V COA	0.0%	0.0%	0.0%	0.0%
	% COARS	0.0%	0.0%	0.0%	0.0%
	% MEDIU	0.0%	0.0%	0.0%	0.0%
	% FINE S	0.0%	0.0%	0.0%	0.0%
	% V FINE	0.0%	0.0%	0.0%	0.0%
	% CLAY:	0.0%	0.0%	0.0%	0.0%

Table B.2 (Continued). Sediment grain-size analysis data for the lower Piscataqua River; GRADISTAT results, gravel not-separated.

	SAMPLE	200209_06_8	200209_07_11	200209_07_3	200209_07_5
	ANALYST				
	SIEVING				
	SAMPLE	Bimodal, Poorly Sorted	Trimodal, Poorly Sorted	Polymodal, Poorly Sorted	Unimodal, Poorly Sorted
	TEXTURA	Sandy Gravel	Gravelly Sand	Sandy Gravel	Sandy Gravel
	SEDIMENT	Sandy Very Fine Gravel	Very Fine Gravelly Fine Sand	Sandy Very Fine Gravel	Sandy Very Fine Gravel
METHOD OF MOMENTS Arithmetic (μm)	MEAN($\overline{x}_a$)	1231.3	822.1	1045.6	1552.7
	SORTING	912.2	859.5	889.1	913.6
	SKEWNE	0.042	0.855	0.448	-0.777
	KURTOS	1.063	1.876	1.281	1.620
METHOD OF MOMENTS Geometric (μm)	MEAN($\overline{x}_g$)	807.5	443.2	660.6	1019.8
	SORTING	2.752	3.103	2.736	3.086
	SKEWNE	-0.332	0.286	-0.004	-0.921
	KURTOS	1.766	1.717	1.733	2.069
METHOD OF MOMENTS Logarithmic (ϕ)	MEAN($\overline{x}_\phi$)	0.309	1.174	0.598	-0.028
	SORTING	1.460	1.633	1.452	1.626
	SKEWNE	0.332	-0.286	0.004	0.921
	KURTOS	1.766	1.717	1.733	2.069
FOLK AND WARD METHOD (μm)	MEAN(M_z)	784.9	473.9	636.2	991.7
	SORTING	2.428	3.205	2.533	2.802
	SKEWNE	-0.040	0.291	0.318	-0.927
	KURTOS	0.523	0.563	0.511	0.570
FOLK AND WARD METHOD (ϕ)	MEAN(M_z)	0.349	1.077	0.652	0.012
	SORTING	1.280	1.680	1.341	1.486
	SKEWNE	0.040	-0.291	-0.318	0.927
	KURTOS	0.523	0.563	0.511	0.570
FOLK AND WARD METHOD (Description)	MEAN:	Coarse Sand	Medium Sand	Coarse Sand	Coarse Sand
	SORTING	Poorly Sorted	Poorly Sorted	Poorly Sorted	Poorly Sorted
	SKEWNE	Symmetrical	Coarse Skewed	Very Coarse Skewed	Very Fine Skewed
	KURTOS	Very Platykurtic	Very Platykurtic	Very Platykurtic	Very Platykurtic
	MODE 1	2180.0	2180.0	2180.0	2180.0
	MODE 2	327.5	196.0	275.0	
	MODE 3		390.0	390.0	
	MODE 1	-1.119	-1.119	-1.119	-1.119
	MODE 2	1.616	2.356	1.868	
	MODE 3		1.364	1.364	
	D_{10} (μm):	250.4	123.1	219.7	168.3
	D_{50} (μm):	775.8	329.8	480.9	2089.1
	D_{90} (μm):	2279.1	2221.5	2258.0	2303.2
	(D_{90} / D_{10})	9.102	18.05	10.28	13.69
	(D_{90} - D_{10})	2028.7	2098.5	2038.4	2134.9
	(D_{75} / D_{25})	6.696	11.09	7.451	7.699
	(D_{75} - D_{25})	1840.0	1845.9	1829.7	1932.0
	D_{10} (ϕ):	-1.188	-1.152	-1.175	-1.204
	D_{50} (ϕ):	0.366	1.600	1.056	-1.063
	D_{90} (ϕ):	1.998	3.022	2.187	2.571
	(D_{90} / D_{10})	-1.681	-2.625	-1.861	-2.136
	(D_{90} - D_{10})	3.186	4.174	3.362	3.775
	(D_{75} / D_{25})	-1.465	-2.400	-1.684	-1.559
	(D_{75} - D_{25})	2.743	3.471	2.898	2.945
	% GRAVE	47.5%	27.4%	37.5%	67.9%
	% SAND:	52.5%	72.6%	62.5%	32.1%
	% MUD:	0.0%	0.0%	0.0%	0.0%
	% V COA	0.0%	0.0%	0.0%	0.0%
	% COARS	0.0%	0.0%	0.0%	0.0%
	% MEDIU	0.0%	0.0%	0.0%	0.0%
	% FINE G	0.0%	0.0%	0.0%	0.0%
	% V FINE	47.5%	27.4%	37.5%	67.9%
	% V COA	1.0%	2.7%	0.0%	0.0%
	% COARS	6.5%	7.5%	10.8%	0.3%
	% MEDIU	35.1%	21.2%	34.2%	10.2%
	% FINE S	7.5%	30.8%	15.0%	18.6%
	% V FINE	2.4%	10.3%	2.5%	3.1%
	% V COA	0.0%	0.0%	0.0%	0.0%
	% COARS	0.0%	0.0%	0.0%	0.0%
	% MEDIU	0.0%	0.0%	0.0%	0.0%
	% FINE S	0.0%	0.0%	0.0%	0.0%
	% V FINE	0.0%	0.0%	0.0%	0.0%
	% CLAY:	0.0%	0.0%	0.0%	0.0%

Table B.2 (Continued). Sediment grain-size analysis data for the lower Piscataqua River; GRADISTAT results, gravel not-separated.

SAMPLE		200209_07_9
	ANALYST	
	SIEVING	
	SAMPLE	Unimodal, Moderately Well Sorted
	TEXTURA	Gravel
	SEDIMENT	Very Fine Gravel
METHOD OF MOMENTS Arithmetic (μm)	MEAN($\overline{x}_a$	1943.4
	SORTING	640.4
	SKEWNE	-2.347
	KURTOSI	6.531
METHOD OF MOMENTS Geometric (μm)	MEAN($\overline{x}_g$	1627.5
	SORTING	2.207
	SKEWNE	-2.446
	KURTOSI	7.166
METHOD OF MOMENTS Logarithmic (ϕ)	MEAN($\overline{x}_\phi$	-0.703
	SORTING	1.142
	SKEWNE	2.446
	KURTOSI	7.166
FOLK AND WARD METHOD (μm)	MEAN(M	2148.1
	SORTING	1.528
	SKEWNE	-0.467
	KURTOSI	11.26
FOLK AND WARD METHOD (ϕ)	MEAN(M	-1.103
	SORTING	0.611
	SKEWNE	0.467
	KURTOSI	11.26
FOLK AND WARD METHOD (Description)	MEAN:	Very Fine Gravel
	SORTING	Moderately Well Sorted
	SKEWNE	Very Fine Skewed
	KURTOSI	Extremely Leptokurtic
	MODE 1 (	2160.0
	MODE 2 (	
	MODE 3 (	
	MODE 1 (	-1.119
	MODE 2 (	
	MODE 3 (	
	D_{10} (μm):	261.4
	D_{50} (μm):	2148.1
	D_{90} (μm):	2316.0
	(D_{50} / D_{10}	8.861
	(D_{50} - D_{10}	2054.6
	(D_{75} / D_{25}	1.099
	(D_{75} - D_{25}	202.2
	D_{10} (ϕ):	-1.212
	D_{50} (ϕ):	-1.103
	D_{90} (ϕ):	1.936
	(D_{50} / D_{10}	-1.598
	(D_{50} - D_{10}	3.147
	(D_{75} / D_{25}	0.884
	(D_{75} - D_{25}	0.136
	% GRAVE	88.0%
	% SAND:	12.0%
	% MUD:	0.0%
	% V COA	0.0%
	% COARS	0.0%
	% MEDIU	0.0%
	% FINE G	0.0%
	% V FINE	88.0%
	% V COA	0.0%
	% COARS	0.4%
	% MEDIU	1.9%
	% FINE S	9.1%
	% V FINE	0.7%
	% V COA	0.0%
	% COARS	0.0%
	% MEDIU	0.0%
	% FINE S	0.0%
	% V FINE	0.0%
	% CLAY:	0.0%

B-3. GRAIN-SIZE STATISTICS FROM GRADISTAT, SAMPLE DATA WITH GRAVEL-SEPARATED

Table B.3. Sediment grain-size analysis data for the lower Piscataqua River; GRADISTAT results, gravel fraction separated.

SAMPLE STATISTICS

		200209_01_2	200209_01_4	200209_01_5
	ANALYST AND DATE:	,	,	,
	SIEVING ERROR:			
	SAMPLE TYPE:	Unimodal, Well Sorted	Polymodal, Poorly Sorted	Trimodal, Very Poorly Sorted
	TEXTURAL GROUP:	Slightly Gravelly Sand	Gravelly Sand	Sandy Gravel
	SEDIMENT NAME:	Slightly Fine Gravelly Fine Sand	Medium Gravelly Fine Sand	Sandy Coarse Gravel
METHOD OF MOMENTS Arithmetic (μm)	MEAN ($\overline{x}_a$):	200.6	1150.0	12504.8
	SORTING (σ_a):	227.2	2395.0	10579.1
	SKEWNESS (Sk_a):	15.56	2.547	-0.159
	KURTOSIS (K_a):	271.3	7.932	1.244
METHOD OF MOMENTS Geometric (μm)	MEAN ($\overline{x}_g$):	180.6	371.3	3279.3
	SORTING (σ_g):	1.415	3.315	9.379
	SKEWNESS (Sk_g):	2.471	1.737	-0.429
	KURTOSIS (K_g):	23.97	4.893	1.286
METHOD OF MOMENTS Logarithmic (ϕ)	MEAN ($\overline{x}_\phi$):	2.469	1.429	-1.713
	SORTING (σ_ϕ):	0.500	1.729	3.229
	SKEWNESS (Sk_ϕ):	-2.471	-1.737	0.429
	KURTOSIS (K_ϕ):	23.97	4.893	1.286
FOLK AND WARD METHOD (μm)	MEAN (M_G):	178.8	281.9	4429.2
	SORTING (σ_G):	1.319	2.369	7.134
	SKEWNESS (Sk_G):	0.057	0.524	-0.839
	KURTOSIS (K_G):	0.921	3.581	0.466
FOLK AND WARD METHOD (ϕ)	MEAN (M_Z):	2.483	1.827	-2.147
	SORTING (σ_I):	0.399	1.244	2.835
	SKEWNESS (Sk_I):	-0.057	-0.524	0.839
	KURTOSIS (K_G):	0.921	3.581	0.466
FOLK AND WARD METHOD (Description)	MEAN:	Fine Sand	Medium Sand	Fine Gravel
	SORTING:	Well Sorted	Poorly Sorted	Very Poorly Sorted
	SKEWNESS:	Symmetrical	Very Coarse Skewed	Very Fine Skewed
	KURTOSIS:	Mesokurtic	Extremely Leptokurtic	Very Platykurtic
	MODE 1 (μm):	196.0	231.0	24450.0
	MODE 2 (μm):		8750.0	17500.0
	MODE 3 (μm):		462.5	231.0
	MODE 1 (ϕ):	2.356	2.119	-4.607
	MODE 2 (ϕ):		-3.124	-4.124
	MODE 3 (ϕ):		1.117	2.119
	D_{10} (μm):	128.8	165.8	185.4
	D_{50} (μm):	177.9	252.2	16809.4
	D_{90} (μm):	257.3	4565.4	25094.6
	(D_{90} / D_{10}) (μm):	1.998	27.54	135.4
	(D_{90} - D_{10}) (μm):	128.6	4399.6	24909.2
	(D_{75} / D_{25}) (μm):	1.489	1.610	92.58
	(D_{75} - D_{25}) (μm):	71.02	125.6	22875.2
	D_{10} (ϕ):	1.958	-2.191	-4.649
	D_{50} (ϕ):	2.491	1.987	-4.071
	D_{90} (ϕ):	2.957	2.593	2.431
	(D_{90} / D_{10}) (ϕ):	1.510	-1.184	-0.523
	(D_{90} - D_{10}) (ϕ):	0.999	4.784	7.081
	(D_{75} / D_{25}) (ϕ):	1.260	1.431	-0.442
	(D_{75} - D_{25}) (ϕ):	0.574	0.687	6.533
	% GRAVEL:	0.5%	14.9%	60.5%
	% SAND:	99.5%	85.1%	39.5%
	% MUD:	0.0%	0.0%	0.0%
	% V COARSE GRAVEL:	0.0%	0.0%	0.0%
	% COARSE GRAVEL:	0.0%	0.0%	57.7%
	% MEDIUM GRAVEL:	0.0%	7.3%	1.1%
	% FINE GRAVEL:	0.2%	4.3%	0.3%
	% V FINE GRAVEL:	0.2%	3.3%	1.4%
	% V COARSE SAND:	0.0%	0.0%	0.0%
	% COARSE SAND:	0.0%	0.0%	0.0%
	% MEDIUM SAND:	10.8%	36.0%	14.4%
	% FINE SAND:	82.4%	45.0%	21.1%
	% V FINE SAND:	6.3%	4.0%	3.9%
	% V COARSE SILT:	0.0%	0.0%	0.0%
	% COARSE SILT:	0.0%	0.0%	0.0%
	% MEDIUM SILT:	0.0%	0.0%	0.0%
	% FINE SILT:	0.0%	0.0%	0.0%
	% V FINE SILT:	0.0%	0.0%	0.0%
	% CLAY:	0.0%	0.0%	0.0%

Table B.3 (Continued). Sediment grain-size analysis data for the lower Piscataqua River; GRADISTAT results, gravel fraction separated.

SAMPLE STATISTICS

		200209_01_7	200209_02_1	200209_02_10
	ANALYST AND DATE:	,	,	,
	SIEVING ERROR:			
	SAMPLE TYPE:	Trimodal, Very Poorly Sorted	Polymodal, Very Poorly Sorted	Polymodal, Very Poorly Sorted
	TEXTURAL GROUP:	Gravel	Gravelly Sand	Sandy Gravel
	SEDIMENT NAME:	Very Coarse Gravel	Fine Gravelly Fine Sand	Sandy Coarse Gravel
METHOD OF MOMENTS Arithmetic (μm)	MEAN ($\overline{x}_a$):	18349.7	2036.6	7329.0
	SORTING (σ_a):	13784.6	3686.4	9651.2
	SKEWNESS (Sk_a):	0.015	2.006	0.997
	KURTOSIS (K_a):	1.431	5.646	2.291
METHOD OF MOMENTS Geometric (μm)	MEAN ($\overline{x}_g$):	7706.7	511.2	1501.3
	SORTING (σ_g):	6.639	4.541	7.840
	SKEWNESS (Sk_g):	-1.182	1.122	0.182
	KURTOSIS (K_g):	2.921	2.704	1.388
METHOD OF MOMENTS Logarithmic (ϕ)	MEAN ($\overline{x}_\phi$):	-2.946	0.968	-0.586
	SORTING (σ_ϕ):	2.731	2.183	2.971
	SKEWNESS (Sk_ϕ):	1.182	-1.122	-0.182
	KURTOSIS (K_ϕ):	2.921	2.704	1.388
FOLK AND WARD METHOD (μm)	MEAN (M_G):	5994.0	603.9	1396.7
	SORTING (σ_G):	7.004	4.500	7.371
	SKEWNESS (Sk_G):	-0.704	0.749	0.477
	KURTOSIS (K_G):	1.064	0.816	0.533
FOLK AND WARD METHOD (ϕ)	MEAN (M_Z):	-2.584	0.728	-0.482
	SORTING (σ_I):	2.808	2.170	2.882
	SKEWNESS (Sk_I):	0.704	-0.749	-0.477
	KURTOSIS (K_G):	1.064	0.816	0.533
FOLK AND WARD METHOD (Description)	MEAN:	Fine Gravel	Coarse Sand	Very Coarse Sand
	SORTING:	Very Poorly Sorted	Very Poorly Sorted	Very Poorly Sorted
	SKEWNESS:	Very Fine Skewed	Very Coarse Skewed	Very Coarse Skewed
	KURTOSIS:	Mesokurtic	Platykurtic	Very Platykurtic
	MODE 1 (μm):	34500.0	231.0	196.0
	MODE 2 (μm):	17500.0	12200.0	2180.0
	MODE 3 (μm):	12200.0	6150.0	327.5
	MODE 1 (ϕ):	-5.103	2.119	2.356
	MODE 2 (ϕ):	-4.124	-3.604	-1.119
	MODE 3 (ϕ):	-3.604	-2.615	1.616
	D_{10} (μm):	257.3	163.2	185.3
	D_{50} (μm):	17230.2	252.2	596.8
	D_{90} (μm):	35790.3	6608.0	24509.0
	(D_{90} / D_{10}) (μm):	139.1	40.50	132.2
	(D_{90} - D_{10}) (μm):	35533.1	6444.9	24323.6
	(D_{75} / D_{25}) (μm):	7.707	10.01	58.23
	(D_{75} - D_{25}) (μm):	29040.8	1821.6	12077.1
	D_{10} (ϕ):	-5.161	-2.724	-4.615
	D_{50} (ϕ):	-4.107	1.987	0.745
	D_{90} (ϕ):	1.959	2.615	2.432
	(D_{90} / D_{10}) (ϕ):	-0.379	-0.960	-0.527
	(D_{90} - D_{10}) (ϕ):	7.120	5.340	7.047
	(D_{75} / D_{25}) (ϕ):	0.418	-2.267	-0.620
	(D_{75} - D_{25}) (ϕ):	2.946	3.323	5.864
	% GRAVEL:	80.1%	25.3%	48.4%
	% SAND:	19.9%	74.7%	51.6%
	% MUD:	0.0%	0.0%	0.0%
	% V COARSE GRAVEL:	34.0%	0.0%	0.0%
	% COARSE GRAVEL:	25.6%	0.0%	21.5%
	% MEDIUM GRAVEL:	10.3%	9.5%	13.8%
	% FINE GRAVEL:	6.4%	11.1%	5.7%
	% V FINE GRAVEL:	3.8%	4.7%	7.4%
	% V COARSE SAND:	0.0%	0.0%	0.0%
	% COARSE SAND:	1.1%	0.7%	3.0%
	% MEDIUM SAND:	9.4%	24.6%	18.2%
	% FINE SAND:	6.4%	44.2%	25.6%
	% V FINE SAND:	3.1%	5.2%	4.8%
	% V COARSE SILT:	0.0%	0.0%	0.0%
	% COARSE SILT:	0.0%	0.0%	0.0%
	% MEDIUM SILT:	0.0%	0.0%	0.0%
	% FINE SILT:	0.0%	0.0%	0.0%
	% V FINE SILT:	0.0%	0.0%	0.0%
	% CLAY:	0.0%	0.0%	0.0%

Table B.3 (Continued). Sediment grain-size analysis data for the lower Piscataqua River; GRADISTAT results, gravel fraction separated.

SAMPLE STATISTICS

		200209_02_2	200209_02_7	200209_02_7rl
	ANALYST AND DATE:	,	,	,
	SIEVING ERROR:			
	SAMPLE TYPE:	Unimodal, Well Sorted	Unimodal, Very Well Sorted	Polymodal, Poorly Sorted
	TEXTURAL GROUP:	Slightly Gravelly Sand	Gravel	Gravelly Sand
	SEDIMENT NAME:	Slightly Fine Gravelly Fine Sand	Very Coarse Gravel	Fine Gravelly Medium Sand
METHOD OF MOMENTS Arithmetic (μm)	MEAN ($\overline{x}_a$):	342.2	46975.8	1427.8
	SORTING (σ_a):	709.1	9425.6	2168.0
	SKEWNESS (Sk_a):	7.004	-4.476	1.951
	KURTOSIS (K_a):	53.70	21.18	5.587
METHOD OF MOMENTS Geometric (μm)	MEAN ($\overline{x}_g$):	241.0	41387.1	625.9
	SORTING (σ_g):	1.747	2.333	3.172
	SKEWNESS (Sk_g):	3.258	-5.601	1.030
	KURTOSIS (K_g):	19.85	34.96	2.898
METHOD OF MOMENTS Logarithmic (ϕ)	MEAN ($\overline{x}_\phi$):	2.053	-5.371	0.676
	SORTING (σ_ϕ):	0.805	1.222	1.665
	SKEWNESS (Sk_ϕ):	-3.258	5.601	-1.030
	KURTOSIS (K_ϕ):	19.85	34.96	2.898
FOLK AND WARD METHOD (μm)	MEAN (M_G):	232.2	48651.1	762.5
	SORTING (σ_G):	1.295	1.054	3.296
	SKEWNESS (Sk_G):	-0.067	0.000	0.643
	KURTOSIS (K_G):	1.239	0.738	1.551
FOLK AND WARD METHOD (ϕ)	MEAN (M_ϕ):	2.107	-5.604	0.391
	SORTING (σ_I):	0.373	0.076	1.721
	SKEWNESS (Sk_I):	0.067	0.000	-0.643
	KURTOSIS (K_G):	1.239	0.738	1.551
FOLK AND WARD METHOD (Description)	MEAN:	Fine Sand	Very Coarse Gravel	Coarse Sand
	SORTING:	Well Sorted	Very Well Sorted	Poorly Sorted
	SKEWNESS:	Symmetrical	Symmetrical	Very Coarse Skewed
	KURTOSIS:	Leptokurtic	Platykurtic	Very Leptokurtic
	MODE 1 (μm):	231.0	49000.0	462.5
	MODE 2 (μm):			327.5
	MODE 3 (μm):			6150.0
	MODE 1 (ϕ):	2.119	-5.610	1.117
	MODE 2 (ϕ):			1.616
	MODE 3 (ϕ):			-2.615
	D_{10} (μm):	165.8	45430.3	242.0
	D_{50} (μm):	231.6	48651.1	414.4
	D_{90} (μm):	314.5	52100.2	5786.5
	(D_{90} / D_{10}) (μm):	1.897	1.147	23.91
	(D_{90} - D_{10}) (μm):	148.7	6669.9	5544.5
	(D_{75} / D_{25}) (μm):	1.372	1.089	2.452
	(D_{75} - D_{25}) (μm):	73.78	4166.7	436.9
	D_{10} (ϕ):	1.669	-5.703	-2.533
	D_{50} (ϕ):	2.110	-5.604	1.271
	D_{90} (ϕ):	2.593	-5.506	2.047
	(D_{90} / D_{10}) (ϕ):	1.554	0.965	-0.808
	(D_{90} - D_{10}) (ϕ):	0.924	0.198	4.580
	(D_{75} / D_{25}) (ϕ):	1.243	0.978	3.950
	(D_{75} - D_{25}) (ϕ):	0.456	0.124	1.294
	% GRAVEL:	2.9%	97.8%	23.8%
	% SAND:	97.1%	2.2%	76.2%
	% MUD:	0.0%	0.0%	0.0%
	% V COARSE GRAVEL:	0.0%	95.6%	0.0%
	% COARSE GRAVEL:	0.0%	0.0%	0.0%
	% MEDIUM GRAVEL:	0.0%	1.0%	2.6%
	% FINE GRAVEL:	1.6%	0.6%	13.5%
	% V FINE GRAVEL:	1.4%	0.7%	7.7%
	% V COARSE SAND:	0.0%	0.0%	0.0%
	% COARSE SAND:	0.0%	0.2%	8.2%
	% MEDIUM SAND:	33.0%	1.2%	56.6%
	% FINE SAND:	60.4%	0.2%	9.7%
	% V FINE SAND:	3.6%	0.5%	1.6%
	% V COARSE SILT:	0.0%	0.0%	0.0%
	% COARSE SILT:	0.0%	0.0%	0.0%
	% MEDIUM SILT:	0.0%	0.0%	0.0%
	% FINE SILT:	0.0%	0.0%	0.0%
	% V FINE SILT:	0.0%	0.0%	0.0%
	% CLAY:	0.0%	0.0%	0.0%

Table B.3 (Continued). Sediment grain-size analysis data for the lower Piscataqua River; GRADISTAT results, gravel fraction separated.

SAMPLE STATISTICS

		200209_03_1	200209_03_10	200209_03_2
	ANALYST AND DATE:	,	,	,
	SIEVING ERROR:			
	SAMPLE TYPE:	Polymodal, Very Poorly Sorted	Polymodal, Very Poorly Sorted	Bimodal, Well Sorted
	TEXTURAL GROUP:	Sandy Gravel	Sandy Gravel	Gravel
	SEDIMENT NAME:	Sandy Medium Gravel	Sandy Very Coarse Gravel	Very Coarse Gravel
METHOD OF MOMENTS Arithmetic (μm)	MEAN ($\overline{x}_a$):	5566.0	15426.3	39893.4
	SORTING (σ_a):	6409.8	14317.2	13349.9
	SKEWNESS (Sk_a):	0.757	0.310	-1.061
	KURTOSIS (K_a):	2.013	1.404	2.933
METHOD OF MOMENTS Geometric (μm)	MEAN ($\overline{x}_g$):	1516.9	4587.5	34621.7
	SORTING (σ_g):	6.740	8.260	2.179
	SKEWNESS (Sk_g):	-0.024	-0.594	-4.862
	KURTOSIS (K_g):	1.366	1.675	32.57
METHOD OF MOMENTS Logarithmic (ϕ)	MEAN ($\overline{x}_\phi$):	-0.601	-2.198	-5.114
	SORTING (σ_ϕ):	2.753	3.046	1.124
	SKEWNESS (Sk_ϕ):	0.024	0.594	4.862
	KURTOSIS (K_ϕ):	1.366	1.675	32.57
FOLK AND WARD METHOD (μm)	MEAN (M_G):	1727.2	4677.6	38532.4
	SORTING (σ_G):	6.168	7.589	1.372
	SKEWNESS (Sk_G):	-0.142	-0.569	-0.757
	KURTOSIS (K_G):	0.548	0.472	0.507
FOLK AND WARD METHOD (ϕ)	MEAN (M_Z):	-0.788	-2.226	-5.268
	SORTING (σ_I):	2.625	2.924	0.456
	SKEWNESS (Sk_I):	0.142	0.569	0.757
	KURTOSIS (K_G):	0.548	0.472	0.507
FOLK AND WARD METHOD (Description)	MEAN:	Very Coarse Sand	Fine Gravel	Very Coarse Gravel
	SORTING:	Very Poorly Sorted	Very Poorly Sorted	Well Sorted
	SKEWNESS:	Fine Skewed	Very Fine Skewed	Very Fine Skewed
	KURTOSIS:	Very Platykurtic	Very Platykurtic	Very Platykurtic
	MODE 1 (μm):	2180.0	12200.0	49000.0
	MODE 2 (μm):	327.5	24450.0	24450.0
	MODE 3 (μm):	231.0	275.0	
	MODE 1 (ϕ):	-1.119	-3.604	-5.610
	MODE 2 (ϕ):	1.616	-4.607	-4.607
	MODE 3 (ϕ):	2.119	1.868	
	D_{10} (μm):	147.2	218.4	23175.9
	D_{50} (μm):	2068.4	11781.5	46841.8
	D_{90} (μm):	16692.0	35397.5	51706.8
	(D_{90} / D_{10}) (μm):	113.4	162.1	2.231
	(D_{90} - D_{10}) (μm):	16544.8	35179.2	28530.9
	(D_{75} / D_{25}) (μm):	45.03	98.76	1.975
	(D_{75} - D_{25}) (μm):	11438.7	32134.1	24603.7
	D_{10} (ϕ):	-4.061	-5.146	-5.692
	D_{50} (ϕ):	-1.049	-3.558	-5.550
	D_{90} (ϕ):	2.764	2.195	-4.535
	(D_{90} / D_{10}) (ϕ):	-0.681	-0.427	0.797
	(D_{90} - D_{10}) (ϕ):	6.825	7.341	1.158
	(D_{75} / D_{25}) (ϕ):	-0.548	-0.320	0.826
	(D_{75} - D_{25}) (ϕ):	5.493	6.626	0.982
	% GRAVEL:	51.6%	69.1%	98.6%
	% SAND:	48.4%	30.9%	1.4%
	% MUD:	0.0%	0.0%	0.0%
	% V COARSE GRAVEL:	0.0%	27.5%	66.2%
	% COARSE GRAVEL:	13.3%	11.9%	29.8%
	% MEDIUM GRAVEL:	22.3%	21.2%	0.7%
	% FINE GRAVEL:	7.9%	3.6%	0.9%
	% V FINE GRAVEL:	8.1%	4.9%	1.0%
	% V COARSE SAND:	0.0%	0.0%	0.0%
	% COARSE SAND:	4.0%	0.0%	0.2%
	% MEDIUM SAND:	20.6%	15.5%	0.4%
	% FINE SAND:	17.0%	12.7%	0.2%
	% V FINE SAND:	6.8%	2.6%	0.5%
	% V COARSE SILT:	0.0%	0.0%	0.0%
	% COARSE SILT:	0.0%	0.0%	0.0%
	% MEDIUM SILT:	0.0%	0.0%	0.0%
	% FINE SILT:	0.0%	0.0%	0.0%
	% V FINE SILT:	0.0%	0.0%	0.0%
	% CLAY:	0.0%	0.0%	0.0%

Table B.3 (Continued). Sediment grain-size analysis data for the lower Piscataqua River; GRADISTAT results, gravel fraction separated.

SAMPLE STATISTICS

		200209_04.1_2	200209_04.1_3	200209_04.1_4
	ANALYST AND DATE:	,	,	,
	SIEVING ERROR:			
	SAMPLE TYPE:	Polymodal, Poorly Sorted	Polymodal, Very Poorly Sorted	Polymodal, Poorly Sorted
	TEXTURAL GROUP:	Sandy Gravel	Gravelly Sand	Gravel
	SEDIMENT NAME:	Sandy Fine Gravel	Fine Gravelly Fine Sand	Medium Gravel
METHOD OF MOMENTS Arithmetic (μm)	MEAN ($\overline{x}_a$):	4931.0	2540.8	18091.0
	SORTING (σ_a):	3931.8	4961.3	12656.8
	SKEWNESS (Sk_a):	0.511	2.160	0.238
	KURTOSIS (K_a):	2.084	6.411	1.571
METHOD OF MOMENTS Geometric (μm)	MEAN ($\overline{x}_g$):	2868.6	453.9	10308.6
	SORTING (σ_g):	3.495	5.573	4.436
	SKEWNESS (Sk_g):	-0.850	1.102	-1.761
	KURTOSIS (K_g):	2.926	2.656	5.492
METHOD OF MOMENTS Logarithmic (ϕ)	MEAN ($\overline{x}_\phi$):	-1.520	1.140	-3.366
	SORTING (σ_ϕ):	1.805	2.478	2.149
	SKEWNESS (Sk_ϕ):	0.850	-1.102	1.761
	KURTOSIS (K_ϕ):	2.926	2.656	5.492
FOLK AND WARD METHOD (μm)	MEAN (M_G):	2826.7	541.6	12555.2
	SORTING (σ_G):	3.397	5.901	3.552
	SKEWNESS (Sk_G):	-0.446	0.684	-0.319
	KURTOSIS (K_G):	0.681	1.106	1.525
FOLK AND WARD METHOD (ϕ)	MEAN (M_Z):	-1.499	0.885	-3.650
	SORTING (σ_I):	1.764	2.561	1.829
	SKEWNESS (Sk_I):	0.446	-0.684	0.319
	KURTOSIS (K_G):	0.681	1.106	1.525
FOLK AND WARD METHOD (Description)	MEAN:	Very Fine Gravel	Coarse Sand	Medium Gravel
	SORTING:	Poorly Sorted	Very Poorly Sorted	Poorly Sorted
	SKEWNESS:	Very Fine Skewed	Very Coarse Skewed	Very Fine Skewed
	KURTOSIS:	Platykurtic	Mesokurtic	Very Leptokurtic
	MODE 1 (μm):	6150.0	196.0	34500.0
	MODE 2 (μm):	2180.0	98.00	12200.0
	MODE 3 (μm):	4375.0	69.00	17500.0
	MODE 1 (ϕ):	-2.615	2.356	-5.103
	MODE 2 (ϕ):	-1.119	3.356	-3.604
	MODE 3 (ϕ):	-2.124	3.863	-4.124
	D_{10} (μm):	462.6	103.1	736.0
	D_{50} (μm):	4443.1	211.6	13021.4
	D_{90} (μm):	11615.5	11216.2	35611.3
	(D_{90} / D_{10}) (μm):	25.11	108.8	48.38
	(D_{90} - D_{10}) (μm):	11152.9	11113.2	34875.3
	(D_{75} / D_{25}) (μm):	7.997	7.230	3.799
	(D_{75} - D_{25}) (μm):	7122.3	971.2	24280.7
	D_{10} (ϕ):	-3.538	-3.488	-5.154
	D_{50} (ϕ):	-2.152	2.240	-3.703
	D_{90} (ϕ):	1.112	3.278	0.442
	(D_{90} / D_{10}) (ϕ):	-0.314	-0.940	-0.086
	(D_{90} - D_{10}) (ϕ):	4.650	6.766	5.596
	(D_{75} / D_{25}) (ϕ):	0.008	-15.540	0.618
	(D_{75} - D_{25}) (ϕ):	3.000	2.854	1.926
	% GRAVEL:	72.1%	24.8%	89.0%
	% SAND:	27.9%	75.2%	11.0%
	% MUD:	0.0%	0.0%	0.0%
	% V COARSE GRAVEL:	0.0%	0.0%	30.7%
	% COARSE GRAVEL:	0.0%	7.1%	17.5%
	% MEDIUM GRAVEL:	26.4%	5.8%	31.4%
	% FINE GRAVEL:	31.2%	8.5%	5.5%
	% V FINE GRAVEL:	14.5%	3.3%	4.0%
	% V COARSE SAND:	3.1%	0.7%	0.2%
	% COARSE SAND:	11.1%	2.2%	2.1%
	% MEDIUM SAND:	11.1%	7.9%	3.8%
	% FINE SAND:	0.5%	48.6%	2.7%
	% V FINE SAND:	2.1%	15.9%	2.2%
	% V COARSE SILT:	0.0%	0.0%	0.0%
	% COARSE SILT:	0.0%	0.0%	0.0%
	% MEDIUM SILT:	0.0%	0.0%	0.0%
	% FINE SILT:	0.0%	0.0%	0.0%
	% V FINE SILT:	0.0%	0.0%	0.0%
	% CLAY:	0.0%	0.0%	0.0%

Table B.3 (Continued). Sediment grain-size analysis data for the lower Piscataqua River; GRADISTAT results, gravel fraction separated.

SAMPLE STATISTICS

		200209_04.1_5	200209_04_1	200209_04_2
	ANALYST AND DATE:	,	,	,
	SIEVING ERROR:			
	SAMPLE TYPE:	Polymodal, Very Poorly Sorted	Bimodal, Moderately Sorted	Unimodal, Well Sorted
	TEXTURAL GROUP:	Sandy Gravel	Gravelly Sand	Slightly Gravelly Sand
	SEDIMENT NAME:	Sandy Coarse Gravel	Very Fine Gravelly Medium Sand	ghtly Very Fine Gravelly Medium Sa
METHOD OF MOMENTS Arithmetic (μm)	MEAN ($\overline{x}_a$):	9944.4	707.7	480.5
	SORTING (σ_a):	9432.6	910.7	396.9
	SKEWNESS (Sk_a):	0.367	4.446	7.474
	KURTOSIS (K_a):	1.624	28.01	75.35
METHOD OF MOMENTS Geometric (μm)	MEAN ($\overline{x}_g$):	3039.0	508.4	427.5
	SORTING (σ_g):	7.361	1.972	1.492
	SKEWNESS (Sk_g):	-0.411	1.400	1.576
	KURTOSIS (K_g):	1.458	6.227	15.60
METHOD OF MOMENTS Logarithmic (ϕ)	MEAN ($\overline{x}_\phi$):	-1.604	0.976	1.226
	SORTING (σ_ϕ):	2.880	0.980	0.577
	SKEWNESS (Sk_ϕ):	0.411	-1.400	-1.576
	KURTOSIS (K_ϕ):	1.458	6.227	15.60
FOLK AND WARD METHOD (μm)	MEAN (M_G):	3870.2	464.5	412.0
	SORTING (σ_G):	6.445	1.718	1.277
	SKEWNESS (Sk_G):	-0.590	0.269	-0.162
	KURTOSIS (K_G):	0.510	2.028	1.206
FOLK AND WARD METHOD (ϕ)	MEAN (M_ϕ):	-1.952	1.106	1.279
	SORTING (σ_I):	2.688	0.781	0.353
	SKEWNESS (Sk_I):	0.590	-0.269	0.162
	KURTOSIS (K_G):	0.510	2.028	1.206
FOLK AND WARD METHOD (Description)	MEAN:	Very Fine Gravel	Medium Sand	Medium Sand
	SORTING:	Very Poorly Sorted	Moderately Sorted	Well Sorted
	SKEWNESS:	Very Fine Skewed	Coarse Skewed	Fine Skewed
	KURTOSIS:	Very Platykurtic	Very Leptokurtic	Leptokurtic
	MODE 1 (μm):	12200.0	462.5	462.5
	MODE 2 (μm):	327.5	2180.0	
	MODE 3 (μm):	462.5		
	MODE 1 (ϕ):	-3.604	1.117	1.117
	MODE 2 (ϕ):	1.616	-1.119	
	MODE 3 (ϕ):	1.117		
	D_{10} (μm):	229.8	277.7	304.5
	D_{50} (μm):	9266.5	452.8	430.4
	D_{90} (μm):	24398.7	2028.2	556.3
	(D_{90} / D_{10}) (μm):	106.2	7.304	1.827
	(D_{90} - D_{10}) (μm):	24168.8	1750.5	251.7
	(D_{75} / D_{25}) (μm):	53.04	1.564	1.354
	(D_{75} - D_{25}) (μm):	17387.5	200.7	125.7
	D_{10} (ϕ):	-4.609	-1.020	0.846
	D_{50} (ϕ):	-3.212	1.143	1.216
	D_{90} (ϕ):	2.121	1.848	1.715
	(D_{90} / D_{10}) (ϕ):	-0.460	-1.812	2.027
	(D_{90} - D_{10}) (ϕ):	6.730	2.869	0.869
	(D_{75} / D_{25}) (ϕ):	-0.381	1.763	1.414
	(D_{75} - D_{25}) (ϕ):	5.729	0.646	0.437
	% GRAVEL:	61.4%	10.7%	2.7%
	% SAND:	38.6%	89.3%	97.3%
	% MUD:	0.0%	0.0%	0.0%
	% V COARSE GRAVEL:	0.0%	0.0%	0.0%
	% COARSE GRAVEL:	31.8%	0.0%	0.0%
	% MEDIUM GRAVEL:	22.1%	0.2%	0.0%
	% FINE GRAVEL:	4.2%	2.3%	0.4%
	% V FINE GRAVEL:	3.2%	8.2%	2.3%
	% V COARSE SAND:	0.0%	0.0%	0.0%
	% COARSE SAND:	2.9%	22.1%	13.5%
	% MEDIUM SAND:	22.7%	61.8%	82.0%
	% FINE SAND:	9.2%	4.4%	1.0%
	% V FINE SAND:	3.8%	1.0%	0.8%
	% V COARSE SILT:	0.0%	0.0%	0.0%
	% COARSE SILT:	0.0%	0.0%	0.0%
	% MEDIUM SILT:	0.0%	0.0%	0.0%
	% FINE SILT:	0.0%	0.0%	0.0%
	% V FINE SILT:	0.0%	0.0%	0.0%
	% CLAY:	0.0%	0.0%	0.0%

Table B.3 (Continued). Sediment grain-size analysis data for the lower Piscataqua River; GRADISTAT results, gravel fraction separated.

SAMPLE STATISTICS

		200209_04_3	200209_04_5	200209_05_3
	ANALYST AND DATE:	,	,	,
	SIEVING ERROR:			
	SAMPLE TYPE:	Trimodal, Moderately Sorted	Bimodal, Moderately Sorted	Unimodal, Well Sorted
	TEXTURAL GROUP:	Gravelly Sand	Gravelly Sand	Gravel
	SEDIMENT NAME:	Very Fine Gravelly Medium Sand	Very Fine Gravelly Medium Sand	Very Coarse Gravel
METHOD OF MOMENTS Arithmetic (μm)	MEAN ($\overline{x}_a$):	502.6	685.1	32327.5
	SORTING (σ_a):	599.7	819.9	7913.9
	SKEWNESS (Sk_a):	4.717	3.884	-3.436
	KURTOSIS (K_a):	30.03	20.76	13.05
METHOD OF MOMENTS Geometric (μm)	MEAN ($\overline{x}_g$):	381.0	502.1	26868.7
	SORTING (σ_g):	1.885	1.947	2.822
	SKEWNESS (Sk_g):	1.083	1.319	-4.621
	KURTOSIS (K_g):	6.914	6.163	23.64
METHOD OF MOMENTS Logarithmic (ϕ)	MEAN ($\overline{x}_\phi$):	1.392	0.994	-4.748
	SORTING (σ_ϕ):	0.915	0.961	1.497
	SKEWNESS (Sk_ϕ):	-1.083	-1.319	4.621
	KURTOSIS (K_ϕ):	6.914	6.163	23.64
FOLK AND WARD METHOD (μm)	MEAN (M_G):	358.5	466.1	34140.1
	SORTING (σ_G):	1.760	1.694	1.295
	SKEWNESS (Sk_G):	0.138	0.327	-0.444
	KURTOSIS (K_G):	2.004	2.307	6.533
FOLK AND WARD METHOD (ϕ)	MEAN (M_Z):	1.480	1.101	-5.093
	SORTING (σ_I):	0.815	0.760	0.373
	SKEWNESS (Sk_I):	-0.138	-0.327	0.444
	KURTOSIS (K_G):	2.004	2.307	6.533
FOLK AND WARD METHOD (Description)	MEAN:	Medium Sand	Medium Sand	Very Coarse Gravel
	SORTING:	Moderately Sorted	Moderately Sorted	Well Sorted
	SKEWNESS:	Coarse Skewed	Very Coarse Skewed	Very Fine Skewed
	KURTOSIS:	Very Leptokurtic	Very Leptokurtic	Extremely Leptokurtic
	MODE 1 (μm):	462.5	462.5	34500.0
	MODE 2 (μm):	327.5	2180.0	
	MODE 3 (μm):	2180.0		
	MODE 1 (ϕ):	1.117	1.117	-5.103
	MODE 2 (ϕ):	1.616	-1.119	
	MODE 3 (ϕ):	-1.119		
	D_{10} (μm):	222.8	299.5	31670.2
	D_{50} (μm):	364.7	445.2	34140.1
	D_{90} (μm):	620.6	2023.7	36802.5
	(D_{90} / D_{10}) (μm):	2.785	6.757	1.162
	(D_{90} - D_{10}) (μm):	397.8	1724.2	5132.3
	(D_{75} / D_{25}) (μm):	1.694	1.473	1.098
	(D_{75} - D_{25}) (μm):	192.0	169.5	3205.9
	D_{10} (ϕ):	0.688	-1.017	-5.202
	D_{50} (ϕ):	1.455	1.167	-5.093
	D_{90} (ϕ):	2.166	1.739	-4.985
	(D_{90} / D_{10}) (ϕ):	3.147	-1.710	0.958
	(D_{90} - D_{10}) (ϕ):	1.478	2.756	0.217
	(D_{75} / D_{25}) (ϕ):	1.696	1.606	0.974
	(D_{75} - D_{25}) (ϕ):	0.760	0.559	0.135
	% GRAVEL:	6.1%	10.6%	96.6%
	% SAND:	93.9%	89.4%	3.4%
	% MUD:	0.0%	0.0%	0.0%
	% V COARSE GRAVEL:	0.0%	0.0%	84.5%
	% COARSE GRAVEL:	0.0%	0.0%	8.4%
	% MEDIUM GRAVEL:	0.0%	0.0%	2.8%
	% FINE GRAVEL:	1.1%	2.2%	0.6%
	% V FINE GRAVEL:	5.1%	8.4%	0.4%
	% V COARSE SAND:	0.0%	0.9%	0.0%
	% COARSE SAND:	10.1%	15.9%	0.0%
	% MEDIUM SAND:	68.0%	67.9%	0.5%
	% FINE SAND:	12.0%	3.5%	1.2%
	% V FINE SAND:	3.8%	1.2%	1.7%
	% V COARSE SILT:	0.0%	0.0%	0.0%
	% COARSE SILT:	0.0%	0.0%	0.0%
	% MEDIUM SILT:	0.0%	0.0%	0.0%
	% FINE SILT:	0.0%	0.0%	0.0%
	% V FINE SILT:	0.0%	0.0%	0.0%
	% CLAY:	0.0%	0.0%	0.0%

Table B.3 (Continued). Sediment grain-size analysis data for the lower Piscataqua River; GRADISTAT results, gravel fraction separated.

SAMPLE STATISTICS

		200209_05_8	200209_05_9	200209_06_1
	ANALYST AND DATE:	,	,	,
	SIEVING ERROR:			
	SAMPLE TYPE:	Polymodal, Very Poorly Sorted	Polymodal, Very Poorly Sorted	Trimodal, Poorly Sorted
	TEXTURAL GROUP:	Sandy Gravel	Sandy Gravel	Gravelly Sand
	SEDIMENT NAME:	Sandy Coarse Gravel	Sandy Coarse Gravel	Medium Gravelly Fine Sand
METHOD OF MOMENTS Arithmetic (μm)	MEAN ($\overline{x}_a$):	11619.9	5947.3	823.8
	SORTING (σ_a):	8958.7	6501.8	1955.3
	SKEWNESS (Sk_a):	0.052	0.858	3.362
	KURTOSIS (K_a):	1.582	2.163	13.13
METHOD OF MOMENTS Geometric (μm)	MEAN ($\overline{x}_g$):	5007.3	2173.2	290.8
	SORTING (σ_g):	5.837	5.424	2.919
	SKEWNESS (Sk_g):	-0.924	-0.335	2.100
	KURTOSIS (K_g):	2.267	1.819	6.744
METHOD OF MOMENTS Logarithmic (ϕ)	MEAN ($\overline{x}_\phi$):	-2.324	-1.120	1.782
	SORTING (σ_ϕ):	2.545	2.439	1.546
	SKEWNESS (Sk_ϕ):	0.924	0.335	-2.100
	KURTOSIS (K_ϕ):	2.267	1.819	6.744
FOLK AND WARD METHOD (μm)	MEAN (M_G):	4593.2	2208.7	233.7
	SORTING (σ_G):	5.855	5.843	2.323
	SKEWNESS (Sk_G):	-0.684	-0.095	0.456
	KURTOSIS (K_G):	0.615	0.664	3.087
FOLK AND WARD METHOD (ϕ)	MEAN (M_ϕ):	-2.199	-1.143	2.097
	SORTING (σ_I):	2.550	2.547	1.216
	SKEWNESS (Sk_I):	0.684	0.095	-0.456
	KURTOSIS (K_G):	0.615	0.664	3.087
FOLK AND WARD METHOD (Description)	MEAN:	Fine Gravel	Very Fine Gravel	Fine Sand
	SORTING:	Very Poorly Sorted	Very Poorly Sorted	Poorly Sorted
	SKEWNESS:	Very Fine Skewed	Symmetrical	Very Coarse Skewed
	KURTOSIS:	Very Platykurtic	Very Platykurtic	Extremely Leptokurtic
	MODE 1 (μm):	12200.0	2180.0	196.0
	MODE 2 (μm):	8750.0	4375.0	8750.0
	MODE 3 (μm):	275.0	550.0	2180.0
	MODE 1 (ϕ):	-3.604	-1.119	2.356
	MODE 2 (ϕ):	-3.124	-2.124	-3.124
	MODE 3 (ϕ):	1.868	0.868	-1.119
	D_{10} (μm):	274.0	158.2	135.3
	D_{50} (μm):	11944.6	2283.5	216.5
	D_{90} (μm):	24314.0	17352.8	2093.7
	(D_{90} / D_{10}) (μm):	88.74	109.7	15.47
	(D_{90} - D_{10}) (μm):	24040.0	17194.6	1958.4
	(D_{75} / D_{25}) (μm):	23.81	21.49	1.708
	(D_{75} - D_{25}) (μm):	17499.3	10690.3	121.8
	D_{10} (ϕ):	-4.604	-4.117	-1.066
	D_{50} (ϕ):	-3.578	-1.191	2.208
	D_{90} (ϕ):	1.868	2.660	2.886
	(D_{90} / D_{10}) (ϕ):	-0.406	-0.646	-2.707
	(D_{90} - D_{10}) (ϕ):	6.472	6.777	3.952
	(D_{75} / D_{25}) (ϕ):	-0.091	-0.269	1.437
	(D_{75} - D_{25}) (ϕ):	4.574	4.426	0.773
	% GRAVEL:	74.2%	61.1%	10.9%
	% SAND:	25.8%	38.9%	89.1%
	% MUD:	0.0%	0.0%	0.0%
	% V COARSE GRAVEL:	0.0%	0.0%	0.0%
	% COARSE GRAVEL:	43.4%	19.0%	0.0%
	% MEDIUM GRAVEL:	20.0%	14.0%	4.5%
	% FINE GRAVEL:	6.7%	14.3%	3.2%
	% V FINE GRAVEL:	4.1%	13.9%	3.1%
	% V COARSE SAND:	0.0%	3.7%	0.0%
	% COARSE SAND:	3.9%	12.0%	0.9%
	% MEDIUM SAND:	14.2%	8.6%	23.0%
	% FINE SAND:	5.6%	9.7%	58.8%
	% V FINE SAND:	2.0%	4.9%	6.4%
	% V COARSE SILT:	0.0%	0.0%	0.0%
	% COARSE SILT:	0.0%	0.0%	0.0%
	% MEDIUM SILT:	0.0%	0.0%	0.0%
	% FINE SILT:	0.0%	0.0%	0.0%
	% V FINE SILT:	0.0%	0.0%	0.0%
	% CLAY:	0.0%	0.0%	0.0%

Table B.3 (Continued). Sediment grain-size analysis data for the lower Piscataqua River; GRADISTAT results, gravel fraction separated.

SAMPLE STATISTICS

		200209_06_2	200209_06_3	200209_06_4
	ANALYST AND DATE:	,	,	,
	SIEVING ERROR:			
	SAMPLE TYPE:	Unimodal, Poorly Sorted	Unimodal, Moderately Sorted	Polymodal, Very Poorly Sorted
	TEXTURAL GROUP:	Gravel	Gravel	Sandy Gravel
	SEDIMENT NAME:	Very Coarse Gravel	Very Coarse Gravel	Sandy Very Coarse Gravel
METHOD OF MOMENTS Arithmetic (μm)	MEAN ($\overline{x}_a$):	31489.1	29371.4	16851.1
	SORTING (σ_a):	8612.8	10304.5	15662.3
	SKEWNESS (Sk_a):	-3.032	-1.647	0.066
	KURTOSIS (K_a):	10.92	4.034	1.136
METHOD OF MOMENTS Geometric (μm)	MEAN ($\overline{x}_g$):	24794.8	24612.8	4690.4
	SORTING (σ_g):	3.162	2.309	7.963
	SKEWNESS (Sk_g):	-3.682	-3.619	-0.318
	KURTOSIS (K_g):	15.07	18.94	1.310
METHOD OF MOMENTS Logarithmic (ϕ)	MEAN ($\overline{x}_\phi$):	-4.632	-4.621	-2.230
	SORTING (σ_ϕ):	1.661	1.207	2.993
	SKEWNESS (Sk_ϕ):	3.682	3.619	0.318
	KURTOSIS (K_ϕ):	15.07	18.94	1.310
FOLK AND WARD METHOD (μm)	MEAN (M_G):	33868.7	25033.2	5557.7
	SORTING (σ_G):	2.029	1.770	6.431
	SKEWNESS (Sk_G):	-0.479	-0.880	-0.558
	KURTOSIS (K_G):	17.87	7.689	0.463
FOLK AND WARD METHOD (ϕ)	MEAN (M_ϕ):	-5.082	-4.646	-2.474
	SORTING (σ_I):	1.021	0.824	2.685
	SKEWNESS (Sk_I):	0.479	0.880	0.558
	KURTOSIS (K_G):	17.87	7.689	0.463
FOLK AND WARD METHOD (Description)	MEAN:	Very Coarse Gravel	Coarse Gravel	Fine Gravel
	SORTING:	Poorly Sorted	Moderately Sorted	Very Poorly Sorted
	SKEWNESS:	Very Fine Skewed	Very Fine Skewed	Very Fine Skewed
	KURTOSIS:	Extremely Leptokurtic	Extremely Leptokurtic	Very Platykurtic
	MODE 1 (μm):	34500.0	34500.0	34500.0
	MODE 2 (μm):			462.5
	MODE 3 (μm):			24450.0
	MODE 1 (ϕ):	-5.103	-5.103	-5.103
	MODE 2 (ϕ):			1.117
	MODE 3 (ϕ):			-4.607
	D_{10} (μm):	24111.0	11589.8	332.8
	D_{50} (μm):	33868.7	33592.2	12721.4
	D_{90} (μm):	36743.8	36683.7	35836.4
	(D_{90} / D_{10}) (μm):	1.524	3.165	107.7
	(D_{90} - D_{10}) (μm):	12632.9	25093.9	35503.5
	(D_{75} / D_{25}) (μm):	1.107	1.116	73.33
	(D_{75} - D_{25}) (μm):	3451.0	3698.6	33021.7
	D_{10} (ϕ):	-5.199	-5.197	-5.163
	D_{50} (ϕ):	-5.082	-5.070	-3.669
	D_{90} (ϕ):	-4.592	-3.535	1.587
	(D_{90} / D_{10}) (ϕ):	0.883	0.680	-0.307
	(D_{90} - D_{10}) (ϕ):	0.608	1.662	6.751
	(D_{75} / D_{25}) (ϕ):	0.971	0.969	-0.223
	(D_{75} - D_{25}) (ϕ):	0.147	0.159	6.196
	% GRAVEL:	94.3%	98.3%	61.5%
	% SAND:	5.7%	1.7%	38.5%
	% MUD:	0.0%	0.0%	0.0%
	% V COARSE GRAVEL:	77.9%	72.1%	35.0%
	% COARSE GRAVEL:	15.6%	10.6%	14.4%
	% MEDIUM GRAVEL:	0.0%	9.2%	4.1%
	% FINE GRAVEL:	0.2%	5.0%	4.3%
	% V FINE GRAVEL:	0.7%	1.5%	3.8%
	% V COARSE SAND:	0.0%	0.0%	0.0%
	% COARSE SAND:	0.3%	0.3%	6.7%
	% MEDIUM SAND:	3.6%	0.5%	28.9%
	% FINE SAND:	1.2%	0.6%	1.9%
	% V FINE SAND:	0.6%	0.3%	1.0%
	% V COARSE SILT:	0.0%	0.0%	0.0%
	% COARSE SILT:	0.0%	0.0%	0.0%
	% MEDIUM SILT:	0.0%	0.0%	0.0%
	% FINE SILT:	0.0%	0.0%	0.0%
	% V FINE SILT:	0.0%	0.0%	0.0%
	% CLAY:	0.0%	0.0%	0.0%

Table B.3 (Continued). Sediment grain-size analysis data for the lower Piscataqua River; GRADISTAT results, gravel fraction separated.

SAMPLE STATISTICS

		200209_06_5	200209_06_8	200209_07_11
	ANALYST AND DATE:	,	,	,
	SIEVING ERROR:			
	SAMPLE TYPE:	Polymodal, Very Poorly Sorted	Polymodal, Very Poorly Sorted	Polymodal, Very Poorly Sorted
	TEXTURAL GROUP:	Sandy Gravel	Sandy Gravel	Gravelly Sand
	SEDIMENT NAME:	Sandy Coarse Gravel	Sandy Coarse Gravel	Very Fine Gravelly Fine Sand
METHOD OF MOMENTS Arithmetic (μm)	MEAN ($\overline{x}_a$):	15676.8	5816.6	1656.5
	SORTING (σ_a):	13692.3	7101.2	2808.3
	SKEWNESS (Sk_a):	0.161	0.815	2.366
	KURTOSIS (K_a):	1.418	1.895	8.088
METHOD OF MOMENTS Geometric (μm)	MEAN ($\overline{x}_g$):	5471.2	1628.5	534.2
	SORTING (σ_g):	6.811	6.014	4.216
	SKEWNESS (Sk_g):	-0.597	0.169	0.700
	KURTOSIS (K_g):	1.694	1.420	2.292
METHOD OF MOMENTS Logarithmic (ϕ)	MEAN ($\overline{x}_\phi$):	-2.452	-0.704	0.905
	SORTING (σ_ϕ):	2.768	2.588	2.076
	SKEWNESS (Sk_ϕ):	0.597	-0.169	-0.700
	KURTOSIS (K_ϕ):	1.694	1.420	2.292
FOLK AND WARD METHOD (μm)	MEAN (M_G):	6001.9	1541.4	587.6
	SORTING (σ_G):	6.390	5.501	4.604
	SKEWNESS (Sk_G):	-0.686	0.453	0.467
	KURTOSIS (K_G):	0.520	0.504	0.782
FOLK AND WARD METHOD (ϕ)	MEAN (M_ϕ):	-2.585	-0.624	0.767
	SORTING (σ_I):	2.676	2.460	2.203
	SKEWNESS (Sk_I):	0.686	-0.453	-0.467
	KURTOSIS (K_G):	0.520	0.504	0.782
FOLK AND WARD METHOD (Description)	MEAN:	Fine Gravel	Very Coarse Sand	Coarse Sand
	SORTING:	Very Poorly Sorted	Very Poorly Sorted	Very Poorly Sorted
	SKEWNESS:	Very Fine Skewed	Very Coarse Skewed	Very Coarse Skewed
	KURTOSIS:	Very Platykurtic	Very Platykurtic	Platykurtic
	MODE 1 (μm):	24450.0	327.5	2180.0
	MODE 2 (μm):	17500.0	462.5	196.0
	MODE 3 (μm):	327.5	2180.0	390.0
	MODE 1 (ϕ):	-4.607	1.616	-1.119
	MODE 2 (ϕ):	-4.124	1.117	2.356
	MODE 3 (ϕ):	1.616	-1.119	1.364
	D_{10} (μm):	320.5	250.5	123.1
	D_{50} (μm):	16661.5	778.8	330.1
	D_{90} (μm):	34830.6	17614.6	5744.6
	(D_{50} / D_{10}) (μm):	108.7	70.33	46.66
	(D_{50} - D_{10}) (μm):	34510.1	17364.2	5621.5
	(D_{75} / D_{25}) (μm):	47.64	38.62	11.34
	(D_{75} - D_{25}) (μm):	25628.6	12155.2	1892.8
	D_{10} (ϕ):	-5.122	-4.139	-2.522
	D_{50} (ϕ):	-4.058	0.361	1.599
	D_{90} (ϕ):	1.641	1.997	3.022
	(D_{50} / D_{10}) (ϕ):	-0.320	-0.483	-1.198
	(D_{50} - D_{10}) (ϕ):	6.764	6.136	5.544
	(D_{75} / D_{25}) (ϕ):	-0.183	-0.448	-2.325
	(D_{75} - D_{25}) (ϕ):	5.574	5.271	3.503
	% GRAVEL:	69.0%	47.5%	27.4%
	% SAND:	31.0%	52.5%	72.6%
	% MUD:	0.0%	0.0%	0.0%
	% V COARSE GRAVEL:	21.5%	0.0%	0.0%
	% COARSE GRAVEL:	30.8%	22.7%	0.0%
	% MEDIUM GRAVEL:	6.1%	8.9%	6.5%
	% FINE GRAVEL:	6.3%	9.5%	10.2%
	% V FINE GRAVEL:	4.4%	6.4%	10.7%
	% V COARSE SAND:	0.9%	1.0%	2.7%
	% COARSE SAND:	6.0%	6.5%	7.5%
	% MEDIUM SAND:	20.8%	35.1%	21.2%
	% FINE SAND:	2.4%	7.5%	30.8%
	% V FINE SAND:	0.9%	2.4%	10.3%
	% V COARSE SILT:	0.0%	0.0%	0.0%
	% COARSE SILT:	0.0%	0.0%	0.0%
	% MEDIUM SILT:	0.0%	0.0%	0.0%
	% FINE SILT:	0.0%	0.0%	0.0%
	% V FINE SILT:	0.0%	0.0%	0.0%
	% CLAY:	0.0%	0.0%	0.0%

Table B.3 (Continued). Sediment grain-size analysis data for the lower Piscataqua River; GRADISTAT results, gravel fraction separated.

SAMPLE STATISTICS

		200209_07_3	200209_07_5	200209_07_9
	ANALYST AND DATE:	,	,	,
	SIEVING ERROR:			
	SAMPLE TYPE:	Polymodal, Very Poorly Sorted	Bimodal, Very Poorly Sorted	Unimodal, Poorly Sorted
	TEXTURAL GROUP:	Sandy Gravel	Sandy Gravel	Gravel
	SEDIMENT NAME:	Sandy Coarse Gravel	Sandy Coarse Gravel	Coarse Gravel
METHOD OF MOMENTS Arithmetic (μm)	MEAN ($\overline{x}_a$):	5108.2	13467.3	20380.3
	SORTING (σ_a):	8496.8	10623.3	8261.7
	SKEWNESS (Sk_a):	1.604	-0.177	-1.748
	KURTOSIS (K_a):	3.870	1.287	4.409
METHOD OF MOMENTS Geometric (μm)	MEAN ($\overline{x}_g$):	1105.0	4276.6	12782.5
	SORTING (σ_g):	5.750	8.487	4.766
	SKEWNESS (Sk_g):	0.677	-0.711	-2.294
	KURTOSIS (K_g):	2.050	1.669	6.440
METHOD OF MOMENTS Logarithmic (ϕ)	MEAN ($\overline{x}_\phi$):	-0.144	-2.096	-3.676
	SORTING (σ_ϕ):	2.523	3.085	2.253
	SKEWNESS (Sk_ϕ):	-0.677	0.711	2.294
	KURTOSIS (K_ϕ):	2.050	1.669	6.440
FOLK AND WARD METHOD (μm)	MEAN (M_G):	1243.0	4050.4	19415.3
	SORTING (σ_G):	6.002	7.344	2.579
	SKEWNESS (Sk_G):	0.647	-0.732	-0.885
	KURTOSIS (K_G):	0.726	0.487	19.17
FOLK AND WARD METHOD (ϕ)	MEAN (M_Z):	-0.314	-2.018	-4.279
	SORTING (σ_I):	2.585	2.877	1.367
	SKEWNESS (Sk_I):	-0.647	0.732	0.885
	KURTOSIS (K_G):	0.726	0.487	19.17
FOLK AND WARD METHOD (Description)	MEAN:	Very Coarse Sand	Fine Gravel	Coarse Gravel
	SORTING:	Very Poorly Sorted	Very Poorly Sorted	Poorly Sorted
	SKEWNESS:	Very Coarse Skewed	Very Fine Skewed	Very Fine Skewed
	KURTOSIS:	Platykurtic	Very Platykurtic	Extremely Leptokurtic
	MODE 1 (μm):	2180.0	24450.0	24450.0
	MODE 2 (μm):	275.0	12200.0	
	MODE 3 (μm):	390.0		
	MODE 1 (ϕ):	-1.119	-4.607	-4.607
	MODE 2 (ϕ):	1.868	-3.604	
	MODE 3 (ϕ):	1.364		
	D_{10} (μm):	219.7	168.4	261.7
	D_{50} (μm):	480.7	12978.3	23811.3
	D_{90} (μm):	23429.0	25473.3	25939.0
	(D_{90} / D_{10}) (μm):	106.7	151.3	99.12
	(D_{90} - D_{10}) (μm):	23209.4	25304.9	25677.3
	(D_{75} / D_{25}) (μm):	15.71	83.15	1.113
	(D_{75} - D_{25}) (μm):	4171.2	23718.6	2548.6
	D_{10} (ϕ):	-4.550	-4.671	-4.697
	D_{50} (ϕ):	1.057	-3.698	-4.574
	D_{90} (ϕ):	2.187	2.570	1.934
	(D_{90} / D_{10}) (ϕ):	-0.481	-0.550	-0.412
	(D_{90} - D_{10}) (ϕ):	6.737	7.241	6.631
	(D_{75} / D_{25}) (ϕ):	-0.844	-0.391	0.967
	(D_{75} - D_{25}) (ϕ):	3.974	6.378	0.154
	% GRAVEL:	37.5%	67.9%	88.0%
	% SAND:	62.5%	32.1%	12.0%
	% MUD:	0.0%	0.0%	0.0%
	% V COARSE GRAVEL:	0.0%	0.0%	0.0%
	% COARSE GRAVEL:	16.4%	48.9%	78.6%
	% MEDIUM GRAVEL:	4.0%	15.4%	9.4%
	% FINE GRAVEL:	7.0%	2.4%	0.0%
	% V FINE GRAVEL:	10.0%	1.2%	0.0%
	% V COARSE SAND:	0.0%	0.0%	0.0%
	% COARSE SAND:	10.8%	0.3%	0.4%
	% MEDIUM SAND:	34.2%	10.2%	1.9%
	% FINE SAND:	15.0%	18.5%	9.1%
	% V FINE SAND:	2.5%	3.0%	0.7%
	% V COARSE SILT:	0.0%	0.0%	0.0%
	% COARSE SILT:	0.0%	0.0%	0.0%
	% MEDIUM SILT:	0.0%	0.0%	0.0%
	% FINE SILT:	0.0%	0.0%	0.0%
	% V FINE SILT:	0.0%	0.0%	0.0%
	% CLAY:	0.0%	0.0%	0.0%

B-4. DISTRIBUTION PLOTS FROM SAMPLES, GRAVEL SEPARATED AND LITHOGENIC AND BIOGENIC PARTS SEPARATED

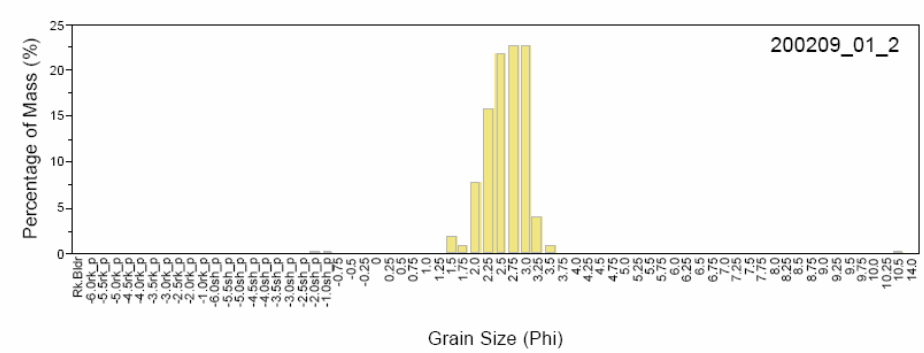
200209_01_2
Percentage of Mass (%)
Grain Size (Phi)

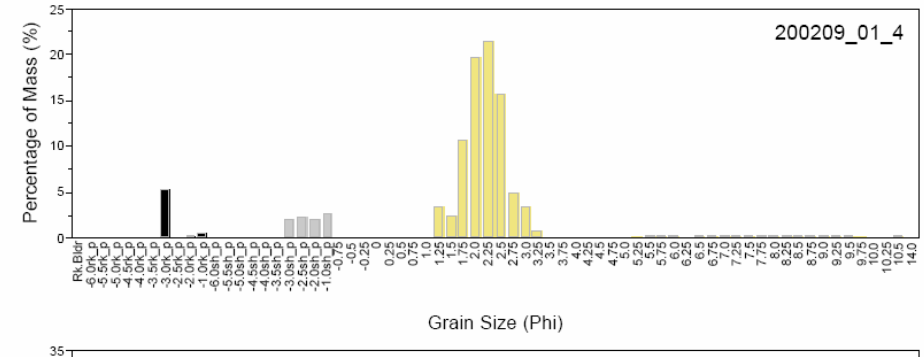
200209_01_4
Percentage of Mass (%)
Grain Size (Phi)

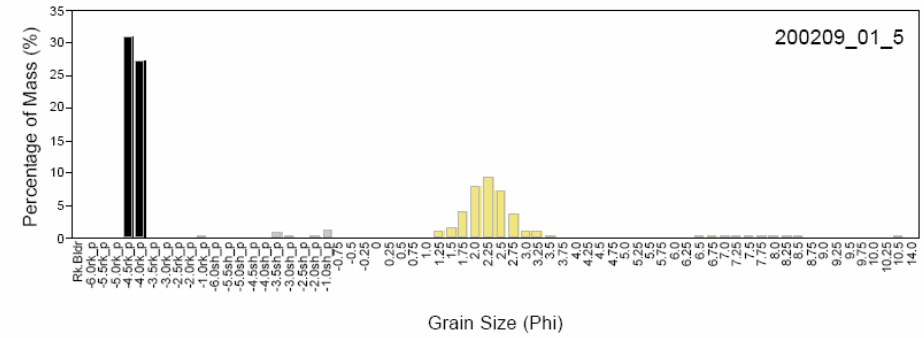
200209_01_5
Percentage of Mass (%)
Grain Size (Phi)

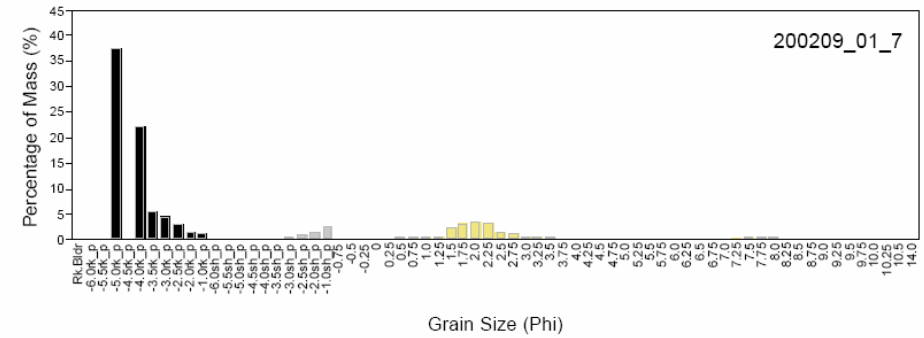
200209_01_7
Percentage of Mass (%)
Grain Size (Phi)

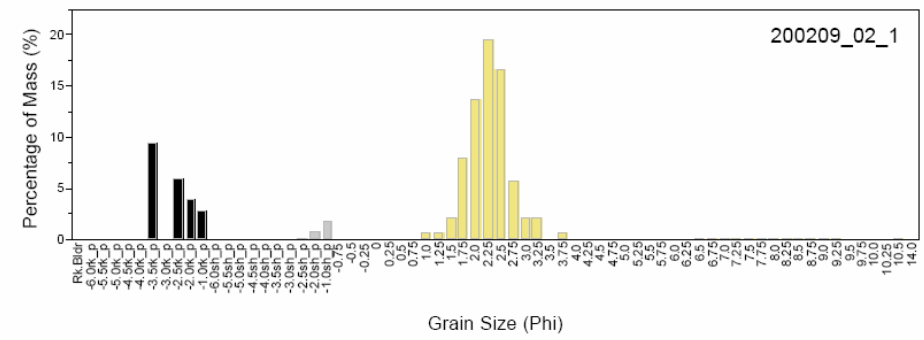
200209_02_1
Percentage of Mass (%)
Grain Size (Phi)

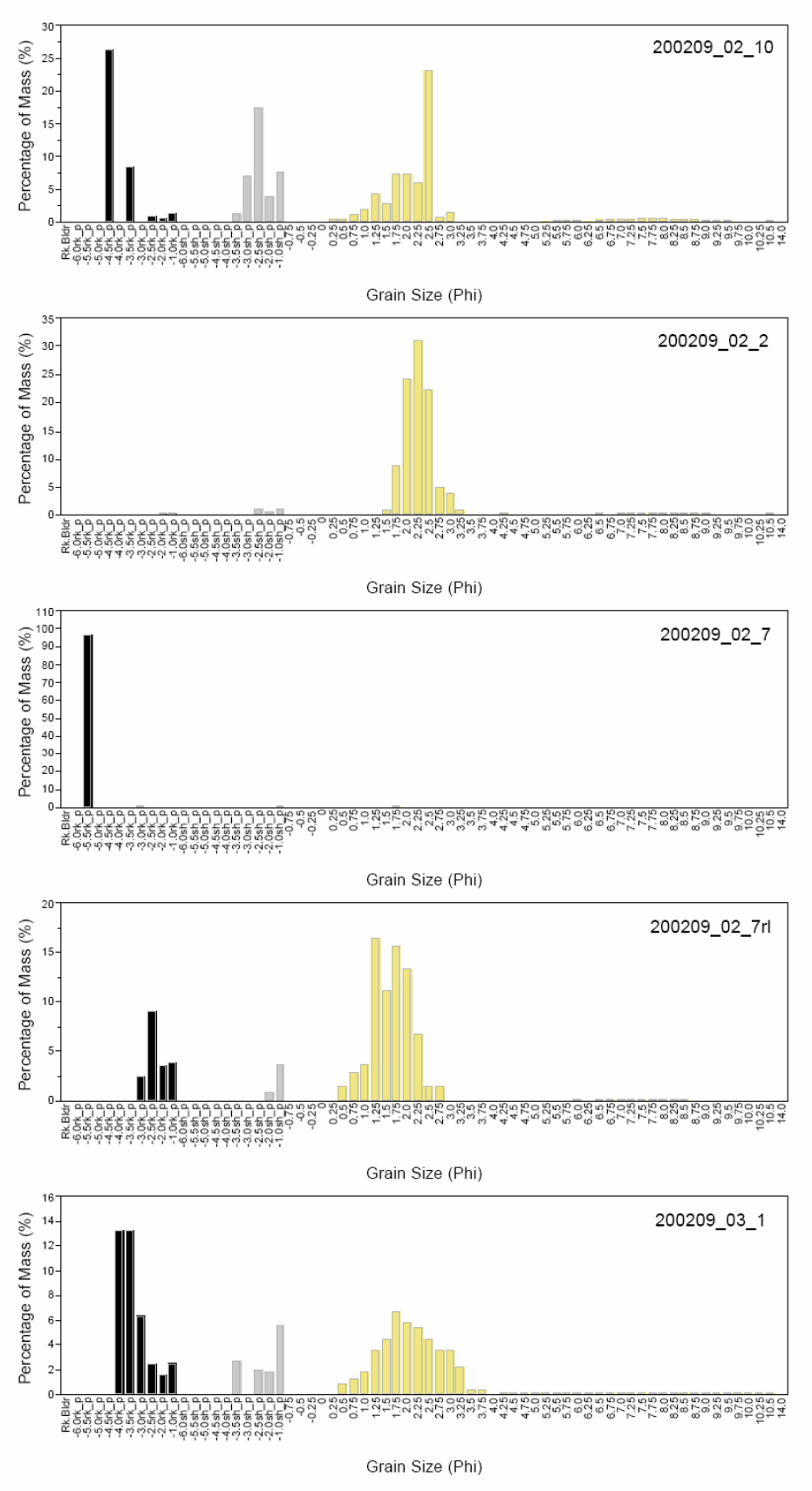
200209_02_10
Percentage of Mass (%)
Grain Size (Phi)
200209_02_2
Percentage of Mass (%)
Grain Size (Phi)
200209_02_7
Percentage of Mass (%)
Grain Size (Phi)
200209_02_7rl
Percentage of Mass (%)
Grain Size (Phi)
200209_03_1
Percentage of Mass (%)
Grain Size (Phi)

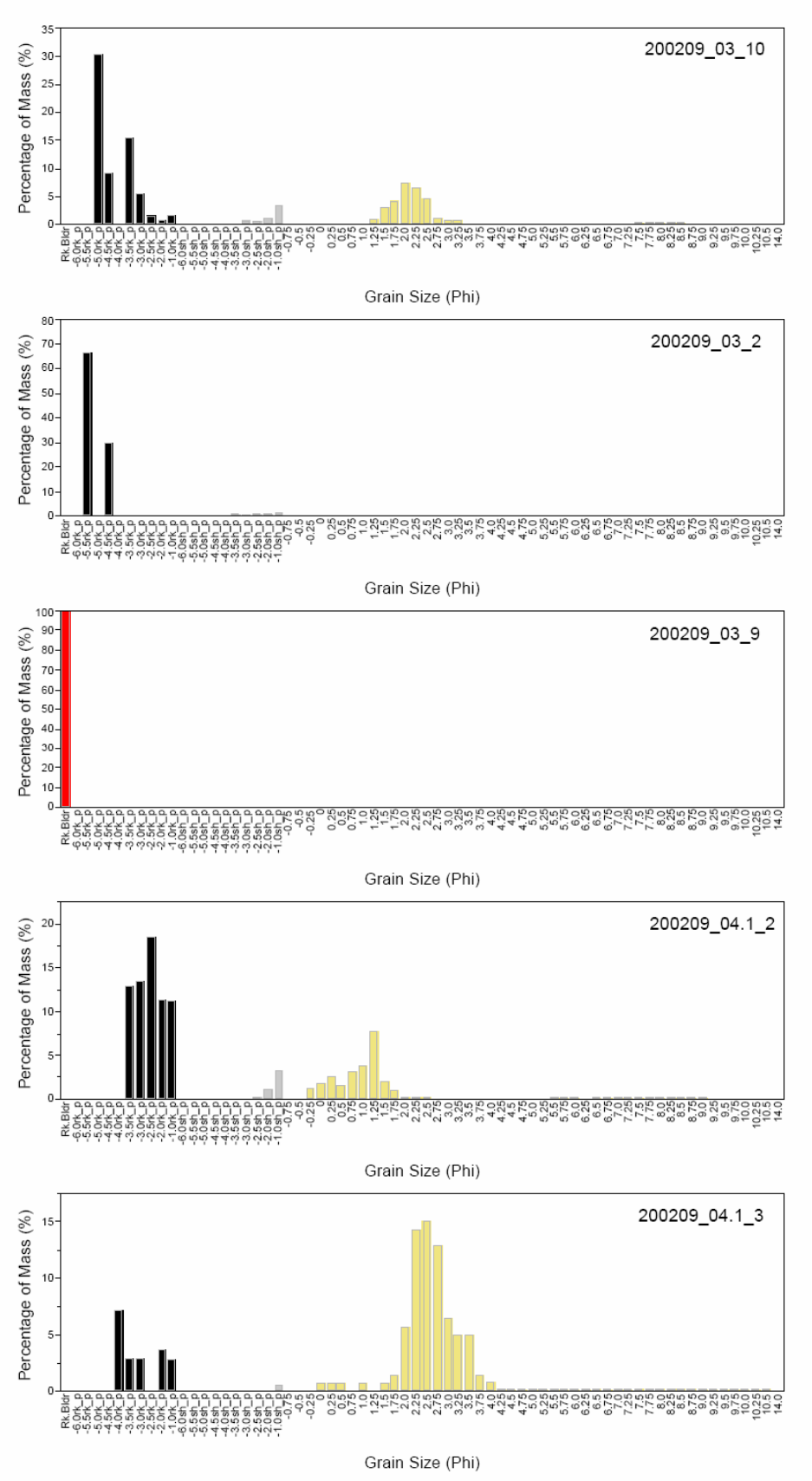
200209_03_10
Percentage of Mass (%)
Grain Size (Phi)
200209_03_2
Percentage of Mass (%)
Grain Size (Phi)
200209_03_9
Percentage of Mass (%)
Grain Size (Phi)
200209_04.1_2
Percentage of Mass (%)
Grain Size (Phi)
200209_04.1_3
Percentage of Mass (%)
Grain Size (Phi)

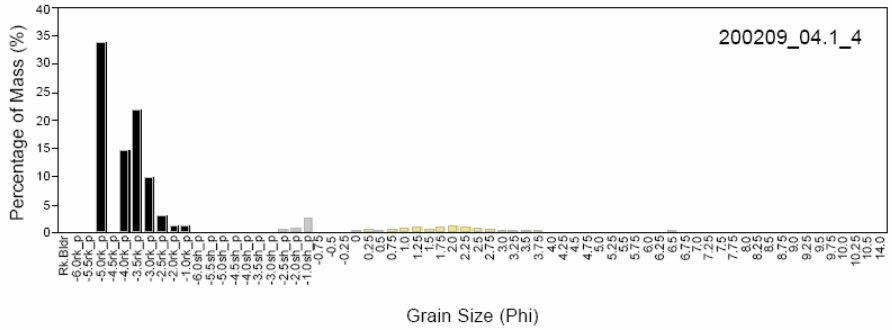
200209_04.1_4
Percentage of Mass (%)
Grain Size (Phi)

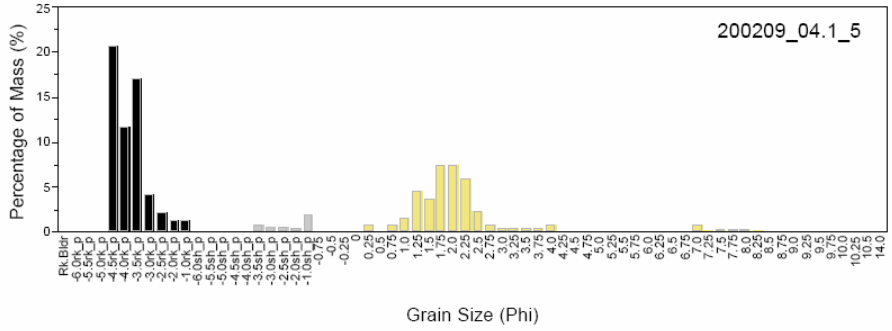
200209_04.1_5
Percentage of Mass (%)
Grain Size (Phi)

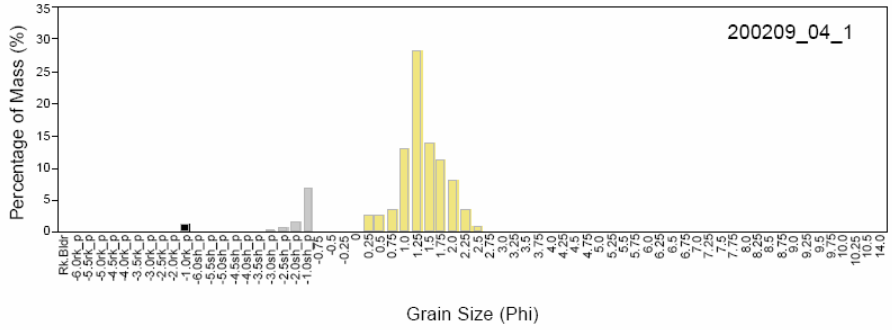
200209_04_1
Percentage of Mass (%)
Grain Size (Phi)

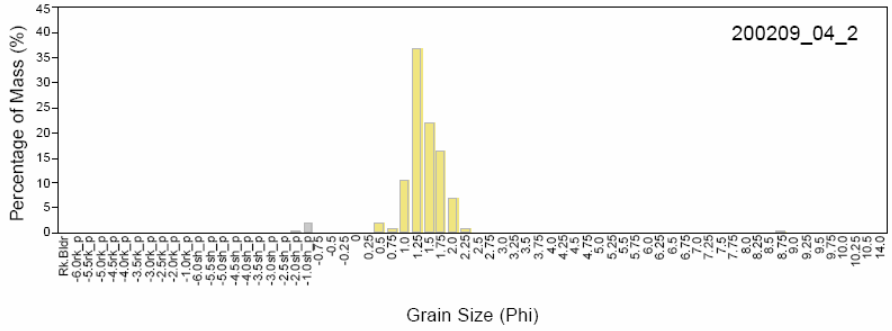
200209_04_2
Percentage of Mass (%)
Grain Size (Phi)

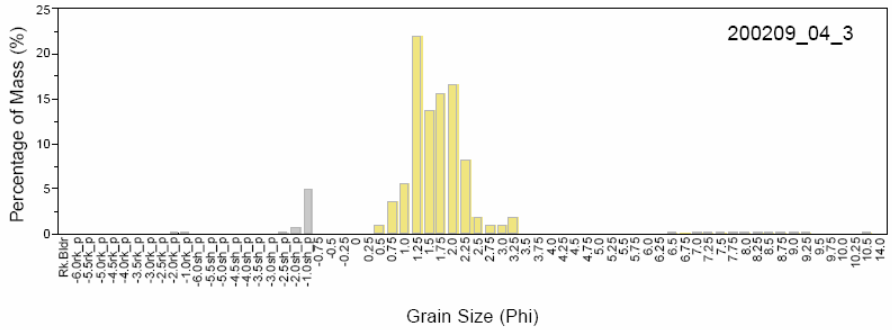
200209_04_3
Percentage of Mass (%)
Grain Size (Phi)

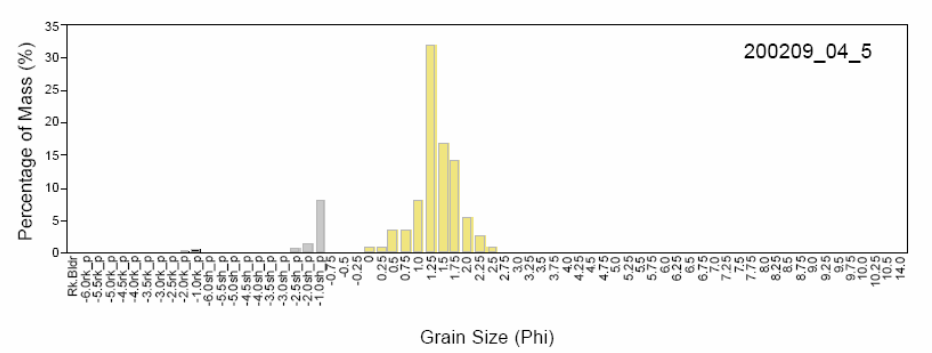
200209_04_5
Percentage of Mass (%)
Grain Size (Phi)

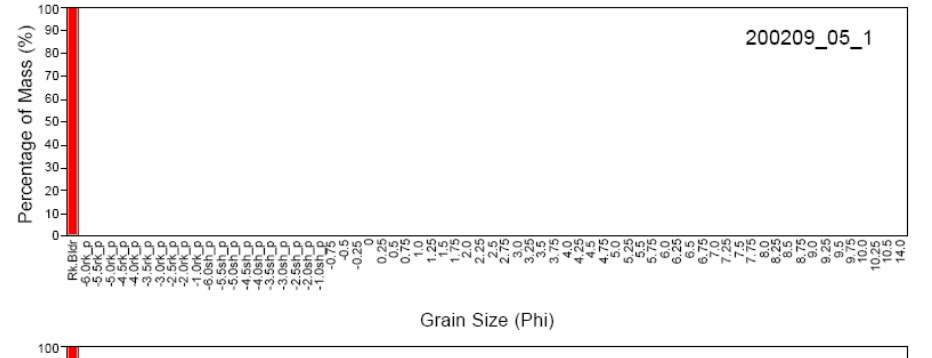
200209_05_1
Percentage of Mass (%)
Grain Size (Phi)

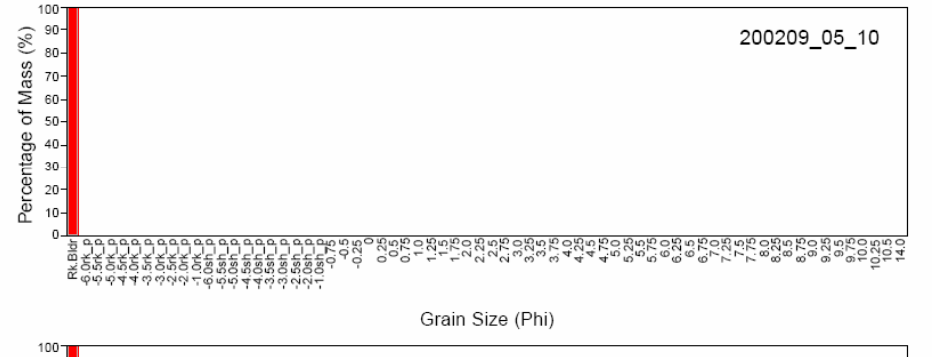
200209_05_10
Percentage of Mass (%)
Grain Size (Phi)

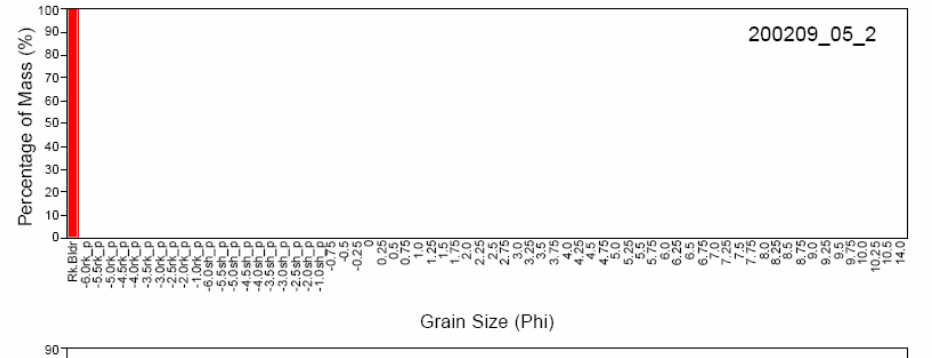
200209_05_2
Percentage of Mass (%)
Grain Size (Phi)

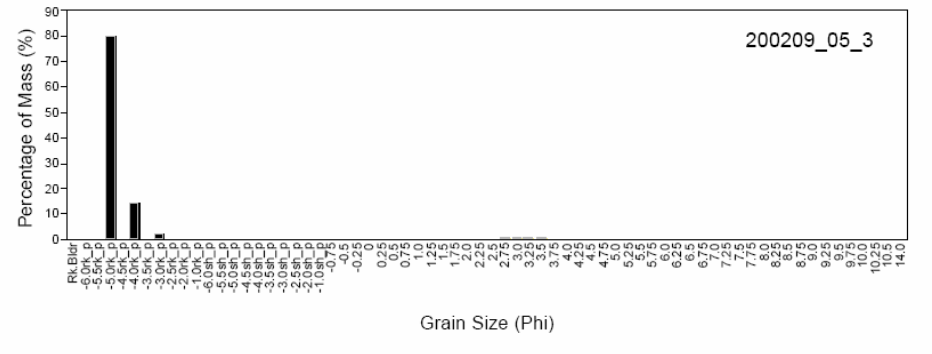
200209_05_3
Percentage of Mass (%)
Grain Size (Phi)

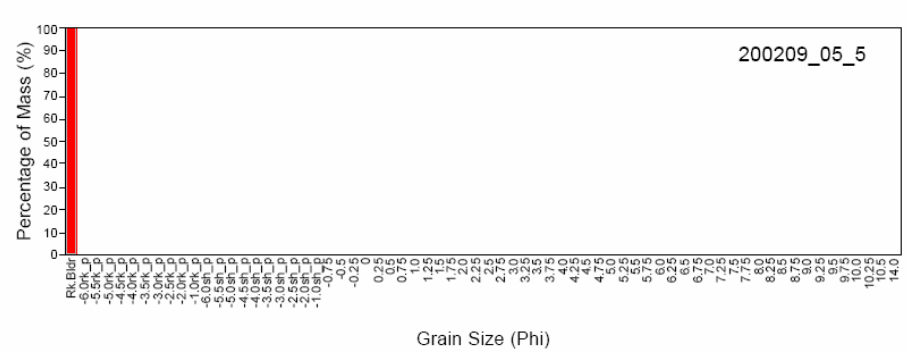
200209_05_5
Percentage of Mass (%)
Grain Size (Phi)

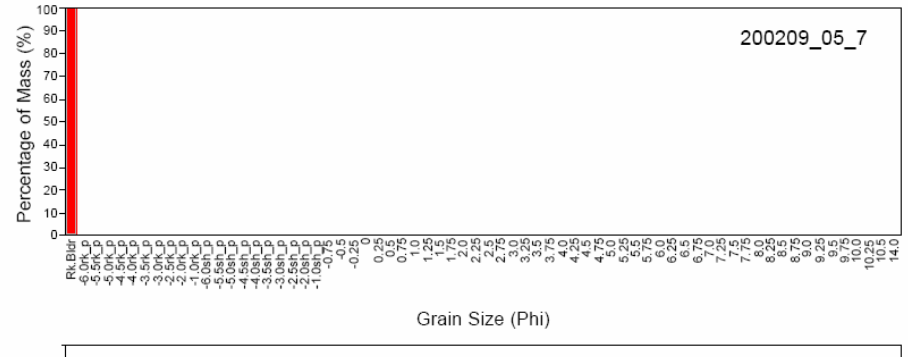
200209_05_7
Percentage of Mass (%)
Grain Size (Phi)

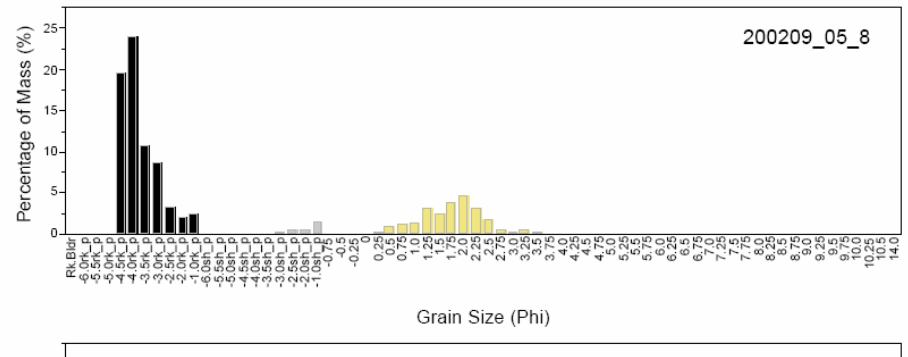
200209_05_8
Percentage of Mass (%)
Grain Size (Phi)

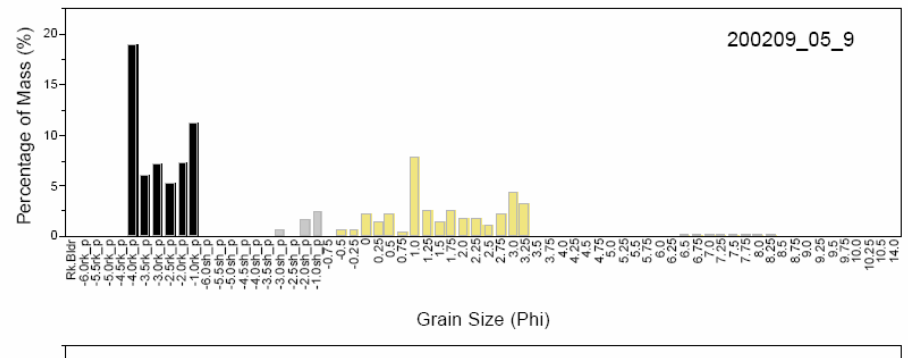
200209_05_9
Percentage of Mass (%)
Grain Size (Phi)

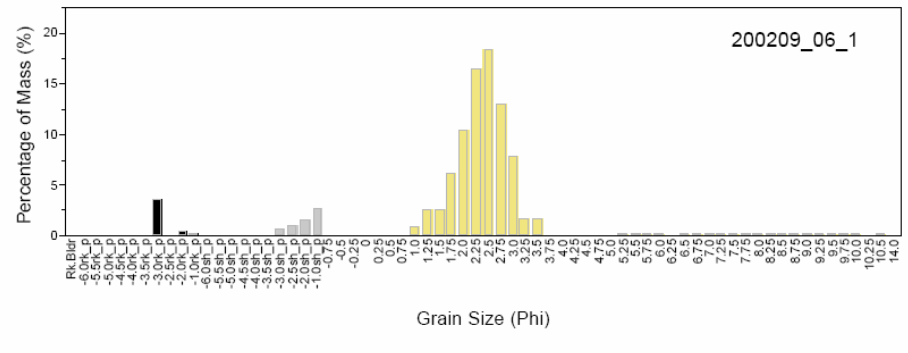
200209_06_1
Percentage of Mass (%)
Grain Size (Phi)

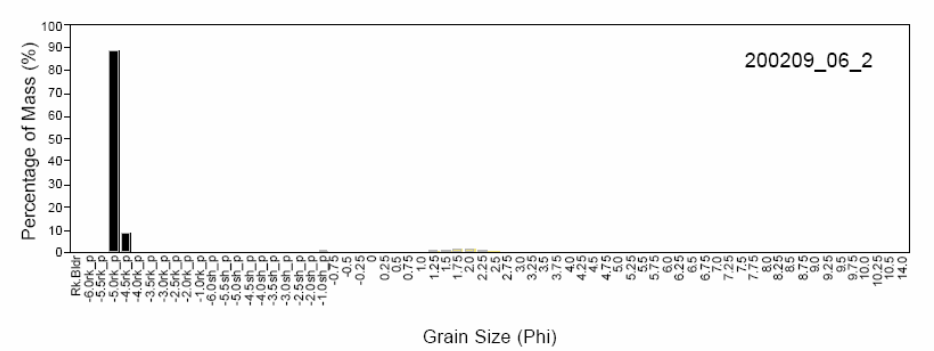
200209_06_2
Percentage of Mass (%)
Grain Size (Phi)

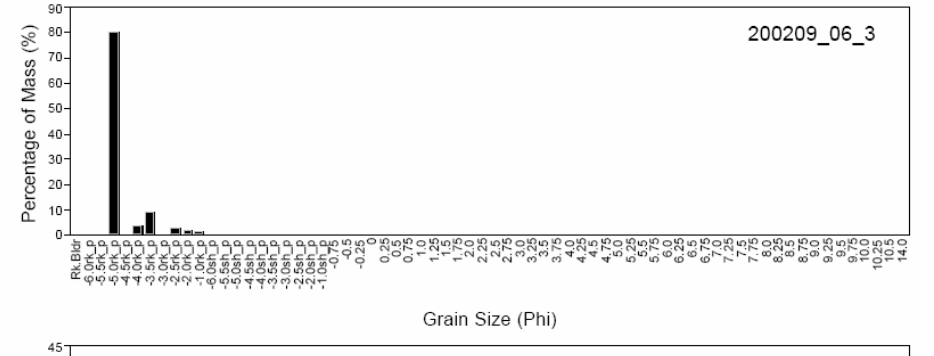
200209_06_3
Percentage of Mass (%)
Grain Size (Phi)

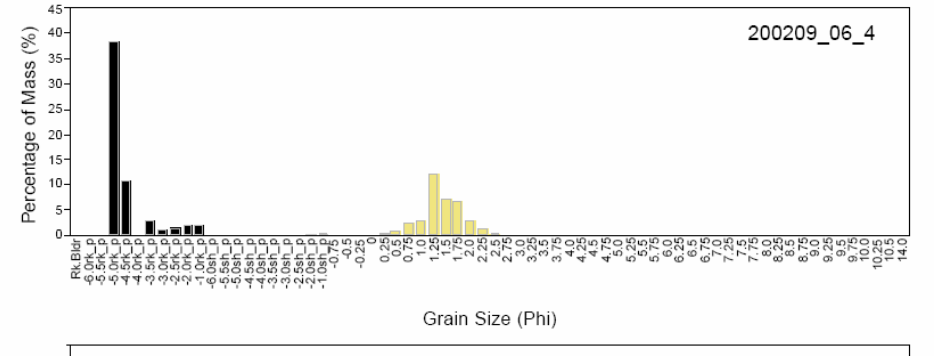
200209_06_4
Percentage of Mass (%)
Grain Size (Phi)

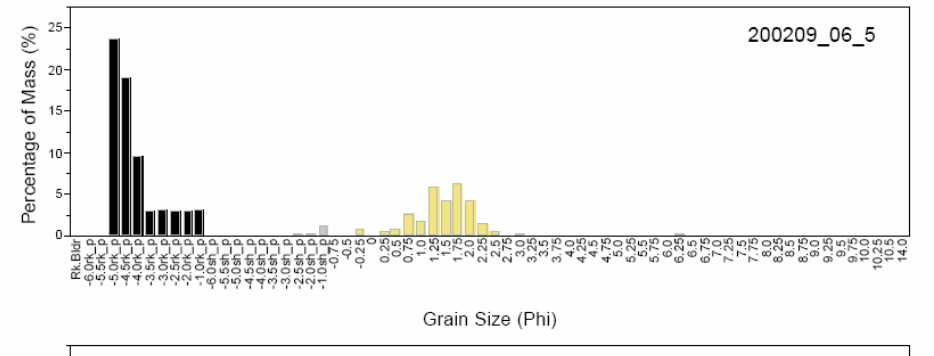
200209_06_5
Percentage of Mass (%)
Grain Size (Phi)

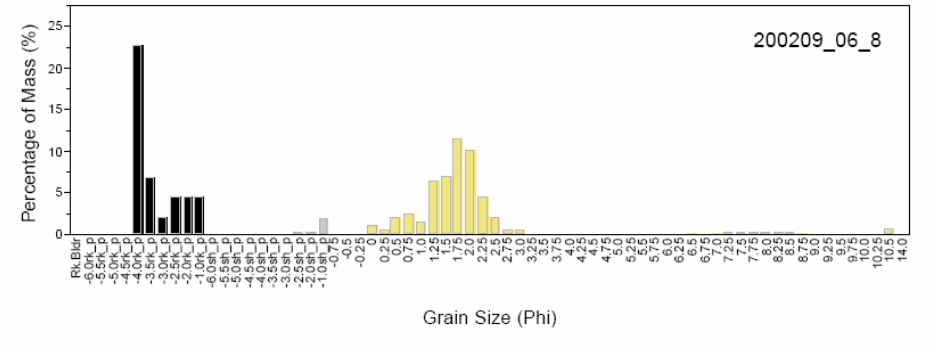
200209_06_8
Percentage of Mass (%)
Grain Size (Phi)

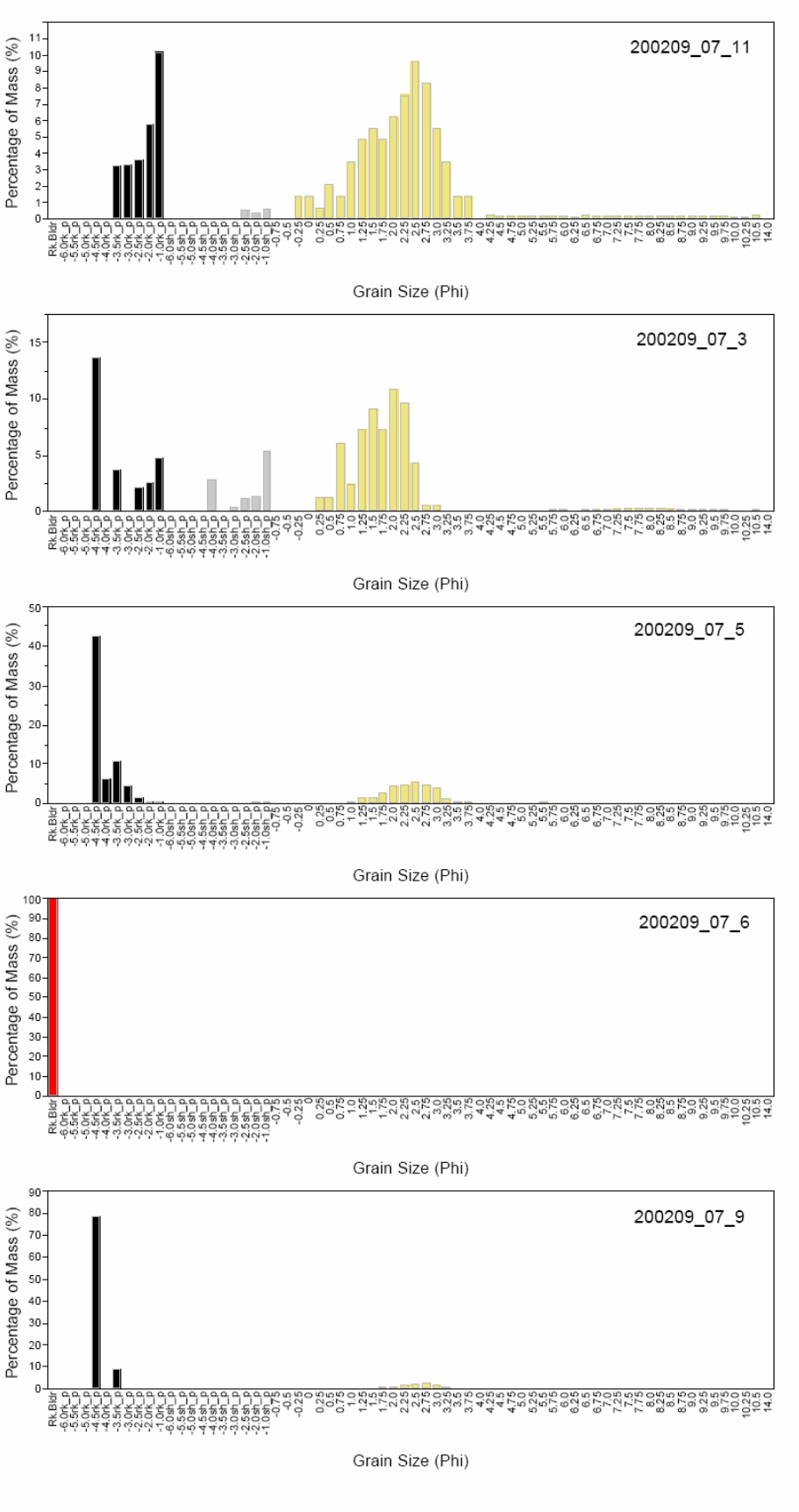
200209_07_11
Percentage of Mass (%)
Grain Size (Phi)
200209_07_3
Percentage of Mass (%)
Grain Size (Phi)
200209_07_5
Percentage of Mass (%)
Grain Size (Phi)
200209_07_6
Percentage of Mass (%)
Grain Size (Phi)
200209_07_9
Percentage of Mass (%)
Grain Size (Phi)

B-5. Images Used For Estimating Sediment Grain Size Percent Coverage Area Distributions

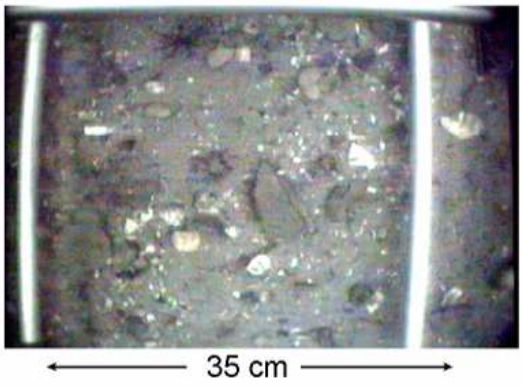

1-2.bmp

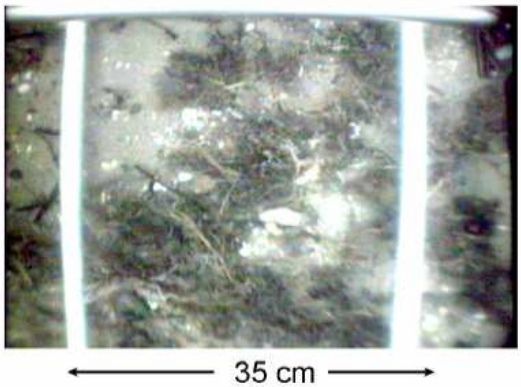

1-4.bmp

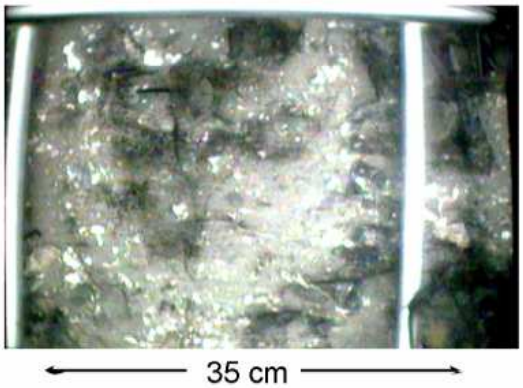

1-5.bmp

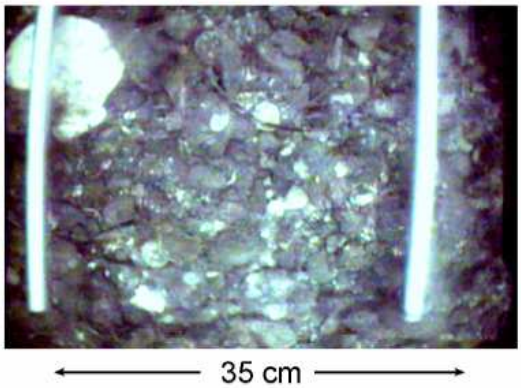

1-7.bmp

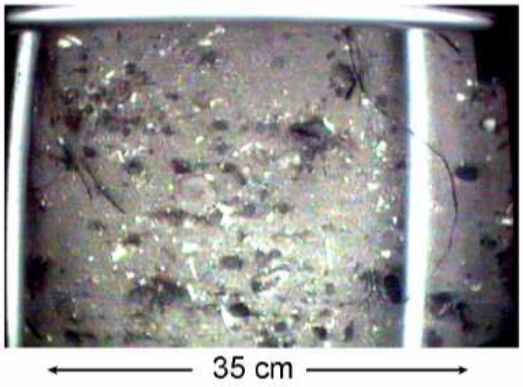

2-1.bmp

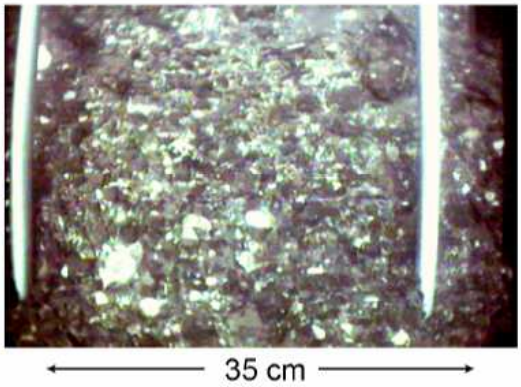

2-10.bmp

2-2b.bmp

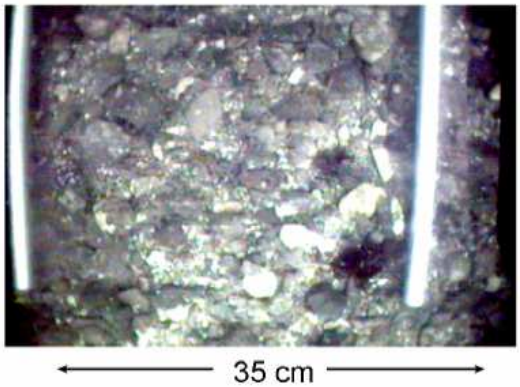

2-7.bmp

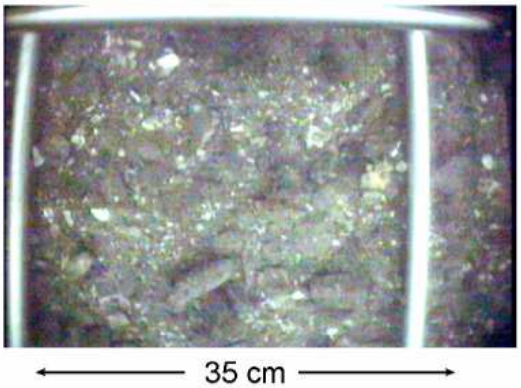

3-1.bmp

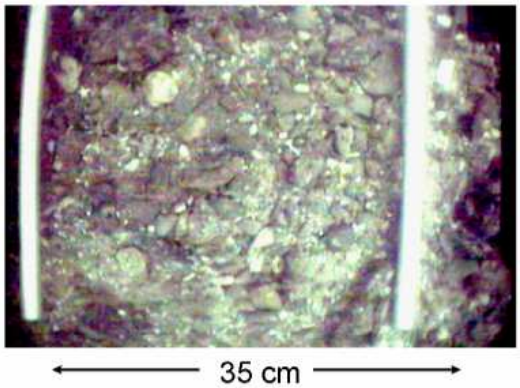

3-10.bmp

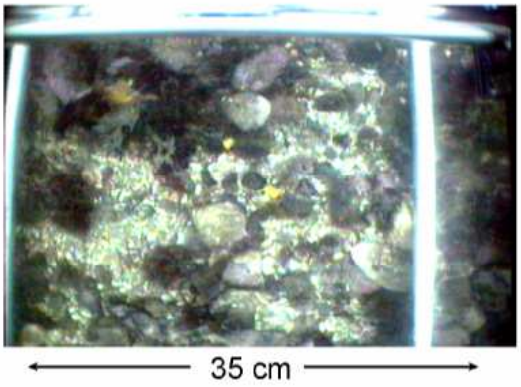

3-2.bmp

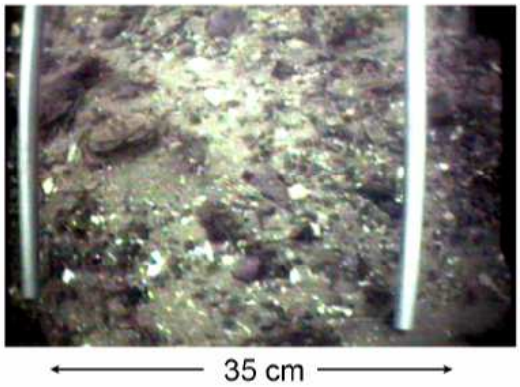

3-7.bmp

3-9.bmp

4.1-2.bmp

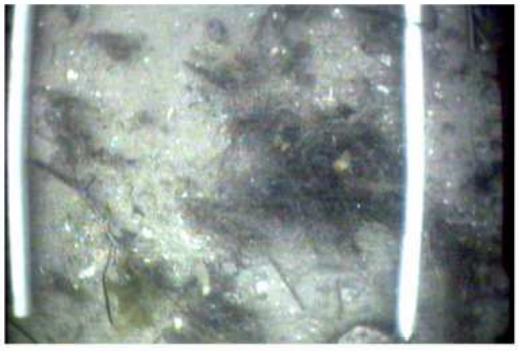

4.1-3.bmp

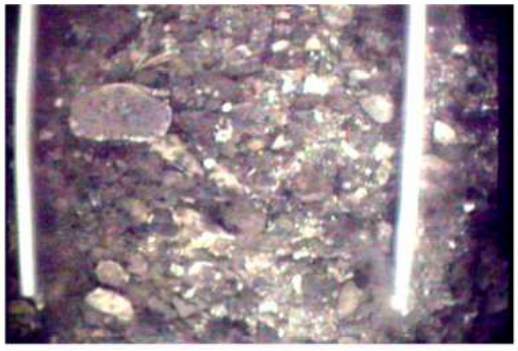

4.1-4.bmp

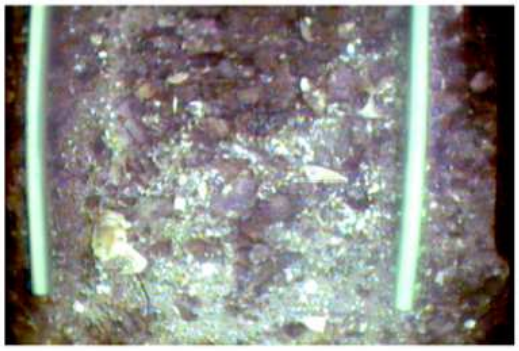

4.1-5.bmp

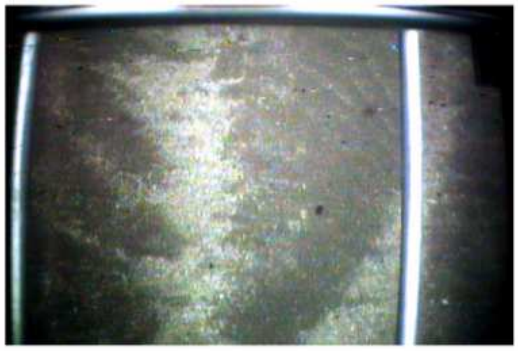

4-1b.bmp

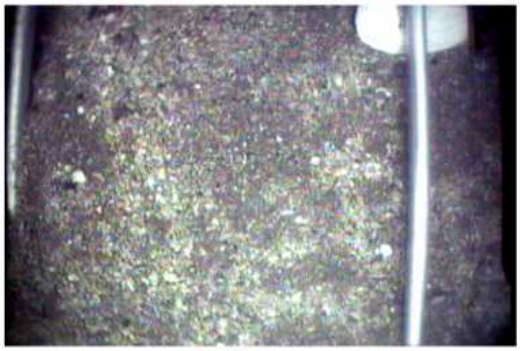

4-2.bmp

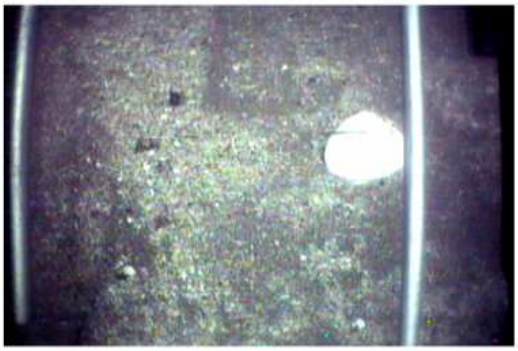

4-2b.bmp

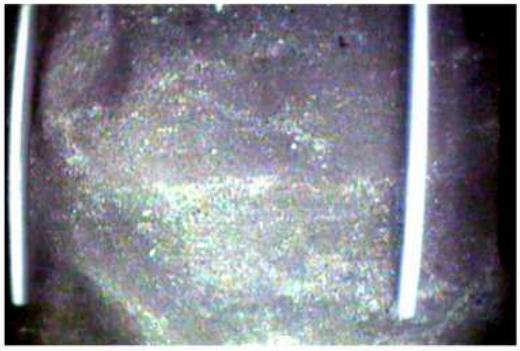

4-3.bmp

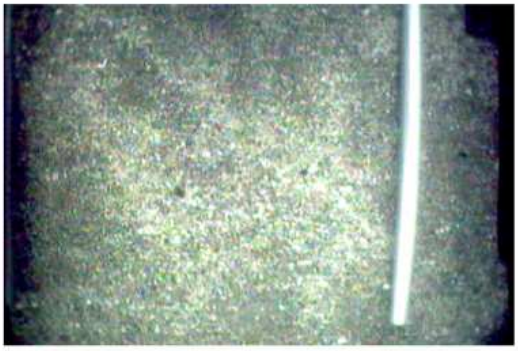

4-5.bmp

5-1.bmp

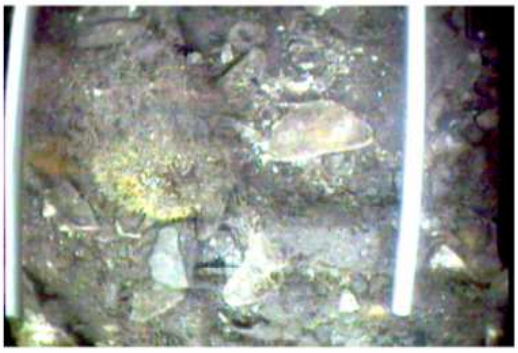

5-10.bmp

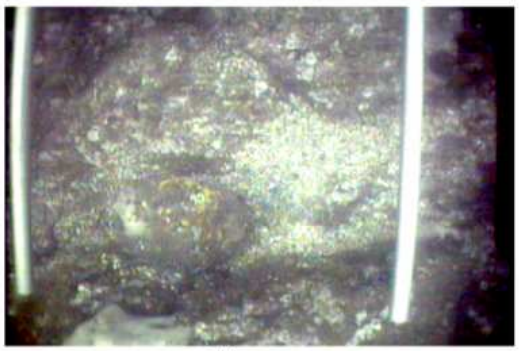

5-2.bmp

5-3.bmp

5-5.bmp

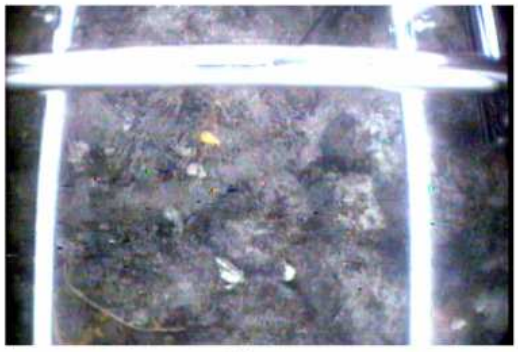

5-7.bmp

5-7b.bmp

5-7c.bmp

5-7d.bmp

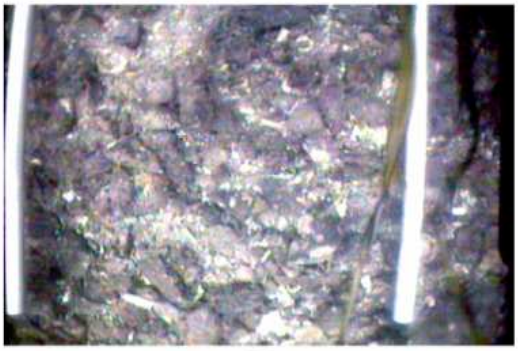

5-8.bmp

5-9.bmp

6-1.bmp

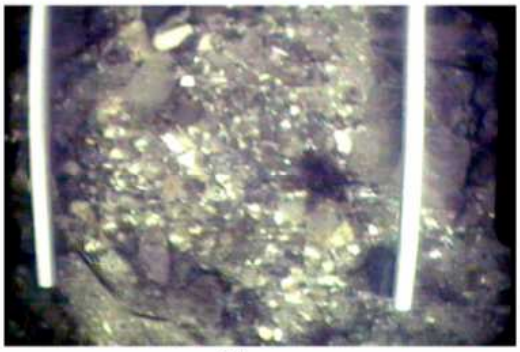

6-2.bmp

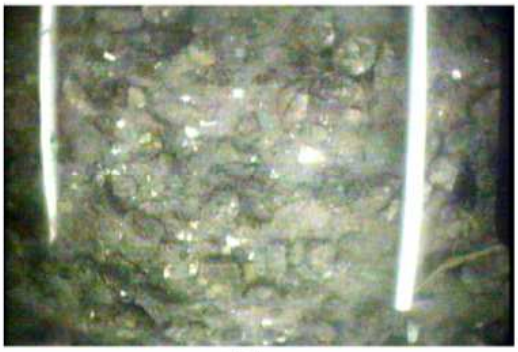

6-3.bmp

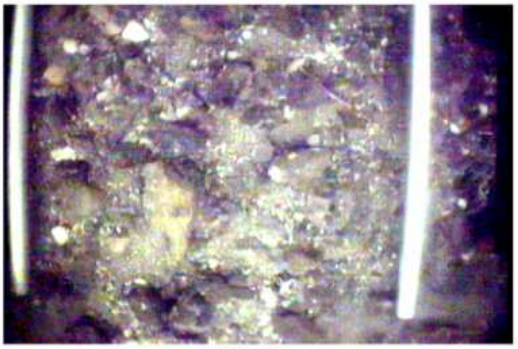

6-4.bmp

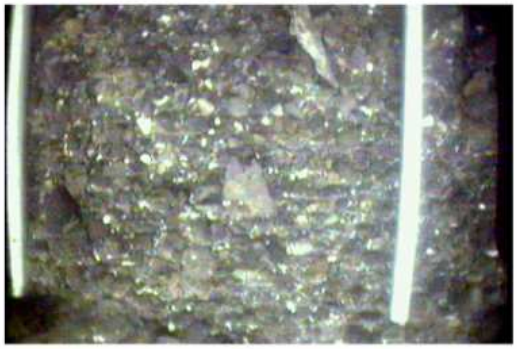

6-5.bmp

6-8.bmp

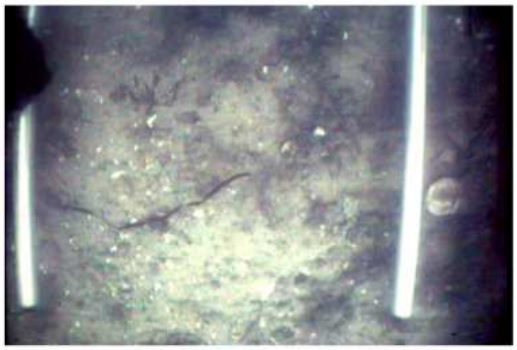

7-11.bmp

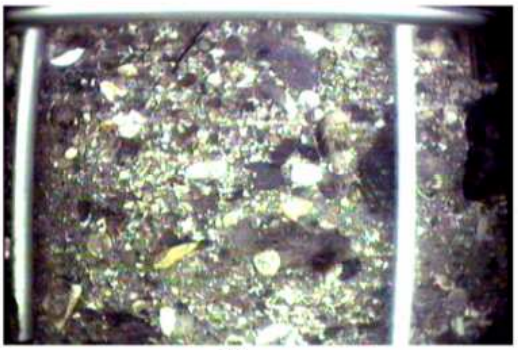

7-3.bmp

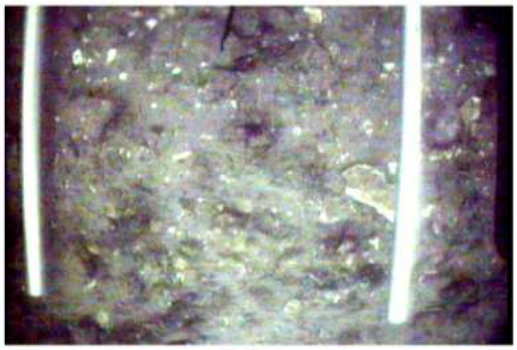

7-5.bmp

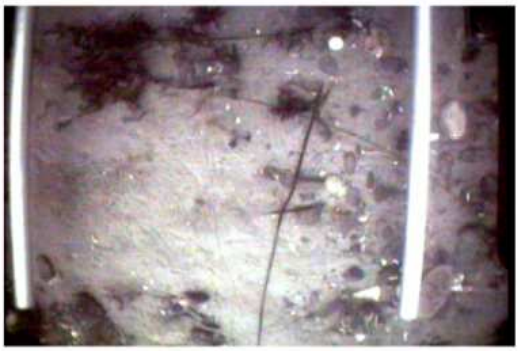

7-6.bmp

7-9.bmp

x2-2.bmp

x2-2c.bmp

x6-1b.bmp

B-6. SAMPLE-VERSUS-IMAGE SEDIMENT GRAIN SIZE HISTOGRAM PLOTS USING RECOMBINED CLASSES

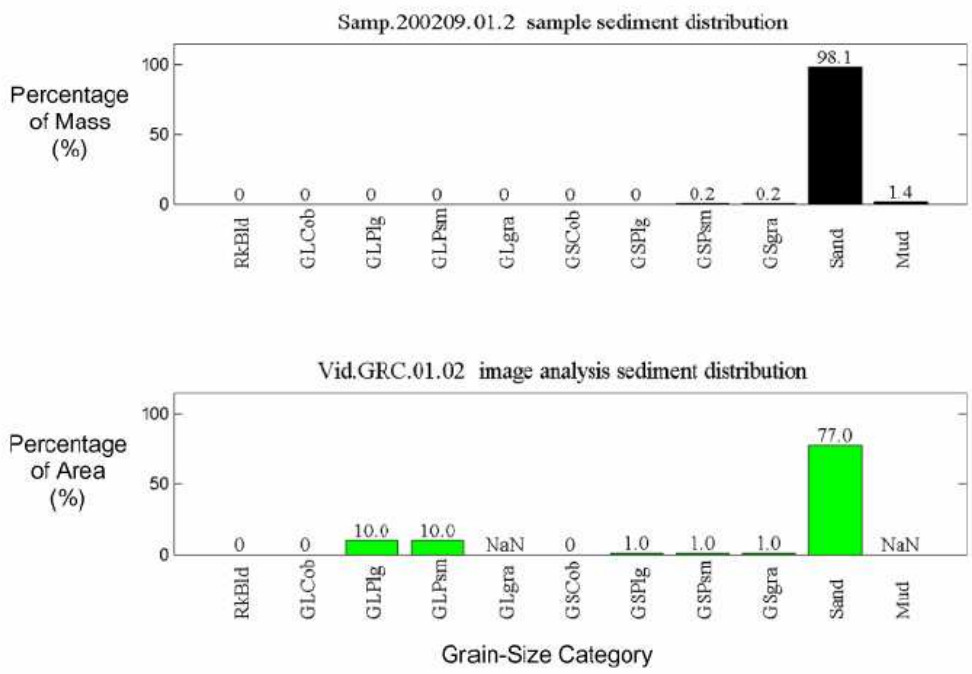

Sed.Samp+Vid.01.02

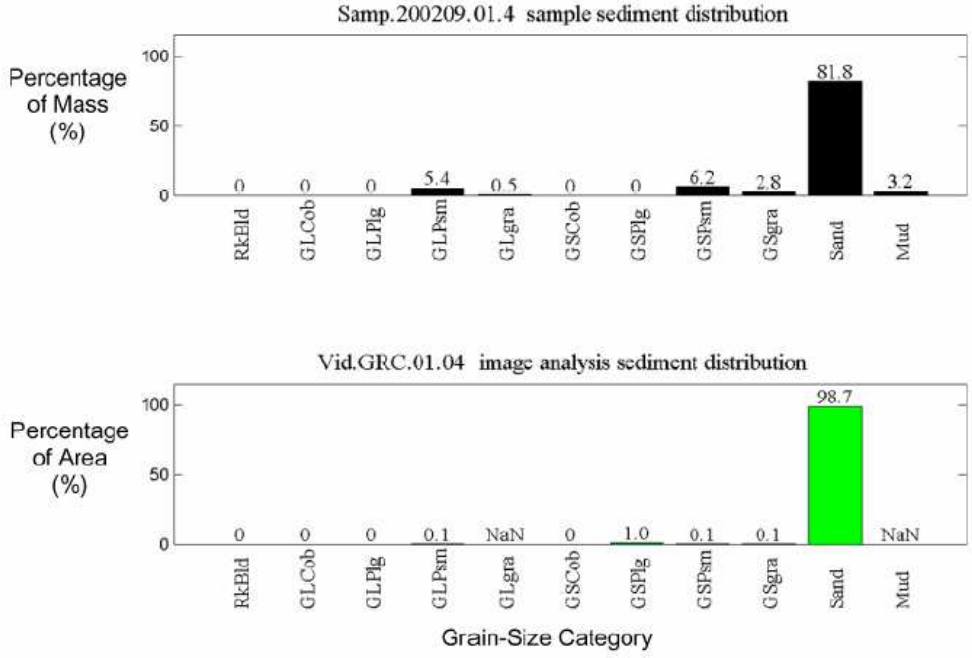

Sed.Samp+Vid.01.04

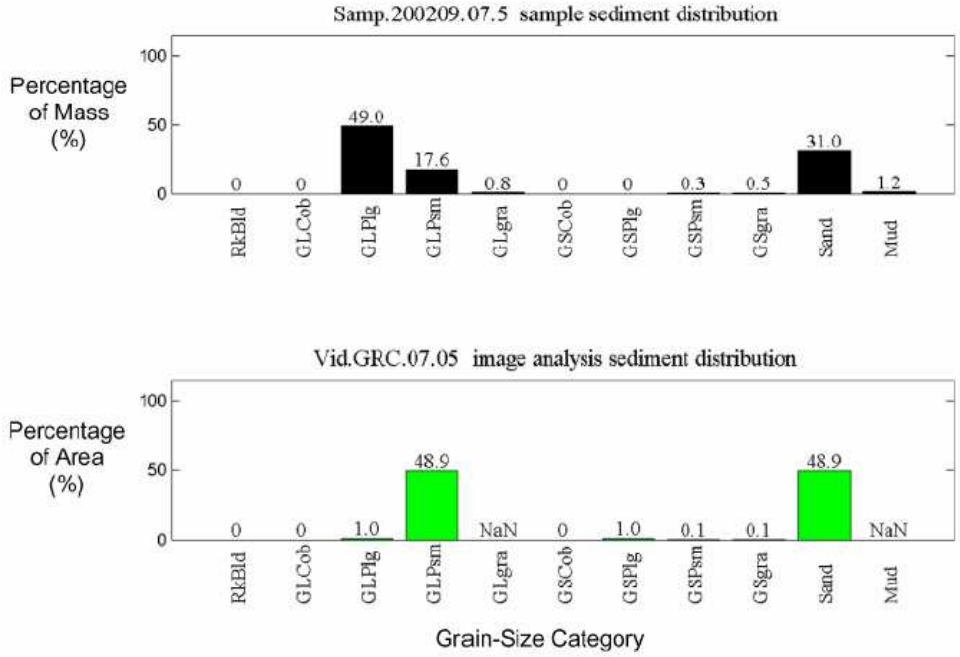

Sed.Samp+Vid.07.05

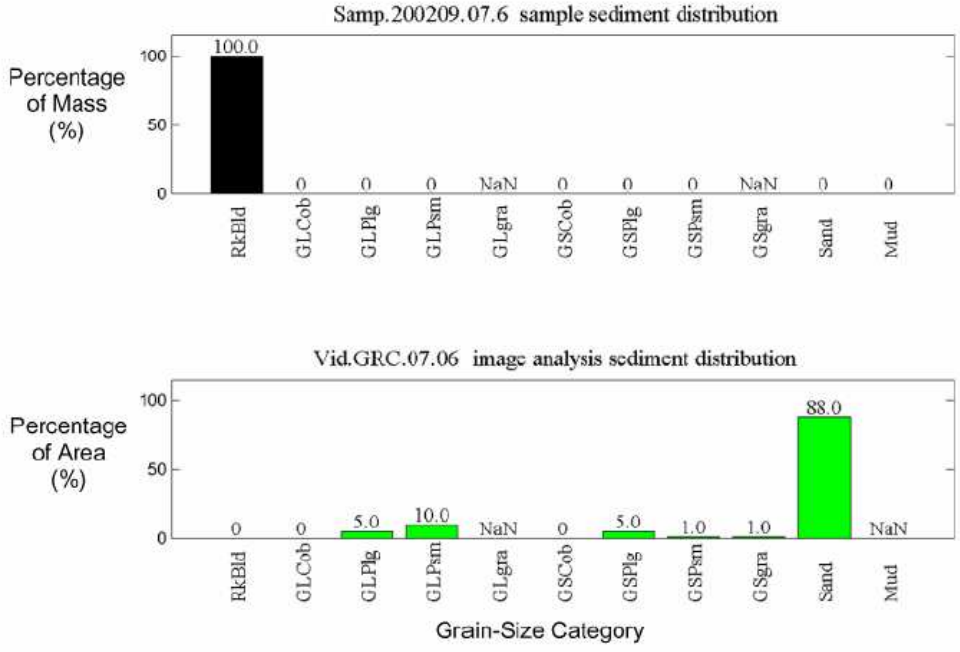

Sed.Samp+Vid.07.06

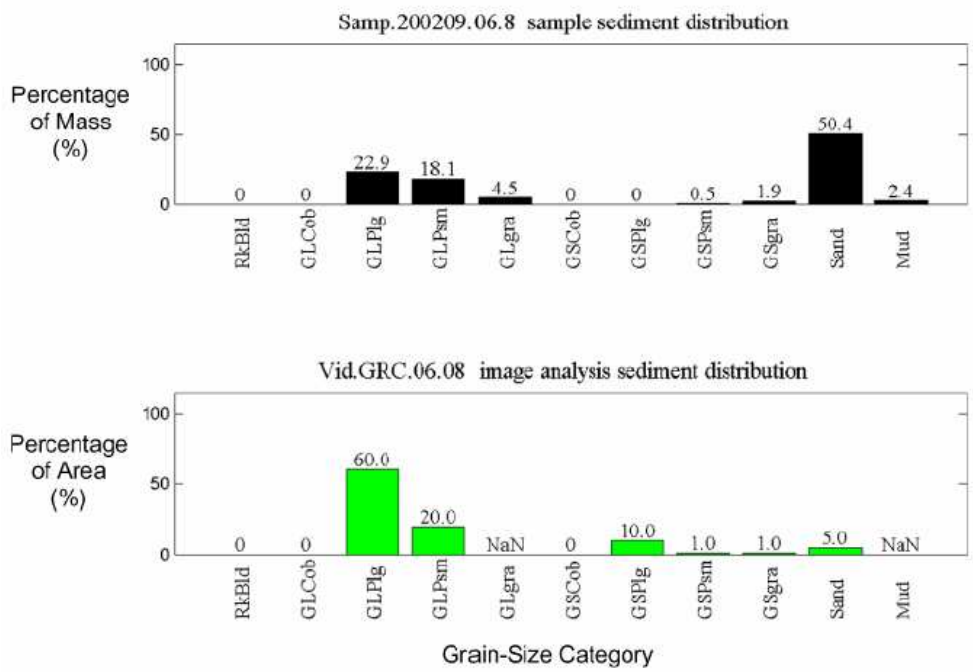

Sed.Samp+Vid.06.08

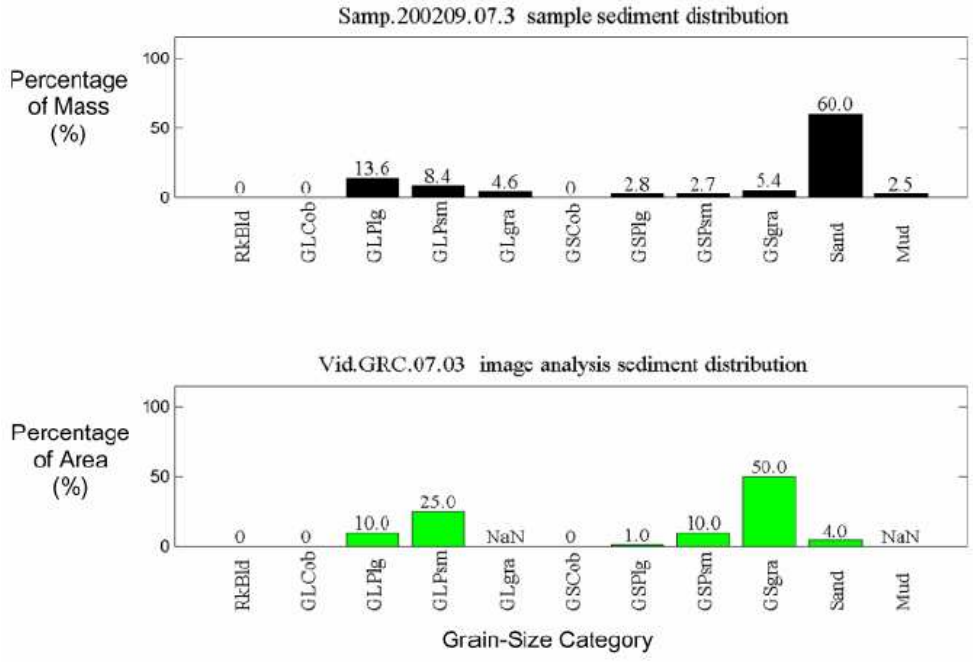

Sed.Samp+Vid.07.03

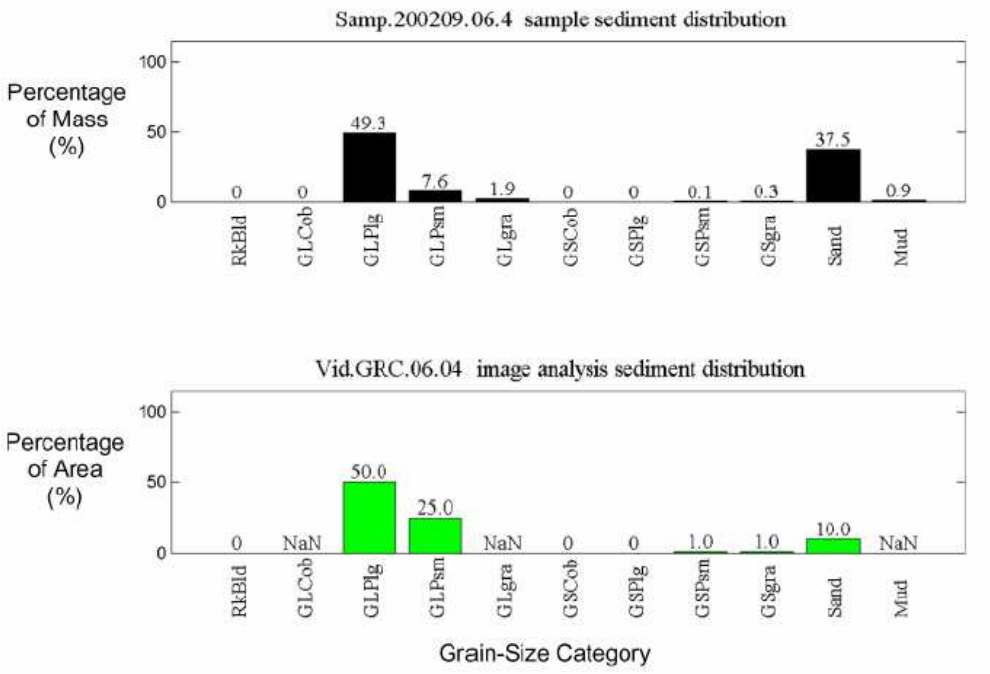

Sed.Samp+Vid.06.04

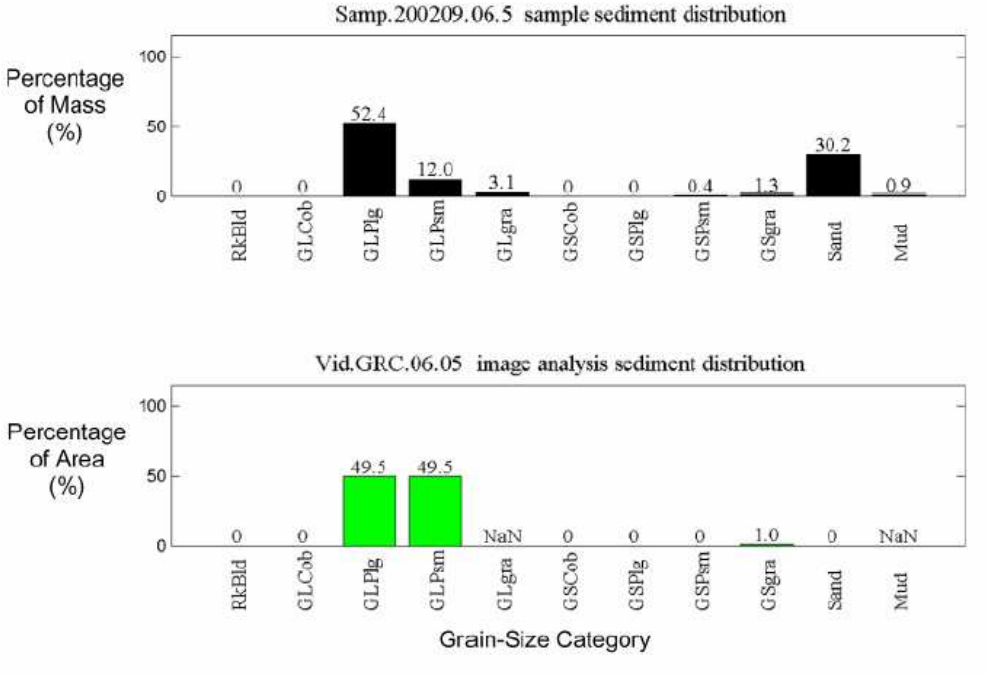

Sed.Samp+Vid.06.05

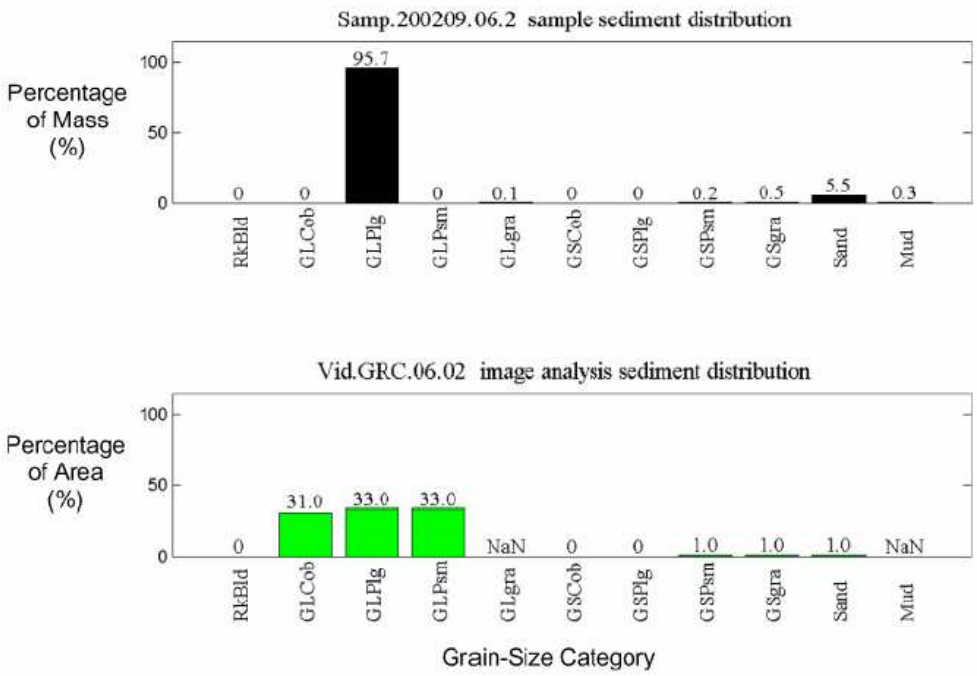

Sed.Samp+Vid.06.02

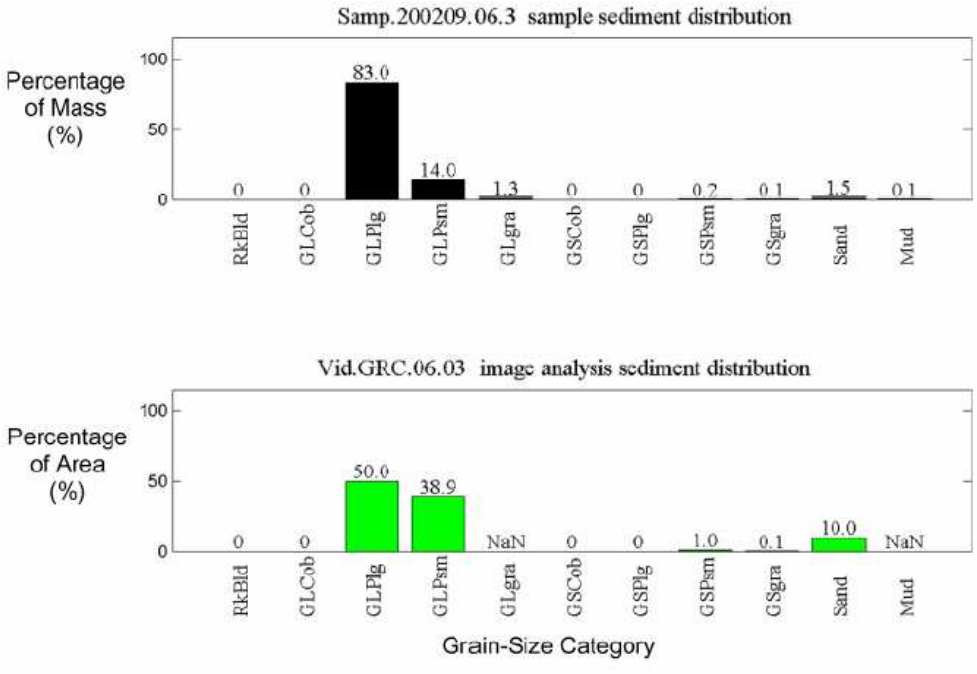

Sed.Samp+Vid.06.03

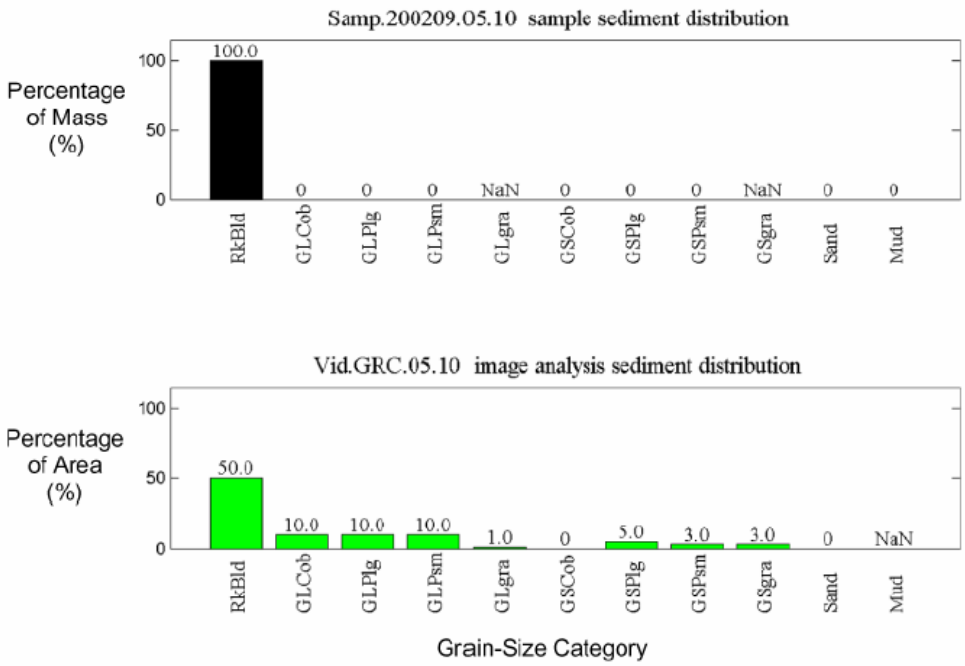

Sed.Samp+Vid.05.10

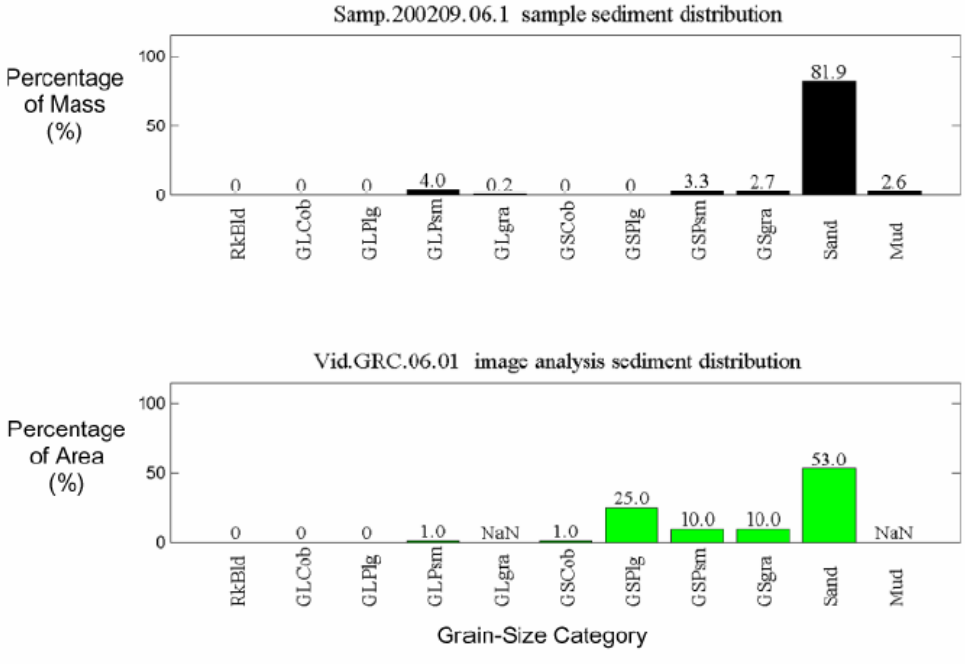

Sed.Samp+Vid.06.01

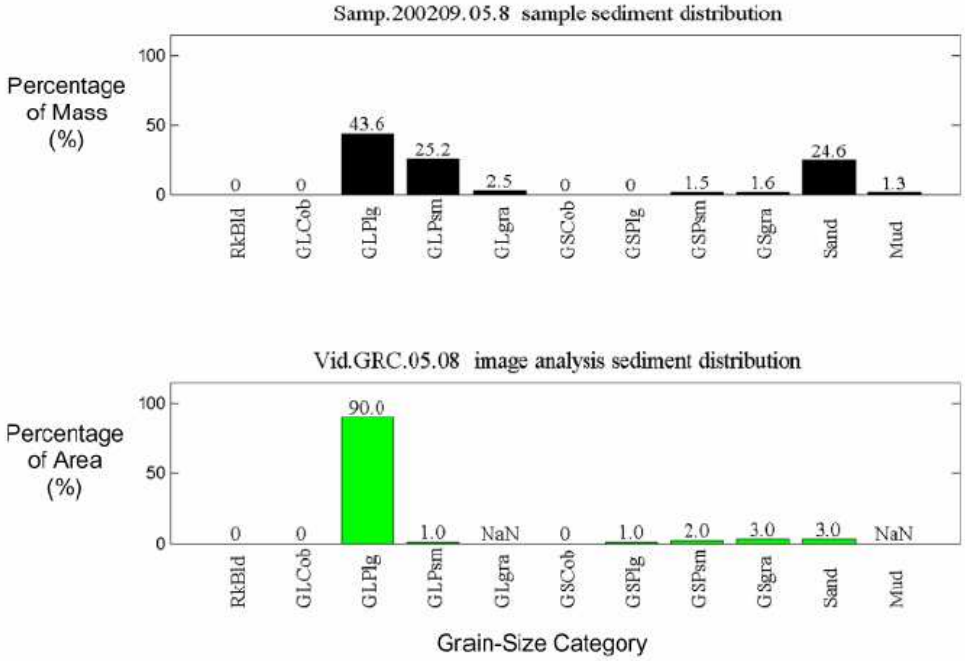

Sed.Samp+Vid.05.08

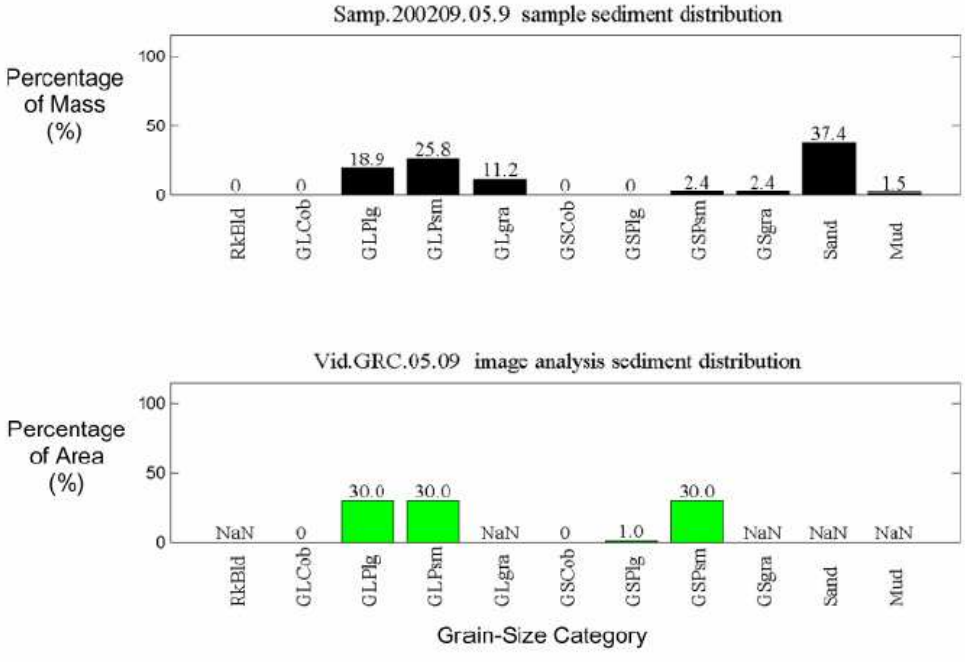

Sed.Samp+Vid.05.09

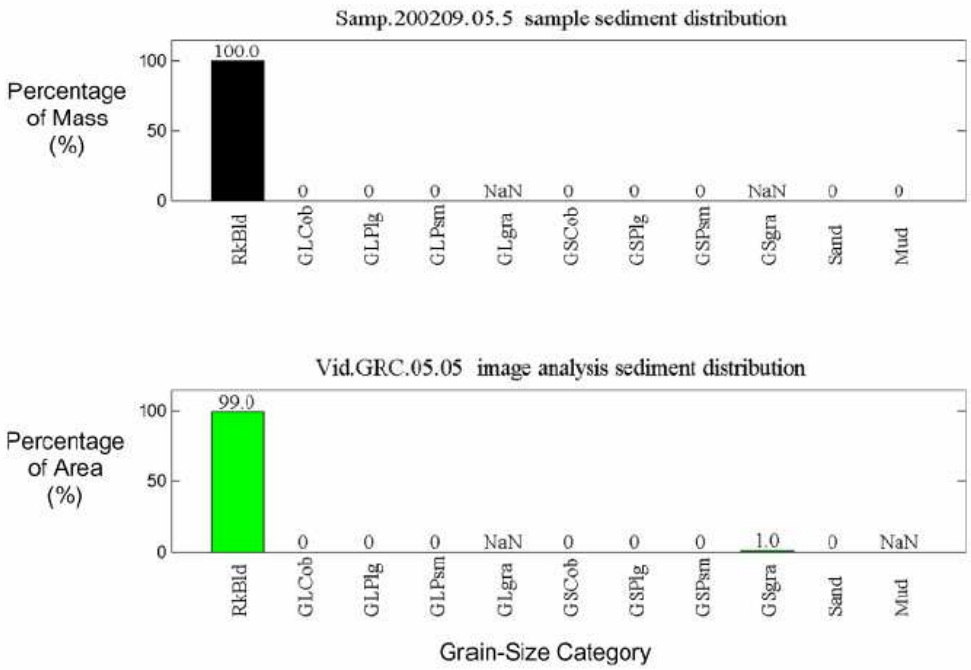

Sed.Samp+Vid.05.05

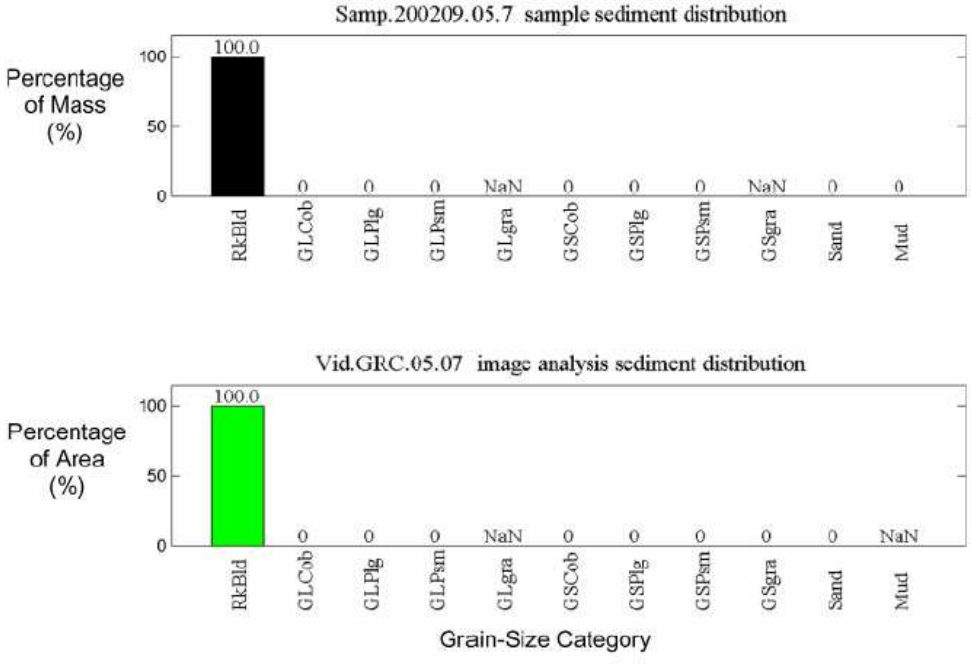

Sed.Samp+Vid.05.07

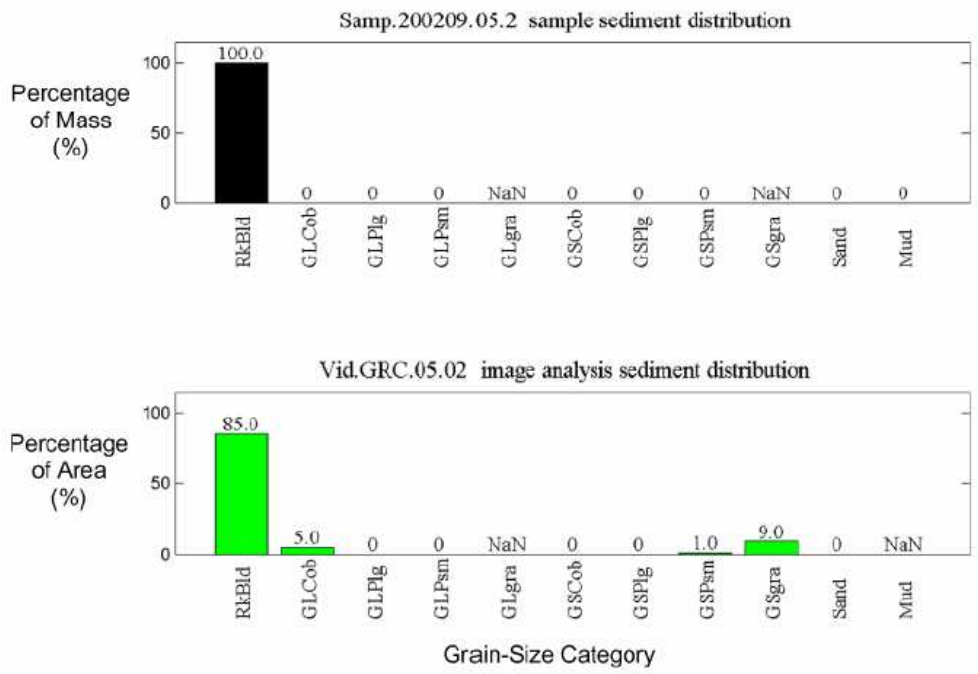

Sed.Samp+Vid.05.02

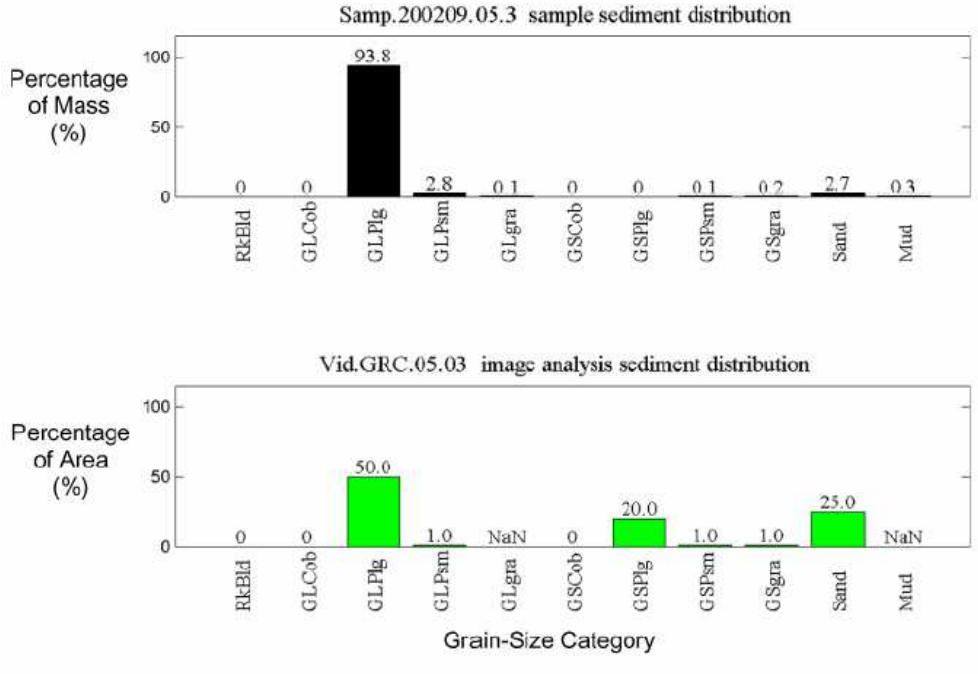

Sed.Samp+Vid.05.03

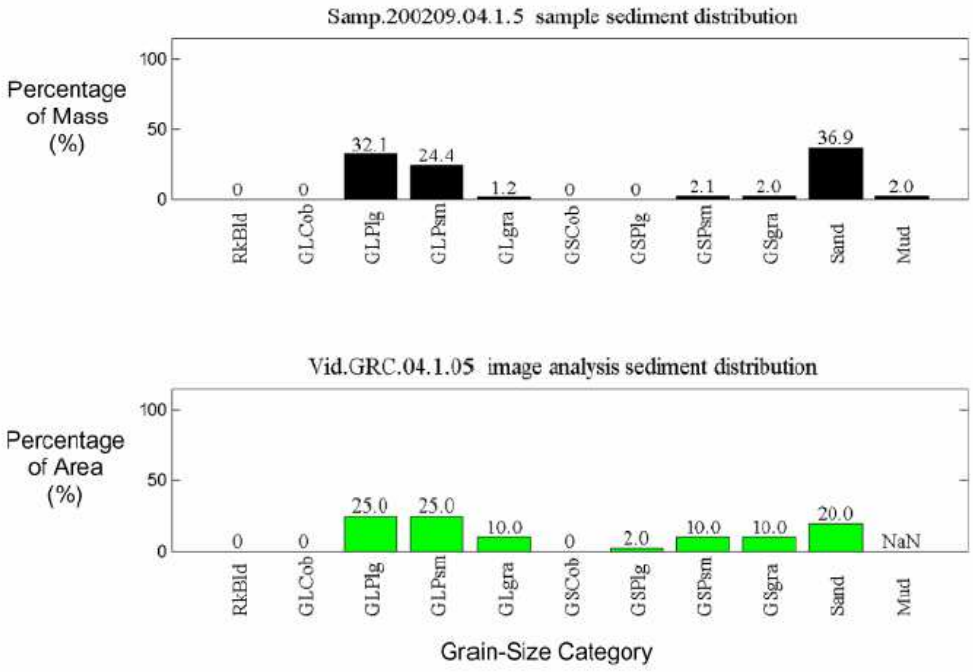

Sed.Samp+Vid.04.1.0:

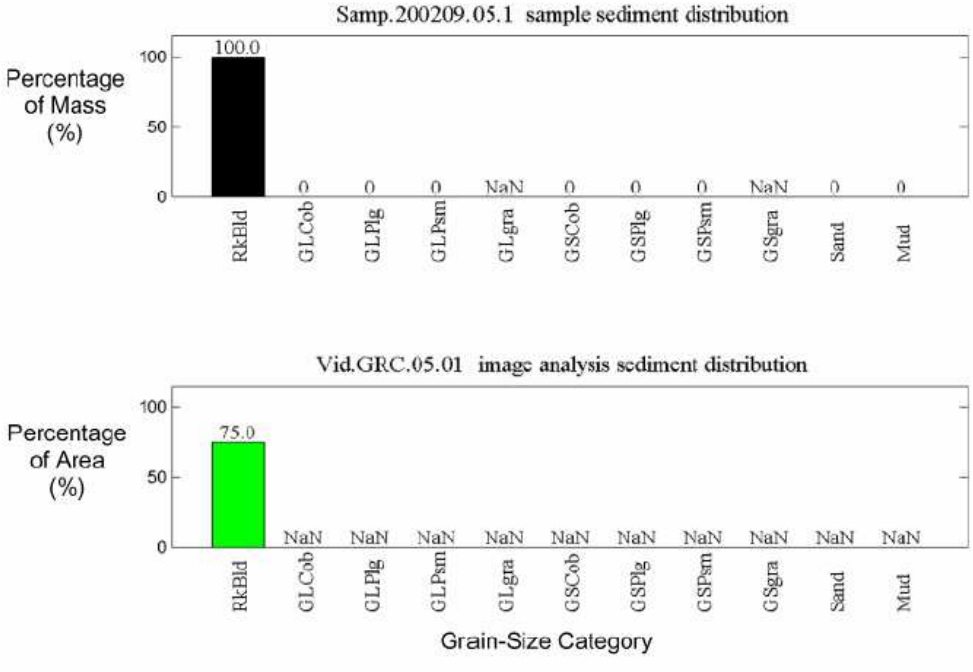

Sed.Samp+Vid.05.01

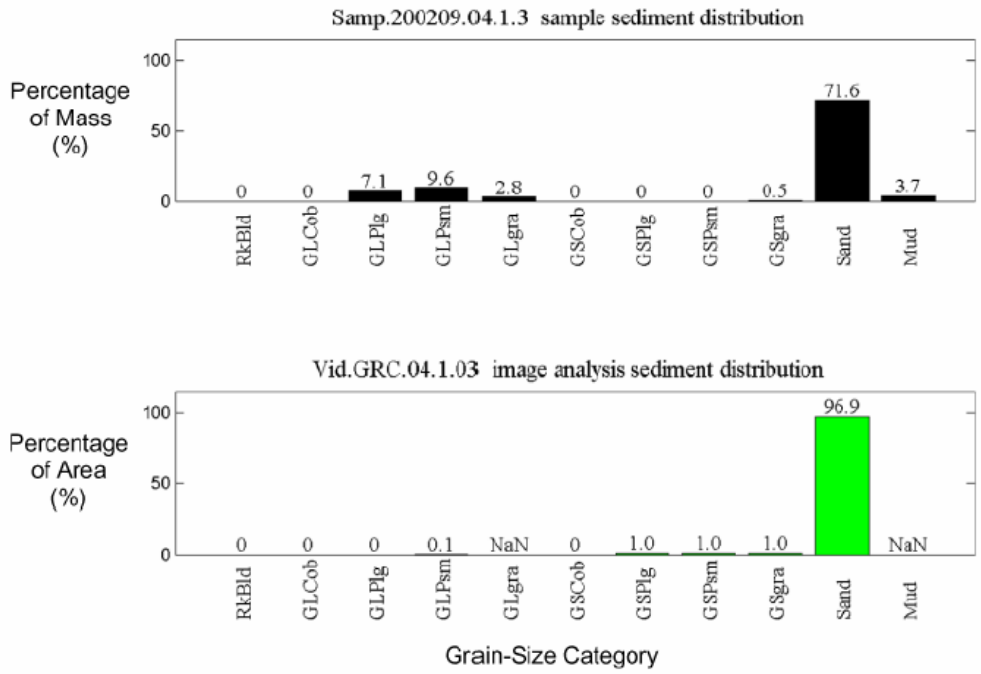

Sed.Samp+Vid.04.1.0

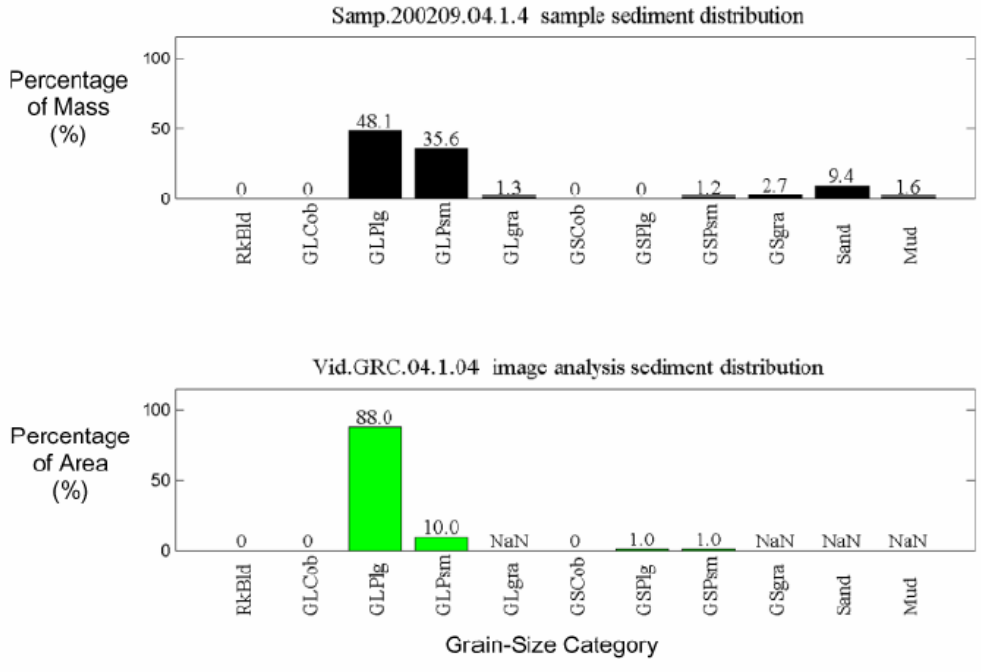

Sed.Samp+Vid.04.1.0

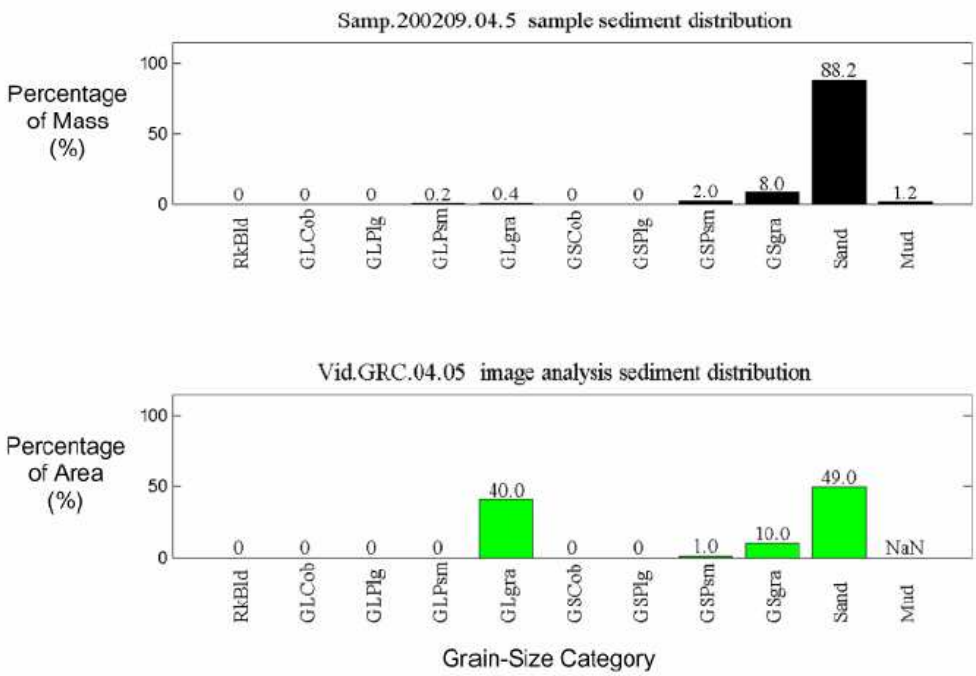

Sed.Samp+Vid.04.05

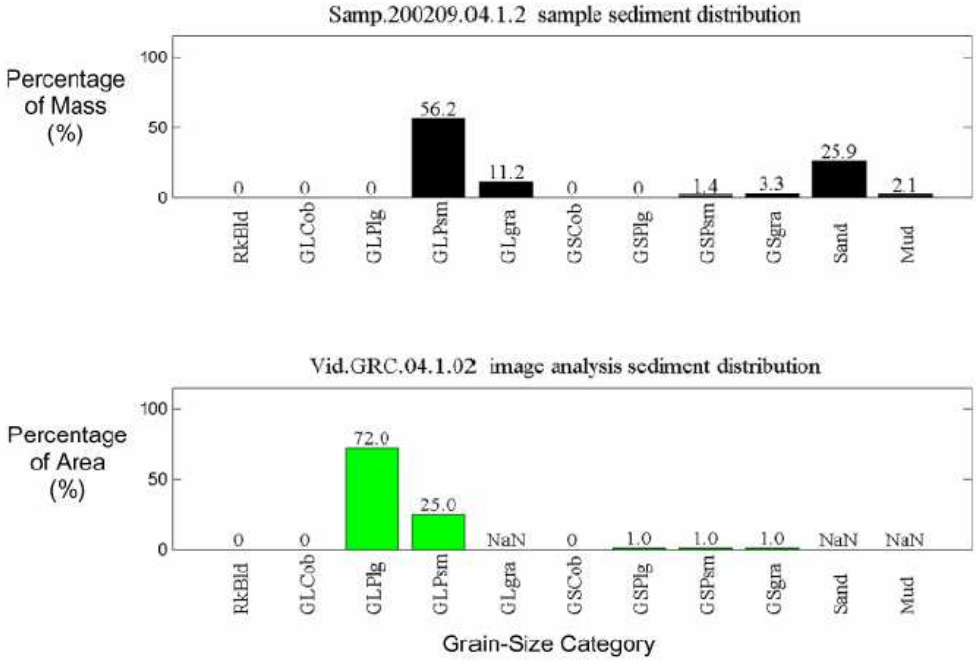

Sed.Samp+Vid.04.1.0

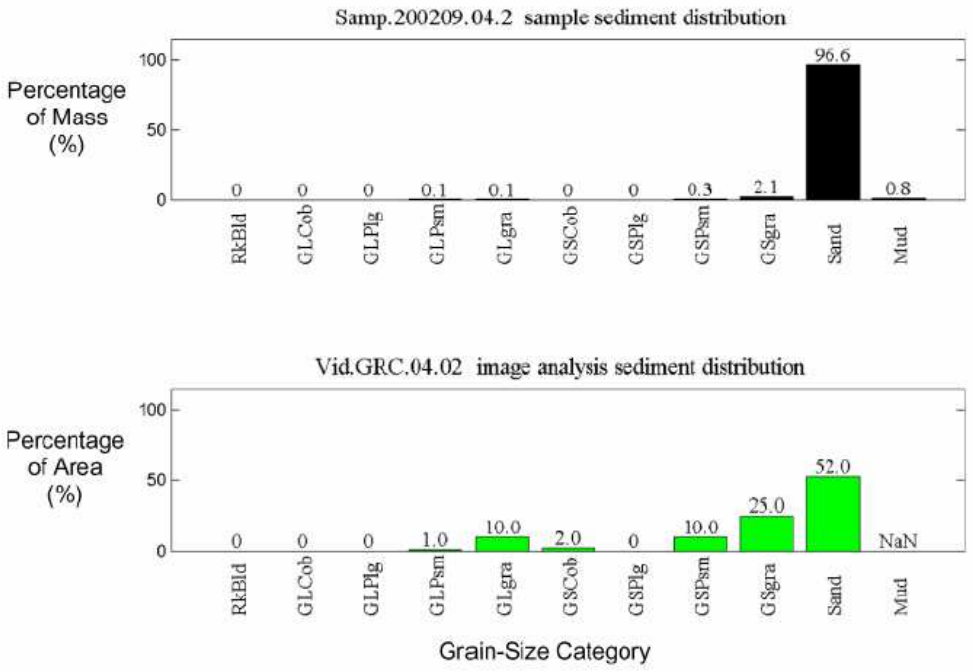

Sed.Samp+Vid.04.02

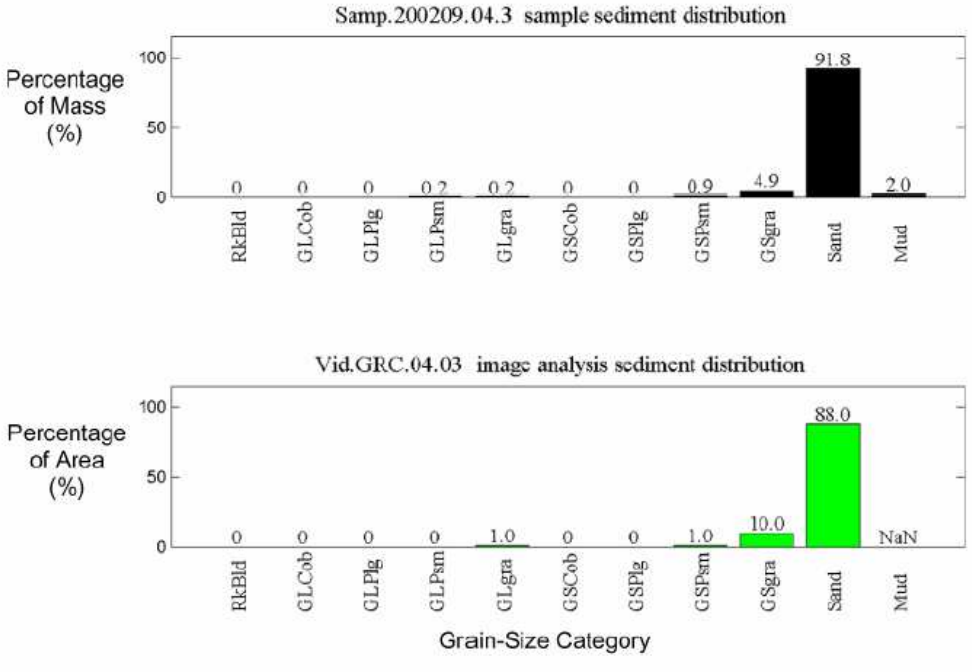

Sed.Samp+Vid.04.03

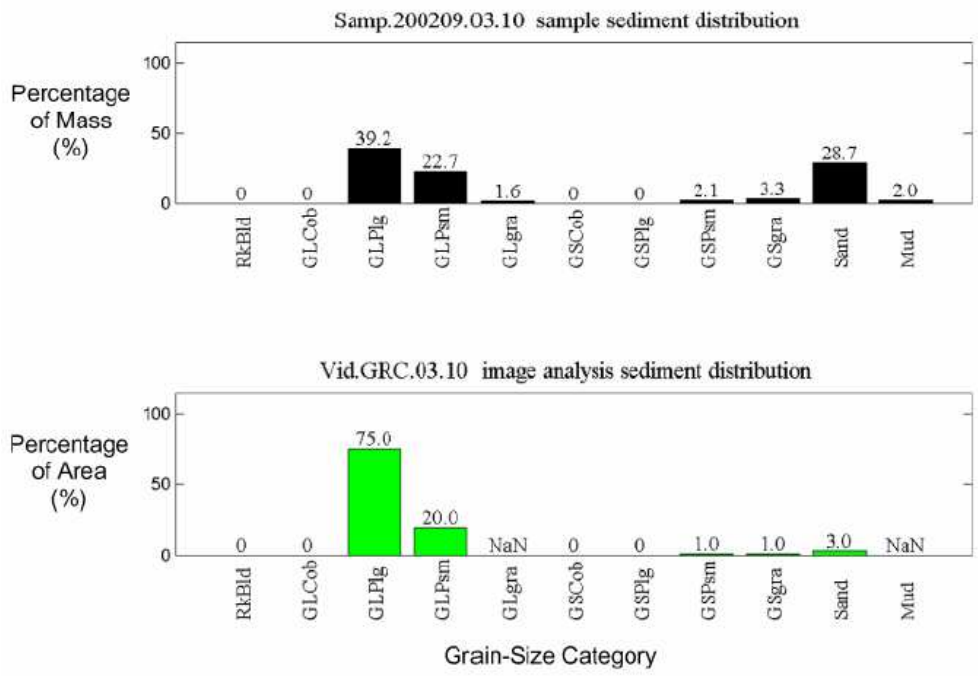

Sed.Samp+Vid.03.10

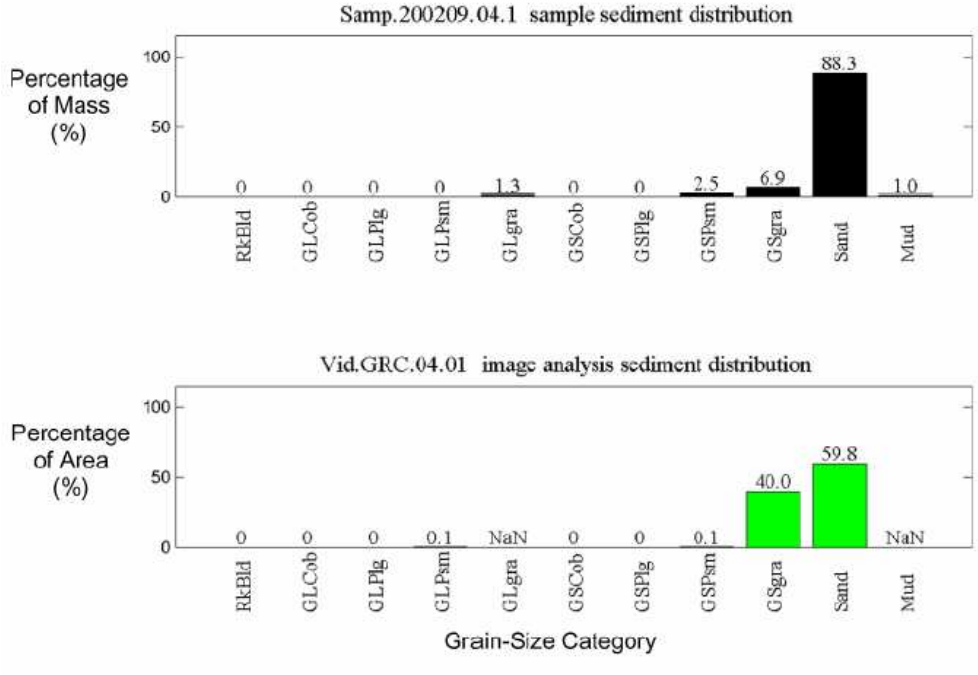

Sed.Samp+Vid.04.01

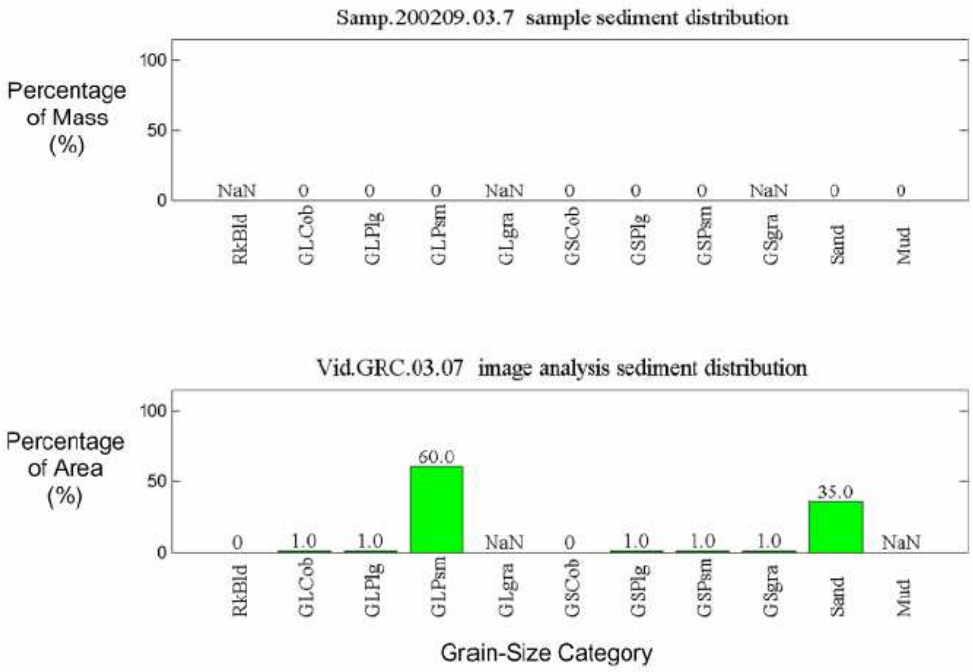

Sed.Samp+Vid.03.07

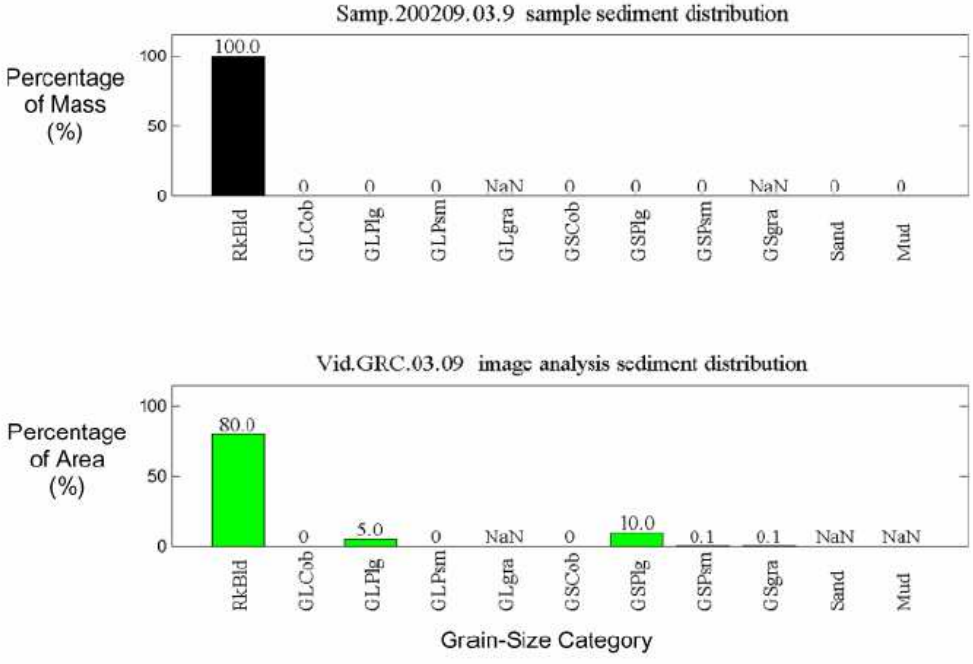

Sed.Samp+Vid.03.09

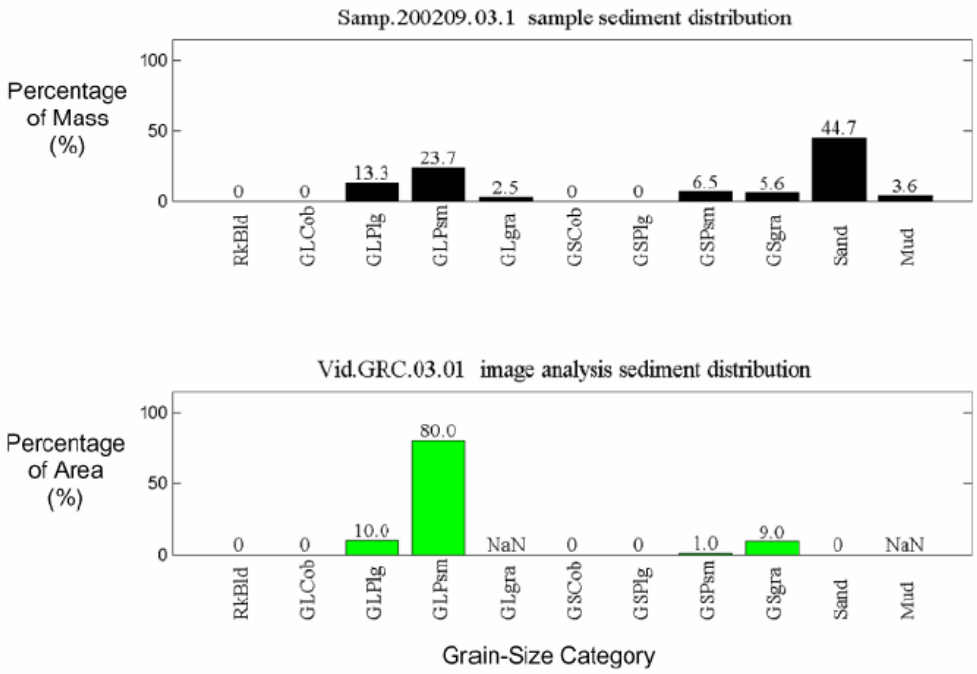

Sed.Samp+Vid.03.01

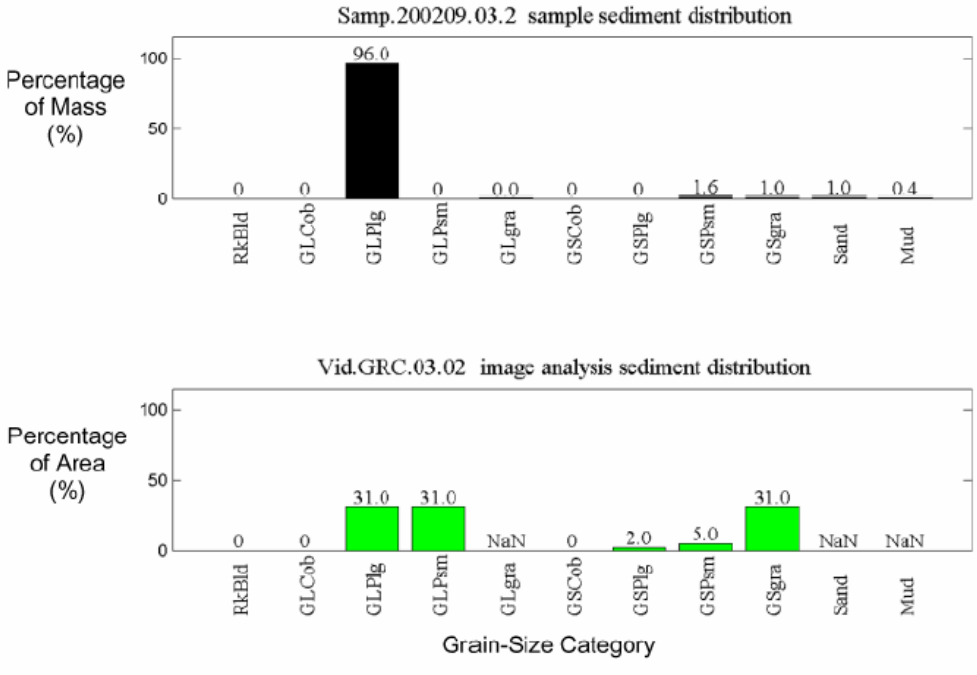

Sed.Samp+Vid.03.02

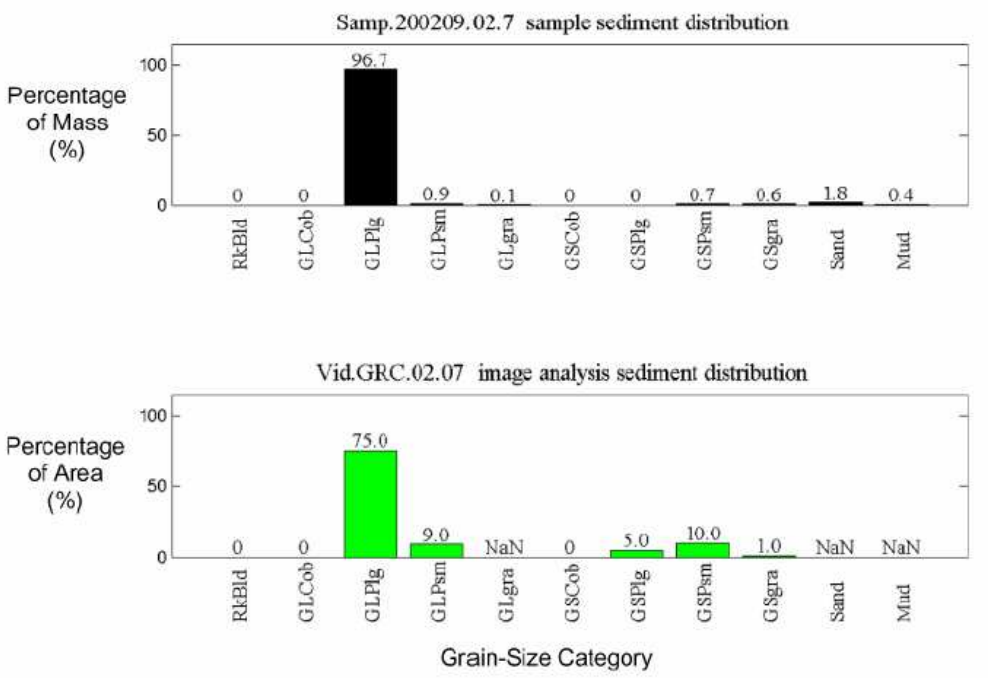

Sed.Samp+Vid.02.07

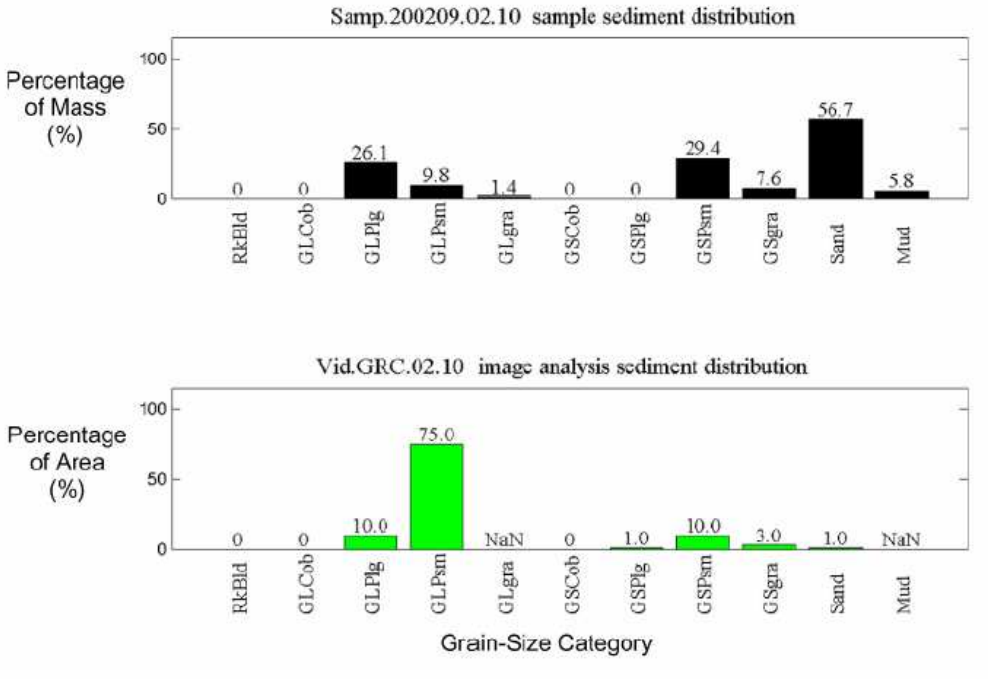

Sed.Samp+Vid.02.10

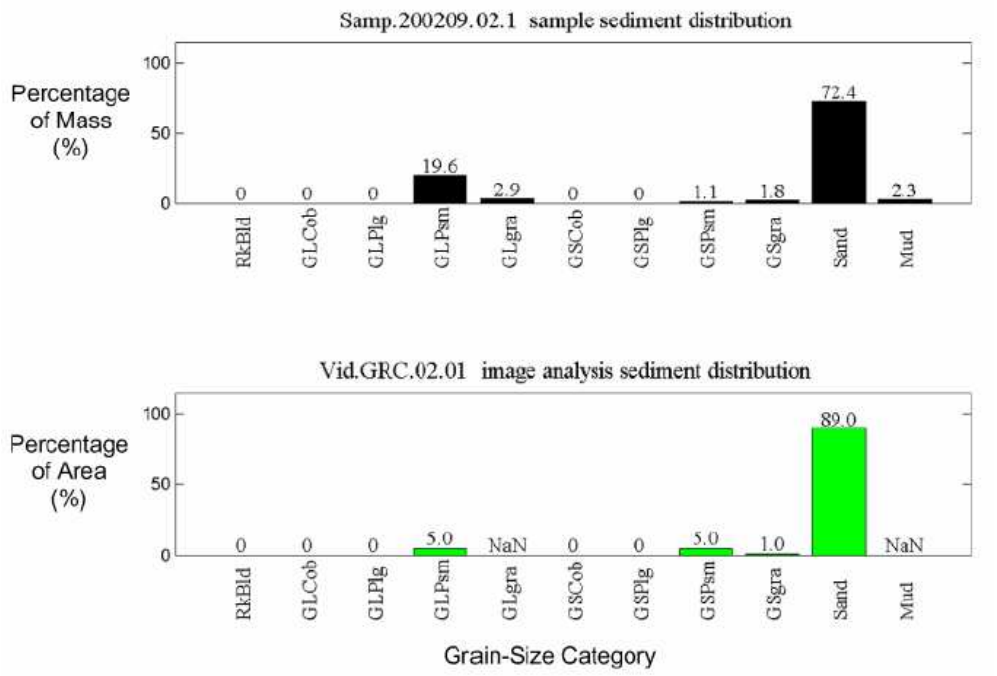

Sed.Samp+Vid.02.01

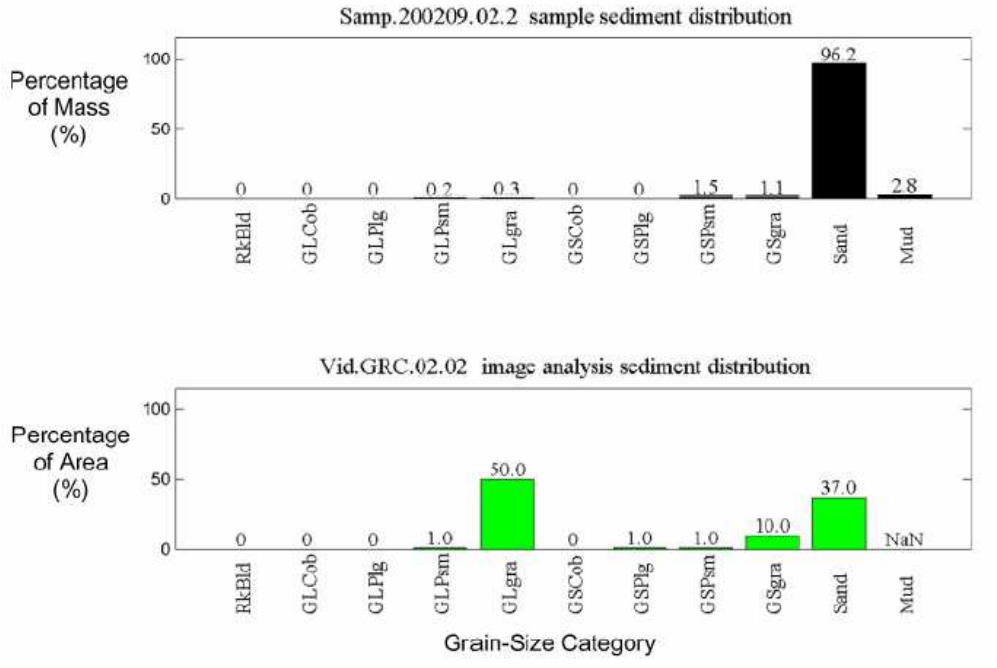

Sed.Samp+Vid.02.02

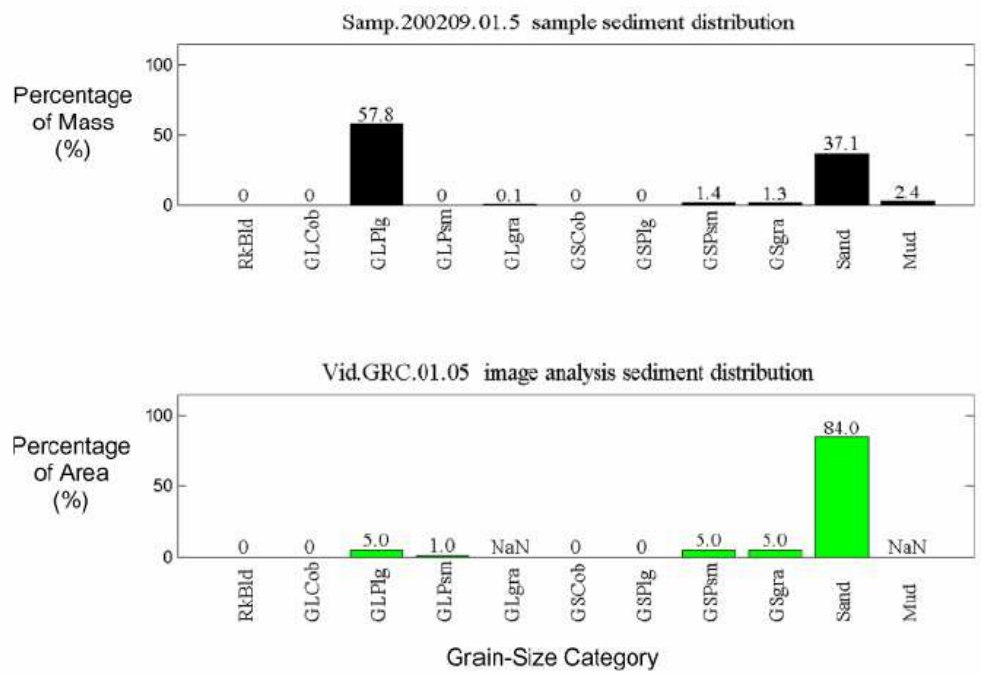

Sed.Samp+Vid.01.05

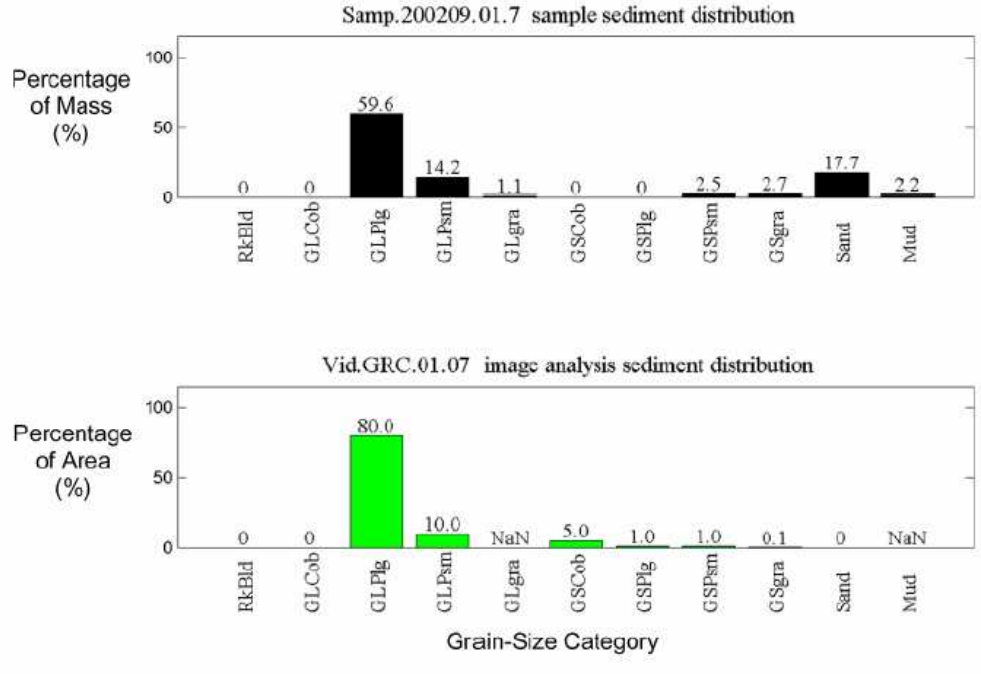

Sed.Samp+Vid.01.07

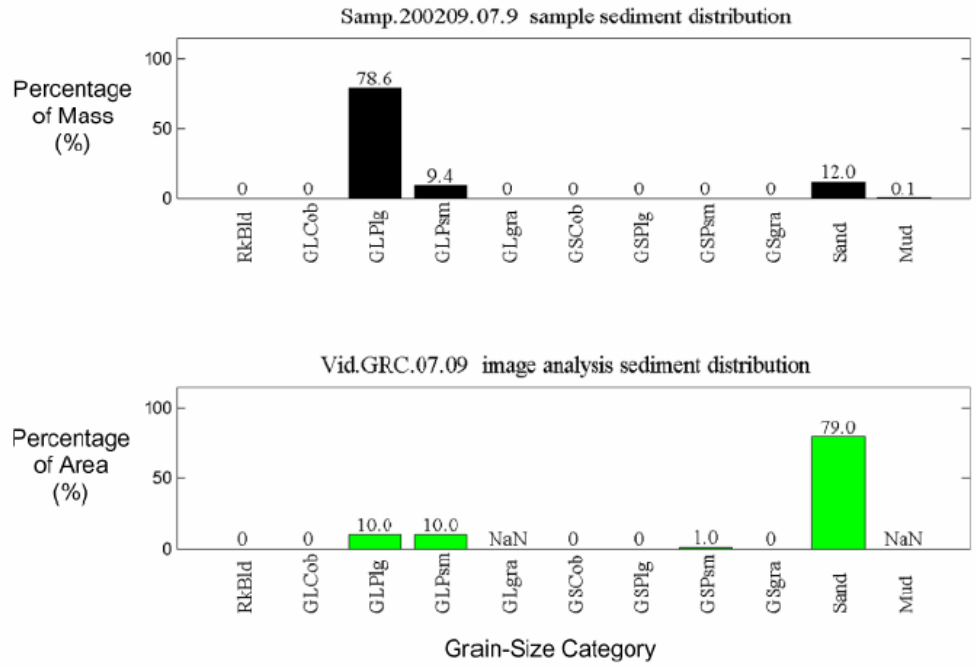

Sed.Samp+Vid.07.09

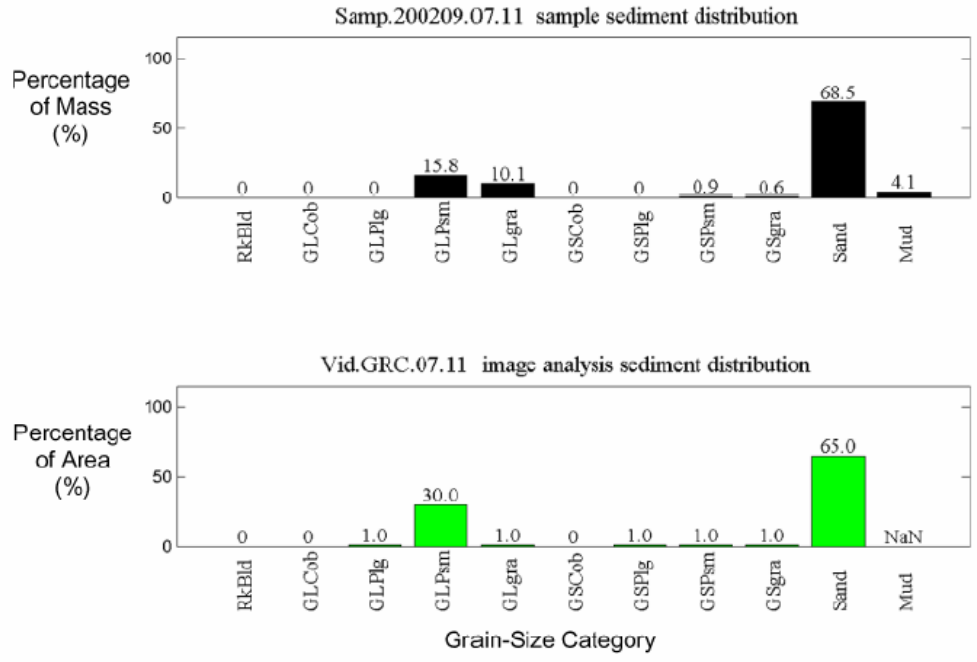

Sed.Samp+Vid.07.11

APPENDIX C

NOAA VIDEO INTERPRETATION METHODOLOGY: USVI 2004

Provided by: T. Battista and M. Kendall (NOAA, NOS, NCCOS, CCMA, Biogeography Program).

The benthic habitat of six seafloor video transects was assessed by visual interpretation. The habitat was classified using three hierarchical levels:

1. Structure
2. Substrate
3. Cover

Structure referred to the broad-scale underlying habitat upon which biotic and abiotic matter or organisms accumulated. The five structure types are:

- Colonized pavement
- Colonized pavement with sand channels
- Sand
- Scattered coral and rock in sand
- Other (if selected was described)

Substrate denotes the visible abiotic components of the bottom which make up the structure and serve as a potential surface on which organisms can grow or attach. Four

substrate classes, considered mutually exclusive and exhaustive, were measured as percent of the visible bottom. These were:

- Consolidated material
- Sand
- Rubble (~2-10 cm)
- Cobble (~20 cm)

Cover referred to the biotic component of the sea floor and was measured as percent of the visible bottom. The biota was divided among four mutually-exclusive categories that are differentiated by their size and shape. A sum of all cover categories is provided in the data as a measure of total colonization. If organisms could not be unquestionably identified into one of the four cover categories it was added to the total colonization sum, but not to any other cover category. Cover was distinguished as:

- Sponge (Phylum Porifera)
- Soft Coral (Subclass Octocorallia and subclass Ceriantipatharia)
- Hard Coral (Subclass Hexacorallia)
- Algae (Phylums Phaeophyta, Chlorophyta and Rhodophyta)

An algal veneer was present on many hard bottom substrates and we attempted to quantify its extent. In many instances the absence of color made quantification impossible. In these instances a value of yes was added to the algal_veneer field. Habitat relief was also recorded. It was defined as either high or low and identified areas where the abiotic vertical range was greater than or less than 1 foot, respectively.

Habitat was evaluated every ten seconds, however due to extreme variability in camera height, not all components of the habitat could be recorded consistently. To compensate for potential problems in scale and unknown data values, each record was differentiated into one of five distance classes. The distinct distance classes were selected based on which components of the habitat, defined hierarchically using structure, substrate and cover, were visible. Notes were recorded to describe special situations when the classification system was not suitable or sufficient. Cover was divided into two groups based on organism size generating two distance classes, because in many assessments large organisms were visible, when smaller ones were not. Each distance class (and the corresponding visible habitat components) is listed below:

1. Too close or too far (no components)
2. Far (only structure)
3. Far (only structure and substrate)
4. Far (only structure, substrate and large organisms)
5. Appropriate Distance (structure, substrate and large and small organisms)

Caveats

Approximate positional accuracy is ~20m. The camera was unable to dive deeper than approximately 100 feet and therefore videos are biased shallow water samples of benthic habitat. Extreme variability in camera height produced unstandardized, inconsistent habitat cover estimates by varying spatial scale. This problem was exaggerated at low camera heights. For instance, when the camera was 1ft from the bottom a single sponge could produce 100% sponge cover estimates, even if most of the

surrounding habitat was sand. At the same location a greater camera height would have greatly reduced the sponge cover estimate. When the camera was very far from the bottom the ten second time interval between observations was inadequate and a large proportion of the same bottom was evaluated in contiguous examinations. The same problem arose when the camera was swinging.

In a few instances camera listing (tilt) caused habitat distortions. When the camera was vertical it was extremely difficult to assess 3-dimensionality. This loss of data impeded identity of cover, probably reduced cover estimates of gorgonians and made it difficult to assess relief.